Development of Photoplethysmography Phantoms for the In Vitro Investigation of Cardiovascular Disease

Redjan Ferizoli

1st Supervisor: Dr James May

2nd Supervisor: Professor Panicos. A. Kyriacou

Thesis submitted for the degree of

Doctor of Philosophy

in Biomedical Engineering

Research Centre for Biomedical Engineering

School of Science and Technology

August 2025

DECLARATION

I declare that the work presented in this thesis is my work. Any idea, result, or illustration originating from the work of other subjects has been acknowledged. I confirm that the work was carried out entirely as part of my Doctor of Philosophy in Biomedical Engineering candidature at City St George's, University of London. This thesis has never been published or submitted elsewhere for obtaining an academic degree or professional qualification.

Redjan Ferizoli

2025

ACKNOWLEDGEMENTS

I would like to begin by sincerely thanking my supervisors. To Dr James May, thank you for supporting me throughout, and for all those timely trips down to the lab whenever I found myself stuck. Thank you to Professor Panicos Kyriacou, who inspired me since my first year at university and had continued to motivate and uplift me ever since. Special thanks to Dr Meha Qassem, for looking out for me and always stopping by, with advice that always seemed to arrive at exactly the right moment.

To my colleagues, thank you for making the lab an incredible place, from unforgettable conversations to the countless shared moments. It seems we skipped 'friends' and went straight to family, both inside and outside the lab.

I would also like to thank my friends for supporting me from the very beginning and for always understanding. There are too many of you to name, but you know who you are. Your encouragement has kept me going, and your friendship has always given me something to look forward to. It means so much to have grown alongside you, to have shared so many stages of life together which have shaped us along the way, and to continue navigating life side by side.

Finally, I want to express my deepest thanks to my family for your unwavering love and sacrifice. To my parents, who gave everything so that we could have the opportunities they never had, without which I could never have even dreamed of embarking on this journey. To my brother Bajram, for showing me this path and paving the way ahead as the eldest brother, so I could walk my own with more confidence. To my brother Endrit, for his persistent encouragement and for always speaking of me with such pride. To my sister Amy, for all our trips to board game cafés across London, and all the memories that came with them. To my sister Vaishali, for always having my back, and for the many iced chais that kept me going. And to my wife, Maisha, for always being there through it all and for brightening even the longest days and nights.

ABSTRACT

Cardiovascular disease (CVD) remains the leading cause of death globally, with arterial stiffness recognised as a key predictor of vascular ageing and disease progression. While photoplethysmography (PPG) shows promise as a non-invasive tool for vascular health monitoring, most research relies on in vivo data, limiting the ability to systematically examine individual physiological factors. This thesis presents a custom-built in vitro testing platform designed to isolate and evaluate the impact of arterial stiffness on PPG signals under controlled conditions.

Custom silicone vessels with adjustable stiffness values, embedded within soft tissue phantoms, were fabricated and tested using a bilateral flow system. The platform enabled direct comparison of healthy and unhealthy vessels under identical haemodynamic environments, producing consistent and reproducible PPG signals across a range of flow settings. A comprehensive feature extraction pipeline was established and validated, identifying PPG waveform features most sensitive to stiffness variation.

The findings demonstrate that PPG features respond dynamically to vascular stiffness and flow conditions, offering a foundation for data-driven algorithm development. Studies across varying vessel stiffnesses showed a pronounced reduction in key morphological features, including amplitude, pulse width, and area under the curve, alongside increases in specific signal indices such as kurtosis, skewness and zero-crossing rate. When examined under different flow rates, these changes were more pronounced in healthy vessels than in their stiffer counterparts, highlighting the heightened sensitivity of PPG features to haemodynamic changes in healthy vessels.

The platform provides a structured environment for generating labelled datasets to support machine learning applications, bridging the gap between controlled experimentation and real-world cardiovascular monitoring. This work contributes to the development of reliable, accessible diagnostic tools for early detection and long-term tracking of vascular health.

TABLE OF CONTENTS

ABBREVIATIONS

AS	Arterial stiffness
AUC	Area under curve
BP	Blood Pressure
CVD	Cardiovascular disease
ECG	Electrocardiogram
FR	Flow Rate
HR	Heart rate
HRV	Heart rate variability
LED	Light emitting diode
PAD	Peripheral arterial disease
PAT	Pulse arrival time
PRV	Pulse rate variability
PTT	Pulse transit time
PWV	Pulse wave velocity
SBP	Systolic blood pressure

List of Figures

LIST OF TABLES

List of Publications

Ferizoli, R., Karimpour, P., May, J.M. and Kyriacou, P.A., 2023, July. A Bilateral In Vitro Model for Cardiovascular Disease Investigations Using Photoplethysmography Sensors. In *2023 IEEE BioSensors Conference (BioSensors)* (pp. 1-4). IEEE.

Ferizoli, R., Karimpour, P., May, J.M. and Kyriacou, P.A., 2024. Arterial stiffness assessment using PPG feature extraction and significance testing in an in vitro cardiovascular system. *Scientific Reports*, *14*(1), p.2024.

Karimpour, P., Ferizoli, R., May, J.M. and Kyriacou, P.A., 2024. Customisable Silicone Vessels and Tissue Phantoms for In Vitro Photoplethysmography Investigations into Cardiovascular Disease. *Sensors*, *24*(5), p.1681.

Karimpour, P., Ferizoli, R., May, J.M. and Kyriacou, P.A., 2024, July. Custom Silicone Vessels for In Vitro Investigations on Vascular Ageing using Photoplethysmography. In *2024 46th Annual International Conference of the IEEE Engineering in Medicine and Biology Society (EMBC)* (pp. 1-4). IEEE.

Publications in Progress

Ferizoli, R., May, J.M. and Kyriacou, P.A. PPG & Vessel Stiffness with Varying Flow Properties utilising Bilateral Custom Vessels

Karimpour, P., Ferizoli, R., May, J.M. and Kyriacou, P.A., A Multimodal Assessment of Arterial Stiffness Using Photoplethysmography and Laser Doppler Flowmetry

1 INTRODUCTION

Cardiovascular disease (CVD) is the leading cause of mortality worldwide, responsible for over 17 million deaths each year, accounting for 32% of all global fatalities (Khan, 2021). Often developing silently over decades, CVD includes conditions such as atherosclerosis, hypertension, and vascular ageing, which can remain undetected until they become major health problems. Early detection and monitoring are essential for effective prevention and treatment, yet current gold-standard diagnostic tools for vascular health, such as pulse wave velocity, rely on specialist equipment and professional training. This limits their accessibility and restricts routine assessment outside of specialist settings (Chang et al., 2024).

Photoplethysmography (PPG) offers a promising alternative. It is a non-invasive, inexpensive and portable light-based technology capable of capturing blood volume changes in peripheral tissue. PPG is already established in smartwatches and consumer health devices for heart rate and oxygen saturation monitoring. Recent research has shown its potential for detecting a wider range of cardiovascular indicators, including arterial stiffness, an early marker of vascular dysfunction (Charlton et al., 2023).

However, much of the existing research is based on in vivo data, where it is difficult to isolate the effect of any one physiological change on the PPG waveform. In practice, waveform morphology can be confounded by factors such as vascular tone, autonomic activity, local tissue composition, sensor contact pressure, temperature, and natural differences between individuals. This makes it challenging to attribute observed changes in PPG features specifically to arterial stiffness or other disease-related mechanical changes, and it limits how confidently findings can be generalised or used to validate feature-based indicators.

This thesis addresses this limitation by developing a controlled in vitro experimental platform for systematic investigation of the relationship

between arterial mechanical changes and PPG signal morphology. The platform comprises custom-fabricated silicone vessels embedded within tissue-mimicking phantoms and integrated into a pulsatile flow rig designed to support optical sensing under reproducible haemodynamic conditions.

A key contribution of this work is the implementation of a bilateral configuration that enables simultaneous assessment of a healthy and a mechanically altered vessel under identical flow conditions. This approach reduces experimental confounding and provides a practical framework for studying asymmetric vascular conditions that are clinically relevant, including peripheral arterial disease and arterial stiffness.

The central motivation of this thesis is to move PPG-based cardiovascular assessment beyond predominantly correlative in vivo observations by providing a reproducible setting in which vessel stiffness can be manipulated, quantified, and directly linked to waveform changes. The novelty of the work lies in three integrated advances: (i) a bilateral in vitro methodology for paired healthy and diseased comparisons under matched haemodynamics, (ii) fabrication of silicone vessels with tuneable mechanical properties to represent progressive arterial stiffening, and (iii) generation of labelled datasets under known mechanical and flow conditions to support statistical feature validation and inform future algorithm development.

Using this platform, this thesis establishes which PPG waveform features are consistently sensitive to stiffness changes and how feature behaviour is modulated by flow dynamics, providing a mechanistic basis for developing and evaluating PPG-based indicators of vascular health prior to clinical testing.

1.1 AIMS & OBJECTIVES

Aim: To investigate the relationship between cardiovascular disease mechanics and photoplethysmography (PPG) signal behaviour using a controlled in vitro platform with bilateral vessel-tissue phantoms.

OBJECTIVES

i. Provide an overview of relevant in vivo and in vitro PPG studies to contextualise research aims.

ii. Develop and validate an in vitro testing platform capable of producing stable PPG signals under controlled flow conditions.

iii. Design and fabricate custom silicone vessels with adjustable mechanical properties representing healthy and diseased arterial conditions.

iv. Implement a bilateral experimental setup to enable simultaneous assessment of healthy and stiffened vessels under identical flow conditions.

v. Extract and quantify key PPG waveform features and apply statistical analysis to identify features sensitive to arterial stiffness variations.

vi. Examine how healthy and unhealthy vessels respond differently to changes in flow dynamics and assess the resulting effects on PPG waveform features.

1.2 CHAPTER OVERVIEW

Chapter 2 – Cardiovascular Disease

Chapter 2 highlights the importance of cardiovascular disease, explaining the motivation behind this research. The causes and mechanisms of CVD: atherosclerosis, hypertension, arterial stiffness, and vascular aging are described to better understand the significance of CVD, how it is caused and how it may be detected using PPG. Current CVD imaging techniques and blood flow measurement devices are described, discussing their advantages, disadvantages and how they relate to each other and photoplethysmography.

Chapter 3 – Photoplethysmography

Chapter 3 introduces photoplethysmography as a technology and a means for blood flow detection and cardiovascular assessment. The physiological principles underpinning PPG are explained to grasp how light can be utilised to detect blood flow. Various aspects of PPG are outlined to provide a holistic understanding including modes of operation, the PPG waveform and feature extraction, the applications, advantages and disadvantages of the technology.

Chapter 4 – Review of Key In Vivo & In Vitro PPG Studies in Cardiovascular Disease

Chapter 4 reviews key PPG investigations from an in vivo and an in vitro perspective. Human studies in peripheral arterial disease and arterial stiffness are described, which form the basis for the in vitro experiment in this project. In vitro experiments are from different topics related to PPG are examined: contact pressure, pulse rate variability, vessel constriction and flow profiles, arterial stiffness and vessel manufacturing.

Chapter 5 – Development of an In Vitro Bilateral Model

Chapter 5 presents the development of a bilateral in vitro model designed to simulate key cardiovascular conditions and support the remaining experiments in this thesis. The components of the system (pump, tubing,

phantoms and sensors) are described, along with the PPG data acquisition and analysis process. A custom feature extraction algorithm was used to process the data, and statistical analysis was carried out to validate the model under varying heart rates, stroke volumes and phantom stiffnesses. Initial results confirmed the system's ability to produce consistent PPG signals, forming the foundation for further studies.

Chapter 6 – Development of Custom Silicone Vessels

Chapter 6 focuses on the development of and testing of custom silicone vessels with adjustable mechanical properties to enhance the in vitro cardiovascular model. The fabrication process using a dip-coating technique is described, alongside mechanical testing for elasticity, hardness and wall thickness. Vessel-tissue phantoms were created and integrated into the flow rig to acquire pulsatile PPG signals, supporting the use of these phantoms for simulating vascular ageing in future experiments.

Chapter 7 – Arterial Stiffness Assessment & PPG Feature Significance Testing

Chapter 7 examines the assessment arterial stiffness using the in vitro rig and custom silicone vessel techniques described in the previous chapter. Vessels with varying elastic properties were tested through morphological PPG feature extraction. Statistical analysis revealed that several features including area, amplitude, and width, significantly correlated with increasing vessel stiffness, demonstrating that PPG signal morphology changes measurably with arterial stiffness.

Chapter 8 – PPG & Vessel Stiffness with Varying Flow Properties Utilising Bilateral Custom Vessels

Chapter 8 investigates how PPG waveforms respond to vessel stiffness under varying flow conditions using a bilateral in vitro setup. Vessel phantoms were assessed simultaneously under identical haemodynamic conditions, enabling controlled comparisons, while flow and heart rate were independently varied. Correlation and regression analysis revealed that the healthy vessel features were more responsive to flow changes than the stiff vessel, providing important considerations for wearable devices.

Chapters 9 & 10 – Discussion & Conclusion

Chapter 9 and Chapter 10 provide the overall discussion and conclusion of the thesis, reflecting on the body of in vitro investigations into PGG for cardiovascular assessment. The chapters synthesis insights from previous experiments, examining how vessel stiffness and flow rate influence PPG waveform morphology and feature behaviour. Broader implications are considered for the design of future PPG systems, including sensor configuration, signal processing and physiological calibration. Limitations of the in vitro approach are acknowledged, alongside open questions and areas for further research. The thesis concludes by highlighting the contribution of this work to understanding the mechanical and optical interactions underlying PPG, and its relevance to the development of non-invasive technologies for cardiovascular monitoring.

2 CARDIOVASCULAR DISEASE

2.1 INTRODUCTION

Cardiovascular disease (CVD) is an umbrella term for conditions affecting the heart and blood vessels (National Health Service, 2017a). CVD is a vital area of research as it is the leading cause of death globally (World Health Organisation, 2021). The World Health Organisation (WHO) recommends we detect CVD as early as possible to reduce the harmful effects and mortality rates. To detect CVD, we must first understand how it develops. Many cardiovascular diseases are caused by atherosclerosis. Atherosclerosis is the build-up of fatty deposits in the walls of the arteries (American Heart Association, 2017). This plaque formation narrows the arteries, restricting blood flow. If a blood clot forms, it can block blood flow, leading to a heart attack or stroke (Stroke Association, 2014).

This project explores photoplethysmography for the assessment of CVD, aiding the detection of arterial stiffness early on before the heart attack or stroke stages through in vitro modelling.

The mechanisms causing CVD are well understood, such as high blood pressure, atherosclerosis and inflammation (Felman, 2019). The relationship of these mechanisms with PPG is an interesting area for investigation. By analysing the PPG wave, we can potentially detect CVD factors non-invasively, with just a fingertip clip-on sensor or even a smartwatch (Saritas et al., 2019).

For PPG technology to reach clinical use for the assessment of CVD, repeated investigations must be carried out to determine how CVD factors are reflected in the PPG wave. Current research involves healthy and unhealthy patients, explored in the review chapter, as well as in vitro cardiovascular models in the following studies.

2.2 CAUSES & MECHANISMS OF CARDIOVASCULAR DISEASE

The causes of cardiovascular disease can vary depending on the specific type. For example, coronary artery disease and peripheral arterial disease are caused by atherosclerosis, plaque build-up in the arteries. When this occurs in the heart vessels, in coronary artery disease, it can lead to an abnormal heart rhythm condition called arrhythmia (CC, 2022a). As such, cardiovascular diseases and causes are interlinked, with certain conditions leading to others, some of which are described in this section.

ATHEROSCLEROSIS

Atherosclerosis is a potentially serious condition where fatty deposits called plaques build up in the arteries, which can lead to other cardiovascular diseases. These plaques cause the arteries to harden and narrow, restricting blood flow and may eventually rupture and trigger a blood clot, shown in FIGURE 2-1 (National Health Service, 2019a). Plaque is made up of fatty substances, cholesterol cellular waste products, calcium and fibrin (JHM, 2022). The thickening and hardening caused by the build-up of these substances directly links atherosclerosis to arterial stiffness. Atherosclerosis can also lead to conditions such as coronary artery disease, peripheral vascular disease and carotid artery stenosis (Asakura and Karino, 1990; Kwak et al., 2014).

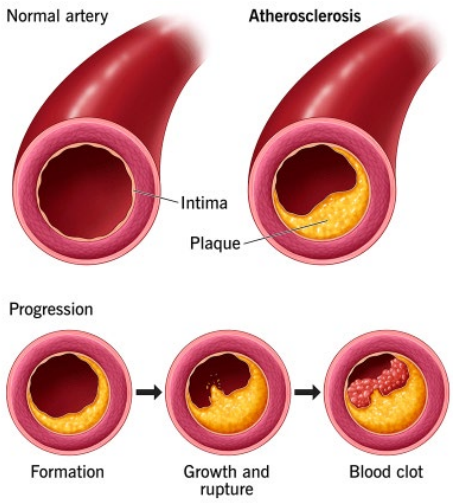

FIGURE 2-1. Atherosclerosis involves the gradual build-up of plaque inside the artery (CC, 2022b).

Hypertension

Hypertension is defined as consistently high blood pressure, and is commonly known as the 'silent killer' because of the damage it causes to your blood vessel walls while not showing any clear symptoms, possibly leading to heart attack or stroke (AHA, 2017; CC, 2021). As a result, around a third of UK adults have high blood pressure, and many will not realise it (National Health Service, 2019b).

Hypertension is associated with other cardiovascular disease risk factors such as smoking, obesity, high cholesterol levels and especially type 2 diabetes. This association increases the risk of vascular complications as well as CVD (Faria et al., 2002; World Health Organisation, 2013).

Arterial Stiffness

Arterial stiffness describes the rigidity of the arterial wall. Stiffening of the arteries occurs as a consequence of aging and atherosclerosis (Cheung, 2010).

Inflammation is a major contributor to arterial stiffness due to its role in atherosclerosis (Mozos et al., 2017). Studies have shown that type 2 diabetes is also a risk factor for functional and structural damage to the arterial wall, resulting in early arterial stiffness (Naka et al., 2012; van der Meer et al., 2007).

Stiffening of the large arteries is the central paradigm for vascular aging, significantly contributing to cardiovascular diseases in older individuals and is associated with hypertension, coronary artery disease, stroke, heart failure and atrial fibrillation (Shirwany and Zou, 2010).

VASCULAR AGING

There is a natural age-related decline in physiological processes in healthy individuals. Vascular aging is associated with changes in the mechanical and structural properties of the vessel wall, leading to the loss of arterial elasticity and reduced arterial compliance (Jani and Rajkumar, 2006). These changes include elastin depletion and fragmentation, as well as collagen deposition.

Studies have related oxidative stress, production of free radicals, and neuroendocrine and genetic changes to vascular aging. These factors acting on myocytes and arteries increases ventricular and vascular stiffness, which is closely related to the cardiovascular aging process, presented in FIGURE 2-2 (Cefalu, 2011).

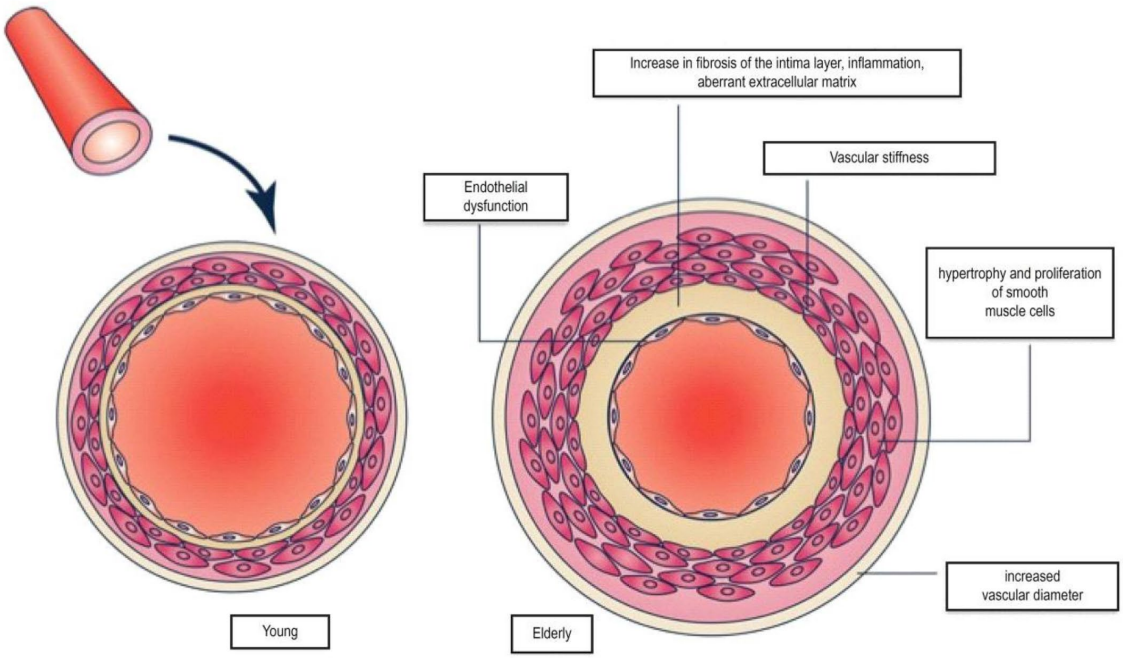

FIGURE 2-2. Pathophysiology of vascular aging (Cefalu, 2011).

2.3 Cardiovascular Monitoring Techniques

Cardiovascular disease assessment involves imaging the heart and blood vessels. This allows healthcare providers to diagnose and manage heart conditions. Many different technologies exist for cardiac imaging exist, each used in different applications with their own and advantages and disadvantages. This chapter describes and discusses some of these techniques and how they are related.

Electrocardiography (ECG)

An electrocardiogram (ECG) is a simple test which records the rhythm, rate and electrical activity of the heart (BHF, 2017a). It is a non-invasive process, but requires placing electrodes, usually on the arms, legs and chest; an example configuration is shown in Figure 2-3. Electrical activity is generated by the heart propagates towards the skin, which can be detected by the electrodes (Farnsworth, 2021).

An advantage of ECG is that it provides information about the contraction of the heart muscles. This allows diagnosis of heart disease and abnormalities such as an irregular heartbeat (Nall, 2022).

As ECG is based on the electrical activity of the heart, not much information is provided about blood flow or pressure. Furthermore, due to the use of electrodes at least two contact points, ECG is typically measured for a specific period of time, such as during rest, bike or treadmill exercise or in an ambulance (National Health Service, 2021). This contrasts with photoplethysmography devices which can measure heart rate and blood oxygen saturation continuously from a single contact point such as the wrist with a smartwatch (Yang et al., 2015).

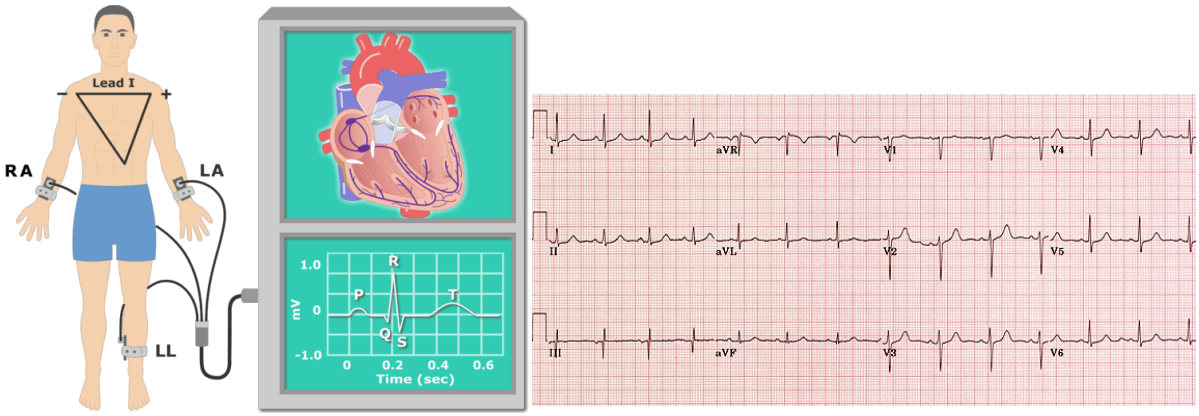

FIGURE 2-3. An electrocardiogram (ECG) configured with three electrodes, showing an ECG wave and a normal 12-lead ECG reading obtained from a ten electrode configuration (Sheffield, 2017; Elentra, 2022).

BLOOD PRESSURE MONITORING

Blood pressure is one of the most widely measured cardiovascular metrics in clinical practice because it is directly linked to cardiovascular risk and long-term outcomes (NICE, 2023). It is routinely assessed in primary care, hospital wards, and during operative monitoring. It is also increasingly measured at home to support hypertension diagnosis and management (Stergiou et al., 2021).

In clinical settings, blood pressure is most commonly measured using an automated oscillometric cuff. The cuff is inflated to temporarily occlude the brachial artery and then gradually deflated while small pulsatile pressure oscillations are recorded, exemplified in FIGURE 2-4 (Sharman et al., 2023). The resulting oscillation envelope is used to estimate mean arterial pressure, and systolic and diastolic pressures are then derived using device-specific algorithms. While this approach is widely adopted due to its practicality, the derived systolic and diastolic values can vary between devices because the underlying decision rules are not standardised across manufacturers (Muntner et al., 2019).

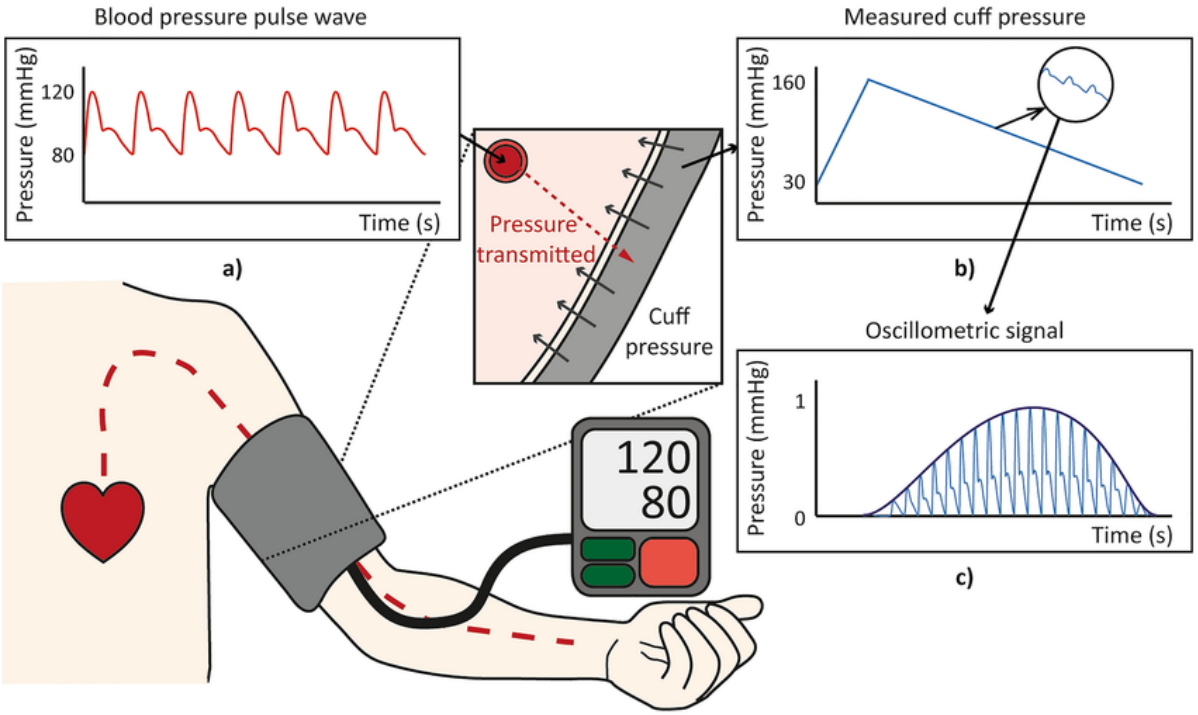

FIGURE 2-4. An oscillometry-based automatic sphygmomanometer. Pulsatile pressure generated by the heart reaches the brachial artery and is transmitted through the upper arm to the cuff. As the cuff inflates then deflates, the device records the cuff pressure and the superimposed oscillations (oscillometric signal) to estimate blood pressure. **a)** Brachial arterial pressure waveform. **b)** Cuff pressure measured by the sphygmomanometer during inflation and deflation. **c)** Oscillometric signal representing cuff pressure oscillations. (Lee et al., 2022a).

APPLANATION TONOMETRY

Alongside cuff-based readings, waveform-based assessment techniques are used to capture the arterial pulse waveform more directly. Applanation tonometry is a non-invasive approach in which a pressure sensor is applied to gently flatten (applanate) a superficial artery (commonly radial or carotid) against an underlying tissue, enabling acquisition of high-fidelity pulsatile pressure waveform for pulse wave analysis, depicted in FIGURE 2-5 (O'Rourke et al., 2001).

Tonometric waveforms are frequently used for arterial stiffness and central haemodynamic assessment, including evaluation of wave reflection and estimation of central aortic pressure (Kwon et al., 2022). Although tonometry measures pressure and PPG measures blood volume changes,

both are shaped by the same underlying arterial pulse and reflected waves. As such, they produce comparable waveform morphologies, such as the systolic upstroke and peak, and the diastolic component, which is linked to wave reflections.

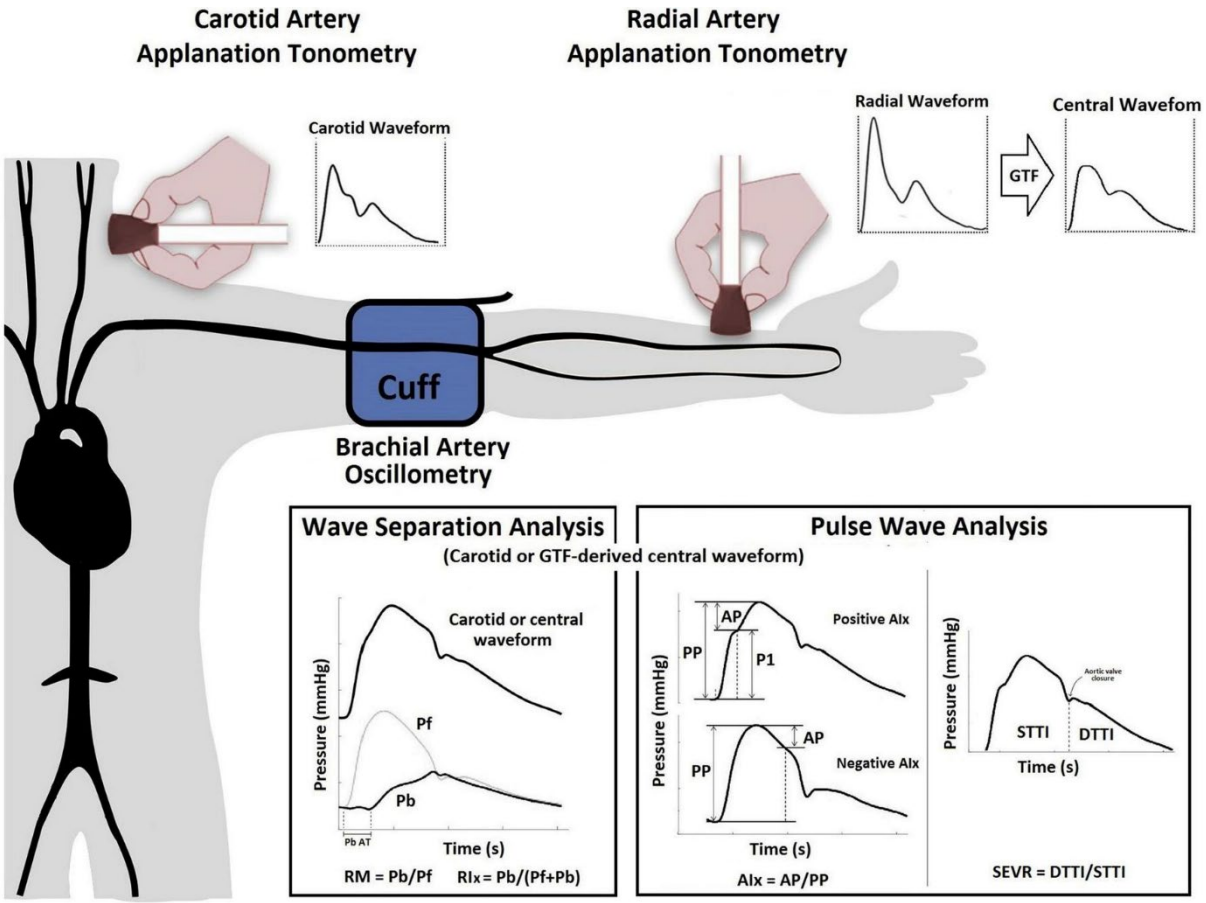

FIGURE 2-5. Use of applanation tonometry at superficial arteries (typically radial or carotid) to record an arterial pressure waveform for pulse wave analysis. The waveform can be used to asses wave reflection and augmentation, supporting arterial stiffness and central haemodynamic assessment, and providing pressure-based morphology comparable to PPG (Pereira et al., 2022).

ECHOCARDIOGRAPHY

An echocardiogram is a type of ultrasound scan, meaning it uses high frequency sound waves to produce an image, shown in FIGURE 2-6 (National Health Service, 2017b). The ultrasound waves are sent out from a handheld probe and travel through the body into the heart. At each boundary, such as between fluid and tissue, some of the sound waves are reflected back to

the transducer (probe), while others continue further (NIBIB, 2016). The speed, direction and distance travelled by the echoes differ from each boundary. This information can be interpreted by a computer to produce a live image (Mayfair, 2020).

Imaging techniques are advantageous as they shows the structures of the heart, such as the muscle or valves, as well as its function (BHF, 2017b). Advancements have led to the development of three-dimensional echocardiography, which offers even more structural and volumetric information (Cheng et al., 2018). Whereas electrocardiography detects the electrical activity which represents the function and rhythm of the heart but does not provide an image showing its structure.

There are innate advantages with this medium – sound waves are harmless and painless, and the probe is non-invasive. Furthermore, processing occurs live for instantaneous imaging. These advantages encourage echocardiography use beyond hospital settings; the handheld probe can be connected to a portable computer, for instantaneous imaging in situations such as emergency ambulatory care (Neskovic et al., 2012).

However, the handheld nature comes with a cost in terms of time and training; physicians and technicians must be well trained in performing and interpreting echocardiograms (Feigenbaum, 1983). Photoplethysmography devices do not require such technical skills, to the point where they are currently used for patient self-monitoring at home, and in smartwatches, where they can monitor blood flow in the background without any user input at all (National Health Service, 2022; D. Han et al., 2019).

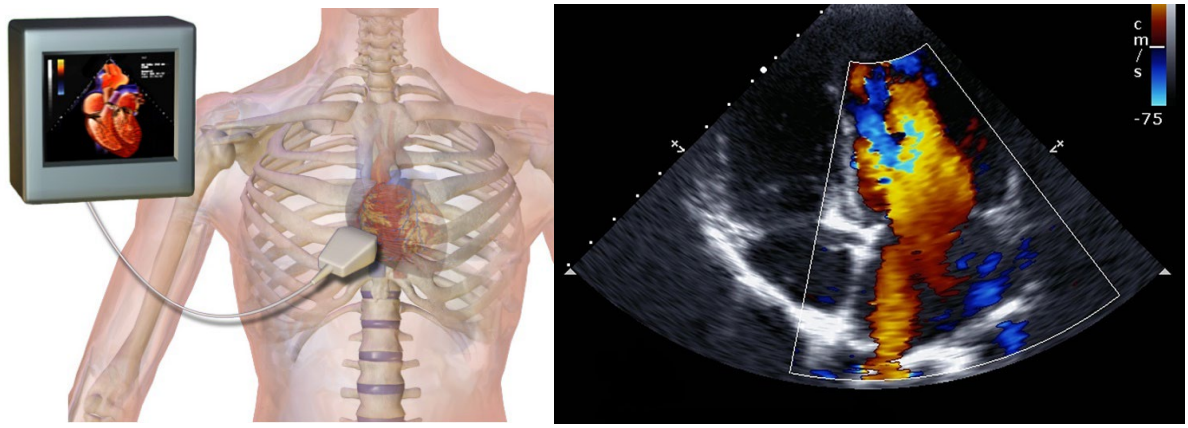

FIGURE 2-6. Echocardiography, a technique using ultrasound to produce scans of the heart (BM, 2017; HPMC, 2015).

MAGNETIC RESONANCE IMAGING (MRI)

Magnetic resonance imaging (MRI) is a type of scan that uses strong magnetic fields and radio waves to produced detailed images of the internal organs, including the heart and blood vessels, seen in FIGURE 2-7 (National Health Service, 2017c). The magnetic fields are produced by powerful cylindrical magnets, with the patient lying inside. They cause the protons in the body to align with that field. With the protons aligned, radiofrequency waves are pulsed through the body, which simulates the protons, causing them to spin out of alignment (NIBIB, 2022a). When the radio waves are turned off, the protons realign with the magnetic field. As they realign, they release their energy as radio waves, which are detected by receiver coils located around the body part being examined (Berger, 2002). The amount of energy released by the protons depends on their type of fluid or tissue, such as muscle, fat or water. These distinct signals are combined to produce detailed images of the inside of the body, called slices, displayed in FIGURE 2-8.

MRI provides detailed images with better contrast between fat, water muscle and other soft tissue than ultrasound, x-ray and computerised tomography (ACR, 2020; FDA, 2017). These images are three dimensional, showing each cross-sectional slice of the body part being scanned, allowing radiologists to see not just inside the body, but inside the organ, such as the brain or heart (Hornak, 1996).

MRI is non-invasive and harmless, not involving any radiation, unlike the following imaging techniques. However, MRI is longer, more expensive and not as immediately available as computerised tomography (Kocak, 2021). Furthermore, not everyone can be scanned with MRI, due to claustrophobia, not being able to fit inside the machine, or incompatible metallic implants (National Health Service, 2017d). The large magnets produce continuous knocking sounds throughout the scan which can reach 110 decibels, the same volume as a rock concert; ear plugs and headphones are used to minimise this (GE, 2019). Combined with the tight space and requirement to stay still for up to 10 minutes at a time, through a total procedure time of up to 90 minutes, makes MRI troublesome for patients with claustrophobia (Chakravorty, 2018; National Health Service, 2018). Again, due to the large magnets, which are strong enough to turn small magnetic objects such as a pen or paperclip into dangerous projectiles, older pacemakers and certain metallic implants are not compatible with MRI (Puiu, 2021; BHF, 2017c).

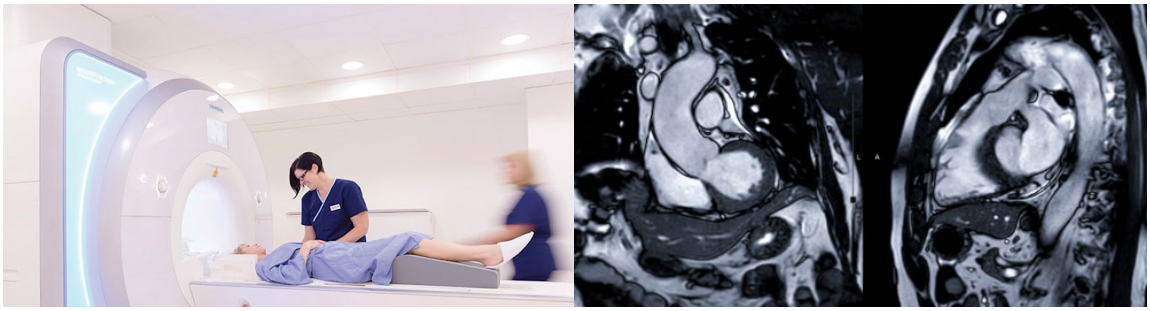

FIGURE 2-7. Magnetic resonance imaging (MRI) machine and scans of the heart (HCA, 2021; VH, 2022).

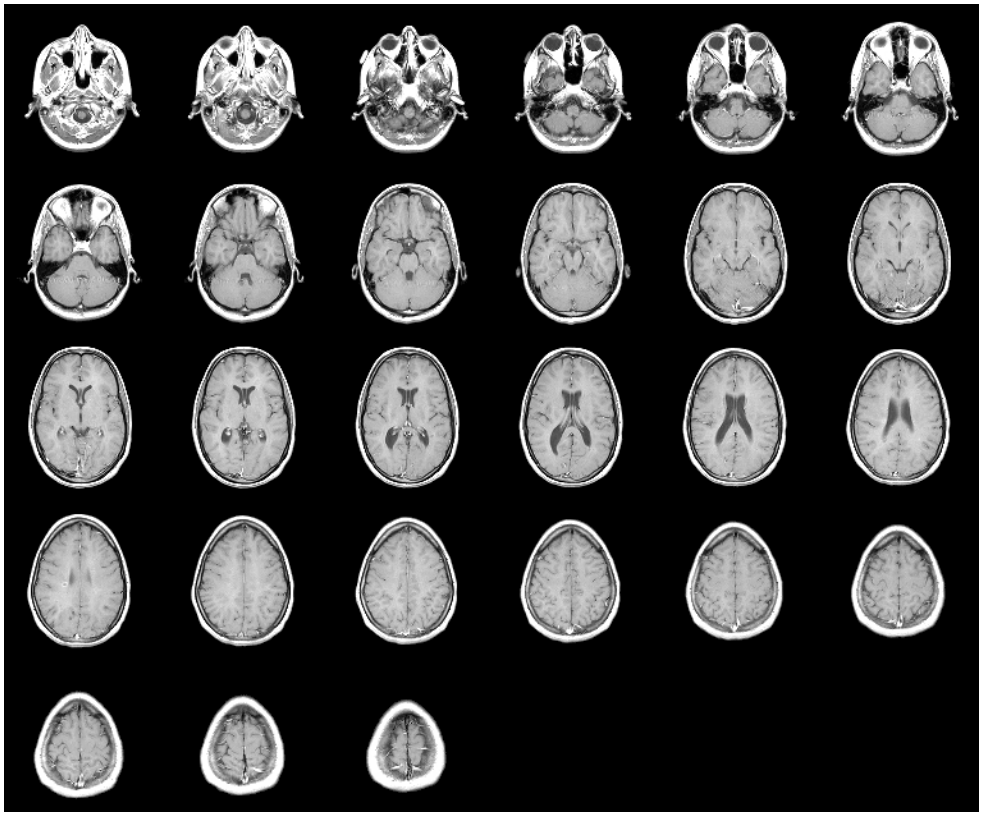

FIGURE 2-8. MRI scan showing multiple horizontal slices of a healthy brain (MW, 2022).

CHEST X-RAY

X-rays are a type of radiation that can pass through the body. As they pass through different parts of the body, such as bones and tissue, different amounts of the x-rays are absorbed (NIBIB, 2022b). In an x-ray scan, they are emitted from a source, pass through the body and reach a detector on the other side, which can be film or digital, where an image is formed, showing contrast depending on the density of the body tissues. Bones and other dense areas show up as white against the black background of the radiograph, while softer tissue such as fat muscle and the lungs appear grey or black, shown in FIGURE 2-9.

Traditional chest x-rays can show the size and outline of the heart and larger vessels – the aorta and pulmonary arteries and veins. This can be used to detect heart failure, aortic aneurysms and calcium deposits (Tsakok and Gleeson, 2018). However, these images are not detailed, with low contrast in soft tissues compared to magnetic resonance imaging (MRI). MRI-like detailed 3D scans can be achieved by taking a series of x-ray images with computerised tomography (CT).

Despite advances in MRI and CT, chest x-rays remain an important tool for initial diagnosis, emergency diagnosis and treatment, and pre-surgery assessment in cardiac patients (Schaefer-Prokop et al., 2008; Tsakok and Gleeson, 2018). These applications are possible because X-ray scans are non-invasive, quick and inexpensive. Initial chest x-ray scans can indicate heart conditions, which are diagnosed with the other CVD assessment techniques (BHF, 2017d).

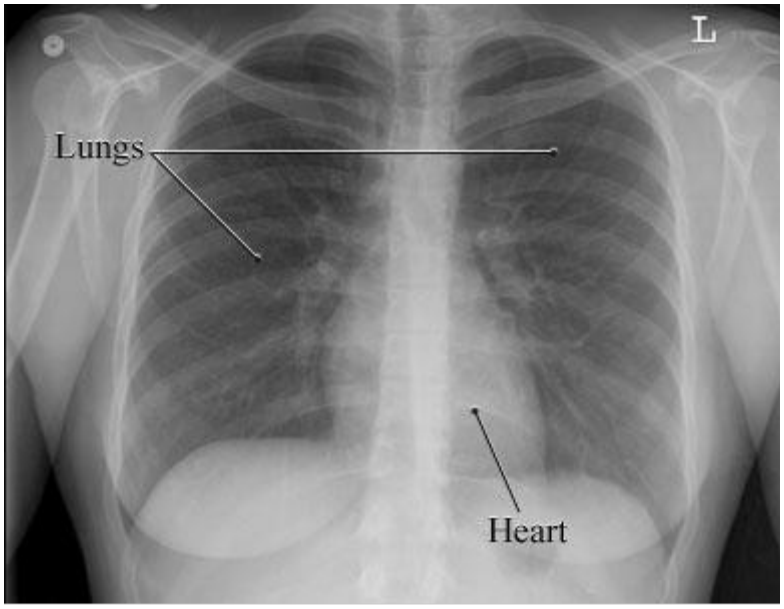

FIGURE 2-9. Chest X-ray showing the lungs and the heart (SVH, 2017).

COMPUTERISED TOMOGRAPHY (CT)

Computerised tomography (CT) uses a series of x-rays from different angles to quickly produce a detailed 3D image of any part of the body, including the bones, muscles, organs and blood vessels. Cardiac CT is routinely performed to detect coronary artery disease and evaluate heart function and pumping volume (Jha, 2021).

The rotating x-ray machine used in CT is non-invasive, however a contrast dye injection is required for cardiac CT to define the blood-tissue interface and improve tissue contrast (Sayyed, 2013). Also, due to the use of multiple x-rays, there is a relatively high dose of ionising radiation from a CT scan compared to other imaging techniques, with a 1 in 2,000 lifetime risk of fatal cancer per scan. This is low compared to the natural incidence of fatal cancer, which is 1 in 5 in the US (FDA, 2018). This means that for any one person, the risk from radiation-induced cancer is much smaller than the natural risk of cancer. This small risk can become a public health concern if large numbers of people undergo medically unnecessary CT screening. Therefore, other imaging techniques are suggested whenever possible, such as ultrasonography and MRI (Schwartz, 2008).

With the advancement of radiation dose reduction strategies and software, in the past decade, CT radiation exposure has reduced significantly, making it less of an issue (Joyce et al., 2020; Rouger, 2022). Benefits of CT include taking detailed 3D images in a short period of time and at a low cost, and accessibility to more patients (Kocak, 2021). CT scans can be performed in 15 minutes, while many magnetic resonance imaging (MRI) scans are over 30 minutes. CT is accessible to more patients, including those with medical implants, prosthesis, or claustrophobia (Rouger, 2022). The advantages and advancements have allowed CT to be an indispensable tool, along with MRI, for imaging of the human body and the heart (Sayyed, 2013).

ANGIOGRAPHY

Angiography is an imaging technique used to visualise the inside of the blood vessels and organs of the body such as the heart. Angiography usually uses x-rays to produce the image, but other imaging technologies such as MRI and CT can be used (SHC, 2017). By visualising the blood flow, angiograms can detect atherosclerosis, peripheral arterial disease, aneurysms and thrombosis (National Health Service, 2020). Contrast agent, also called contrast dye, is injected into the blood stream to reveal the blood vessels in x-rays. They can be also be used to improve contrast in blood vessels or tissues in CT, MRI or ultrasound (UVAH, 2017). Radiographic agents, used in x-ray and CT, work by absorbing the x-rays, which shows up on the x-ray film or CT scanner; as the agent has been injected into the blood vessels or tissues, those areas will be detected (Cluett, 2022).

Coronary angiography is used to visualise the arteries supplying blood to the heart, making it important for the diagnosis of heart conditions such as angina. This method is invasive as it requires cardiac catheterisation, involving a flexible tube threaded through the groin to the heart or coronary arteries (MC, 2022). Invasive angiography remains the gold standard for diagnosing most intravascular pathologies (Omeh and Shlofmitz, 2022).

Angiography achieves real-time, dynamic imaging using traditional x-ray and CT devices, exemplified in FIGURE 2-10, offering therapeutic options at the time of initial diagnosis. Angiography is a versatile technique as it can be applied invasively with catheterisation for, or using minimally invasive contrast agent injections (Omeh and Shlofmitz, 2022). Furthermore, advancements have been made in non-invasive angiography using CT and MRI (Kohsaka and Makaryus, 2008; Estornell Erill, 2004).

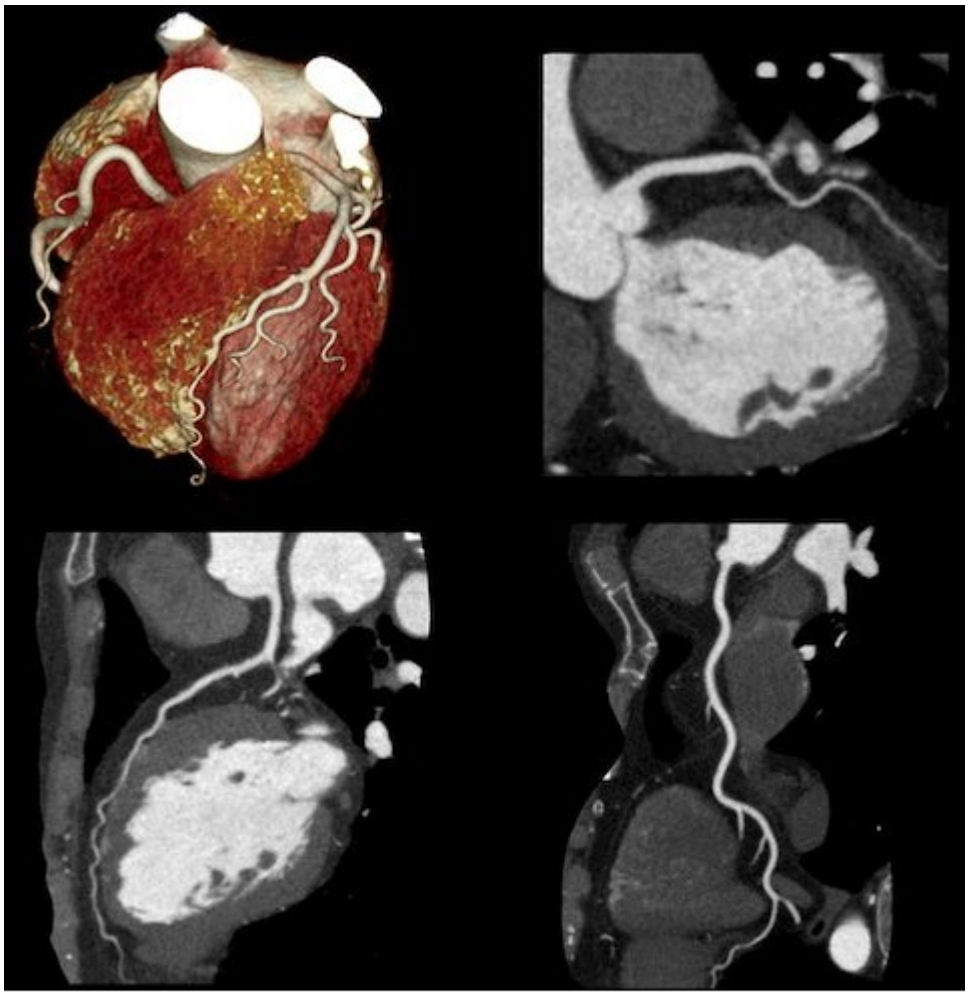

FIGURE 2-10. Cardiac coronary computed tomography angiography (CCTA) exam showing different views of the myocardium and the coronary arteries (ITN, 2020).

2.4 Blood Flow Monitoring Devices

Doppler Ultrasound

Vascular ultrasound is a technique utilising a Doppler probe to send and detect ultrasound waves which undergo Doppler shift, to produce an image of the bodies vessels and calculate blood flow velocity (National Health Service, 2014). Doppler shift is a phenomena which causes the frequency (wavelength) of sound to change when reflected by moving objects, including red blood cells (GSFC, 2020). The difference in frequencies between the emitted and reflected waves is used to calculate the velocity of blood (ESP, 2018). Combined with the differences in speed, direction and distance travelled by the echoes from each tissue boundary, such as the blood and vessel walls, this information can be interpreted to produce a live image of the blood vessels, shown in Figure 2-11 (Aldrich, 2007).

Ultrasonic blood flow meters are non-invasive as they use sound waves which are naturally harmless and painless (SMIL, 2022). Another advantage is that they produce a continuous, real-time image feed, allowing for instantaneous blood flow measurement. Although they can be connected to a portable computer, allowing for monitoring outside of hospitals, they must be operated by trained physicians. This is a key area where photoplethysmography devices have an advantage as they can be used by patients for self-monitoring, and can monitor blood flow continuously throughout the day without user input (National Health Service, 2022; D. Han et al., 2019).

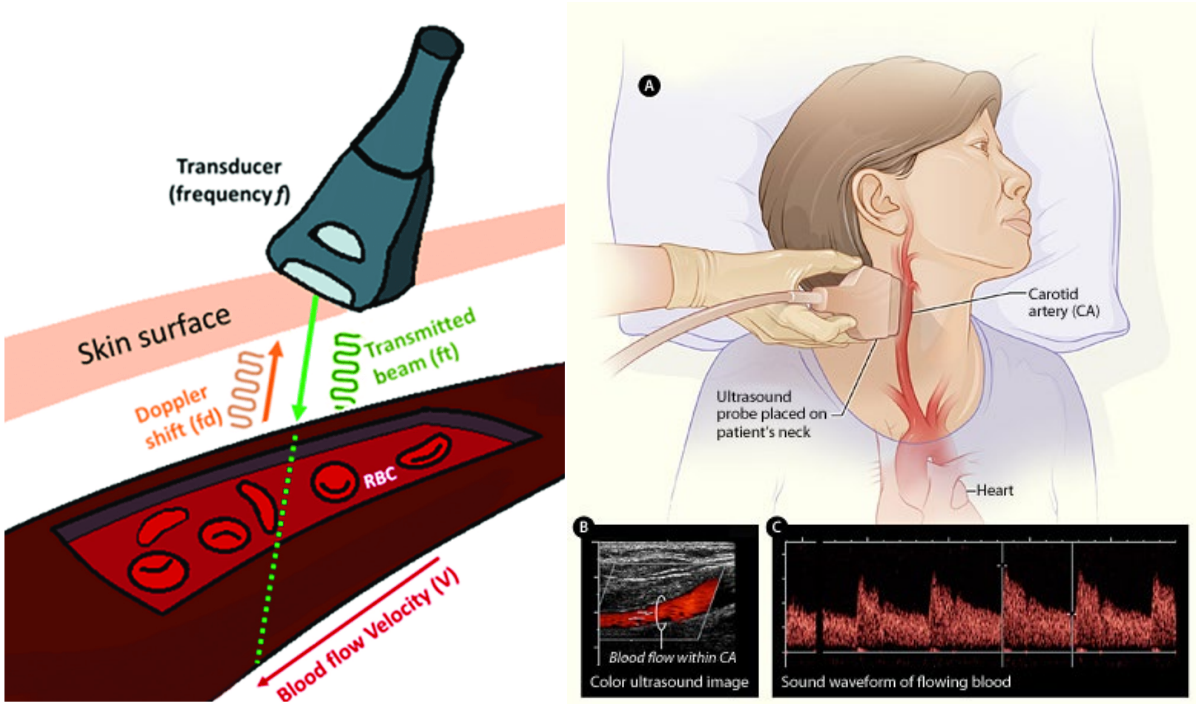

FIGURE 2-11. Ultrasound transducer utilising the Doppler shift from moving red blood cells to measure blood flow velocity (Baratchi et al., 2019). The differences in the echoes from different tissue boundaries are used to produce images of the blood vessels. Applied on a patient, this allows for imaging and blood flow measurement of the carotid artery (NHLBI, 2013).

LASER Doppler Flowmetry (LDF)

Laser Doppler flowmetry (LDF) is a blood flow measurement technique utilising laser light which undergoes Doppler shift (Micheels et al., 1984). This allows for the measurement of blood perfusion as well as relative velocity (Riva et al., 1992). With the combination of light in the form of lasers and the Doppler effect, LDF can be seen as a bridge between photoplethysmography and Doppler ultrasound. Like both of these techniques, LDF is non-invasive and continuous, using a probe placed over an area of interest, such as the brain (Pouratian and Toga, 2002).

A beam of low power laser light is led by an optical fibre to a probe head, from which it is emitted into the tissue, where it hits the flowing red blood cells within the tissue vessels and reflects back. The motion of the blood cells causes a Doppler shift in the reflected light. The surrounding tissue

also reflects the light but in an unshifted manner as there is no movement, depicted in FIGURE 2-12 (Micheels et al., 1984).

Laser doppler flowmetry is used for reliable, real-time microcirculation and perfusion diagnostics, like photoplethysmography, in experimental studies such as patients with burns, hypothermia or shock (Stoyneva, 2012; Micheels et al., 1984). The similarity between LDF and PPG extends to their advantages as well as disadvantages. Being light-based, both modalities provide continuous, non-invasive, and real-time measurement capabilities but are also susceptible to motion artefacts. These devices cannot be calibrated in absolute units, instead using relative, arbitrary units, producing an output which is not linearly related to blood flow rate (Matthews and Vongsavan, 1993). For example, if the output signal increases by 100%, this does not mean that the blood flow rate has increased by 100%.

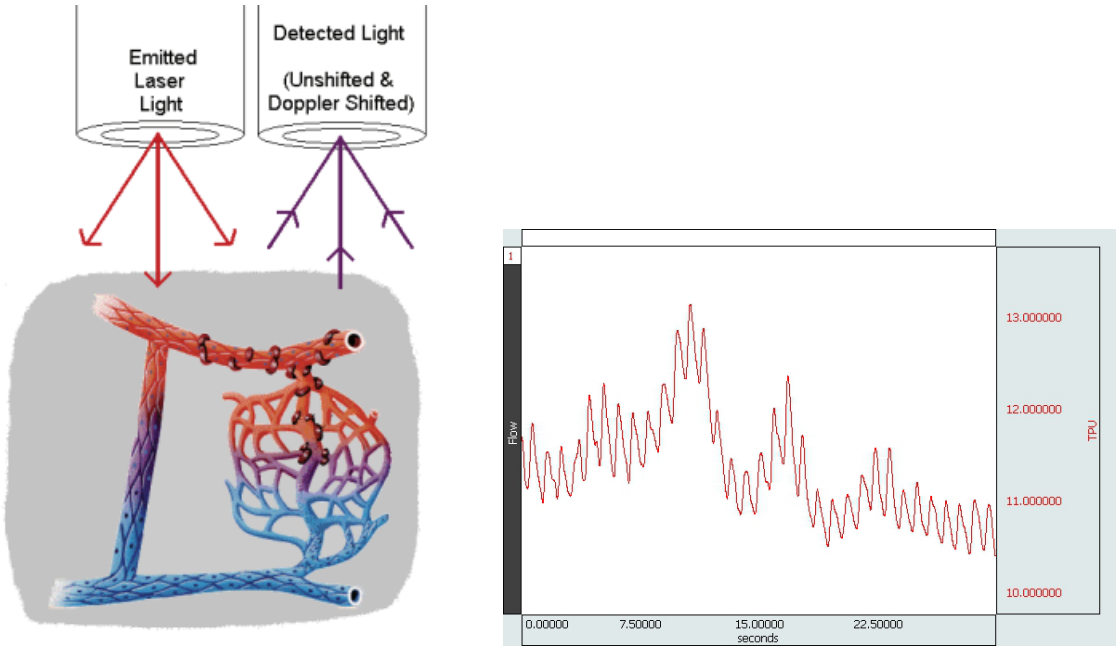

FIGURE 2-12. Excitation and detection of blood vessels with laser doppler flowmetry, producing an example of microvascular data (BIOPAC, 2021).

Electromagnetic Blood Flow Meters

Electromagnetic blood flow meters use the laws of electromagnetic induction to measure blood flow in blood vessels throughout the circulatory system (Scott and Sandler, 1978). Faraday's law of electromagnetic induction states that when a conductor is moved at a right angle both to the magnetic field and it's length, and electromotive force (EMF) is induced in the conductor (Sadiku, 2001). External coils generate the magnetic field and non-contact electrodes measure the electromotive force, displayed in Figure 2-13.

Predominately used in research in experiments such as blood flow profile studies, electromagnetic blood flow meters can also clinically measure blood flow invasively or non-invasively to diagnose flow related problems and during surgery (Scott and Sandler, 1978; Teferra, 2017).

Electromagnetic flow meters are able to measure blood flow rate in ml/min with high accuracy and precision. As a benchmark for blood flow measurement, they are used to calibrate other blood flow meters (Zouridakis, 2003). They also have a rapid response to blood flow changes, meaning that sudden changes in flow velocity can also be measured (Folts, 1974). As these devices are based on Faraday's law, they wrap around the vessel, which can be invasive or non-invasive. This is not required in photoplethysmography, which measures from a single contact point, allowing for wider applications.

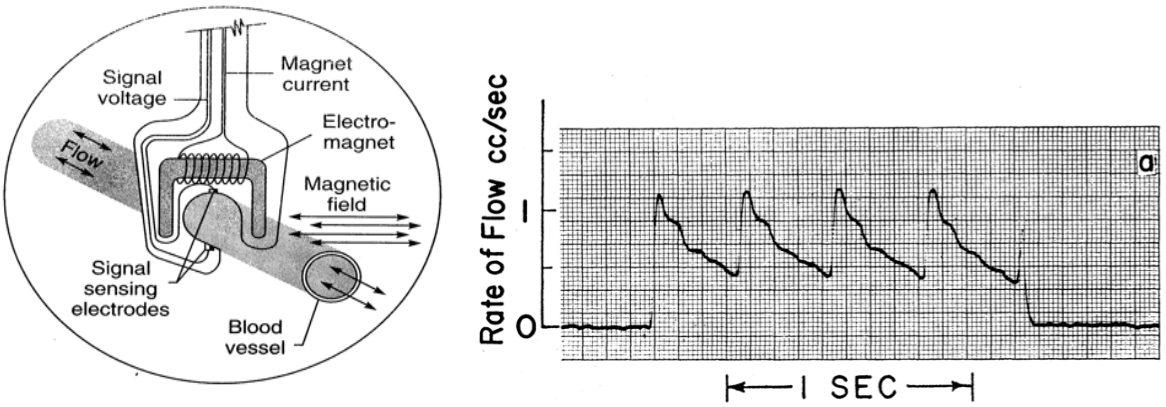

FIGURE 2-13. Electromagnetic blood flow meter device and recordings (Electricalvoice, 2017; Kolin, 1959).

IMPEDANCE PHOTOPLETHYSMOGRAPHY (IPG)

Impedance plethysmography (IPG) is a non-invasive technique used to measure blood volume changes through variations in electrical impedance. A small alternating current is passed through the tissue using surface electrodes, and the resulting voltage is measured to determine impedance. As blood volume within the measured segment changes during the cardiac cycle, the electrical impedance also changes, producing a pulsatile waveform (Thomson and Jung, 2025).

This allows IPG to be used for the assessment of peripheral blood flow and vascular function. Unlike PPG, which relies on optical absorption, IPG is based on the electrical properties of blood and tissue. However, both techniques are used to detect pulsatile volume-related changes, making IPG a useful electrical analogue when considering non-invasive monitoring methods (Liu et al., 2017).

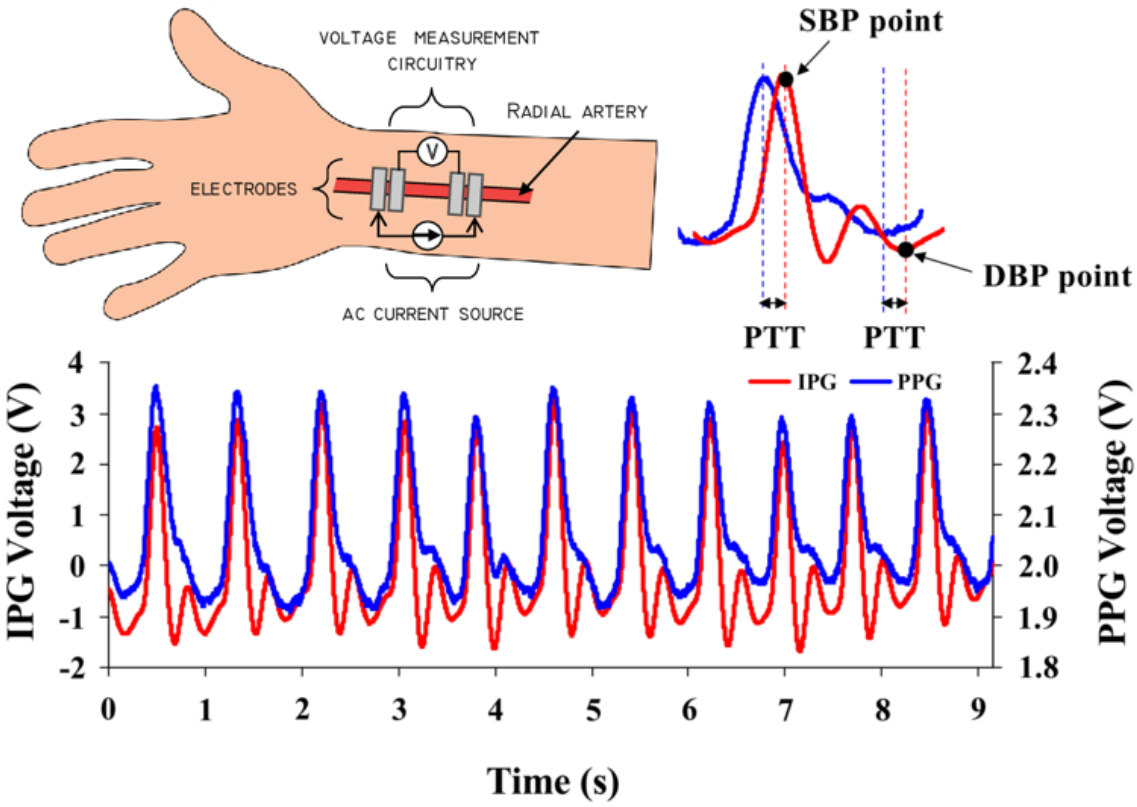

FIGURE 2-14. Synchronous impedance plethysmography (IPG) waveform measurement at the radial artery region. Surface electrodes are placed on the wrist and a small alternating current is applied to detect pulsatile changes in electrical impedance associated with blood volume changed during the cardiac cycle. The recorded IPG waveform shows characteristic pulse features that can be used for vascular assessment and blood pressure-related feature analysis, with waveform morphology comparable to PPG (de Pinho Ferreira et al., 2020a; Wang et al., 2020).

Impedance Cardiography

A related impedance-based technique is impedance cardiography, in which thoracic impedance changes are measured to estimate stroke volume and cardiac output non-invasively. Small surface electrodes are placed on the neck and lower thorax and during systole, the impedance signal changes as blood is ejected into the great vessels, allowing beat-to-beat haemodynamic patterns to be derived (Mansouri et al., 2018).

Although it does not replace invasive reference methods in all clinical settings, impedance cardiography has been widely used as a practical non-invasive approach for monitoring cardiac output trends (Nguyen and Squara, 2017). Its main advantages are that it is continuous, relatively simple to apply, and does not require arterial catheterisation, making it attractive for haemodynamic monitoring where a less invasive method is preferred (Cybulski, 2011).

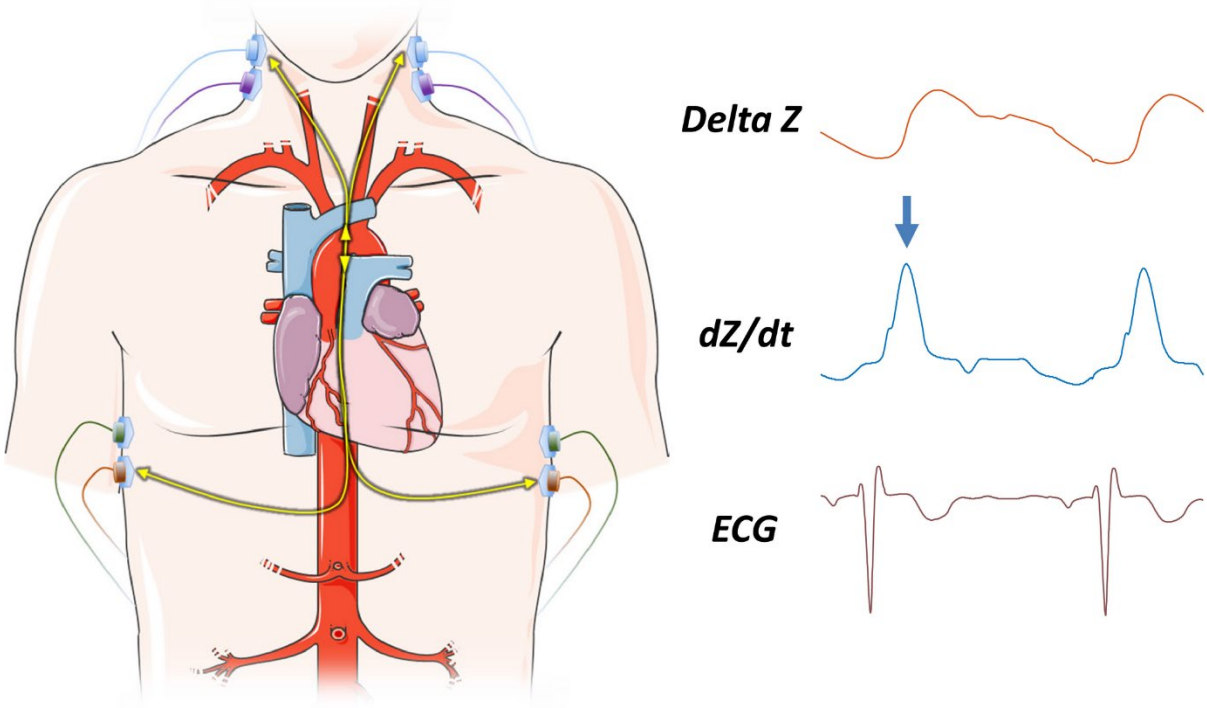

Figure 2-15. Impedance cardiography setup showing thoracic electrode placement and example signals. Changes in thoracic electrical impedance during the cardiac cycle produce a pulsatile waveform that can be analysed alongside the electrocardiogram (ECG) to assess cardiac timing and estimate haemodynamic

parameters such as stroke volume and cardiac output (Medina-Lezama et al., 2018).

PHOTOPLETHYSMOGRAPHY

Photoplethysmography (PPG), a light-based, non-invasive, real-time technique is the chosen blood flow monitoring modality in this study for cardiovascular disease assessment. Other advantages of PPG are its inexpensive, compact sensor design with a single contact point for continuous measurement. The next chapter provides an overview discussing the physiology behind PPG, its applications, advantages, and disadvantages.

2.5 SUMMARY

This chapter presents on overview of cardiovascular disease (CVD), detailing its primary causes and mechanisms including atherosclerosis, hypertension, arterial stiffness, and vascular ageing. Establishing techniques used for CVD assessment are reviewed, such as electrocardiography (ECG), echocardiography, magnetic resonance imaging (MRI), chest X-ray, computerised tomography (CT), and angiography, discussing their principles, applications, advantages, and limitations.

Additionally, the chapter examines blood flow measurement devices including Doppler ultrasound, laser Doppler flowmetry, electromagnetic blood flow meters, and photoplethysmography (PPG). Emphasis is placed on PPG's non-invasive, continuous monitoring capabilities and its suitability for cardiovascular assessment, highlighting its potential over other modalities in terms of simplicity, cost and user accessibility. This foundation establishes the context for the thesis focus on PPG as a tool for early detection and monitoring of CVD.

3 PHOTOPLETHYSMOGRAPHY

3.1 INTRODUCTION

In the previous chapter, the cardiovascular system was outlined, as well as diseases and assessment techniques related to it. Photoplethysmography (PPG) is the primary technique to be utilised in this investigation of cardiovascular disease biomarkers.

PPG is an established optical sensing technology commonly used for blood oxygen level and heart -rate measurements in healthcare and wearable devices, with a huge potential for cardiovascular health assessment.

First, let us delve into the physiological principles underpinning PPG, what makes it an effective and attractive technology and how it is used in routine clinical practice.

The human body is commonly considered to be opaque, although transmission of light through the skin can be observed, for example, by placing the finger on a mobile phone flashlight. As blood flows through the finger, slight variations in the amount of transmitted light occur, invisible to the naked eye. This phenomenon is the basis for PPG. The word photoplethysmography originates from the Greek words photo (meaning light), plethysmos (increasing, filling up) and graph (to write). As such, PPG is an optical technique, harnessing the power of light to non-invasively measure the volume changes in the blood vessels (Elgendi et al., 2019).

Devices utilising PPG can be placed on various body sites such as the fingertip, wrist and ears. A typical PPG device consists of two main components: a light source, such as an LED, to illuminate the tissue at the body site, and a photodetector to measure the reflected light (Castaneda et al., 2018). Change in the amount of light reflected is proportional to blood volume variations (Wang et al., 2013). These variations in blood volume are represented in a photoplethysmograph, FIGURE 3-1, indicating

the change in blood volume over time as the heart cycles through the systolic and diastolic phases.

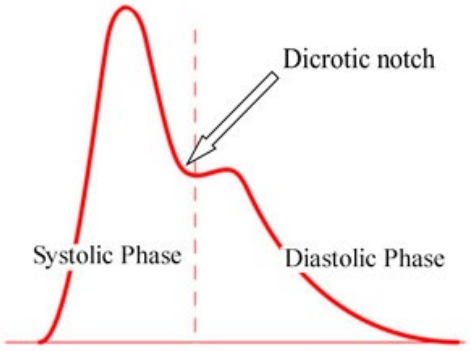

FIGURE 3-1. Cycle of a normal PPG waveform, divided into the systolic and diastolic phases of the cardiac cycle (Nara et al., 2014).

3.2 PRINCIPLES & PHYSIOLOGY

TRANSMISSION & REFLECTANCE MODES

PPG devices can be placed on different parts of the body including the forehead, arm, wrist, finger and toe as seen in FIGURE 3-5A, to obtain various types of physiological information (Hartmann et al., 2019). Depending on the body site, the sensor will operate in either transmission or reflectance mode.

Transmission mode requires light to pass through the body part, so it is used at smaller extremities such as the finger, toe and ear lobe. In transmission mode, light from the LEDs, usually red and infrared, passes through the body part, where it's detected by the photodetector on the other side (Přibil et al., 2020).

Reflectance mode can be used at other body sites, where a photodetector would not work on the other side as light cannot reach, as with the forehead, arm and wrist. In reflectance mode, light from the LEDs, usually red or green, enters the tissue and reflects into the photodetector (Sviridova et al., 2018). With reflectance mode, PPG measurements can be taken from virtually any part of the body. However, the physiological information received is dependent on the tissue depth that the light can

reach. This distance can be set depending on the LED colour used and its separation distance with the photodetector (Nomoni et al., 2019).

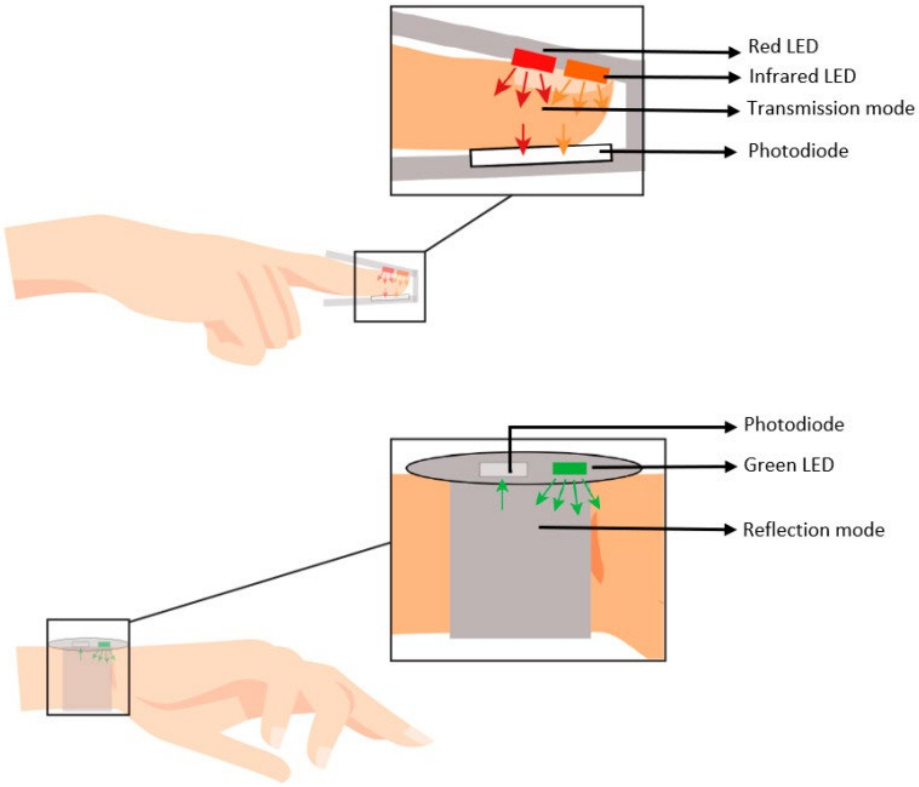

FIGURE 3-2. PPG devices shown in transmission and reflectance mode (Almarshad et al., 2022).

OPTICAL PATHWAYS & LIGHT-TISSUE INTERACTIONS IN SKIN

Light is the fundamental element of PPG used to illuminate skin under the sensor for blood flow measurements. These optical interactions with the skin and tissue contribute to the non-pulsatile component of the PPG signal (Njoum, 2017). Reviewing the light-tissue interactions helps to further understand how PPG devices work, which allows for more reliable and specific sensor designs for certain applications.

Skin has a complex structure of multiple layers consisting of different cells and fibres, with vessel and capillary networks embedded (Yousef et al., 2022). As light from the sensor traverses the skin, it interacts with each layer differently, creating multiple optical pathways. For this model, the cellular level is assumed to be homogenous, only considering the different properties between layers (Krishnaswamy and Baranoski, 2004). This

allows us to estimate the optical properties of each layer of skin. Furthermore, we consider absorption and scattering to be uniformly distributed across skin layers (Nielsen et al., 2008).

Longer wavelengths of light penetrate deeper into the skin, shown in FIGURE 3-3 (Clement et al., 2005). Shorter wavelengths carry more energy, making them more reactive with the skin, preventing them from reaching as far. This effect is like electromagnetic waves in the non-visible spectrum, which are ionising and do not travel far due to their high energy and frequency, and low wavelength (D'Orazio et al., 2013).

Starting at the surface of the skin, the stratus corneum, some of the incident light is reflected and scattered. In the deeper layers of the epidermis and dermis, subsurface light is scattered, reflected and absorbed by pigments such as melanin and haemoglobin (Lee et al., 2018). These interactions are depicted in FIGURE 3-3. Below the skin surface, in the epidermis, the natural chromophore melanin is mostly responsible for the absorption properties (Njoum, 2017). As such, absorption levels vary between individuals, depending on skin tone.

The dermis is an opaque layer with a lower melanin content. It is primarily composed of dense, irregular connective tissue with varying sizes of nerves and blood vessels (Sandell and Zhu, 2011). Due to its vast network of collagen fibres, a significant amount of scattering takes place, described as multiple scattering.

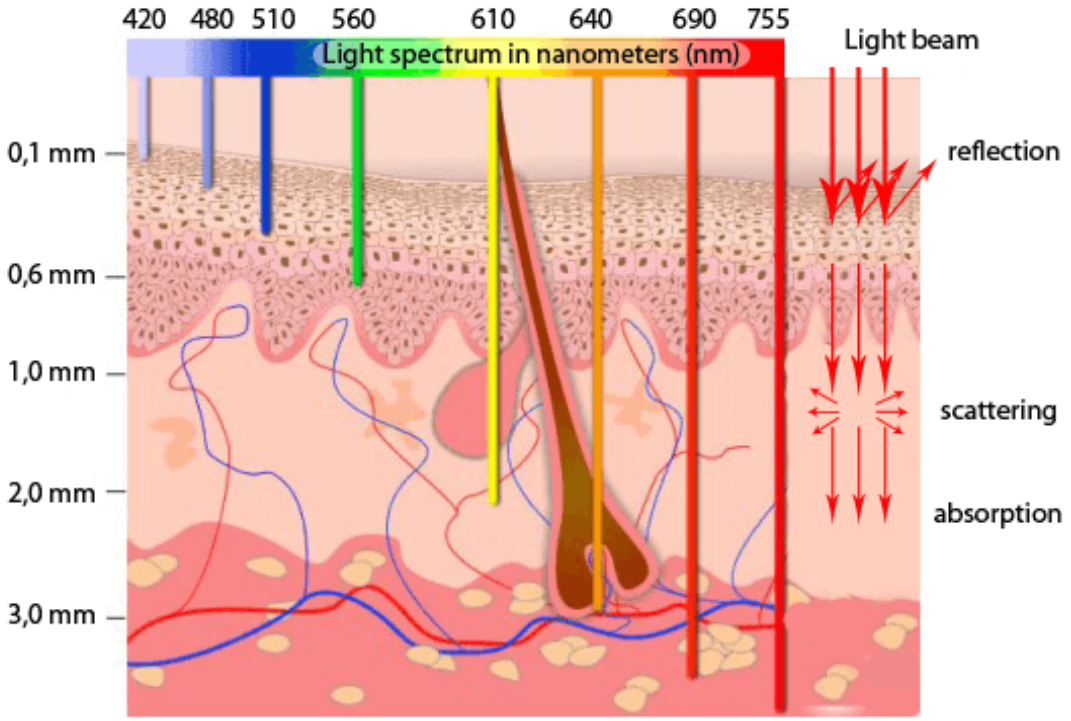

FIGURE 3-3. Propagation of light of different wavelengths in layers of the skin (GBS, 2015).

ORIGIN

Although PPG is a widely used and advantageous technology, origin of its waveform has still not been completely confirmed. It is a subject of debate, with different hypotheses currently being tested (Chatterjee et al., 2020). Key factors affecting PPG have been identified including blood volume, blood vessel wall movement and orientation of red blood cells (Aoyagi, 2003; Daly and Leahy, 2013; Nitzan et al., 2013). It is widely accepted that PPG provides a recording of the pulsatile changes in the microvascular bed of tissue (Njoum, 2017).

WAVELENGTH

When designing a PPG sensor, considering the optical pathways helps determine the ideal LEDs to use for the application. We have seen that longer wavelengths have deeper penetration and shorter wavelengths are absorbed near the surface. The most commonly used wavelengths in PPG sensors are red and infrared, usually used in combination in blood flow sensors, and green light, used in fitness devices such as smart watches.

Red and infrared light are on the longer wavelength end of the spectrum, capable of reaching deeper into the tissue where the blood vessels reside. This makes it possible to retrieve physiological information from blood flow and produce better PPG signals. As such, red and infrared light are commonly used in pulse oximetry devices and other PPG applications (Nitzan et al., 2014).

Green light has been used in fitness wearables, such as Apple Watch, Fitbit and Garmin, despite the better signal quality and blood flow information retrieved from red and infrared ("Red light, green light," 2017). One reason for this is that green light performs better during motion, making it useful for wearables which are worn during exercise and daily activities (Lee et al., 2013). This contrasts with a clinical setting where a pulse oximeter is clipped onto a patient's finger while they are still. However, some companies have avoided green light even for fitness wearables, suggesting that 'the future is red' (BSX Technologies, 2016). Furthermore, green light has been found to not be effective with all skin tones (Fine et al., 2021). It is difficult to make a conclusion as this area of research is still undergoing, with another study finding that green light PPG had greater resolution regardless of skin type (Fallow et al., 2013).

Waveform

Two main components make up the PPG waveform: the pulsatile AC component and a steady, non-pulsating DC component, displayed in Figure 3-4a. The AC component is synchronised with the heartbeat and related to the blood pulse in the arteries. While the DC component relates to light absorption in the tissues and veins, which are naturally non-pulsating (Lee et al., 2011). In many applications, the DC component is filtered out using a low-pass filter (as the steady part is low frequency), to analyse the pulsatile AC component (Lao et al., 2012). This is done by feature analysis, described in the next section. The AC component is analysed for patterns in a technique called feature extraction, described in the following sections.

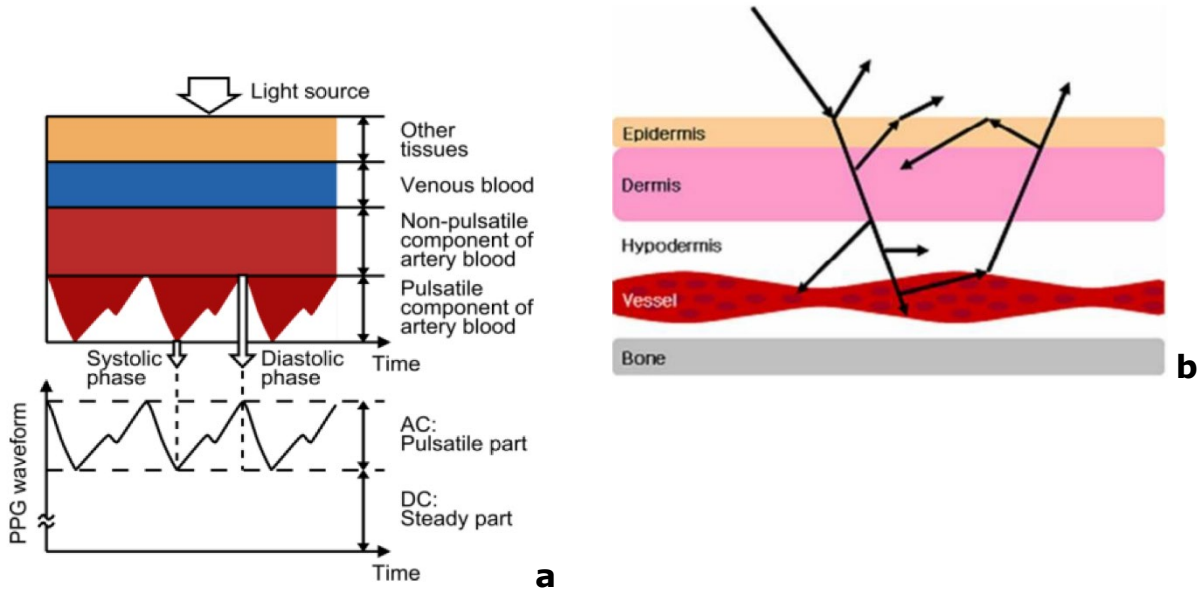

FIGURE 3-4. a) PPG waveform divided into pulsatile AC and steady, non-pulsating DC components. Variation in attenuation of light through arterial blood causes the AC component, which is synchronised with the heartbeat. The DC component relates to the tissue and veins which are non-pulsating by nature (Tamura et al., 2014). **b) Absorption and diffusion of light in the body tissues and blood vessels, the physiological phenomenon which enables PPG** (Reguig, 2016).

FEATURES

PPG signals carry valuable information about the human body, cardiovascular health and blood flow that can be used for the screening and diagnosis of diseases. Feature extraction is a method for analysing PPG waves to determine if they can indicate these conditions, such as arterial stiffness (Park et al., 2022).

The approach for feature extraction involves analysing each cycle of the PPG wave and calculating shape characteristics such as amplitude, width, and area under the curve. These features can be time-based such as rise time and pulse width, amplitude related as in systolic peak amplitude, or geometric which are based on slopes and angles such as upslope and downslope, shown in FIGURE 3-5 (May et al., 2021).

Further analysis can be done by computing the rate of change of the PPG signal to produce first and second derivatives, respectively called velocity

PPG (VPG) and acceleration PPG (APG). Extracting features from these time-based transformations reveals more valuable information than only analysing the original signal, specifically the second derivative which contains further features and reflects the acceleration of blood flow (Elgendi, 2020).

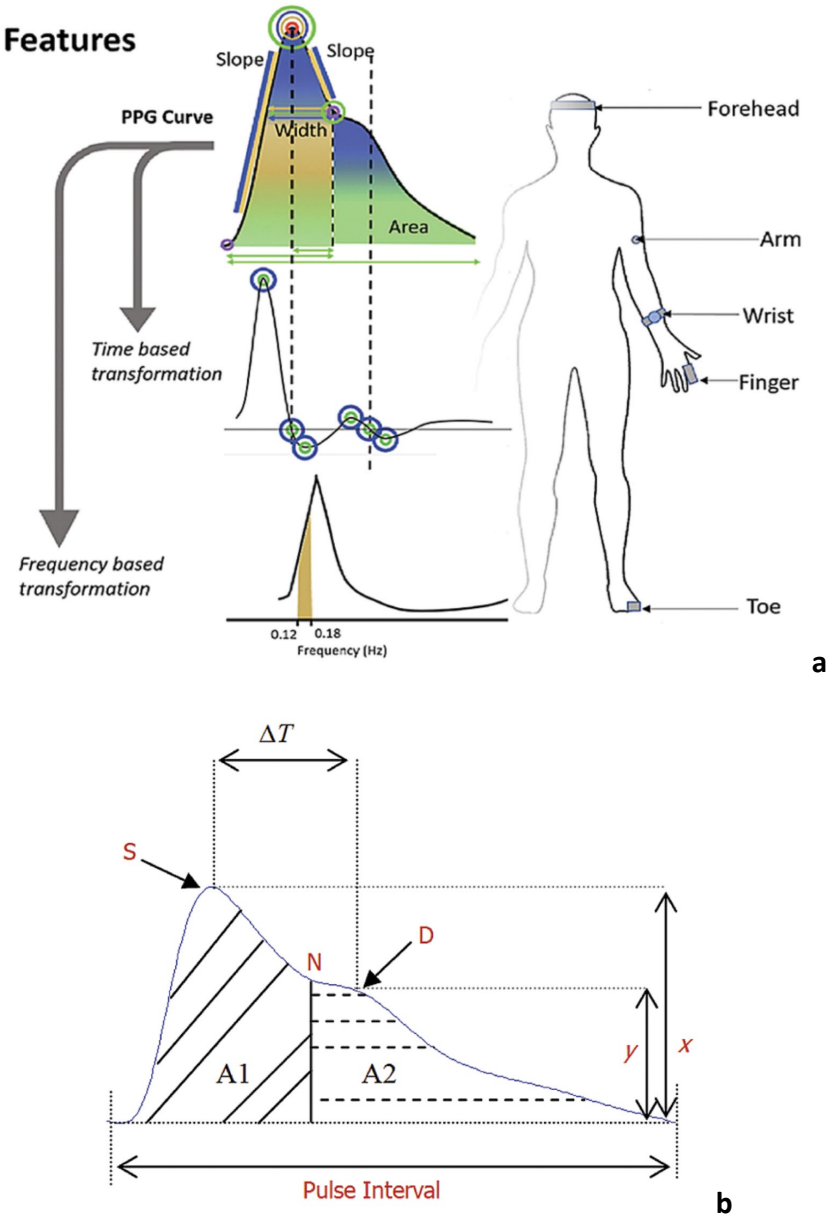

FIGURE 3-5. a) PPG feature extraction through it's derivative (time-based transformation) and frequency-based transformations. Fingertip PPG features have been most widely used and validated (Elgendi, 2020). **b) Features of a PPG curve**. **S** systolic peak, **D** diastolic peak, **N** dicrotic notch, x systolic amplitude, y diastolic amplitude, **ΔT** systolic-diastolic peak-to-peak, **A1** and **A2**

pulse area, split into systolic and diastolic areas by dividing at the dicrotic notch (Elgendi, 2020).

3.3 ADVANTAGES

PPG technology has many advantages which have allowed it to become widely used in medical and consumer devices such as pulse oximeters and smartwatches, including non-invasive measurement, low cost, simple design leading to compact and portable devices. These applications will be covered in the following chapters, after looking at the advantages that have allowed PPG to become popular and the current limitations of the technology.

NON-INVASIVE

As PPG is a light-based technique, it can be used non-invasively. Both modes of operation, transmittance and reflectance, allow for blood flow measurement at various sites of the body such as the finger, wrist and forehead. The light from the LED simply enters then exits the tissue, either by transmission or reflectance, and reaches the detector. This takes place with the device resting at the surface of the skin – using only light, there is no need to insert any probes into the skin.

The non-invasive nature of PPG has led to it becoming routinely used for pulse oximetry measurements and common in fitness devices. It is a convenient way of making blood oxygen and heart rate measurements as only a single sensor is required, which can be easily placed at a favourable location such as the finger or wrist. This is comfortable for the patient and consumer, leading to PPG devices being used with all ages, including new-borns and elderly, as well as smartwatches for children and adults (Brown et al., 2020; Van Son and Eti, 2021).

Although the majority of PPG applications are non-invasive, there have been invasive applications such as measurements from the oesophagus, showing the wide potential of applications for PPG in different areas (Kyriacou, 2006; Kyriacou et al., 2001; Phillips et al., 2011).

Low Cost

The low cost of PPG devices has also aided its widespread use in hospitals, clinics and homes. For example, pulse oximeters were given to COVID-19 patients to self-monitor their progress from home (NHS, 2020).

Pulse oximeters, utilising PPG, are also commonly used in hospitals and routine clinics for oxygen saturation and heart rate measurement, where they can be simple clip-on devices or also incorporated into other devices such as cardiac monitors (Medtronic, 2016).

Simplicity and low cost have allowed PPG to become ubiquitous in consumer wearables. In 2018, Henriksen et al identified 423 unique wrist-worn wearables from 132 different brands. Out of these, PPG was the most common sensor, with 71% of new devices including a PPG sensor (Henriksen et al., 2018).

As PPG technology and algorithms improve, for example motion artefact reduction using the gyroscopes already present in wearables, it will be included in more upcoming devices (Casson et al., 2016).

Simple & Portable

As well as low cost, simple components and circuit requirements have allowed PPG sensors to become extremely portable and compact. Only two basic electrical components are needed to build a PG sensor: an LED and a photodetector (Scardulla et al., 2023). Both parts are inexpensive and can be miniaturised. As such, we have seen portable applications of PPG in smartwatches, fitness bands and clip-on pulse oximeters (Castaneda et al., 2018).

PPG is not limited to hospital or clinical use – these devices are able to take PPG measurements throughout the day, including during physical activity, adding to the convenience of PPG and encouraging home monitoring. Many new wrist-worn wearables have included a PPG sensor due to its compact nature as well as the low cost, making it easy to incorporate (Kim and Baek, 2023).

Compact

Smartwatches are far from the smallest PPG devices. The Oura is a commercially available ring which measures blood oxygen during activity and sleep using PPG (Cao et al., 2022).

As technology advances and components become even smaller, more devices are expected to include PPG, such as upcoming sports earphones, which also can be used for non-invasive blood pressure assessment (Apple, 2020; Xing et al., 2021).

PPG sensors have also been built in the form of optical fibres for assessment in the human oesophagus as well as spinal cord tissue in rats (Phillips et al., 2011, 2013; Davenport et al., 2017).

Single-spot Measurement

Most of the devices mentioned, including smart watches, earphones and rings, only require a single contact point to take PPG measurements (Sun and Thakor, 2016). Single-point recording allows the continuous daily PPG measurements accomplished by these devices, often in the background without any discomfort or engagement with the user. Electrocardiography (ECG), in contrast, detects heart activity using at least two electrodes, and usually requires a third reference electrode attached to the leg (Hsieh et al., 2019). The multiple electrode ECG setup is useful for assessment, but not practical for continuous daily recordings.

Advancements in wearable technology have made it possible to take ECG recordings with a smartwatch by placing a finger on the watch button, but this still requires two contact points, with first being the watch itself on the wrist, for Lead I ECG recordings (Spaccarotella et al., 2021). This is more practical for general daily use than electrodes, but still limited to finite measurement at specified times, as the finger must be kept on the watch during the recording. In terms of convenience and portability, PPG sensors therefore have an advantage, allowing them to be used for daily heart rate and blood oxygen measurements.

Multi-site Measurement

Single-site PPG is convenient, but there is also the option of multi-site PPG for more thorough analysis, such as comparing signals from different body ports and timing blood pulses.

Multi-site PPG recordings are used for blood pressure estimation and the assessment of aging, peripheral arterial disease assessment, coronary artery disease, described in the literature review section (Chan et al., 2019; Allen et al., 2020; Bentham et al., 2018; Ouyang et al., 2021). There are multiple measurement locations: fingers, toes, ears, and configurations: single-site and various multi-site configurations, making PPG a versatile technology with many uses.

Single-site smartwatches are useful for fitness and continuous heart rate and blood oxygen measurements throughout the day; and pulse oximeters are useful for taking these measurements accurately and comfortably in a hospital setting. Multi-site configurations are useful for conducting studies on cardiovascular diseases as well as more advanced clinical measurements such as blood pressure and arterial stiffness.

Summary

Ease of use, convenience and low cost have allowed PPG to become a ubiquitous technology in clinical practice and lifestyle, as well as an attractive area of research biomedical communities. PPG research can be with human participants, as well as experimental models, which are discussed in the literature review chapter.

With both types of research, there are a few challenges to be overcome when using PPG which we will discuss in the following section. By investigating the relationship between PPG signals and cardiovascular disease risk factors, we can reach the next step for medical device and wearable health assessment.

3.4 CHALLENGES

Although there are many advantages for PPG which have encouraged its widespread use, there are still challenges to be overcome. Skin tone, ambient light and motion all affect PPG readings. By keeping these challenges in mind when designing PPG sensors for lifestyle, clinical and experimental applications, they can be mitigated or lessened. This section discusses how these sources of variation or noise are caused and the methods to reduce them.

SKIN TONES

PPG is a light-based technique, dependent on changes in light absorption, which is determined by the level of chromophores, such as melanin, in the skin. As such, participants with darker skin tones have found higher error in heart rate measurements by PPG wearables, however, further studies are required to confirm the influence of skin type on PPG devices (Shcherbina et al., 2017; Colvonen, 2021; Feiner et al., 2007). Similarly, nail polish suppresses PPG signals, with darker colours showing greater effect (Haq et al., 2018).

Pulse oximetry was first used to measure oxygen saturation in blood in 1974 (Bhattacharya, 2020). It was soon realised that it may be limited by melanin concentration, and methods to standardise PPG measurement across skin types were developed (Kraudel, 2021). For example, by dynamically adjusting light intensity depending on skin tone, so that light transmission is kept constant. Another approach has been to implement multiwavelength sensors. These techniques devices such as the Nonin finger clip, have shown that wearable sensors can work accurately for all skin tones, as long as the best design practices are implemented (Kraudel, 2021).

Ambient Light

Naturally, surrounding light, such as sunlight or indoor lighting, will affect PPG device readings. This effect should be considered when designing wearables as well as experimental protocols.

For measurement devices such as pulse oximeters, the sensor is incorporated into a clip to reduce interference from ambient light and motion. Everyday wearables like smartwatches usually cannot use clips to shield light. In these instances, signal processing techniques are employed to reduce ambient light and motion artefacts (Patterson and Guang-Zhong Yang, 2011; Hayes and Smith, 1998).

In this in vitro experiment, a similar approach was taken to design the sensor and phantom holder with ambient light shielding, as well as conducting experiments in a dark room.

Motion

Movement of the sensor creates noise in the signal called motion artefacts. Motion artefacts are the greatest cause of artefact noise in PPG signals (Njoum, 2017). This is reduced with clip-on devices such as pulse-oximeters, but partially limits PPG monitoring capabilities with smartwatches and in real-world environments where activity and motion are common, such as homecare, ambulances and sports (Sun and Thakor, 2016).

When discussing wavelengths, we saw that green light is less affected by motion in PPG sensors, however it does not achieve the depth of red and infrared light. Work has been done to remove motion artefacts from PPG signals, with various methods and signal processing techniques developed using accelerometers, gyroscopes and even ambient light (Seok et al., 2021; de Pinho Ferreira et al., 2020b).

In vitro setups can also be affected by motion artefacts, originating from the motion in a mechanical pump. This depends on the type of pump and

can be reduced by using a pump with less mechanical motion such as a diaphragm pump.

As motion artefact compensation algorithms improve, PPG devices will become more accurate, as will the physiological and experimental information obtained.

Summary

Along with the advantages, there are some limitations when using PPG devices on people as well as experimental projects. Physiologically, PPG is dependent on light-tissue interactions, which are influenced by skin tone. Being a light-based technique, ambient light will also interfere with PPG measurements. Similar artefacts are seen during motion, which is the greatest source of noise in PPG signals. All these effects should be considered when designing PPG sensors for public use, as well as in vitro experiments. By doing so, we can overcome these challenges using dynamic sensors with adjustable light sources and multiple wavelengths. Post-processing algorithms are also employed to reduce interference from motion and ambient light.

3.5 Applications

This section focuses on current and emerging applications of PPG in healthcare. PPG is already embedded in a wide range of clinical tools and consumer devices, providing vital signs such as heart rate and oxygen saturation in a non-invasive, continuous matter. Alongside established uses, a growing body of research is expanding its clinical potential, extending to blood pressure estimation, vascular assessment, cardiac output monitoring and autonomic function analysis. The following sections explore both routine clinical applications and those currently under development.

Clinical Practice

Currently, PPG is clinically used in pulse oximetry devices for blood oxygen level and heart rate measurement, with commercial devices for blood

pressure estimation, arterial stiffness measurement and peripheral arterial disease testing available. These applications are discussed, outlining their clinical importance and how they can be measured using PPG.

Heart Rate

Measured in conjunction with oxygen saturation in finger pulse oximeters, heart rate is an important measurement due to the vital function of the heart (Shmerling, 2017). The PPG pulse wave is synchronous with the heartbeat, allowing heart rate to be derived.

Pulse oximetry is universally used in hospitals for the monitoring respiratory status of ICU patients (Jubran, 2015). Pulse oximetry devices simultaneously measure heart rate, giving rise to the potential for heart rate variability calculation. Research shows promise for fingertip and wrist-worn PPG heart rate variability measurement in the future (Sahroni et al., 2019; Hoog Antink et al., 2021; Mejía-Mejía and Kyriacou, 2022).

Blood Oxygen Saturation

Pulse oximetry, the measurement of oxygen levels in the blood, has been one of the most significant technological advancements in clinical patient monitoring over the last few decades, even described as the 'fifth vital sign' (Webster, 1997; Mower et al., 1997).

Using red and infrared PPG measurements, pulse oximetry is also a non-invasive light-based technology. Oxygen saturation in the blood (SpO_2) is calculated from the ratio of red to infrared signal (Jubran, 2015).

Pulse oximetry is widely used in medical practice for blood oxygen and heart rate measurements. Areas include monitoring during anaesthetic surgery or with cardiovascular disease patients, neonatal and paediatric care and sleep studies.

Tissue Oxygen Saturation

Near-infrared spectroscopy (NIRS) is non-invasive optical technique used to monitor local tissue oxygenation by measuring the absorption of near-infrared light in biological tissues.

Unlike pulse oximetry, which focuses on arterial blood, NIRS captures oxygen saturation across venous, capillary and arterial compartments using the DC component of the PPG signal (Scheeren et al., 2012). Tissue oxygen saturation (StO_2) is calculated from the differential absorption of multiple wavelengths in the near-infrared spectrum.

NIRS is routinely used in clinical settings to monitor cerebral oxygenation during cardiac surgery and intensive care, as well as to assess tissue viability in neonatal units, trauma care, and reconstructive surgery (Ward et al., 2006).

Blood Pressure Estimation

High blood pressure increases risk of long-term conditions such as coronary heart disease and kidney disease (National Health Service, 2019c). Blood pressure is also routinely measured in clinical practice, either invasively, or non-invasively with an inflatable cuff (Picone et al., 2017). The non-invasive and comfortable nature of PPG devices make them an ideal technology to replace both these methods of traditional blood pressure measurement.

Blood pressure estimation has been achieved through the single-site PPG measurements of existing wearables and specifically designed smartwatches (Slapničar et al., 2019; Cao et al., 2021; Lazazzera et al., 2019). More accurate blood pressure measurement has been achieved with newly developed devices involving small finger-cuffs or force sensors (Finapres, 2008; Mukkamala et al., 2022). To become standard use, improved reliability and understanding of blood pressure estimation accuracy are essential (Hosanee et al., 2020).

Recent work has also suggested that in some clinical settings, it may be more practical to detect clinically meaningful blood pressure changes rather than continuously estimate absolute values. PPG has been used for threshold-based classification of systolic, diastolic and mean blood pressure changes in real time (Hong et al., 2026). This is particularly relevant in

settings where rapid identification of haemodynamic deterioration or recovery may be more important than obtaining an exact cuffless blood pressure value at every time point.

This change-based approach is also important because absolute blood pressure estimation from PPG remains challenging. The relationship between PPG morphology blood pressure is influenced by physiological variability, noise, and subject-specific factors, which can limit the reliability of regression-based absolute estimates (Mehta et al., 2024). In contrast, focussing on whether haemodynamic quantities are increasing, stable, or decreasing may provide a more robust and clinically useful framework for continuous monitoring, particularly for alerting and trend detection.

Arterial Stiffness & Peripheral Arterial Disease

Thickening of the arterial wall, caused by aging and fatty deposits, reduces its rigidity, leading to arterial stiffness (Anderson et al., 2009). Arterial stiffness is a growing epidemic associated with aging and cardiovascular disease (Kohn et al., 2015; Zieman et al., 2005).

Commercial devices exist for non-invasive arterial stiffness measurement, using PPG (Thomas-Jean et al., 2016). This is determined from pulse wave velocity, calculated by comparing finger and toe PPG signals (Axelife, 2019).

Peripheral arterial disease, the narrowing of arteries leading to reduced blood flow to the arms and legs, is associated with arterial stiffness (Zahner et al., 2017). By taking PPG measurements at each body site, such as both arms and both legs, the left and right-side signals can be compared to assess peripheral arterial disease at a specific body part. This method is discussed in detail and related to aging in the following review chapter. Multi-site PPG systems are currently available for arterial stiffness measurement and peripheral arterial disease screening (SMT Medical, 2013; Allen, 2007).

RESEARCH

For a PPG application to be routinely used in clinical practice or a device to become commercially available, as in pulse oximetry, an adequate quantity of research is required. PPG investigations are ongoing from teams across the globe. There are many more exciting applications of PPG in healthcare, which are currently being researched and headed towards clinical adoption. Following the previous section, these applications are outlined by explaining their importance and how they are being investigated with PPG.

Respiration

A person's breathing rate is important in clinical settings such as critical and neonatal care, sleep studies and surgery involving anaesthetics (Nicolò et al., 2020). Respiration contributes to fluctuations in peripheral blood flow, making it possible to monitor breathing using a PPG sensor (Khoo and Chalacheva, 2019; Allen, 2007). These fluctuations are low frequency, represented by slight shifts in the baseline of the PPG signal, called respiratory-induced intensity variation (RIIV). Respiratory rate is extracted by analysing these variations (Dehkordi et al., 2018).

Heart Rate Variability

Heart rate is currently clinically monitored as an indicator of patient health and risk of mortality (Thaulow and Erikssen, 1991). Heart rate variability (HRV), the change in time between heartbeats, is related to PPG pulse rate variability (PRV). However, they are not equivalent as they are caused by different physiological mechanisms (Georgiou et al., 2018). As such, in clinical practice heart rate variability is obtained through ECG or chest-strap devices, until the accuracy of PPG methods is developed (Electrophysiology, 1996; Cleveland Clinic, 2021; Pinheiro et al., 2016)

As pulse oximetry is a well-established technique for blood oxygen and heart rate measurement, the addition of heart rate variability measurement would expand clinical non-invasive monitoring (MHRA, 2021). Researchers

have begun to investigate the physiological link by analysing PPG pulse rate variability in vitro, in the absence of HRV (Mejía-Mejía and Kyriacou, 2022).

Cardiac Output

Cardiac Output is a measure of how much blood the heart pumps in one minute, usually around 5 litres for a healthy adult (Smith and Sachdev, 2022). Maintaining cardiac output is important to ensure sufficient supply of oxygen to the brain and other vital organs (Pai, 2021). Continuous non-invasive cardiac output measurement would also be useful for first-dose drug therapy monitoring as well as hypertension and heart failure treatment, especially in the elderly (Remmen et al., 2002).

Cardiac output is calculated by multiplying heart rate with stroke volume. PPG devices such as pulse oximeters and smartwatches are regularly used for heart rate measurement. This could be paired with stroke volume, which is the volume of blood pumped by the left ventricle of the heart in each beat (Bruss and Raja, 2022).

Stroke volume has been estimated using the blood pressure pulse contour method and Windkessel model. The aorta is modelled as a capacitor – storing blood ejected during systole, whereas the arterioles represent a resistor for blood ejected into the arterial system (Bartels and Thiele, 2015). With this technique, stroke volume can be calculated for each beat, allowing cardiac output to be determined.

These techniques have been explored in combination with the volumetric pulses of PPG waveforms, showing potential for multi-modal measurement (Colquhoun et al., 2013).

Vascular Assessment

While arterial stiffness and peripheral arterial disease may be assessed in clinical practice using PPG-based devices, ongoing research is expanding its role in vascular assessment beyond current applications. Studies have investigated the utility of PPG in identifying arterial abnormalities associated with coronary artery disease, cerebral artery stenosis and

thoracic outlet syndrome (Al Fahoum et al., 2023; Hersant et al., 2021; Kang et al., 2018; Schultz-Ehrenburg and Blazek, 2001, 2001). These conditions often lead to waveform alterations such as delayed upstroke, reduced amplitude or increased reflection components, which can be quantified using time-domain or frequency-domain feature extraction.

Recent investigations have also explored the use of PPG in assessing microvascular function and endothelial reactivity, areas traditionally limited to invasive or pharmacologically intensive methods (Armañac-Julián et al., 2025). Conditions such as Raynaud's phenomenon, diabetic microangiopathy and sepsis-related perfusion changes have shown measurable effects on PPG waveform morphology and variability (Bogusz-Górna et al., 2023; E et al., 2010).

Research into viscoelastic arterial properties using in vitro flow systems further supports PPG's potential as a diagnostic and monitoring tool in vascular biomechanics (Nomoni et al., 2020a). These approaches aim to characterise vascular stiffness, compliance, and tone in greater detail, enabling earlier detection of dysfunction and providing deeper insight into the progression of vascular disease (Njoum and Kyriacou, 2018).

Autonomic Function

Outside of physiological monitoring and vascular assessment, autonomic functions of the body are also possible to investigate using PPG. Ongoing research includes vasomotor function, thermoregulation, orthostatic intolerance and neurology (Allen, 2007; Liu et al., 2021; Mizeva et al., 2025; Tanaka, 2022).

HEALTH & FITNESS DEVICES

PPG has a strong presence outside of clinical use, in home care and consumer technology. Wearable PPG devices allow continuous measurements throughout the day, during physical activity and encourage home monitoring. Wearables are synonymous with PPG, with 71% of new

wrist-worn devices in 2018 using a PPG sensor, making it the most widely used technology in this area (Henriksen et al., 2018).

Commercial smartwatches can measure heart rate, blood oxygen levels, respiratory rate and blood pressure using PPG. By combining PPG readings with accelerometer data, more information can be measured including calorie expenditure, sleep stages and maximal oxygen uptake (Charlton and Marozas, 2022).

Wearables come in different forms, not only limited to wrist watches and straps. PPG sensors have been built into commercial devices such as rings, ear buds, arm bands, goggles and socks for holistic body measurements.

3.6 SUMMARY

This chapter introduced the principles and applications of PPG. The physiological light-based phenomena that create the PPG waveform and how features can be extracted from it has been described. The behaviour of light when interacting with tissue informs our decisions when designing a PPG sensor, such as wavelength of choice and mode of operation. As do the challenges which are connected to light-tissue interactions such as sensor movement and accounting for different skin tones.

PPG technology has risen due to its various advantages and technological development, which allow for the non-invasive monitoring of blood and tissue at a low cost. PPG is universally used across hospitals in pulse oximeters and in smart wearables, where PPG is the most common sensor. There are many more more physiological, vascular, and autonomic applications possible with PPG, which are currently being researched. As research continues, PPG accuracy improves, and feature extraction algorithms develop, more of these applications will materialise. This ongoing PPG research has taken the form of physiological measurements to study waveforms in disease and in health, as well as experimental models utilising appliances to model the human cardiovascular system.

The in vitro investigations in the following studies, utilise a pulsatile pump, silicone tubing and tissue phantoms to simulate the human heart and blood vessels. Optical phantoms allow light to interact with tissue in the similar way to the human body, making them useful for medical research, especially with PPG. The next chapter reviews key in vivo and in vitro studies investigating PPG in relation to cardiovascular disease.

4 Review of Key In Vivo & In Vitro PPG Studies in Cardiovascular Disease

4.1 Introduction

Photoplethysmography (PPG) is an established technology mainly utilised in medical care technologies such as the pulse oximeter or Near-Infrared spectroscopy (NIRS) monitoring of tissue oxygenation (Abay and Kyriacou, 2018). Consumer devices such as health trackers and smart watched also employ PPG to track heart rate (Shcherbina et al., 2017).

Lately there has been a surge of research in PPG for the assessment of cardiovascular disease (CVD) (Busati et al., 2025; Ejiyi et al., 2024, 2024; Karimpour et al., 2023; Weng et al., 2024). Multiple research groups have investigated the relationship between PPG and human physiology in vivo, on healthy subjects and CVD patients, as well as subjects from different demographic groups, i.e., age, gender pathology.

Additional studies have investigated the relationship between PPG and human physiology with cardiovascular models, in vitro (May et al., 2021; Mejía-Mejía and Kyriacou, 2022; Njoum, 2017; Nomoni et al., 2020a; Pilt et al., 2021; Roldan and Chatterjee, 2021). In vitro studies help improve the understanding of PPG under specific controlled conditions, such as the effect of vessel properties or blood flow mechanics.

Although this chapter focuses on in vivo and in vitro investigations, it is worth noting that the relationship between PPG and human physiology has also been explored in silico using computational cardiovascular models. Such studies have simulated PPG pulse waves under controlled changes in haemodynamic vascular properties, including ageing, arterial stiffness blood pressure, cardiac output and peripheral resistance (Charlton et al., 2019; Hong et al., 2026; Xing et al., 2023). These approaches complement experimental work by allowing individual parameters to be varied systematically, providing a mechanistic framework for interpreting

waveform morphology, and generating virtual datasets for algorithm development and comparison with in vivo findings.

This review discusses examples from both in vivo and in vitro PPG studies and applying the findings to help design new in vitro investigations into CVD research utilising PPG.

4.2 In vivo PPG studies

In vivo PPG studies have played a key role in demonstrating the physiological relevance of PPG waveform features in relation to vascular health. By collecting signals from human subjects, both healthy and with diagnosed cardiovascular conditions, researchers have explored how PPG reflects factors such as arterial stiffness, ageing, and peripheral arterial disease. Key in vivo PPG studies investigating peripheral vascular characteristics are summarised in Table 4-1. The table presents selected studies using multi-site or bilateral PPG measurements to assess waveform features, age-related changes, and arterial stiffness.

Table 4-1. Summary of key in vivo PPG studies investigating peripheral vascular characteristics.

Study	Measurements	Main Findings
Similarity in bilateral photoplethysmographic peripheral pulse wave characteristics at the ears, thumbs and toes (Allen and Murray, 2000)	• PPG from six sites (left and right ear, thumb, toe) • Root mean square error (RSME) • Cross-correlation coefficient	• High symmetry between left and right waveforms in healthy individuals at all levels. • Low RMSE confirming signal similarity. • Established normative bilateral data for future comparisons with vascular patients.
Age-related changes in the characteristics of the photoplethysmographic	• Multi-site bilateral PPG • Systolic rising edge	• Subtle, significant age-related changes observed at all sites.

pulse shape at various body sites (Allen and Murray, 2003)	• Dicrotic notch • Pulse normalisation	• Elongation of systolic rise and damping of dicrotic notch with age. • Effects varied by site (greatest at ear/finger). • Age-matched reference pulses proposed for vascular assessment.
A novel device for measuring arterial stiffness using finger-toe pulse wave velocity: Validation study of the pOpmètre® (Alivon et al, 2015)	• Finger-toe PPG using commercial device • Compared ft-PWV to cf-PWV (Shphygmo-Cor) • Cold pressor test • Repeatability testing	• ft-PWV showed moderate correlation with cf-PWV, especially in transit time. • Reacted similarly to sympathetic stimulation.
Innovative Multi-Site Photoplethysmography Analysis for Quantifying Pulse Amplitude and Timing Variability Characteristics in Peripheral Arterial Disease (Bentham et al., 2018)	• Multi-site bilateral PPG • Beat-to-beat and PAT variability • Time-domain SD/IQR • Frequency domain MSC	• PAD patients showed significantly lower amplitude variability and higher PAT variability in both fingers and toes. • Frequency-domain coherence was reduced bilaterally across key frequency bands in PAD, suggesting loss of vascular control.
Age-related changes in pulse risetime measured by multi-site photoplethysmography (Allen et al, 2020)	• Multi-site bilateral PPG • Risetime • SBP, HR, height	• Risetime increased linearly with age at all sites, and was inversely correlated with heart rate.

	• Multivariate regression showed age and HR as dominant factors. • Normative risetime ranges were established across body sites.

PERIPHERAL ARTERIAL DISEASE

Blood flow in the peripheral arteries is often monitored to assess health and disease. The peripheral pulse is particularly useful for assessing the cardiovascular system, for example heart rate and pulsatility (Aminuddin et al., 2018). These measurements provide an insight into the properties of the blood vessels such as arterial elasticity and narrowing of the arteries due to stenosis with occlusive diseases (Allen et al., 2020).

Photoplethysmography readings can be taken from various locations on the body, with different waveform morphologies being shown at each site. Allen and Murray looked at PPG signals from the ears, thumbs and toes, and comparing the signals from the right and left sides of healthy volunteers. Six peripheral sites were measured: the left and right ears, thumbs and big toes, using a multi-site PPG measurement system (Allen and Murray, 2000).

The purpose of this study was to determine the similarity of the pulse characteristics of the PPG signals from each side, with the hypothesis that in healthy individuals with no peripheral vascular disease, there would be a high degree of similarity in features such as timing, amplitude and waveform shape. Different characteristics observed included pulse transit time (the time taken for the pulse wave to travel from the heart to a particular site), strength and shape, and variation of each over time.

Right-to-left channel similarity was calculated using two methods: root mean square error (RMSE) to provide a measure of differences and cross-

correlation analysis to measure the degree of similarity. For the validation data, very low levels of RMSE and correlation coefficients close to unity were found. The similarity confirmed good right–left channel matching. As such, the multi-site PPG measurement system phase differences would not affect the physiological data of the subjects, so it could be used for the experiment.

The RMSE and cross-correlation of the healthy patient data showed high correlation for the left and right PPG signals of normal subjects, confirming that PPG waveforms received at the left and right-side ears, thumbs and toes are similar. This leads to the next study which compares the left and right-side PPG signals of patients with peripheral arterial disease (PAD) (Bentham et al., 2018). By confirming the similarity in normal subjects, any bilateral PPG differences seen in subjects with PAD can be attributed to the disease, rather than inherently different left and right PPG signals.

Furthermore, as this data was collected from normal subjects, it can be used to compare differences with patients of specific vascular diseases. For example, in FIGURE 4-1 a patient with unilateral left iliac arterial occlusive disease, a disease of the lower body, produces normal PPG signals at the ears and thumbs, but a clear difference at the toes (Allen and Murray, 2000).

The validation and similarity analysis methods outlined can be applied in vitro models to ensure that branches show similar PPG signals before introducing a pathology into a specific branch.

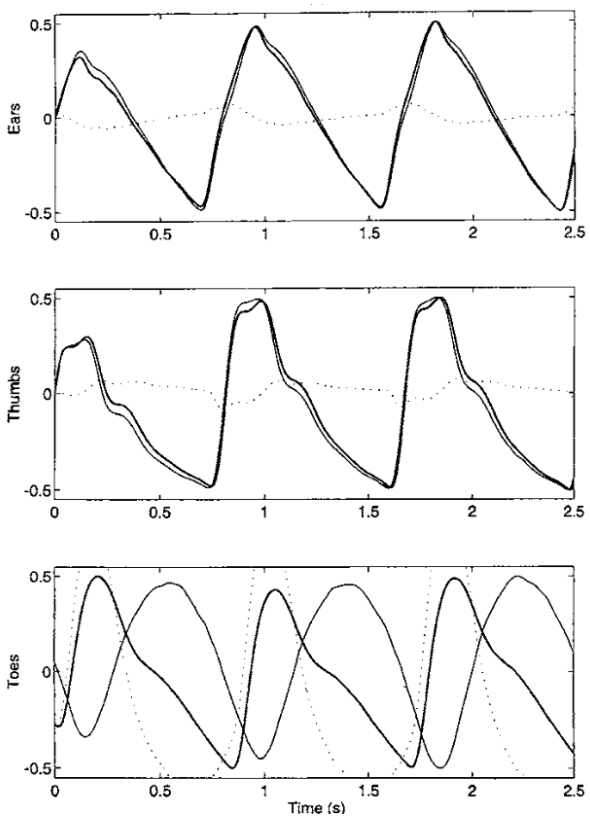

FIGURE 4-1. PPG pulse waveforms from the right and left ears (top), thumbs (middle) and toes (bottom) for a patient with an occlusion in the left iliac artery. This artery leads to the lower body, where a clear difference in the PPG signals is seen, while the ear and thumb PPGs are very similar (Allen and Murray, 2000).

While previous studies collected left and right-side photoplethysmography (PPG) signals of normal subjects, Bentham et al collected the signals from patients with PAD. PAD is a common condition, estimated to affect 15-20% of people over 70 years of age, that has a negative impact on quality of life and life expectancy. Only a quarter of the people affected display symptoms, making non-invasive, inexpensive early diagnosis even more important (Bentham et al., 2018).

Using a similar multi-site PPG system, shown in FIGURE 4-2, recordings from healthy control subjects and patients with PAD were compared and analysed beat-to-beat (Bentham et al., 2018). With this method, PPG waves are separated into cycles with each heartbeat. Analysing individual cycles enables the study of the variability of pulse features, such as amplitude and pulse arrival time (PAT). These features can then be

quantified in the time and frequency domains, which can provide information on the perfusion changes associated with PAD.

Beat-to-beat pulse amplitude and PAT were calculated and also their variability was quantified in the time and frequency domains. This enables the study of patterns and changes that could not be seen otherwise. Two simple statistical measures were used for time-domain analysis of amplitude and PAT: standard deviation (SD) and interquartile range (IQR). Quantification in the frequency-domain was done using magnitude squared coherence (MSC). In the time-domain analysis, patients with PAD had significantly reduced amplitude variability and significantly increased PAT variability. In the frequency-domain, PAD patients had significantly lower MSC values across a range of frequency bands. These significant changes in amplitude and PAT variabilities suggest a loss of right-to-left body side coherence and cardiovascular control in PAD. The loss of coherence is visible when comparing the left and right-side PPGs in FIGURE 4-3.

This is another bilateral PPG study using methods that can be employed in vitro as well as in vivo. When designing an in vitro study with tissue phantoms and silicone vessels, properties can be changed to match PAD patients, such as vessel stiffness and diameter. The results from both in vivo and in vitro studies can then be compared.

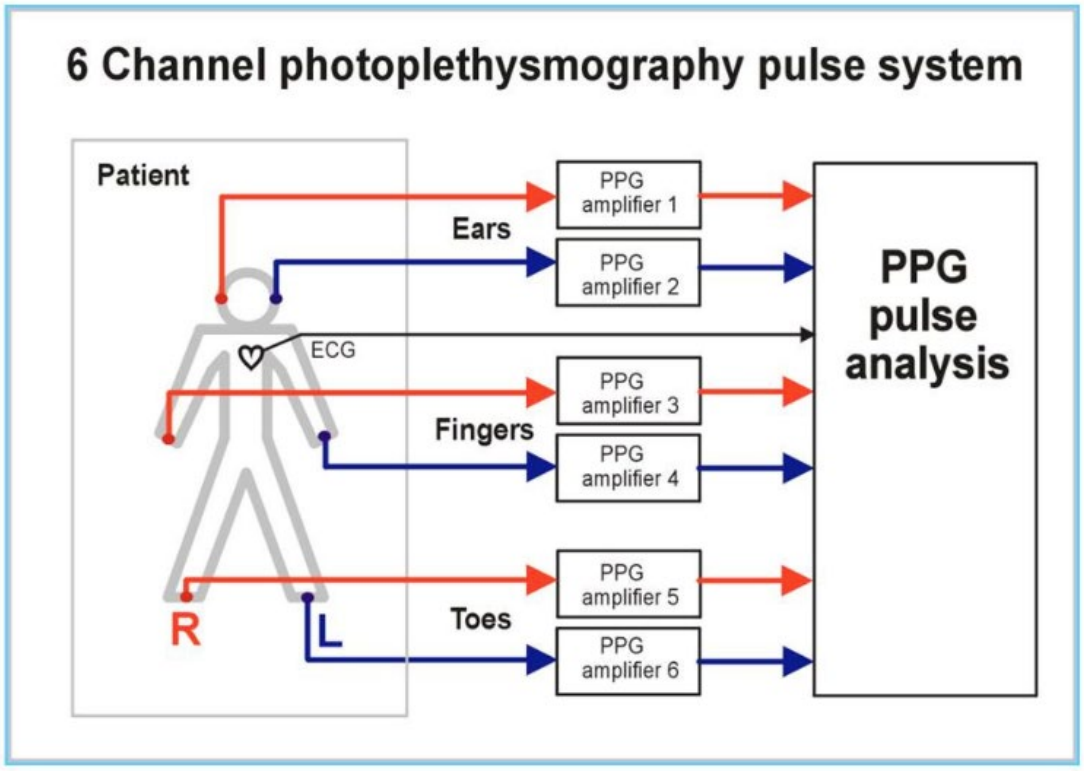

FIGURE 4-2. Multi-site photoplethysmography (PPG) pulse measurement and analysis system (Bentham et al., 2018).

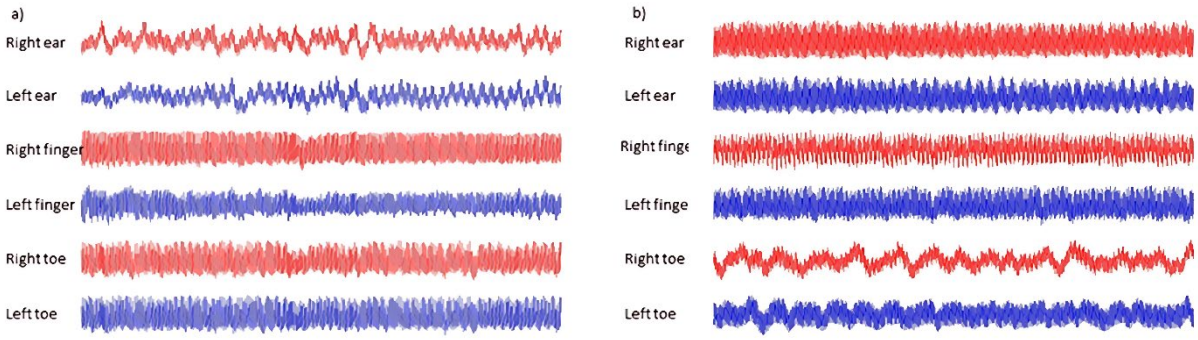

FIGURE 4-3. Multi-site PPG recordings (a) a healthy control and (b) a peripheral arterial disease (PAD) patient (Bentham et al., 2018).

ARTERIAL STIFFNESS

Arterial stiffness describes the rigidity of the arterial wall and is determined by the structural components such as elastin and collagen (Najjar et al., 2011). An increase in arterial stiffness can lead to increasing pulsatility and systolic pressure, which causes damage to the cardiovascular system, leading to cardiovascular disease. As such, arterial stiffness is another valuable measurement to observe through photoplethysmography (PPG).

The pOpmètre device asses arterial stiffness by continuously recording pulse waves using two PPG sensors, on the finger and at the toe to calculate the difference in pulse transit time between the finger and toe (ft-TT) shown in FIGURE 4-4A (Axelife, 2022). For this calculation, distance travelled in the blood vessels is estimated based on subject height, as measuring the true distance requires magnetic resonance imaging (Van Bortel et al., 2012).

A validation study was conducted to evaluate the accuracy of the device for clinical practice. The method for this evaluation can be applied to in vitro experiments for the investigation of arterial stiffness. The validation consisted of three studies. The first study compared finger-toe pulse wave velocity (ft-PWV) with carotid-femoral PWV (cf-pWV), which is the velocity of the pulse wave calculated based on the distanced travelled from the arteries in the neck to the upper leg, seen in FIGURE 4-4B. ft-PWV was calculated by pOpmètre, the device being evaluated and cf-PWV was calculated by the reference method SphygmoCor®. Results showed that both PWVs from the finger to toe and the carotid to femoral arteries correlated significantly. However, there was a better correlation in terms of transit time. When the transit times were translated into velocities, the agreement decreased. Interestingly, the discrepancy between transit times was related to age. At younger ages, ft-TT was overestimated compared to cf-TT. This indicated that ft-TT captures additional information about the aging process, which is not seen with cf-TT. Other age-related changes in PPG characteristics have been found which are discussed next in this review (Allen et al., 2020; Allen and Murray, 2003).

The second study compared changes in ft-PWV and cf-PWV during a cold pressor test. The cold pressor test is considered a stimulus of the cardiovascular and sympathetic nervous systems, causing an increase in blood pressure (Bellinazzi et al., 2014). When immersing the right hand into an ice water container for one minute, aortic stiffness increased with parallel changes in ft-PWV and cf-PWV shown. cf-PWV increased from the start of the cold pressor test, while the change in ft-PWV was only

significant at the end of the cold exposure. Aortic stiffness and the PWVs then decreased during the recovery period. The third study assessed repeatability by measuring the ft-PWV of different patients including healthy and unhealthy, showing good intra-session repeatability.

Conclusions drawn from the study allowed the measurement of arterial stiffness in routine clinical practice with a non-invasive PPG device. This reflects the potential of PPG for early screening of cardiovascular diseases. Furthermore, the evaluative nature of this study can be repeated when conducting in vitro studies. For example, the intra-session repeatability can be assessed with different vessel and tissue phantom combinations. PPG is used in a range of scenarios. This device utilises PPG at the finger and toe for pulse transit time and pulse wave velocity calculation for the measurement of arterial stiffness. This technique is based in the time domain, by looking at the time difference between PPG pulses. Other methods for PPG analysis are available, for example area and shape of the wave. These techniques, which are utilised in the next study, allow the assessment of arterial stiffness and aging at a single measurement site, rather than detecting the time difference from two sites (finger and toe). In vitro studies can also be setup to improve the understanding of the relationship between arterial stiffness and these characteristics of the PPG wave.

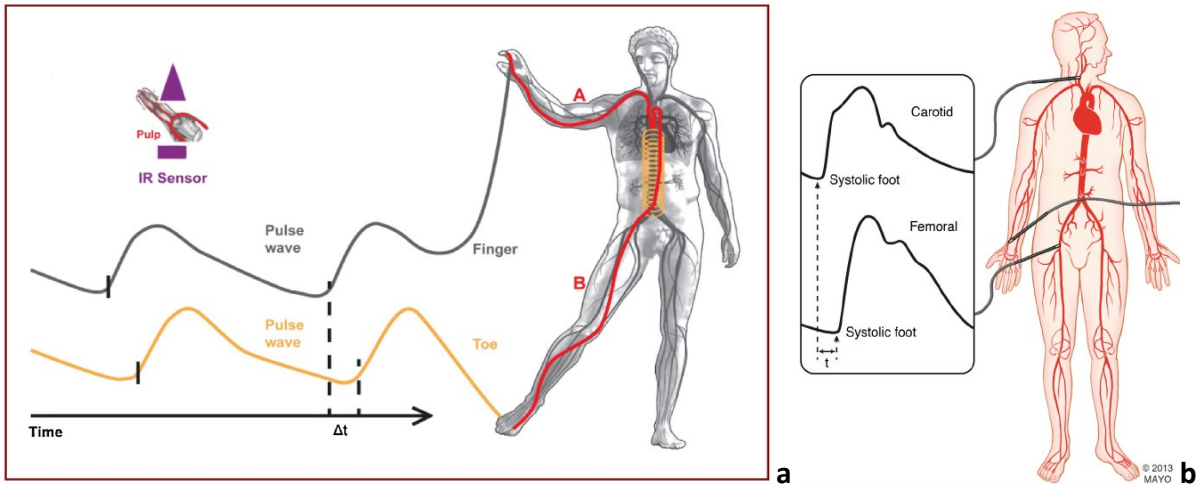

FIGURE 4-4. Illustration of peripheral and central pulse wave velocity (PWV) measurement techniques using PPG and

pressure wave analysis. Pulse wave velocity is calculated based on the estimated distance travelled and the time of the pulse waves at **a)** the finger and toe (Alivon et al., 2015) and **b)** the carotid and femoral arteries (Coutinho, 2014).

Arterial stiffness, which is closely associated with cardiovascular disease, is known to increase with age. This is due to decreases in the ratio of elastin to collagen in the arterial wall structure (Kyriacou and Allen, 2022). The link to cardiovascular disease make arterial stiffness and aging important topics to research. The arterial wall changes are reflected in the propagation of the blood pulse waves to the peripheral arteries, suggesting that analysing peripheral pulse timing and shape characteristics, which can be done with photoplethysmography (PPG), could be a key to the non-invasive, early screening of arterial stiffness and cardiovascular disease.

Allen and Murray looked at the link between arterial stiffness and aging from the perspective of PPG. By observing the changes in pulse wave characteristics, such as shape and area, across generations, a pattern could be found (Allen and Murray, 2003). These characteristics were observed from PPGs at the ears, fingers and toes of people across four age groups, ranging from below 30 to over 50 years old. Changes seen were subtle but significant, which occurred gradually across the age groups, visible in FIGURE 4-5. At the ears, a gradual flattening of the notches is seen. A dampening of the dicrotic notch occurred at all sites with age. Another universal change was the overall elongation of the systolic rising edge with age at all three sites. The data shows that when evaluating pulses from patients with possible vascular disease, age-matched normal ranges should be considered. Focussing on the elongation of the systolic rising edge, the next study analyses the changes in the pulse risetime with age.

The confirmation of changes in the PPG pulse shape with age at all sites shows how much we can learn about a person's cardiovascular health from a single point of contact such as the finger, without any discomfort. This is in contrast other methods which are invasive, or the pulse wave velocity calculations as in the previous study which require two points, the finger

and toe. Pulse shape analysis can be improved, and further changes can be studied by in vitro experiments. Similar studies with specific, known arterial stiffnesses could help determine the pulse shape changes at smaller intervals of stiffness translating to smaller age gaps in vivo.

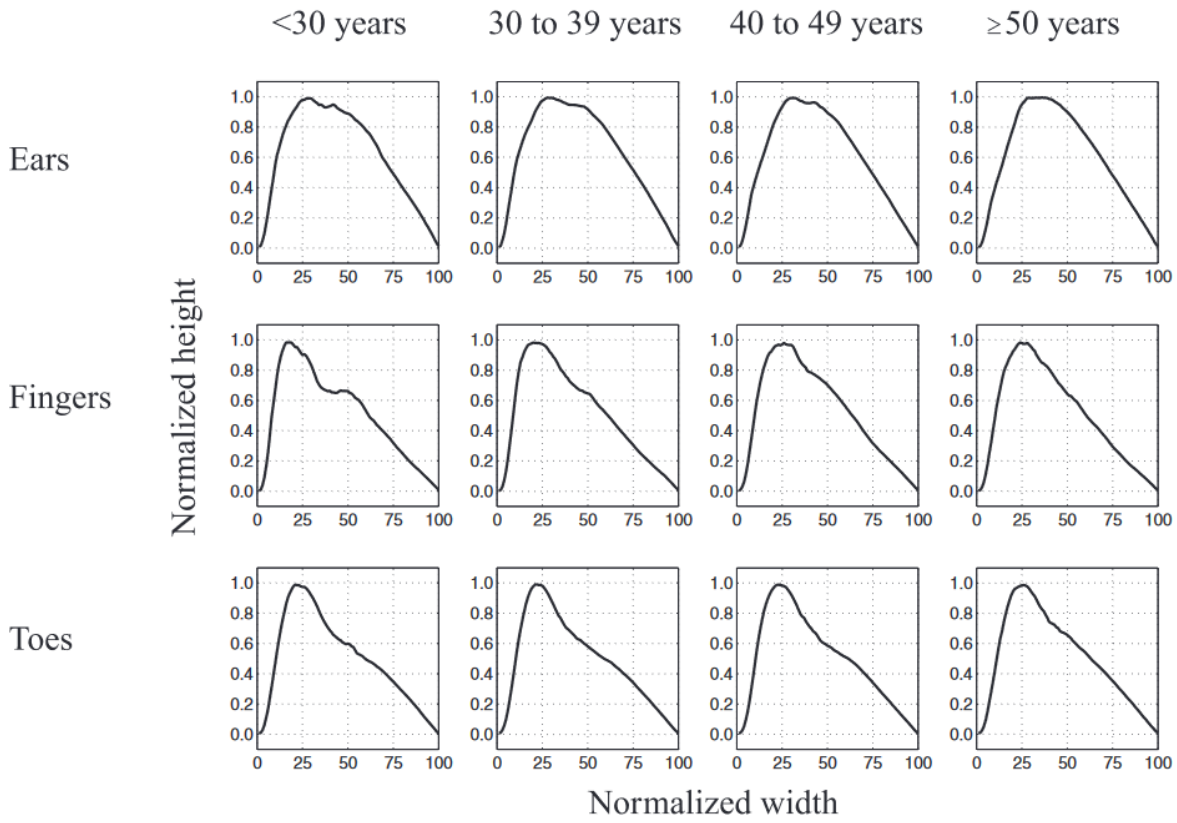

FIGURE 4-5. Changes in PPG pulse waves across four age groups. A reduction in the dicrotic notch with age is seen as well as a slight elongation of the systolic rising edge (Allen and Murray, 2003).

In the previous study, elongation of the systolic rising edge changed with age. Pulse risetime, the time between the foot of a pulse and its peak, is a quantifiable feature of the systolic part of the wave. Determining the association between age and pulse risetime could lead to the measurement of arterial stiffness and cardiovascular disease with PPG.

This study followed an 8-decade range at the same sites (ears, fingers and toes) and also considered systolic blood pressure (SBP), height and heart rate. Univariate regression analysis of the pulse risetime changes

showed positive correlation with pulse risetime with age and clear inverse association with heart rate (Allen et al., 2020).

Similarly, pulse transit time (PTT), the time taken for the blood pulse wave to travel from the heart to the various body sites, has also been previously associated with age. Using multi-site PPG and electrocardiography (ECG), it was found that PTT decreased with age and with increased blood pressure (Allen and Murray, 2002).

These in vivo studies have revealed a link between photoplethysmography and cardiovascular disease, which can be rigorously studied in vitro to draw specific conclusions.

4.3 In vitro PPG studies

By building experimental models to simulate the human cardiovascular system, consisting of pumps, vessels and phantoms, it is possible to do in vitro studies parallel to the previous in vivo studies mentioned. This can help improve the understanding and optimisation of photoplethysmography (PPG) technology and characteristics in areas such as contact pressure, haemorheology, pulse rate variability, and vessel properties. Key experimental setups and findings from in vitro PPG research, including vessel-tissue phantoms, controlled flow conditions, and blood-mimicking fluids are highlighted in Table **4-2**.

TABLE 4-2. Summary of in vitro PPG studies exploring haemodynamics, vessel models, and signal behaviour.

Study	Setup	Main Findings
Photoplethysmography for the Assessment of Haemorheology (Njoum & Kyriacou, 2017)	• Shear rate adjusted via syringe pump • Clotting induced chemically • Custom vessel-tissue phantoms • Equine blood	• PPG-AC amplitude decreased and PPG-DC increased with higher shear rates and during clot formation.
In vitro validation of measurement of volume elastic modulus using photoplethysmography (Njoum & Kyriacou, 2018)	• Dual-model arterial flow loop simulating healthy (silicone) and diseased (PVC) arteries • Catheter pressure transducer • Optical fluid used cobalt nitrate solution • Volume elastic modulus testing	• Volume elastic modulus showed sensitivity to pulse frequency and stroke volume, outperforming PTT.
Novel Polydimethylsiloxane (PDMS) Pulsatile Vascular Tissue Phantoms for the In-Vitro Investigation of Light Tissue Interaction in Photoplethysmography (Nomoni et al, 2020)	• Mimicking finger anatomy • Custom dip-coated PDMS vessels • Optically tuned PDMS tissue	• Custom vessels with thin walls (~60 μm) significantly improved signal-to-noise ratio and PPG waveform quality vs. commercial tubing

Effects of Contact Pressure in Reflectance Photoplethysmography in an In Vitro Tissue-Vessel Phantom (May et al, 2021)	• Linear actuator • Custom vessel-tissue phantoms • Pulsatile pump • 17 morphological features	• Identified an optimal contact pressure range (25.1–48.1 mmHg) for highest signal quality. • Time-domain features (e.g. pulse duration, rise time) were least affected by pressure. • Amplitude and geometric features changed significantly.
In-Vitro investigation of flow profiles in arteries using the Photoplethysmograph (Pilt et al, 2021)	• Doppler ultrasound and pressure sensors • PVC arterial model • India ink water solution used as optical fluid • Steady-state flow from gear pump	• Waveform shape and frequency content with flow profile. • Turbulent flow showed increased high-frequency components. • Downstream PPG was sensitive to stenosis-induced turbulence.
Photoplethysmography-Based Pulse Rate Variability and Haemodynamic Changes in the Absence of Heart Rate Variability: An In-Vitro Study (Mejía-Mejía & Kyriacou, 2022)	• Anatomically inspired upper-limb in-vitro model for radial and palmar sites • Custom silicone vessels • Tissue phantoms • Artificial blood • Pressure sensors	• Demonstrated that PRV indices (time, frequency and non-linear) change significantly with stroke rate and flow, despite no heart rate variability present. • Confirms PRV is modulated by haemodynamic factors alone, highlighting key differences from HRV.

CONTACT PRESSURE

Wearable technology for the benefit of health has continued to grow and expand. PPG is a key component in this rapidly developing area of healthcare technology, currently present in many smartwatches. May et al used an in vitro setup to improve the understanding of how contact pressure effects PPG signals. Specifically, the signal-to-noise ratio of the PPG wave and its morphological features were analysed (May et al., 2021). Contact pressure of the PPG device connected to a tissue-vessel phantom, displayed in FIGURE 4-6, was adjusted.

PPG signals were recorded at different contact pressures and blood pressures. The results revealed the optimum sensor contact pressure to be between 35.1 mmHg and 48.1 mmHg. Time-based features were less affected by contact pressure, suggesting that parameters such as heart rate and respiration rate are not dependant on contact pressure. Conversely, amplitude and geometric features of the PPG wave showed significant change.

These results are important to consider when designing a PPG sensor, building an in vitro system or using morphological analysis for cardiovascular assessment.

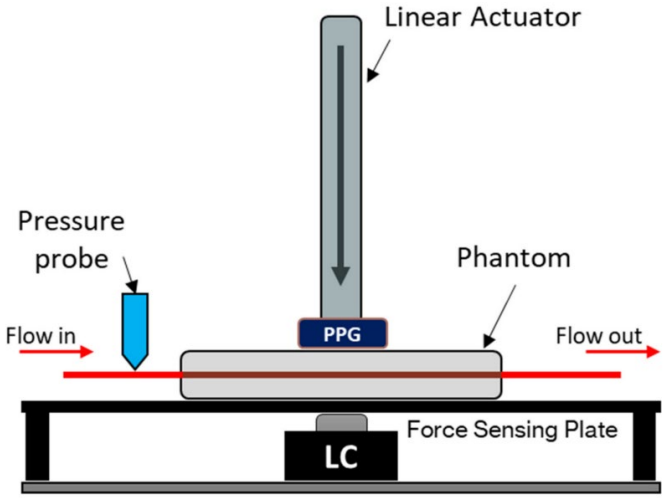

FIGURE 4-6. Vessel-tissue phantom and PPG sensor, attached to a linear actuator, for the adjustment of contact pressure (May et al., 2021).

Pulse Rate Variability

Pulse rate variability (PRV) measures how much the pulse rate is changing over time. It can be measured from the heartbeat on an electrocardiogram (ECG), as heart rate variability (HRV), or from a pulsatile signal such as the photoplethysmogram (PPG), compared in Figure 4-7.

Recent studies have reported PRV as a surrogate for HRV, however, studies have confirmed there is a discrepancy between PRV and HRV, due to the several steps of physical transformation from ECG R wave to PPG pulse wave: electromagnetic coupling, conversions from force to volume, volume to pressure, pressure impulse to wave, pressure wave to volume, and volume to light intensity (Yuda et al., 2020).

Mejía-Mejía and Kyriacou built an in vitro model to better understand the factors affecting the relationship between PRV and HRV, by analysing PRV on its own, in the absence of HRV (Mejía-Mejía and Kyriacou, 2022). The model was designed to simulate the upper-circulatory system, Figure 4-8.

Haemodynamic changes were induced by changing stroke rate and target flow, while PPG signals were being acquired. The signals were used to calculate PRV and time-domain, frequency-domain and non-linear indices were extracted. Factorial analyses showed that changing stroke rate and target flow had a significant effect on the PRV indices, helping explain some of the differences between HRV and PRV.

This study is an example of using in-vitro models to isolate and study specific characteristics relating to the cardiovascular system and PPG, which can be replicated for the study of cardiovascular diseases.

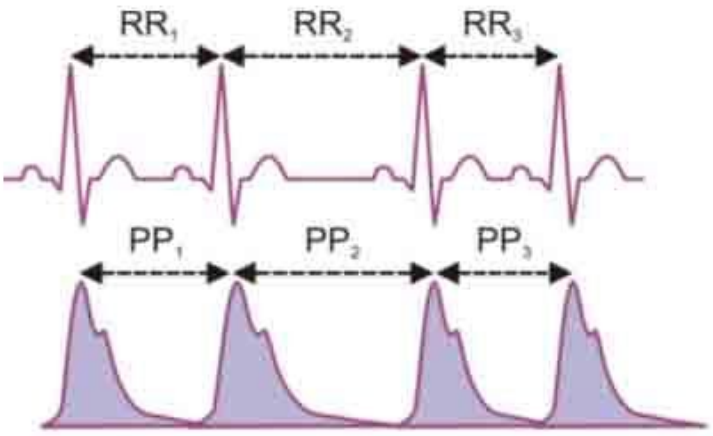

FIGURE 4-7. An electrocardiogram (ECG), top and a photoplethysmograph (PPG) for heart rate calculation. Heart rate is calculated from the time difference between the R peaks of the ECG and pulse rate is calculated from the pulse peaks of the PPG.

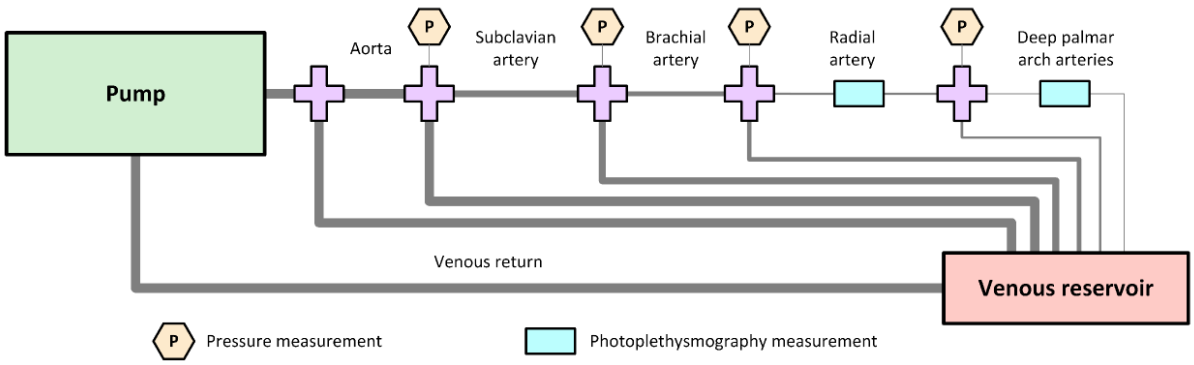

FIGURE 4-8. In-vitro model simulating the upper-circulatory system for the assessment of pulse rate variability (PRV) of a photoplethysmography (PPG) signal (Mejía-Mejía and Kyriacou, 2022).

The blood flow profile in the arteries is an indication of the health of the vessel and the arterial system. Turbulent blood flow is linked to a range of cardiovascular diseases and can damage red blood cells and the endothelial cells of the artery wall, leading to atherosclerosis. Haemorheology, the study of blood flow mechanics and components, has been long identified as an early biomarker for cardiovascular diseases.

VESSEL CONSTRICTION & FLOW PROFILES

Pilt et al used an in vitro model of a simplified arterial system to investigate the effect of flow profiles on photoplethysmography (PPG) signals at

different steady state flow ates and levels of vessel constriction (Pilt et al., 2021). The model consisted of a steady state flow pump and PVC vinyl tubing, FIGURE 4-9.

Results showed that during laminar flow, the PPG waveform was stable but during turbulent flow, the PPG waveforms fluctuate irregularly. This is an indication that PPG can be used to assess blood flow profiles in the arteries.

Previously mentioned in vivo studies have analysed the morphology of the PPG wave with regards to peripheral arterial disease. Similar analyses can be done on PPG in vivo with different flow profiles with healthy subjects and those with arterial diseases, as well as with an in vitro model, show that in vivo and in vitro investigations can complement one another. This study also utilised ultrasound doppler probes for the calculation of flow velocity, a useful technique which can be used in future in vitro setups.

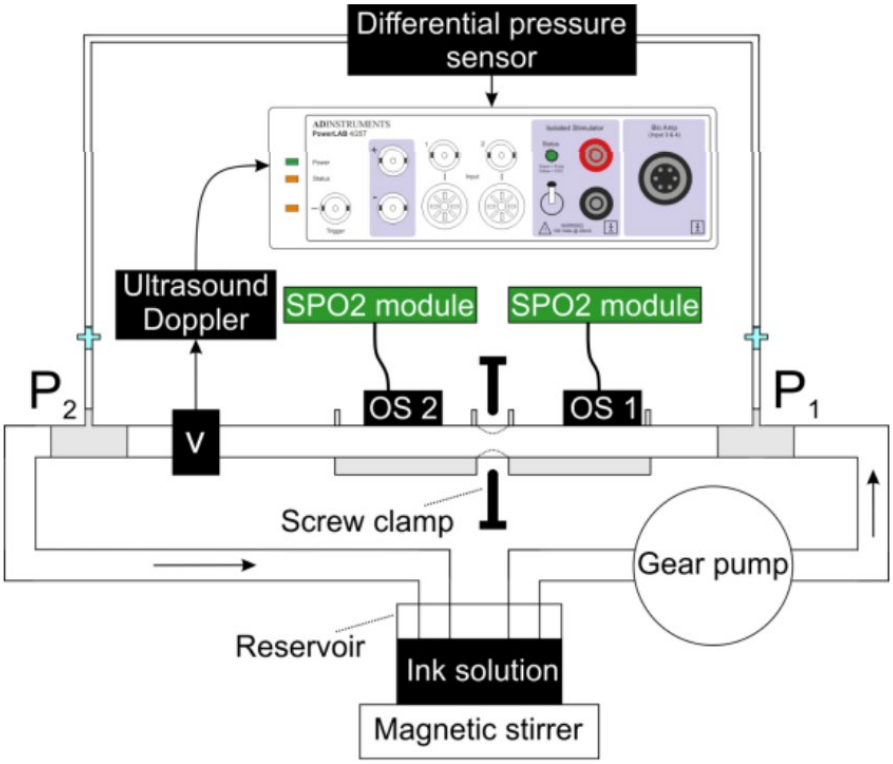

FIGURE 4-9. In vitro model of a simplified arterial system, consisting of a steady state flow gear pump and PVC vinyl tubing, to investigate the effect of flow profiles on photoplethysmography (Pilt et al., 2021).

Another aspect of blood flow and haemorheology that has been studied in relation to PPG is shear rate. Njoum and Kyriacou built an in vitro setup to mimic the human circulation, with various arterial models shown in FIGURE 4-10.

Shear rate was investigated by pumping fluid at various frequencies and thromboplastin activation was investigated by using a chemical trigger, both while PPG was being observed. PPG levels showed significant changes when shear rate was increased and an immediate change after thromboplastin activation, suggesting that PPG could non-invasively detect blood characteristics, including disaggregation, radial migration and cross-linking fibrin formations (Njoum and Kyriacou, 2017).

Detecting these characteristics would allow anticoagulants and clotting-activators to be assessed and could be used for the early non-invasive assessment of cardiovascular diseases. This study used equine blood, showing that blood components such as red blood cells can be investigated with in vitro.

ARTERIAL STIFFNESS

Njoum and Kyriacou also used an in vitro setup to measure arterial stiffness and volume elastic modulus using PPG. At varying flow dynamics, PPG signals were recorded along with pressure and flow using an ultrasonic Doppler flowmeter (Njoum and Kyriacou, 2018). With one branch simulating normal human circulation, and another simulating arterial stiffness, volume elastic modulus values were calculated for each branch and compared to the gold standard mechanical testing techniques using a tensile testing machine.

The values obtained through PPG showed no significant difference compared to the tensile test, confirming that volume elastic modulus and arterial stiffness can be directly measured with PPG in an in vitro setup, which paired with emerging non-invasive blood pressure methods and future in vivo studies, such as the arterial stiffness and aging studies

reviewed in the previous section, opens the possibility for the direct quantification of arterial stiffness in vivo.

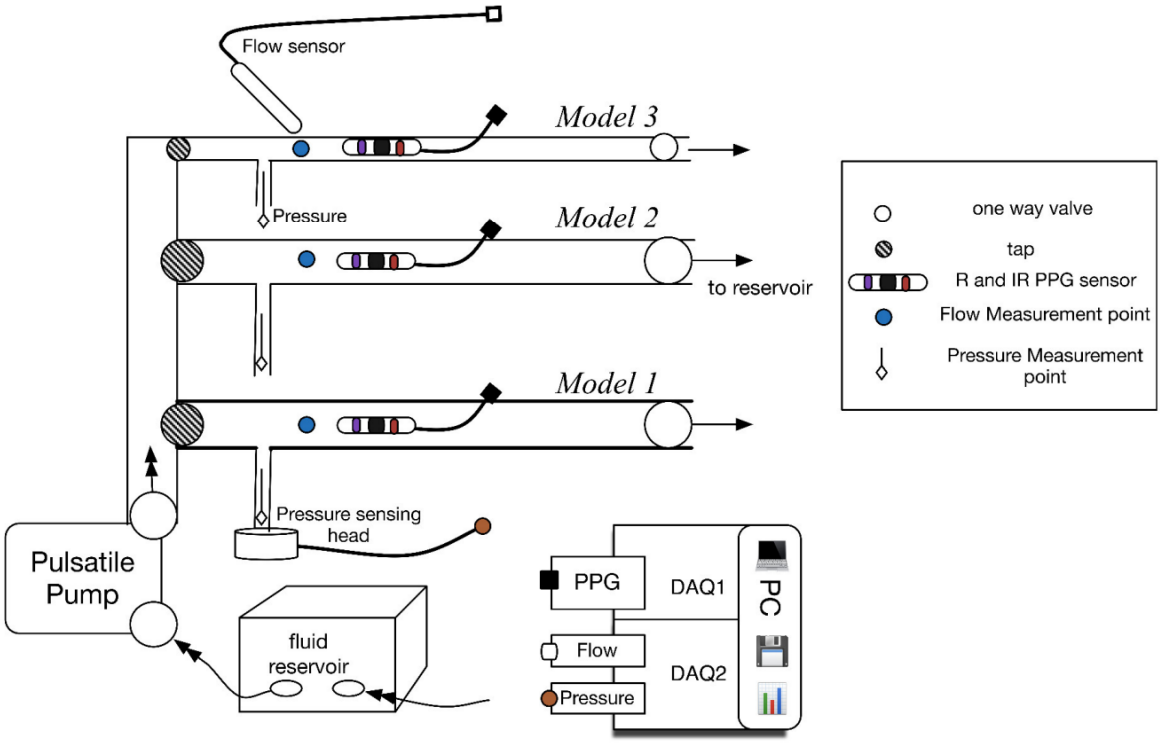

FIGURE 4-10. In vitro setup for the assessment of haemorheology and measurement of volume elastic modulus using photoplethysmography (PPG) (Njoum, 2017).

SILICONE VESSELS

Vessel and tissue phantoms form the vascular basis of many in vitro cardiovascular models (Boice et al., 2022). Nomoni et al have developed a novel method for creating phantoms providing high-quality PPG signals, attributed to the low vessel wall thickness compared to commercial tubing. The artificial vessels were formulated with polydimethylsiloxane (PDMS), and constructed in a custom continuous dip-coating process, FIGURE 4-11A (Nomoni et al., 2020a).

An in vitro setup was used to test the phantoms, FIGURE 4-11B; this confirmed flow profiles similar to human blood flow and high signal-to-noise ratios. The design, fabrication and evaluation methods described are useful for future in vitro studies and models resembling the human vascular system, especially for the study of PPG.

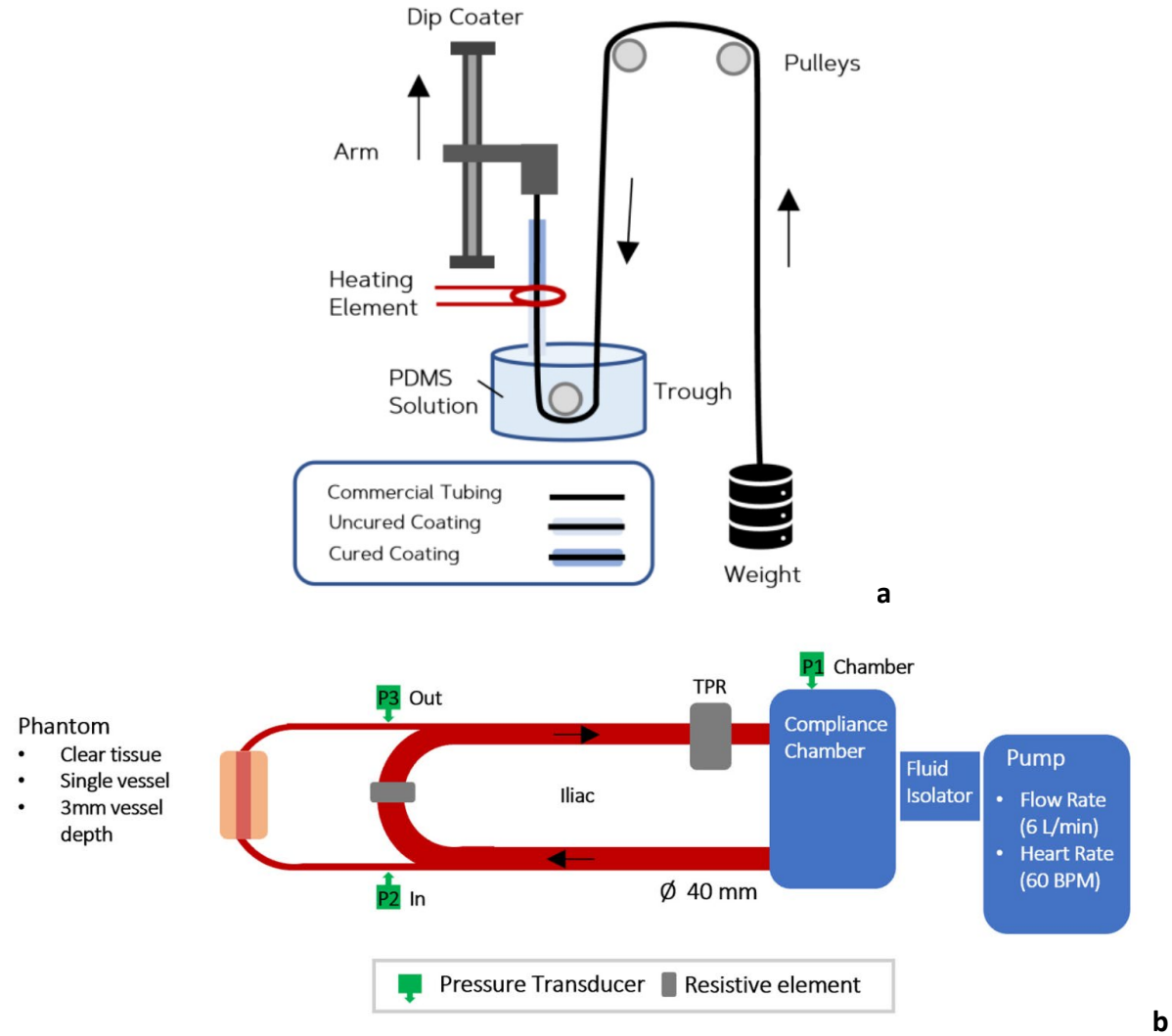

FIGURE 4-11. Schematic overview of vessel fabrication and flow testing setup for in vitro PPG analysis. a) Custom dip-coating process for the fabrication of vessel phantoms with properties similar to human blood vessels. **b)** Experimental flow rig for testing phantoms. (Nomoni et al., 2020a)

4.4 Discussion & Conlusions

Experiments by different groups have investigated PPG with different approaches, with people as well as cardiovascular models. In vivo studies have been conducted on healthy subjects, patients with cardiovascular diseases such as peripheral arterial disease (PAD) and arterial stiffness, and subjects across age groups (Allen and Murray, 2003, 2000; Bentham et al., 2018). Peripheral arterial disease is a condition that affects the quality of life and life expectancy of subjects. It is common, especially in the older population, yet hard to detect – only a quarter of patients display symptoms. Therefore, early screening technologies such as photoplethysmography (PPG) are paramount. For widespread use, non-invasive and inexpensive devices are required, which are the advantages of PPG.

Allen and Murray first investigated with normal, healthy subjects to determine the validity of such a device for PPG measurements on both sides of the body, potentially useful to detect PAD (Allen and Murray, 2000). After verifying that PPG signals on both sides of the body were similar, the system could be used in pathological in vivo studies such as investigations of PAD and aging. With PAD patients, a clear difference in the PPG signals were seen between the left and right-side, specifically at the site leading from the area of occlusion. For example, with an occlusion in the left iliac artery (situated in the lower body), the difference in the PPG signals at the toes was clearly visible, but at the ears and thumbs, left and right PPG signals were identical (Bentham et al., 2018). This supports PPG for a non-invasive clinical cardiovascular assessment and shows the importance of measuring at different body sites. When investigating variability, PAD patients also showed significantly reduced amplitude variability and increased pulse arrival time (PAT) variability. The changes in the time and frequency domains signified the loss of right-to-left body side coherence. This is seen through signal analysis as well as simply viewing the PPG

graph, making it a potential method for early screening of cardiovascular diseases.

Arterial stiffness is another contributor to cardiovascular disease that has been studied with photoplethysmography (Karimpour et al., 2023). Arterial stiffness is the loss of arterial compliance due to changes in the arterial wall properties such as wall thickness and components such as elastin and collagen (Coutinho, 2014). Arterial stiffness can lead to increased blood pressure and pulsatility, which damages the cardiovascular system. This link with cardiovascular disease makes arterial stiffness clinically significant. A device for non-invasive arterial stiffness measurement, based on PPG, currently exists. The validation study allows the use of the non-invasive PPG device for measurement of arterial stiffness in routine clinical practice (Alivon et al., 2015). Similar evaluations can be made with in vitro studies, such as assessing intra-session repeatability with different vessel-tissue phantom combinations. The current arterial stiffness measurement device is based on finger-toe pulse wave velocity, meaning a PPG sensor is required at the finger and the toe. This could be improved if the arterial stiffness could be measured with ear and wrist PPG sensors, as these can be embedded into a smart watch and earbuds, which would be more convenient and comfortable for patients. This may be achieved by utilising in vitro studies to study PPG pulse transit times and velocities at different distances and stiffnesses. The controlled nature of in vitro studies makes them useful for isolating specific parameters such as arterial stiffness and studying them in the absence of other physiological factors.

Aging, which links to arterial stiffness has been studied in terms of PPG. Again, by looking at PPGs from different body sites, a full picture of the cardiovascular trends can be obtained. The dicrotic notch clearly disappears across older age groups, at all tested body sites (Allen et al., 2020). Arterial stiffness likely has a role to play in this disappearance over time, due to the link between aging and arterial stiffness. This is another area where in vitro studies could provide a detailed understanding of the changes in PPG

due to specific parameters, without other physiological factors interfering. For example, by using models with vessel tubing of different thicknesses and stiffnesses, while keeping all other components of the model the same, the morphology of the PPG wave can be studied in response to increasing arterial stiffness.

The development and assessment of custom vessels is an example of such in vitro studies. These vessels were much closer to the properties of human blood vessels than commercially available, producing high quality PPG signals (Nomoni et al., 2020a). They allow for in vitro setups to give PPG readings as good or better than on human subjects, which widens the potential for PPG feature analysis and cardiovascular disease investigations.

Further in vitro investigations using similar components and methods have investigated how PPG can be used to assess flow profiles, haemorheology and arterial stiffness (Njoum and Kyriacou, 2018, 2017; Pilt et al., 2021). In vitro models have also been used to improve the understanding of the relationship between PPG and contact pressure and pulse rate variability (May et al., 2021; Mejía-Mejía and Kyriacou, 2022). Such research highlights the breadth of potential physiological parameters that could be studied through PPG and cardiovascular models.

The reviewed in vitro studies reveal several gaps that limit broader translation of PPG research. Many systems focus on a single factor in isolation, but do not combine controlled haemodynamics with vessel-specific modification to allow direct comparison between healthy and diseased conditions under matched flow. Others rely on simplified tubing or phantom structures that do not fully capture the mechanical or optical conditions needed for reproducible vascular assessment, while few provide bilateral configurations suited to investigating asymmetry, despite its relevance to PAD. Furthermore, there is room in the body of work for a pipeline to generate labelled PPG datasets under known mechanical conditions for systematic feature validation. These areas form the basis for the present thesis, which aims to develop a more controlled bilateral in vitro

platform with customisable vessel properties for investigating stiffness-related PPG changes under reproducible conditions.

By using the in vitro model developments and techniques, combined with in vivo investigations, we can combine the two realms for a holistic study of PPG and cardiovascular disease. This is a sure path for the realisation of non-invasive, early screening of cardiovascular diseases in routine clinical practice.

4.5 SUMMARY

This chapter reviewed key in vivo and in vitro PPG studies investigating cardiovascular disease indicators such as arterial stiffness, peripheral arterial disease (PAD), ageing, and haemodynamic changes. In vivo studies demonstrated how waveform features from multi-site and bilateral PPG recordings reflect differences between healthy individuals and those with vascular conditions. Key findings included significant waveform alterations with age, and clear differences in amplitude and timing variability in patients with vascular disease.

In vitro models were described for replicating cardiovascular conditions using synthetic vessels, controlled flow loops and blood-mimicking fluids. These setups allowed research to systematically vary parameters such as vessel stiffness, shear rate, and contact pressure to observe their effects on PPG waveforms. In vitro experiments confirmed that PPG could detect changes in vessel elasticity, thrombosis and heart haemodynamic variability.

The review highlights how combining in vivo and in vitro approaches offers a robust framework for understanding PPG signal behaviour and its clinical relevance. In vivo data provide physiological grounding, while in vitro models offer controlled environments to test hypotheses and refined sensor or model design. This dual approach supports the ongoing development of non-invasive, accessible and reliable PPG-based tools for early detection and monitoring of cardiovascular disease.

5 DEVELOPMENT OF AN IN VITRO BILATERAL MODEL

5.1 INTRODUCTION

The review of previous PPG has shown that controlled experimental setups provide valuable information about the relationship between PPG and cardiovascular mechanics, through PPG waveform feature extraction and morphological analysis. An interest is taken to apply vascular mechanical changes and PPG waveform analysis for the assessment of cardiovascular disease. An in vitro setup has been designed to investigate this by pumping fluid to two tissue phantoms, one healthy and one simulating cardiovascular disease. This chapter describes the design and implementation of this setup, as well as the protocols that will be used to study these pathologies.

5.2 METHODS

The in vitro setup consists of a pulsatile pump, tubing and connectors, a blood mimicking fluid, photoplethysmography and pressure sensors and a data acquisition system. The layout is shown in FIGURE 5-1, with each part of the setup described below.

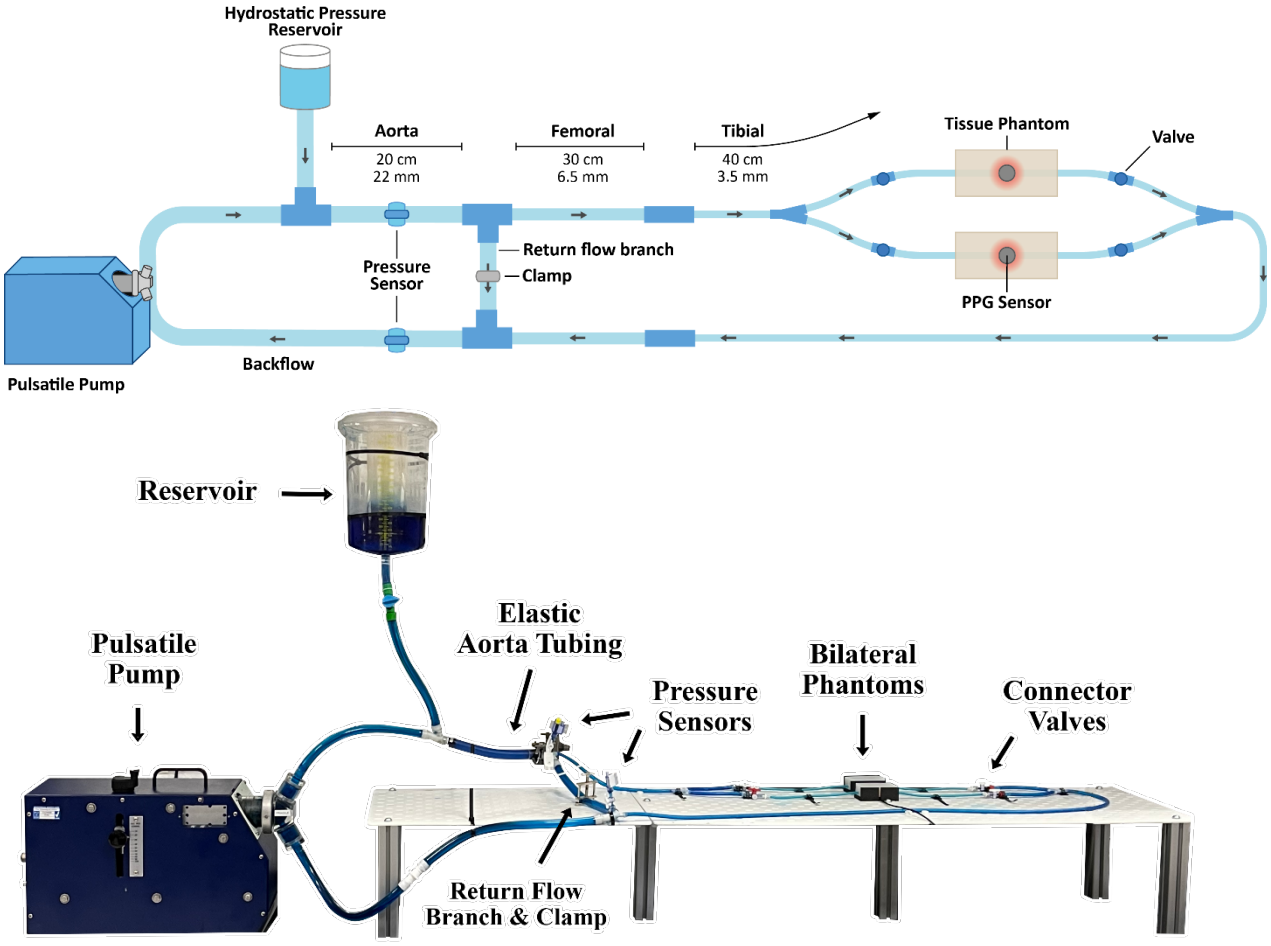

FIGURE 5-1. Bilateral in vitro setup for cardiovascular disease simulation and assessment. Two tissue phantoms simulate a healthy vessel and arterial stiffness. A return flow branch reduces cavitation in the system, with a clamp to adjust pressure.

PUMP

A pulsatile pump (Model 1423 PBP, Harvard Apparatus, US) was used to simulate the human heartbeat and create a pulsatile flow in the system, producing a realistic PPG wave. The pump settings that can be controlled are stroke volume, pumping rate and diastolic/systolic time ratio.

Experiments were run at varying pump settings, described in the protocol, to see how this would affect the results shown in the PPG waves.

RESERVOIR

A hydrostatic pressure reservoir (Unfiltered Cardiotomy Reservoir, Sorin, IT) that would serve two purposes: Firstly, the reservoir would contain the fluid, without filtering out the dye or ink, and allow it to enter the system to be pumped around by opening a valve. This is required as the pump doesn't have a built-in reservoir, so fluid must be added separately with a leak-proof method, usually a separate reservoir connected to the system. Secondly, as the reservoir is positioned higher up, it acts adds hydrostatic pressure to the system, helping the pump to send the fluid all the way around with an increased pressure. This force can be adjusted by repositioning the reservoir at different heights.

TUBING

The arterial model comprised of clear silicone rubber tubing (Hilltop Products, UK). Thin-walled tubing of less than 1 mm was chosen to improve elasticity in the model, mimicking that of the human aorta and other arteries. Elastic tubing also intensified the presence of the dicrotic notch in the PPG wave. Properties considered when deciding tubing options are inner diameter, wall thickness and outer diameter. These were chosen based on the human equivalent artery properties. Tubings with matching properties were used for artery thickness and stiffness experiments. For these experiments, tubing with the same inner diameter but different wall thicknesses were paired, shown in FIGURE 5-2. The tubing from the reservoir was supported by a clamp stand. The rest of the tubing was laid out flat on pegboard. This was originally a vertical board layout, pictured in FIGURE 5-3, before being updated to the lay-flat horizontal pegboard with holes for practicality and spillage collection into the spill tray below.

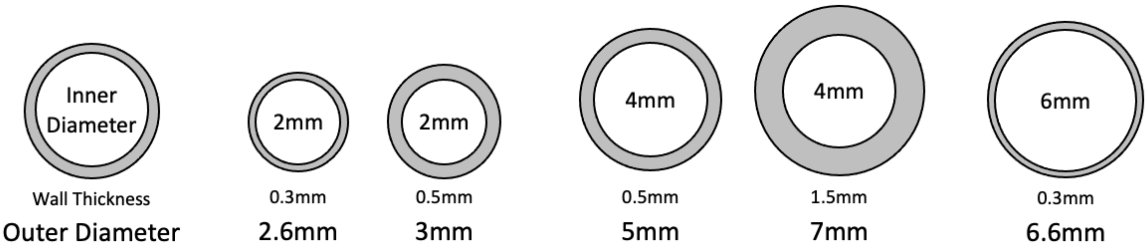

FIGURE 5-2. Silicone tubing, used for simulation of blood vessels in an in vitro model. The different diameters and thicknesses can be chosen based on the human arterial system as well as matching properties for bilateral studies. For example, here tubings with the same inner diameter (ID) but different wall thicknesses (WT) have been paired for vessel thickness and stiffness experiments. Also, similar outer diameters with different inner diameters and thicknesses can be compared, such as the 4mm ID, 1.5mm WT with the 6mm ID, which has a much lower wall thickness but a similar outer diameter.

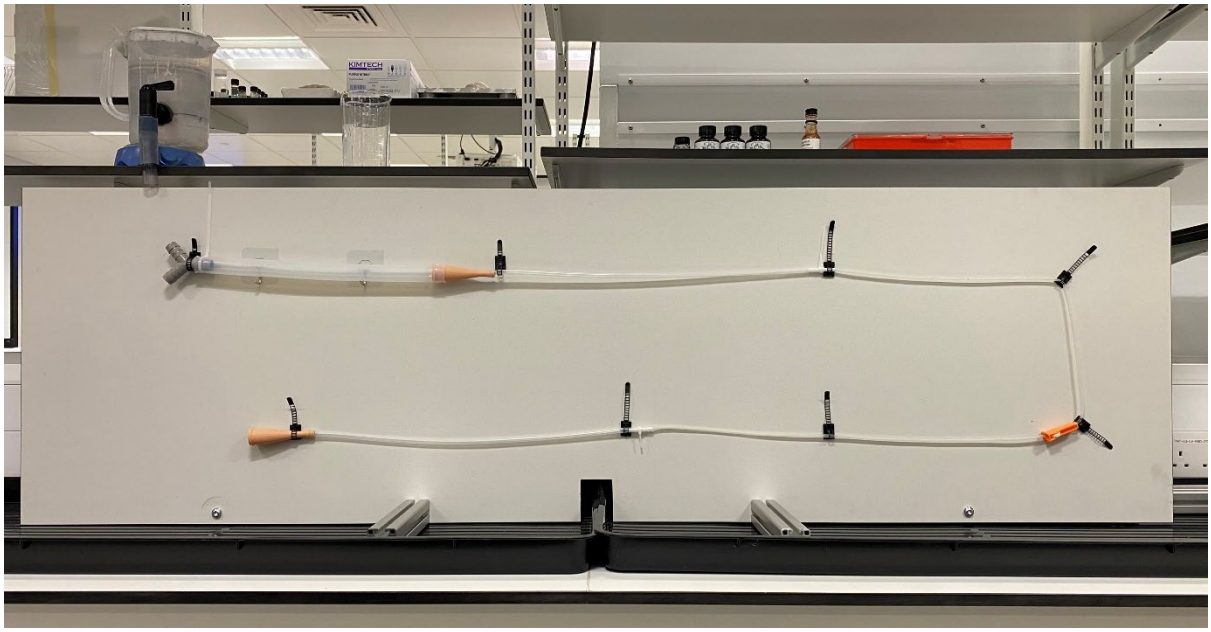

FIGURE 5-3. Previous vertical board and tubing layout design. This original format was tested before being updated to the lay-flat horizontal pegboard design.

CONNECTORS

Due to the varying diameters of tubing and setup requirements such as reservoirs and pressure sensors, custom connectors were often required. These were designed in Fusion 360 (Autodesk, US) and 3D printed using an Elegoo Saturn 3D resin printer (Elegoo, China) with standard photopolymer resin. This allowed for specific diameters, unique connections such as curved and angled Y-connectors, and luer connections for in-line pressure sensor attachment, shown in FIGURE 5-4. For the phantoms, stop-valves were used at each end of the vessel so that the phantoms and vessels could be changed easily with minimal leak, displayed in FIGURE 5-5.

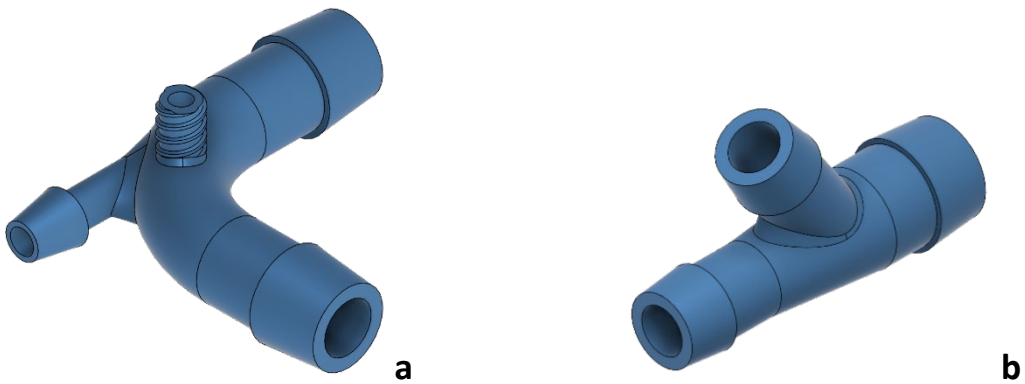

FIGURE 5-4. Designs for custom 3D printed Y-connectors. a) Curved with different diameters for each branch. Featuring a separate luer branch for pressure sensor attachment**. b) Connector for tubing from hydrostatic pressuer reservoir.** Fluid enters the system at an angle so that the laminar flow from the pump is preserved.

FIGURE 5-5. Stop valve with luer connectors. Added to each end of the phantom vessels, making it easier to change phantoms for experiments with minimal leak (Cole-Parmer, UK).

Fluid

To create a simple blood mimicking fluid (BMF), methylene blue dye (Thermo Fisher Scientific, UK) was mixed with deionised water to increase the absorption of red and infrared wavelengths and improve PPG signal quality. As PPG is a volumetric measurement, based on the amount of light absorbed, clear water does not provide strong signals as most of the light passes through without being absorbed. Methylene blue was chosen for the dye due its strong absorption of red light, between 650 nm and 700nm, Figure 5-6a, matching the red light used in the PPG sensor for this experiment and many other PPG devices. The amount of dye used was determined from the literature initially. With a concentration of 20 mg/L, absorbance would be around 1 at 650 nm max (Eduok et al., 2012), shown in Figure 5-6b, indicating a light absorbance of 90% (McNaught and Wilkinson, 1997).

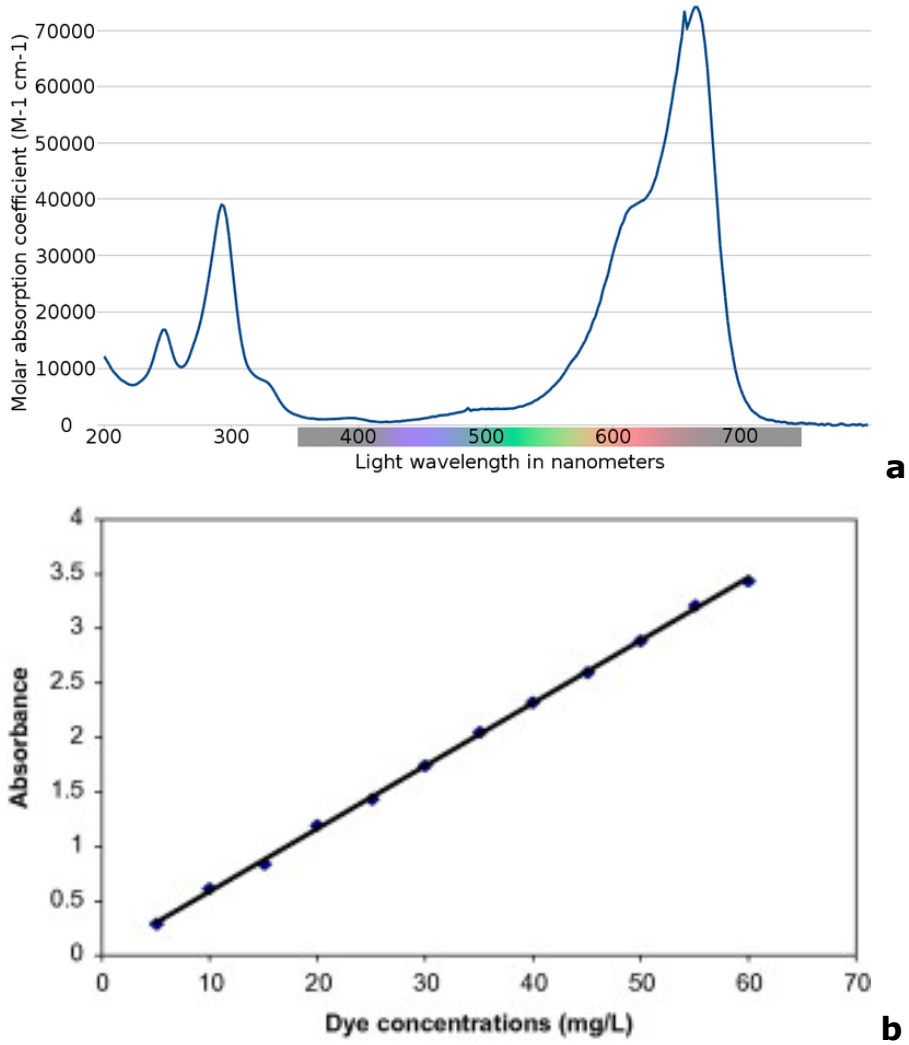

FIGURE 5-6. a) Absorption spectrum of methylene blue. This dye was chosen to simulate blood and improve the PPG quality by increasing the absorbance of the fluid, specifically in the red light region. (Pharmattila, 2019) **b) Methylene blue absorbance of light at different concentrations.** A dye concentration of 20 mg/L was used for an absorbance of approximately 1 at 650 nm max, which is means the fluid absorbs 90 percent of light. This concentration also appeared similar in darkness to human blood. (Eduok et al., 2012)

TISSUE PHANTOM MOULD

Development of the tissue phantoms requires a mould to pour the silicone elastomer in and allow it to set. The mould design displayed in FIGURE 5-7 incorporated removable side doors that allowed the removal of the phantom without breaking the mould or damaging the vessels, making it reusable so that multiple phantoms could be made with the same mould. This design is customisable as the sides can be reprinted with different vessel depths and diameters, without reprinting the entire mould.

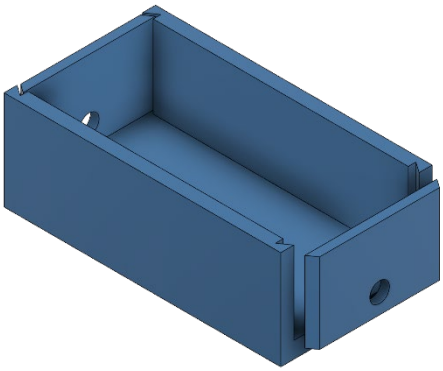

FIGURE 5-7. Tissue phantom mould 3D print design. Removable sides were incorporated so that the cured tissue phantom could be removed without damaging the vessel, allowing a single mould to be reused to make multiple phantoms. The sides are also interchangeable to adjust vessel depth or diameter.

The tissue phantom moulds were also designed in Fusion 360 (Autodesk, US) and 3D printed using an Elegoo Saturn 3D resin printer (Elegoo, China) with standard photopolymer resin. The printing settings were set to a wall thickness of 4 mm, with a thicker base of 5 mm, and a layer distance of 0.05 mm, with a layer setting time of 50 seconds. These settings were found to produce consistent moulds where the walls were fully formed, exhibited in FIGURE 5-8.

FIGURE 5-8. Tissue phantom mould 3D print attempts and final prototype.

TISSUE PHANTOMS

Tissue phantoms were made to simulate the tissue surrounding the blood vessels. PlatSil Gel-00 and Gel-10 silicone rubber (Polytek, USA) were used as the primary silicone media in this work and come as a two-part kit. Mixing part A with part B initiates the silicone curing process. A hardener or deadener additive can be added to adjust the tissue stiffness, and a retarder additive can be added to adjust the cure time.

The phantom manufacturing process involves pouring the mixed two-part silicone into the tissue phantom mould, shown in FIGURE 5-9, with deadener and/or retarder added if required, then allowing it to cure for a minimum of 6 hours, before removing it from the mould, seen in FIGURE 5-10. The standard hardness was 0030 shore (Shore 00 scale), measured using an AD-100-OO Precision Shore Durometer (Checkline Europe, Netherlands), in line with reported porcine tissue hardness (Jafary et al., 2022). With 50% deadener for the soft phantom, this was reduced to below 005 shore. 3% retarder was mixed for both phantoms, to allow more time for mixing, removing bubbles in a vacuum chamber and making multiple identical phantoms in one batch. During the curing process, copper rods were used to maintain the shape of the tubing and prevent it from collapsing when the silicone was poured.

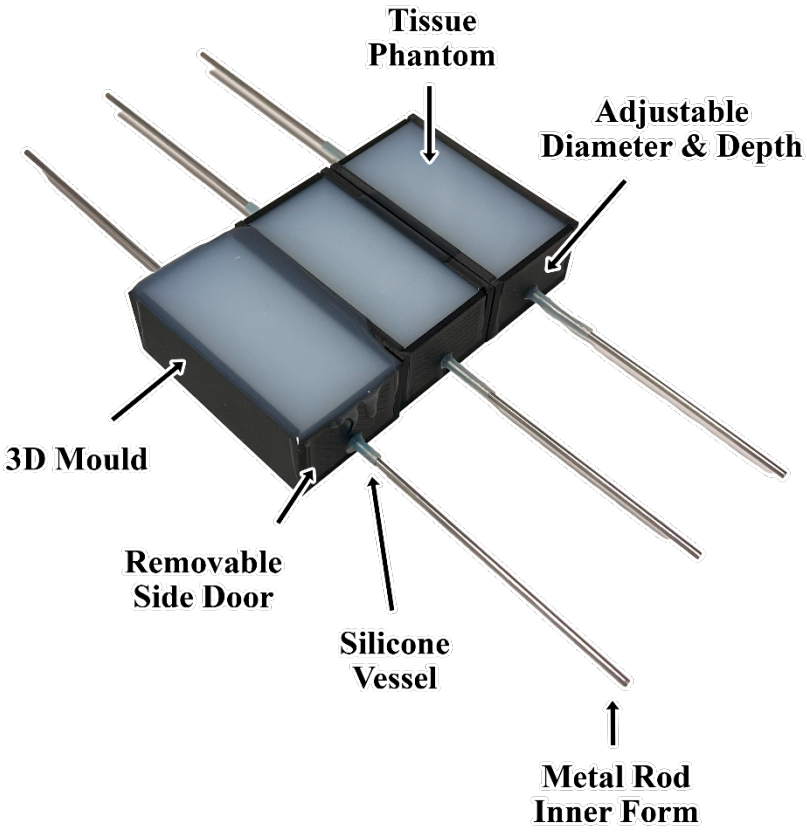

FIGURE 5-9. Tissue phantoms setting inside 3D moulds, with silicone vessels supported by inner metal rod forms.

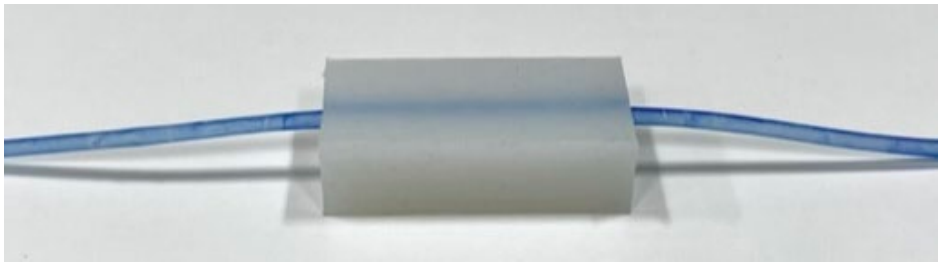

FIGURE 5-10. Cured tissue phantom with vessel tubing.

SENSORS

Two custom-built identical reflectance-mode PPG sensors were used with red and IR LEDs (640 nm and 900 nm) and a photodiode (900 nm peak sensitivity) (BPW34, Osram Germany). These components were situated in a black plastic housing, with a barrier between them, to minimise optical coupling (Pilt et al., 2021).

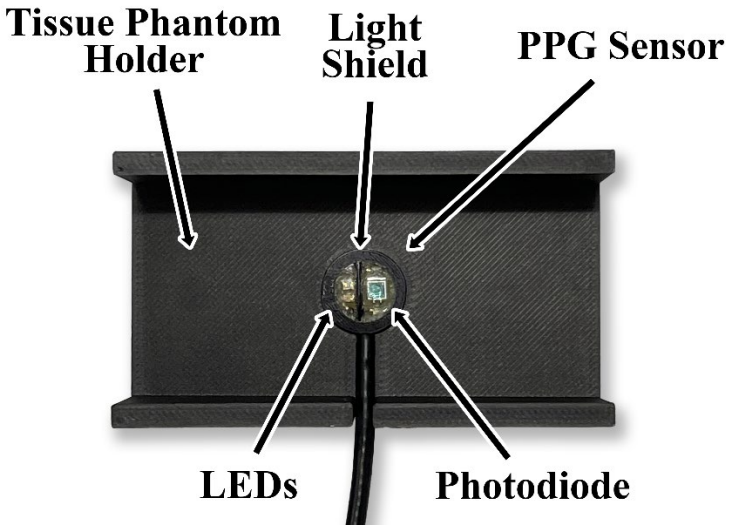

FIGURE 5-11. Custom built PPG-sensor embedded into a custom 3D-printed phantom holder, for consistent signal recordings.

Pressure sensors were positioned at the beginning and end of the system to record reference pressure waveforms during PPG acquisition. In-line pressure sensors (PRESS-S-000, PendoTECH, US) illustrated in FIGURE 5-12, were attached to the custom connector via its luer attachment. These readings were acquired using a data acquisition card (NI cDAQ-9178, National Instruments, US) connected to a computer running LabVIEW (National Instruments, US).

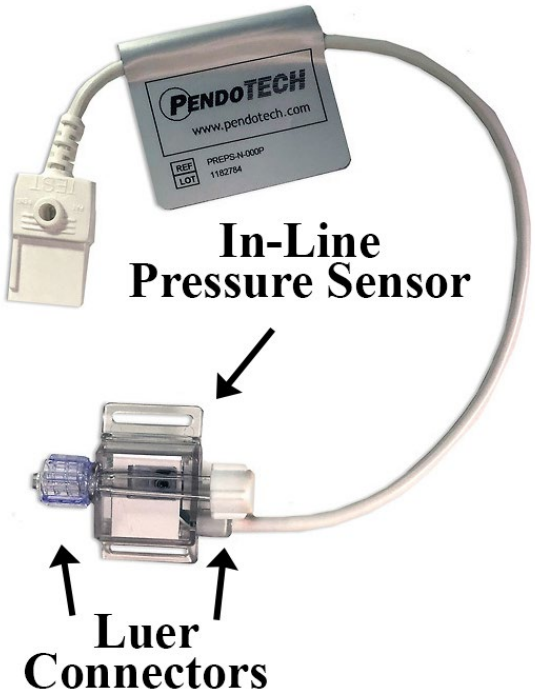

FIGURE 5-12. In-line pressure sensor featuring built-in luer connections. Pressure readings were obtained for reference and validation. (PendoTECH, US).

DATA ACQUISITION

The PPG sensors were connected to a ZenPPG system, seen in FIGURE 5-13, a custom-made dual-channel device for PPG signal acquisition and processing, developed in the Research Centre for Biomedical Engineering at City St George's, University of London (Budidha et al., 2018). From the ZenPPG, the output was sent to a data acquisition card (NI USB-6162, National Instruments, US) connected to a computer running LabVIEW (National Instruments, US).

FIGURE 5-13. The outside and inside structure of the ZenPPG. Used for dual-channel PPG signal acquisition and processing.

Feature Extraction

The feature extraction pipeline was implemented in Python, utilising a custom code developed at City St George's, University of London (Bradley and Kyriacou, 2024) and outlined in Figure 5-14. The first step divides the raw PPG data into fixed-length analysis windows of customisable time periods (set to 10 second windows). Each window is passed through a Chebyshev II 2nd order filter, as suggested in the literature (Liang et al., 2018) to remove low-frequency drift and high-frequency noise while preserving the morphology of the pulse waveform.

Pulse detection is then performed, illustrated in Figure 5-15, using a moving-average baseline to locate crossing points, which indicate peak and trough regions. Within each region, peaks and troughs are identified and refined by removing physiologically implausible or anomalous beats based on amplitude, prominence and inter-beat intervals. For each accepted pulse, the onset, systolic peak and end points are stored, allowing calculation of morphological, temporal and derivative-based features. These include amplitude, width, rise and decay times, areas under the curve and ratios derived from these measures. Features are combined with experimental data and stored in a long-format structured CSV output for statistical analysis.

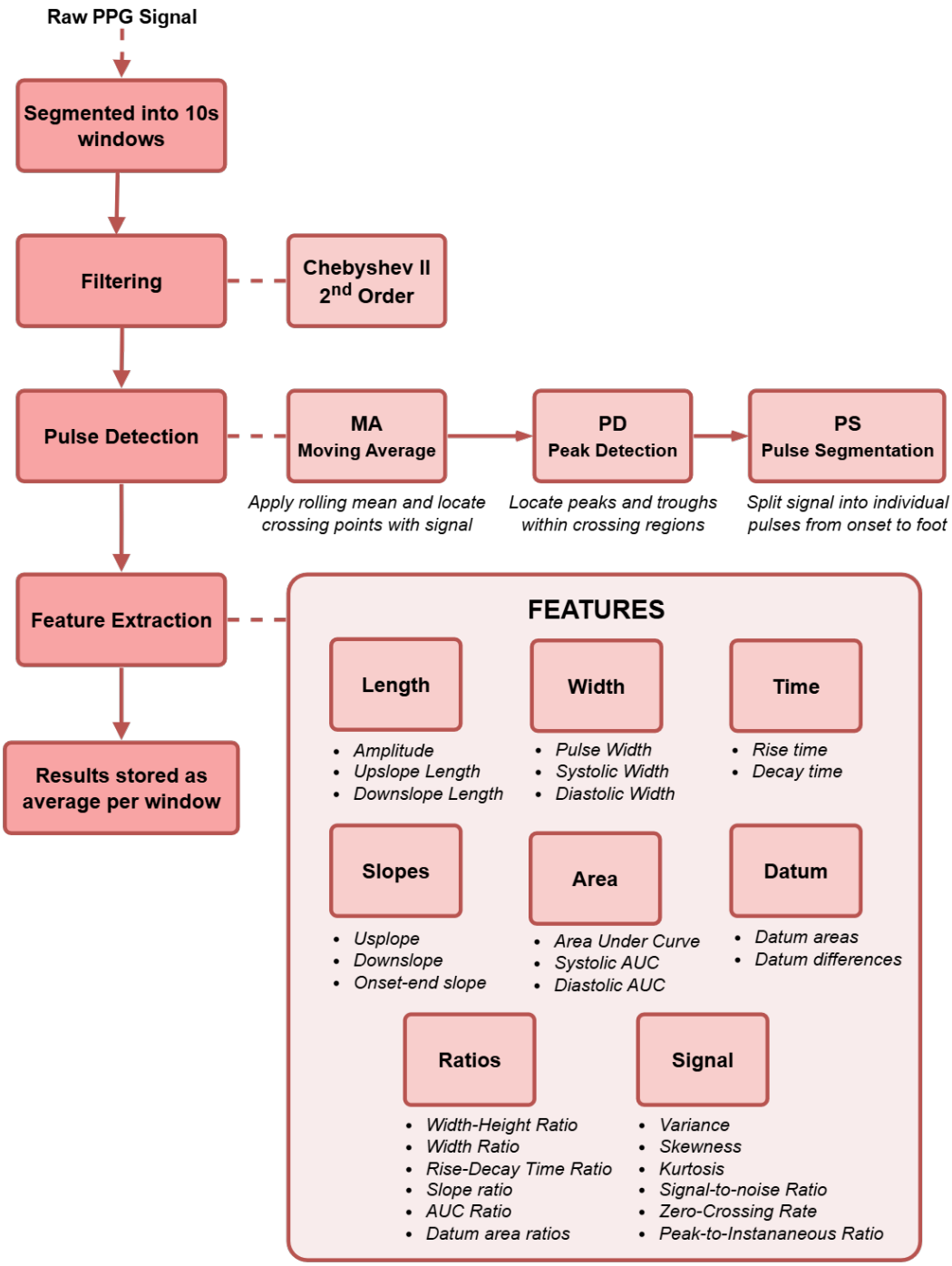

FIGURE 5-14. Overview of the PPG feature extraction pipeline. Raw PPG data is segmented into 10 second windows and filtered with a bandpass Chebyshev II 2nd order filter. Pulses are detected through a moving average baseline which produces crossing points with signal, combined with a peak detector to indicate individual pulses. Finally, based on the onset, peak and foot points, features are a range of features are extracted including morphological, temporal, slope and area-based features. These are stored as averages for each window.

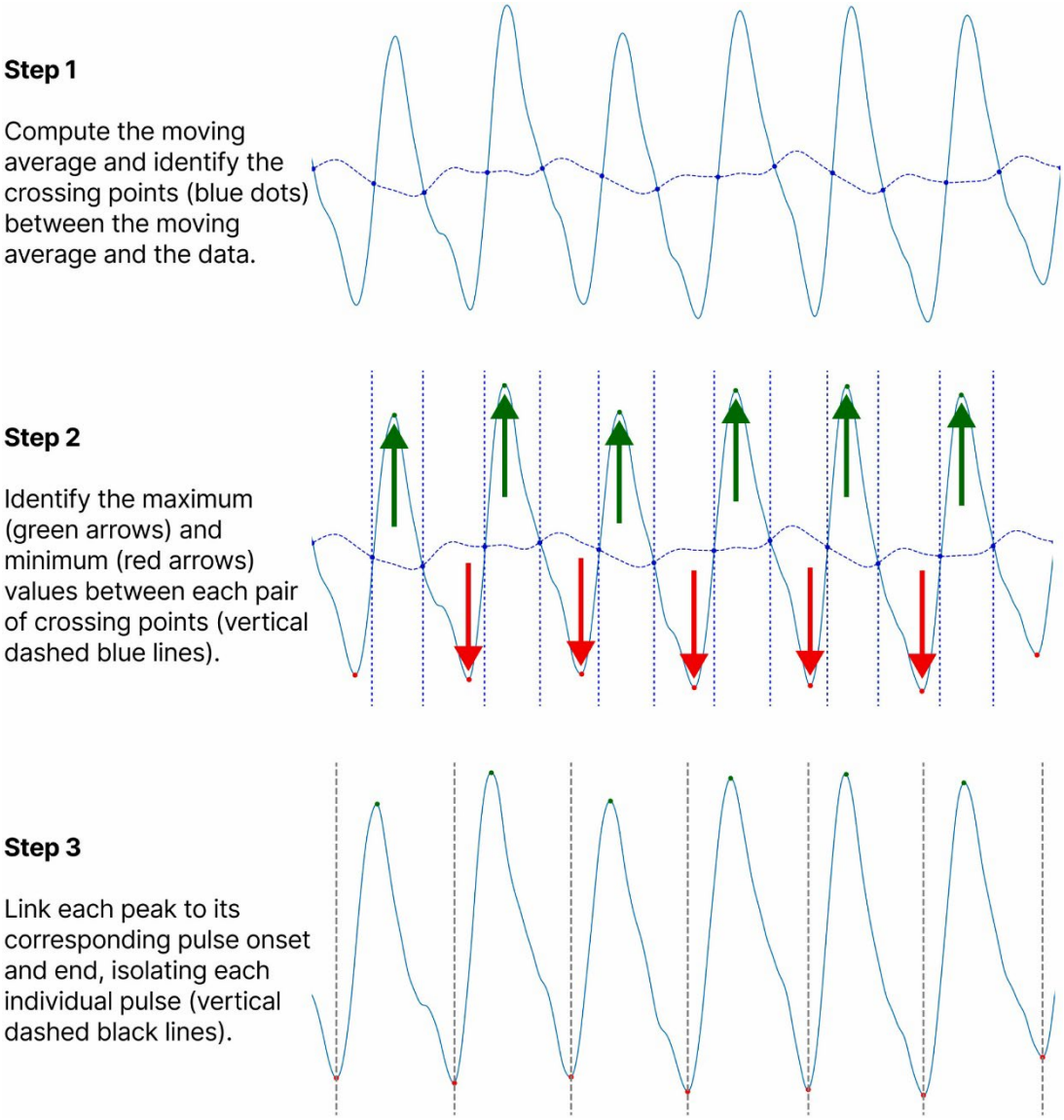

FIGURE 5-15. Illustration of the pulse detection process. (1) Apply a moving-average baseline and identify crossing points (blue dots) between the baseline and the filtered signal. **(2)** Within each region bounded by crossing points, locate the maximum (green arrows) and minimum (red arrows) values to identify candidate peaks and troughs. **(3)** Pair each detected peak with its preceding and following troughs to define the pulse onset and end, thereby isolating individual cardiac pulses, (Bradley and Kyriacou, 2024).

EXPERIMENT PROTOCOL

Two vessel-tissue phantoms in the bifurcation setup, depicted in FIGURE 5-16, were run through a protocol to simulate changing arterial stiffness, heart rate and stroke volume. Firstly, identical phantoms of shore 0050 hardness were used to verify that both sides of the bifurcation have statistically similar fluid flow properties. Next, one of the phantoms was changed with the lower shore 0025 hardness phantom. This difference in shore hardness simulates vessels of varying stiffness in human anatomy, for example during atherosclerosis. Finally, the other phantom was changed so there would be two shore 0025 phantoms. Again, this was to verify the signals and features detected from identical phantoms, to ensure that they would be the same. Therefore, we could be sure that any detected changes in the signal features were caused by the change in phantom tissue stiffness.

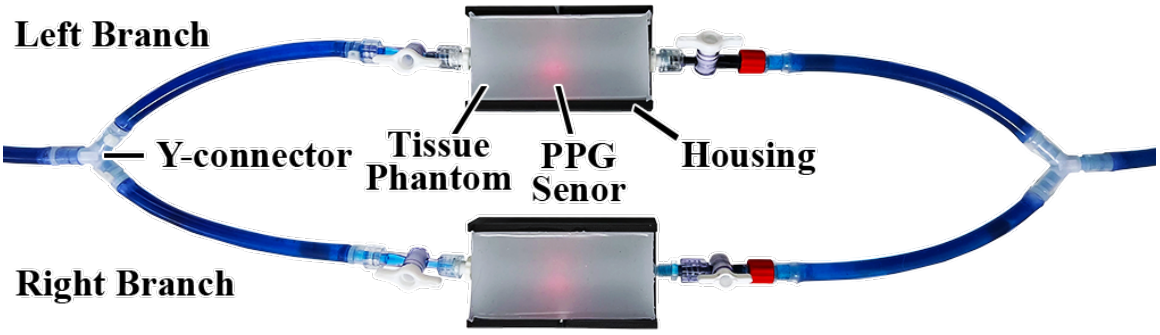

FIGURE 5-16. Tissue phantoms in bilateral configuration. 3D-printed housing situates PPG sensors for simultaneous measurement.

The experiment was run at varying heart rates of 60, 80 and 100 beats per minute. These values were chosen to simulate human heart rates during rest and physical activity, and also to induce changes in the PPG signal. A similar decision was taken with stroke volumes of 15, 20 and 25 ml/stroke. The phase ratio of the pump for the systolic/diastolic phase was set to 25/75 to create a steeper gradient in one phase of the PPG, rather than a sinusoid.

PPG signals were acquired from two phantoms at a time in a bifurcation setup, consisting of varying tissue hardness as a proxy for vessel stiffness.

Each phantom was inside a custom 3D-printed case. This held the phantom in place, resting on the housed PPG sensor within the case. The custom-built sensors were connected to the dual-channel ZenPPG device, which allows the accessing and recording of raw AC and DC PPG signals (Budidha et al., 2018). These signals were sent through a data acquisition card to be processed and recorded in LabVIEW. Each sensor produced and detected red and infrared wavelengths, producing two channels for each phantom.

Signals from all the experiment runs were processed for feature extraction (Bradley and Kyriacou, 2024) and this data was arranged into a table of experiment variables (such as stiffness, heart rate, stroke volume) and features (such as amplitude, half peak width and upslope). This was then analysed in MATLAB (The MathWorks, USA) using Kruskal-Wallis one-way analysis of variance for statistical differences in the features for each variable.

5.3 Results

PPG & Pressure Signals

Representative pressure waveforms measured at the beginning and end of the rig are shown in Figure 5-17. Both sensor locations exhibited a stable pulsatile waveform over repeated cycles, with clear systolic peaks and diastolic decay. While there were slight differences in waveform shape between the two measurement sites, the overall morphology was preserved, indicating that the pulsatile pressure generated by the pump was maintained through the system during PPG acquisition.

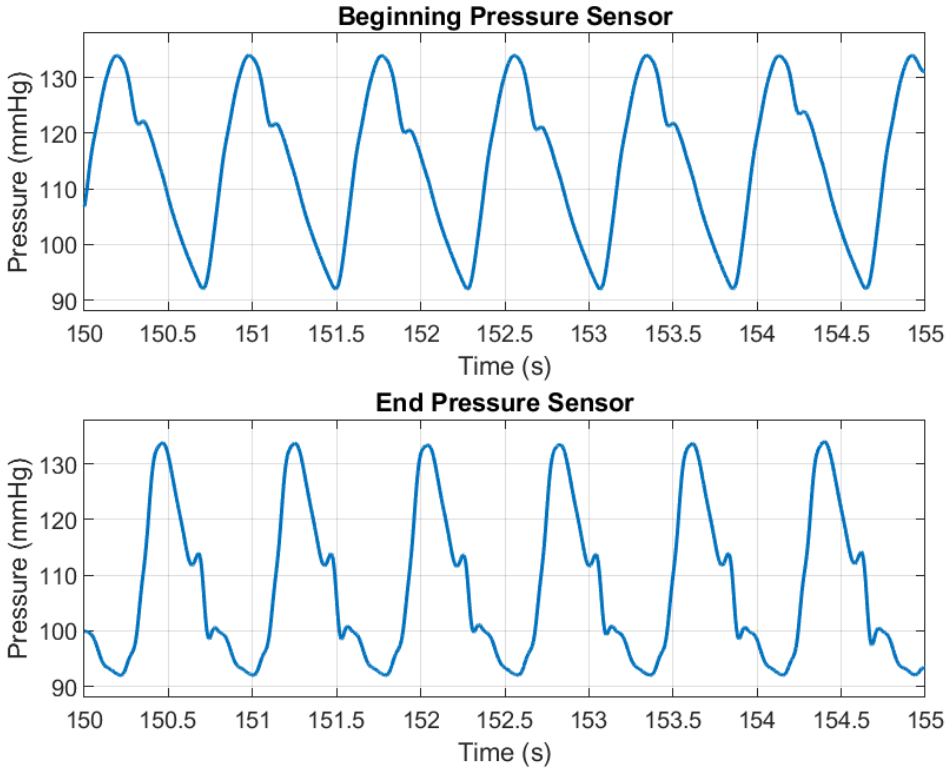

FIGURE 5-17. Representative pressure waveforms measured at the beginning and end of the in vitro system during PPG acquisition. Both traces show a stable pulsatile pressure waveform with clear systolic and diastolic phases, confirming that pulsatility generated by the pump was preserved through the model.

Different filter types were compared before conducting feature extraction of the signals. The raw PPG signal is the data acquired with LabVIEW, from the Data Acquisition Card which was connected to the ZenPPG device. Two custom-built PPG sensors were connected to the dual-channel ZenPPG, each with a red and infrared signal. Butterworth, Chebyshev and Elliptic filters were compared for effectiveness in removing noise while maintaining features of the PPG signals. These features were the peaks and notches of the PPG, while the foot required smoothing as there was more noise in that area. The Chebyshev II 4^{th} order filter is seen to excel in these areas, highlighted in FIGURE 5-18. All the filters reduced noise, with the Chebyshev II filter producing a smoother signal at the peaks and troughs yet maintaining the notch. This filtered signal was used in the feature extraction process.

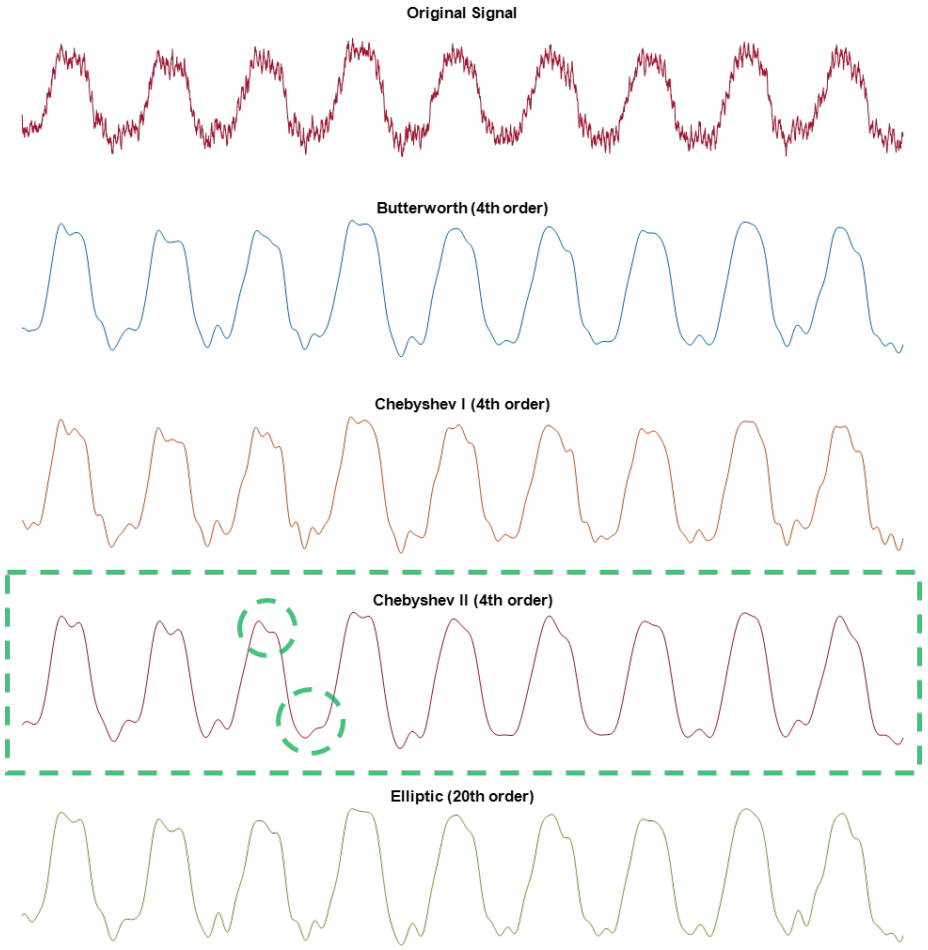

FIGURE 5-18. Comparison of filter types on the raw PPG signal.

Signals received from the shore 0050 phantom and the shore 0025 phantom were compared for any visual differences. As seen in FIGURE 5-19, there are no visible differences between the phantoms in either the red or infrared channels, as the signals appear similar. The peaks, notches and feet of the signals can be identified, suggesting that feature extraction is possible, which is conducted in the next section. The red and infrared signals initially appear similar, however statistical analysis later revealed significant differences between them.

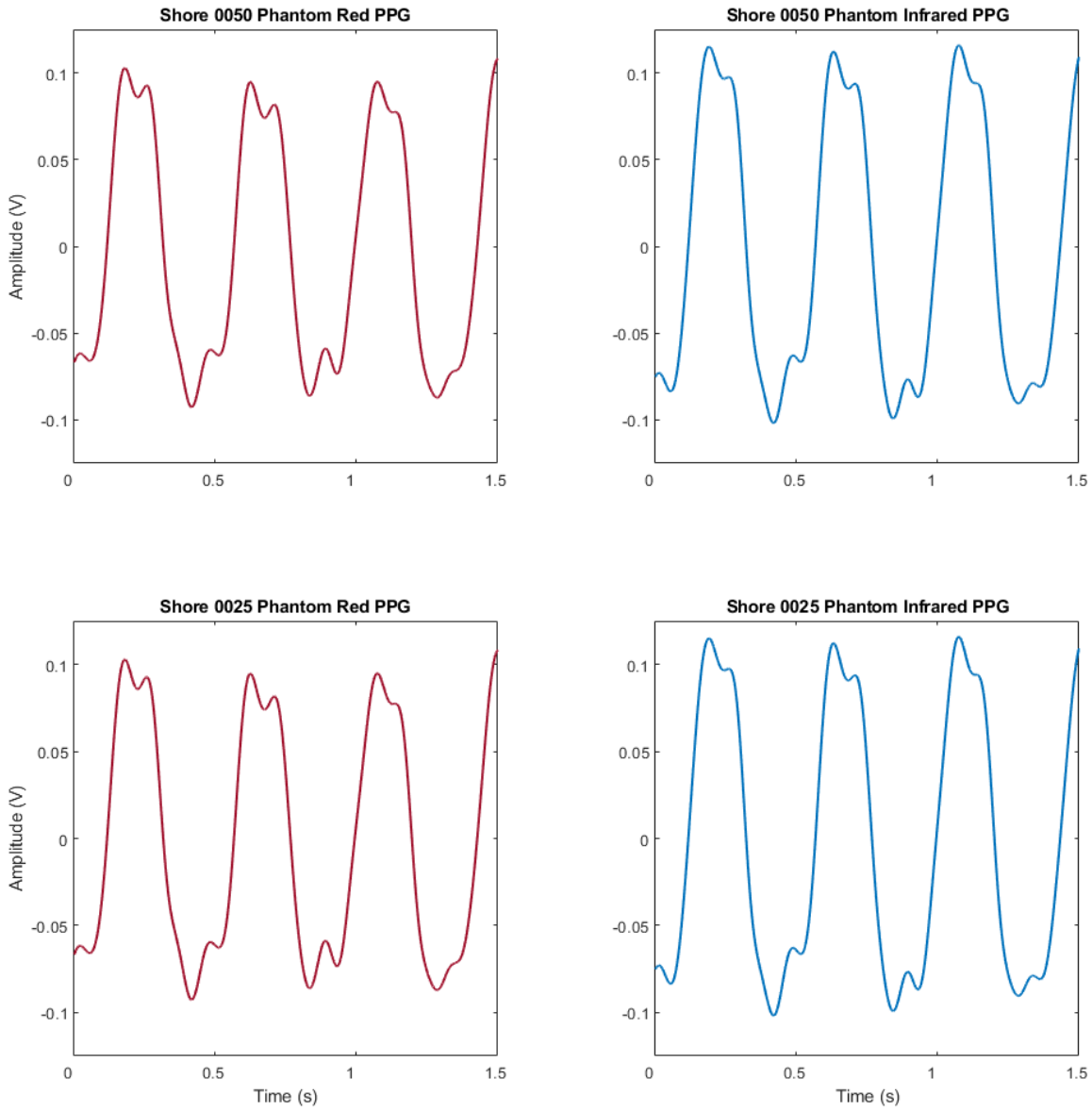

FIGURE 5-19. Red and Infrared PPG signals from phantoms of different stiffnesses. Shore 0050 and shore 0025 phantoms were tested.

The PPG signals were also inspected in terms of varying heart rate and stroke volume. The experiment was conducted at heart rates of 60, 80 and 100 beats per minute. Displaying the PPG signals at these varying heart rates in FIGURE 5-20 showed significant noise occurring at 60 bpm, suggesting the need for more elastic vessels. This was reduced as heart rate increased to 80 bpm, but still present. At 100 bpm, the noise is only seen at the foot of the PPG wave. As such, PPG signals from the 100-bpm protocol were prioritised for the feature extraction and statistical analysis.

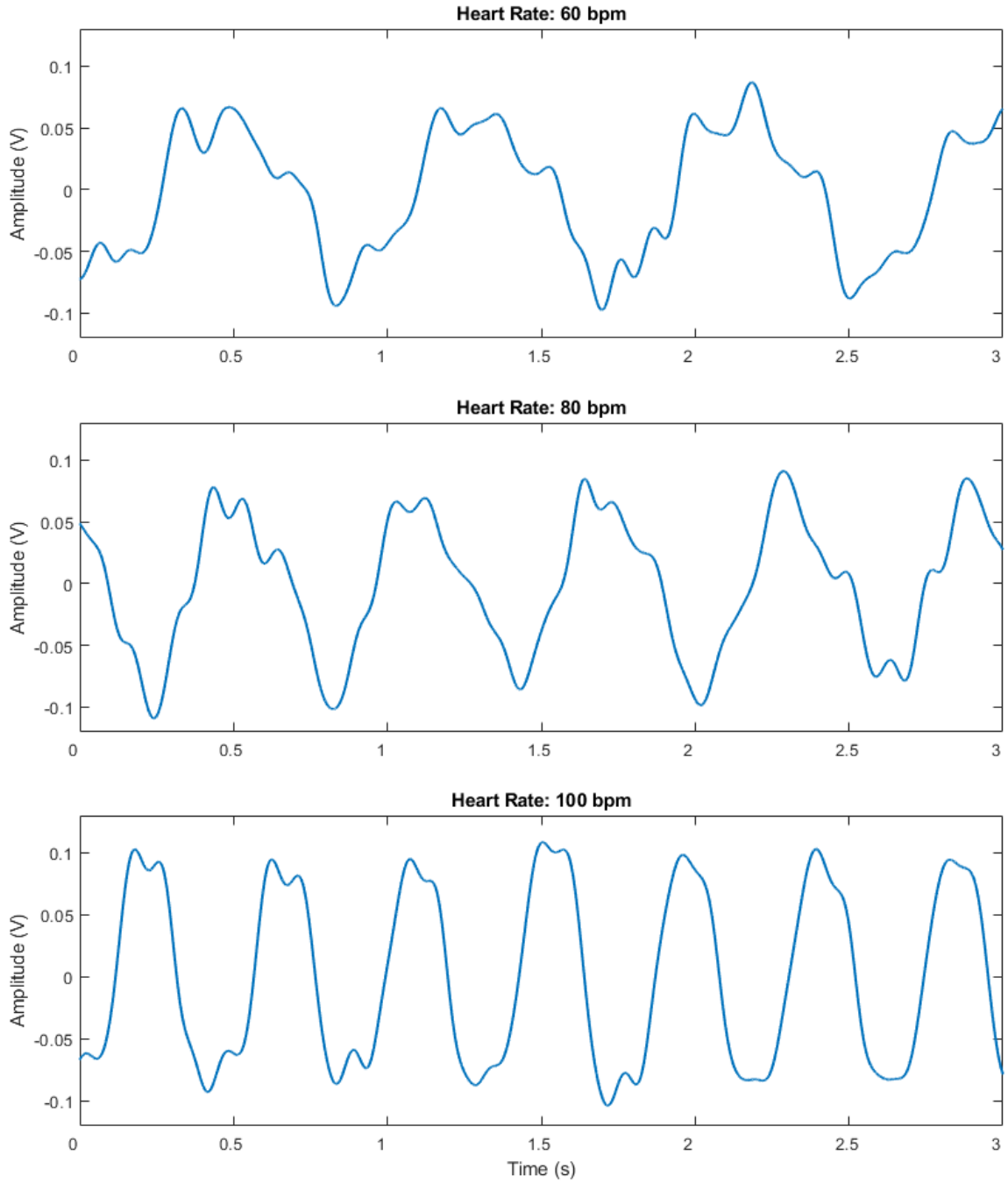

FIGURE 5-20. PPG signals at varying heart rates.

Comparing PPG signals obtained during different stroke volume settings indicated a small change in amplitude, shown in FIGURE 5-21. The same analysis was conducted on a tissue phantom with no inner vessel, which showed a greater starting amplitude as well as difference in amplitude as stroke volume increased.

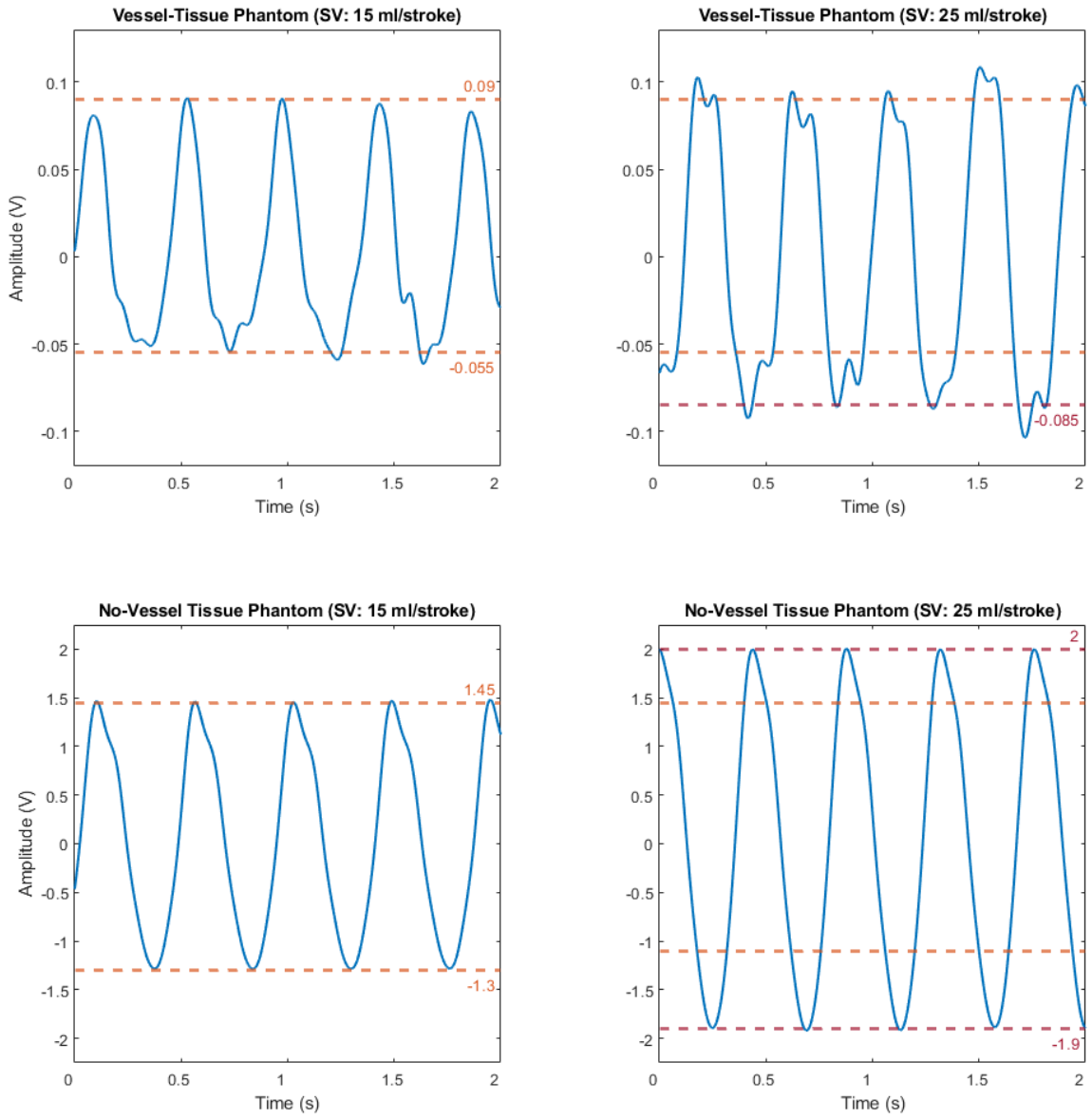

FIGURE 5-21. PPG signals at varying stroke volumes. 15 ml, left and 25 ml/stroke, right; obtained from a vessel-tissue phantom (top) and a tissue-only phantom with no inner vessel (bottom).

Feature Extraction

After observing the filtered signals at varying heart rates and stroke volumes, the custom feature extraction algorithm was tested. Amplitude and half peak width were successfully detected, indicated in Figure 5-22. Upslope and downslope gradients were also detected, along with rise time and decay time, displayed in Figure 5-23. Finally, area under the curve was measured and split into the systolic and diastolic phases, in Figure 5-24.

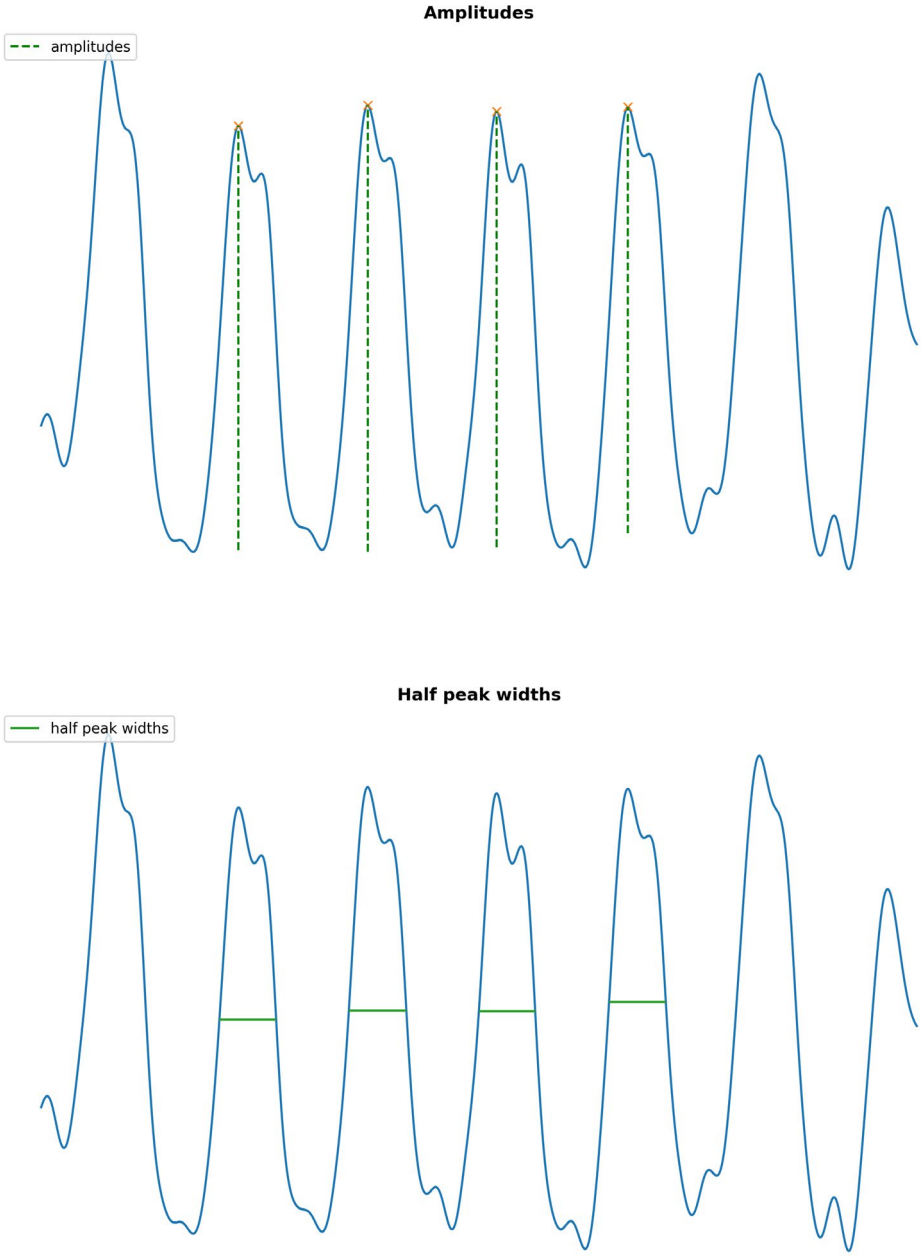

Figure 5-22. Feature extraction of amplitude and half peak width from PPG signal.

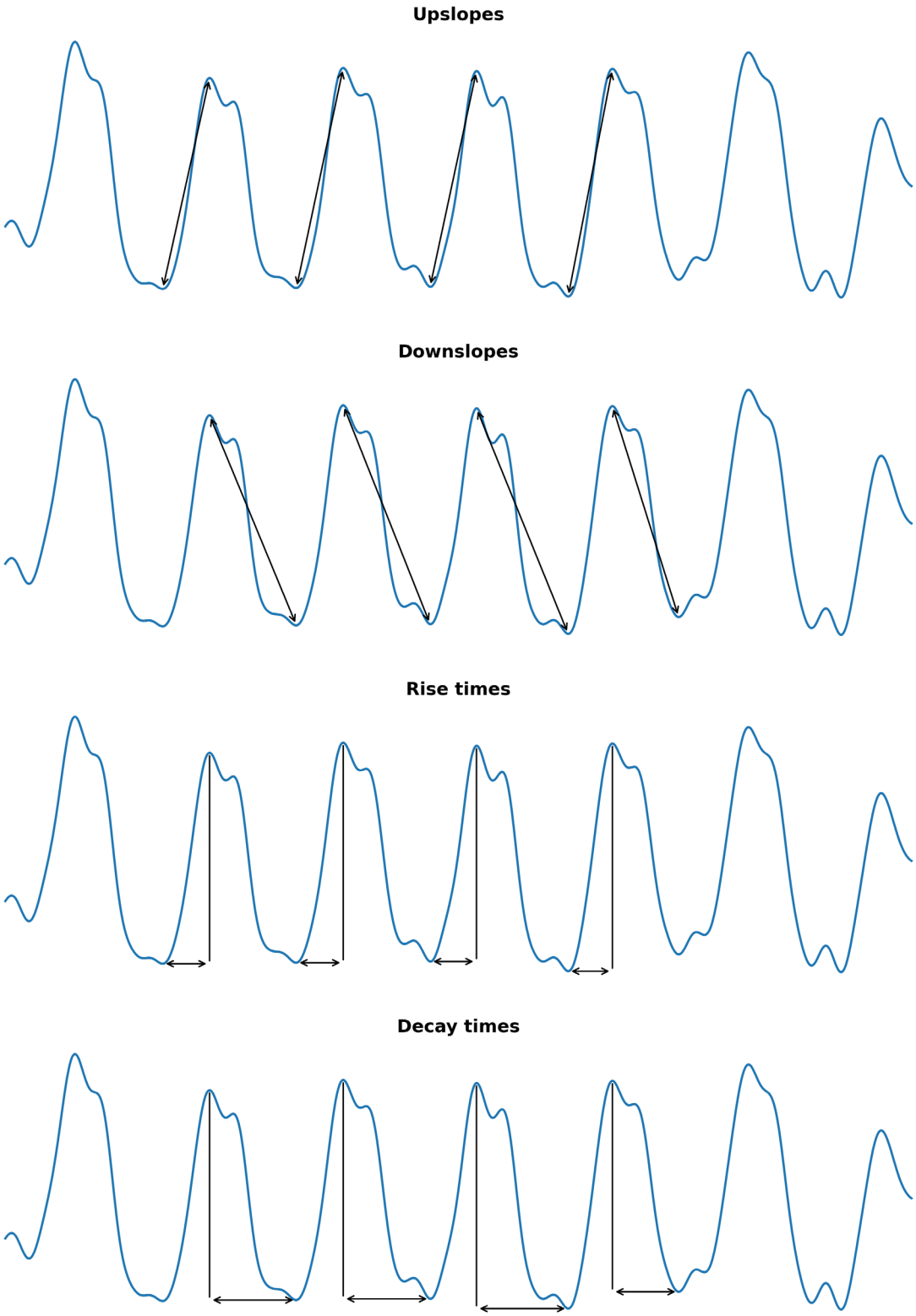

FIGURE 5-23. Extraction of upslopes, downslopes, rise times and decay times.

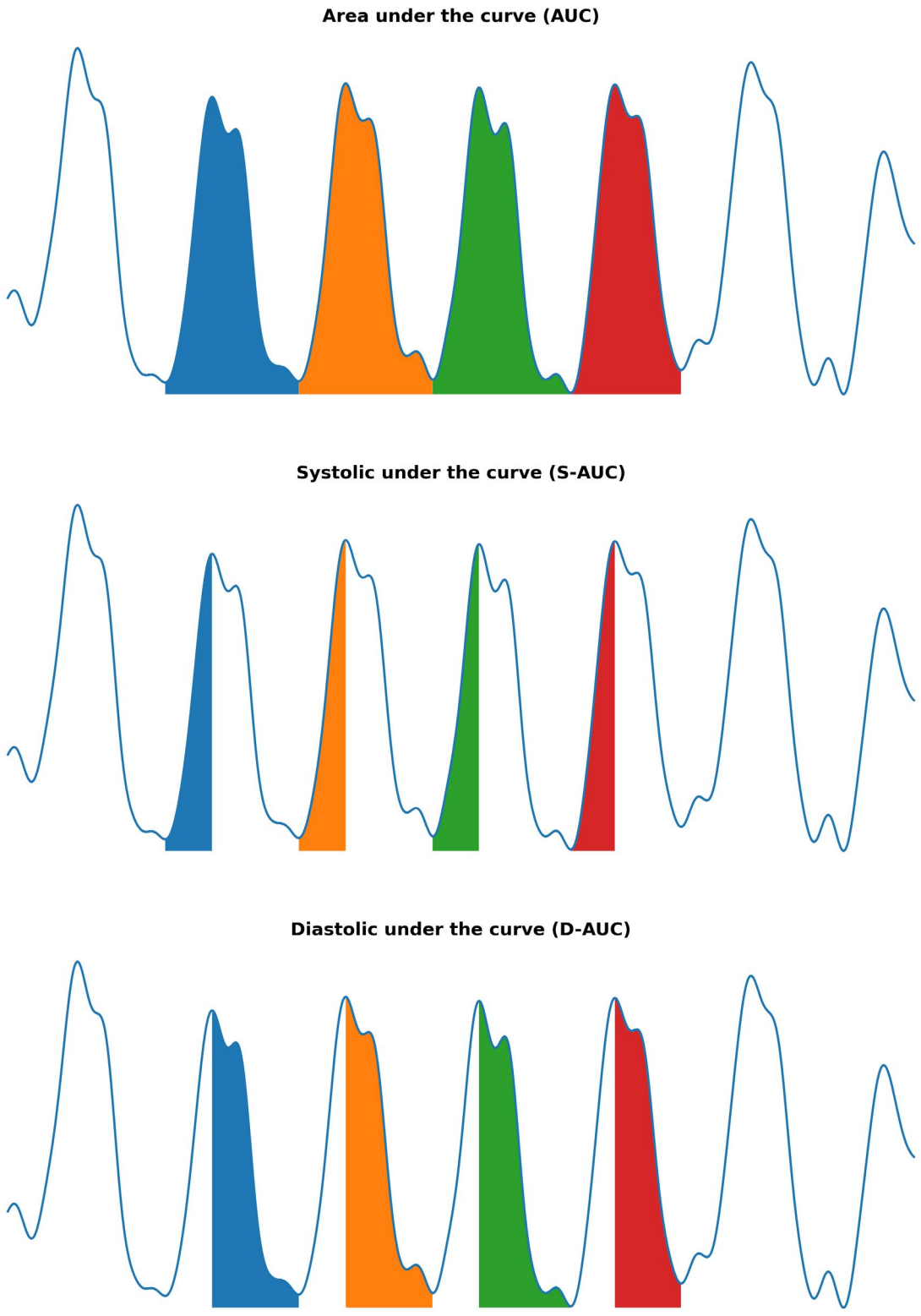

FIGURE 5-24. Extraction of area under the curve, divided into systolic and diastolic areas.

Statistical Analysis

With the filtered signals and feature extraction verified, statistical analysis was carried out on the resultant features from the algorithm. The method for significant difference calculation used was the Kruskal-Wallis test. The results for the phantom stiffness comparisons are shown in Figure 5-25 and Figure 5-26, with corresponding p-values listed in Table 5-1 and Table 5-2. For the red PPG signals, *amplitude*, *upslope*, *downslope*, *rise time*, *decay time* and the *area*-based features showed no significant differences between the identical and mixed-phantom conditions; while *half peak width* was the only feature that showed a significant difference, however this was present even for identical phantoms. For the infrared signals, *amplitude* and *total* and *diastolic area under the curve* remained comparatively stable, whereas half *peak width* and *rise time* showed significant variation, which was again seen in the identical phantoms as well.

The effects of changing heart rate and stroke volume are shown in Figure 5-27 and Figure 5-28. Increasing heart rate produced the clearest and most consistent feature changes, with lower *half peak widths*, *rise time*, *decay time* and *area*-based measures, together with steeper *upslopes*, reflecting the visually narrower and more frequent pulses seen in the waveform traces. In contrast, stroke volume produced smaller overall changes, although higher stroke volumes were associated with an increase in *half peak width* and modest increases in *total* and *diastolic area under the curve*. These results show that the feature extraction pipeline was sensitive to controlled haemodynamic changes in heart rate and stroke volume, while the stiffness contrast used in this chapter produced only limited separation across most extracted features.

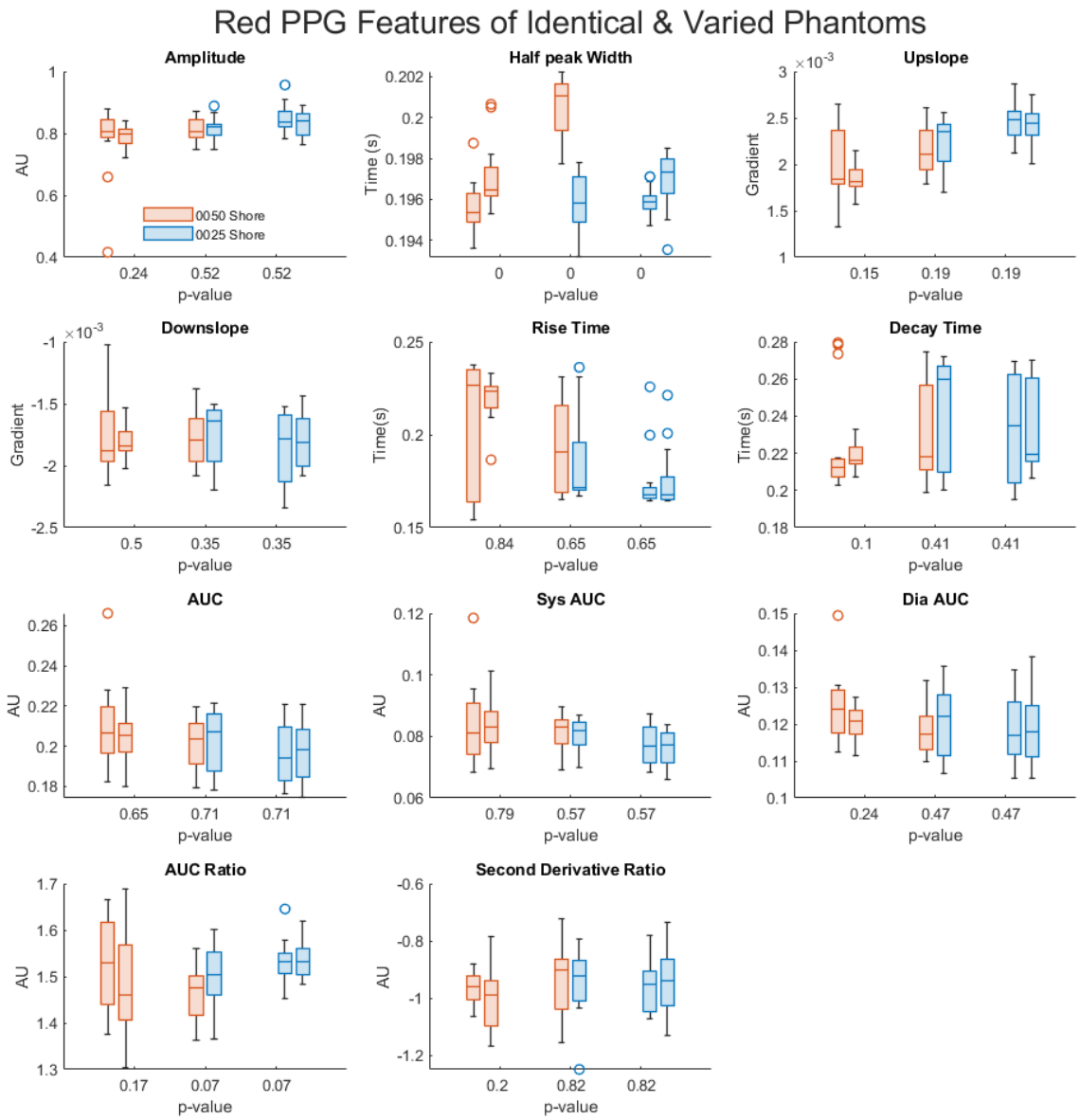

FIGURE 5-25. Boxplots and p-values of Red PPG features extracted from identical phantoms and phantoms with a varied tissue stiffness of 0025 and 0050 shore hardness.

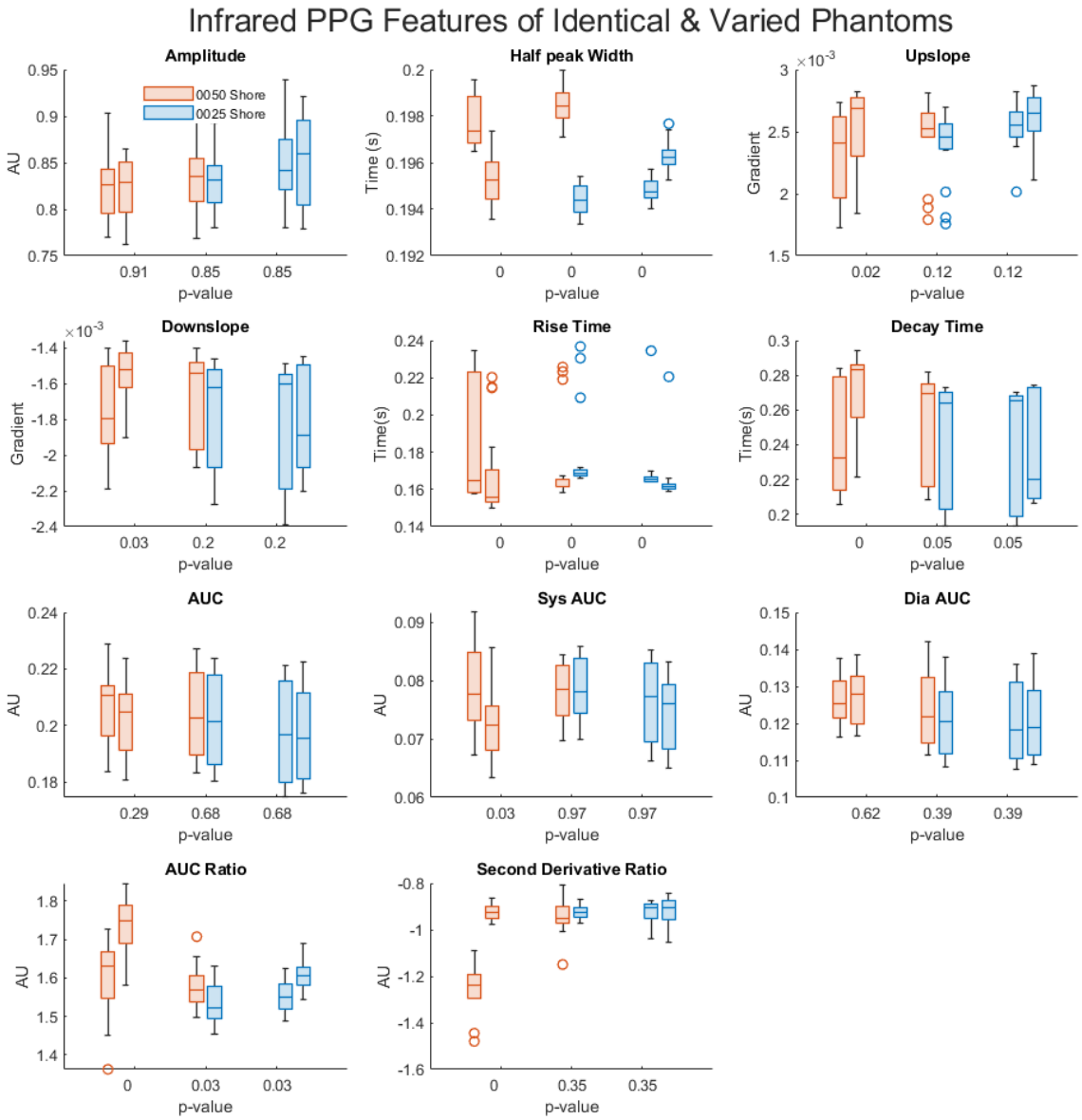

FIGURE 5-26. Boxplots and p-values of Infrared PPG features extracted from identical phantoms and phantoms with varied tissue stiffness.

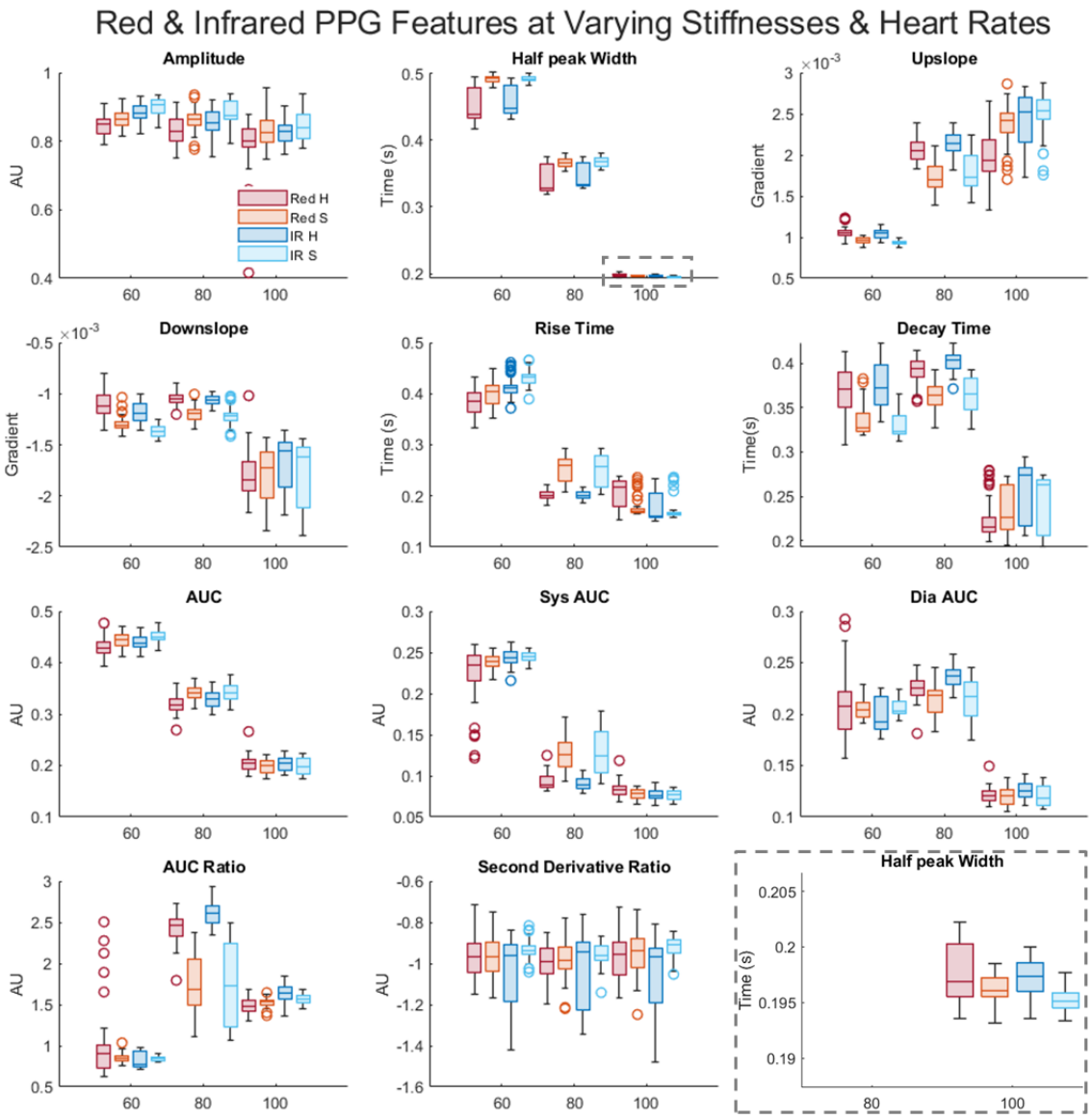

FIGURE 5-27. Boxplots of red and infrared PPG features from phantoms of varied stiffnesses, at a range of Heart Rates. The shore 0050 and 0025 phantoms have been abbreviated to 'H' and 'S' for hard and soft.

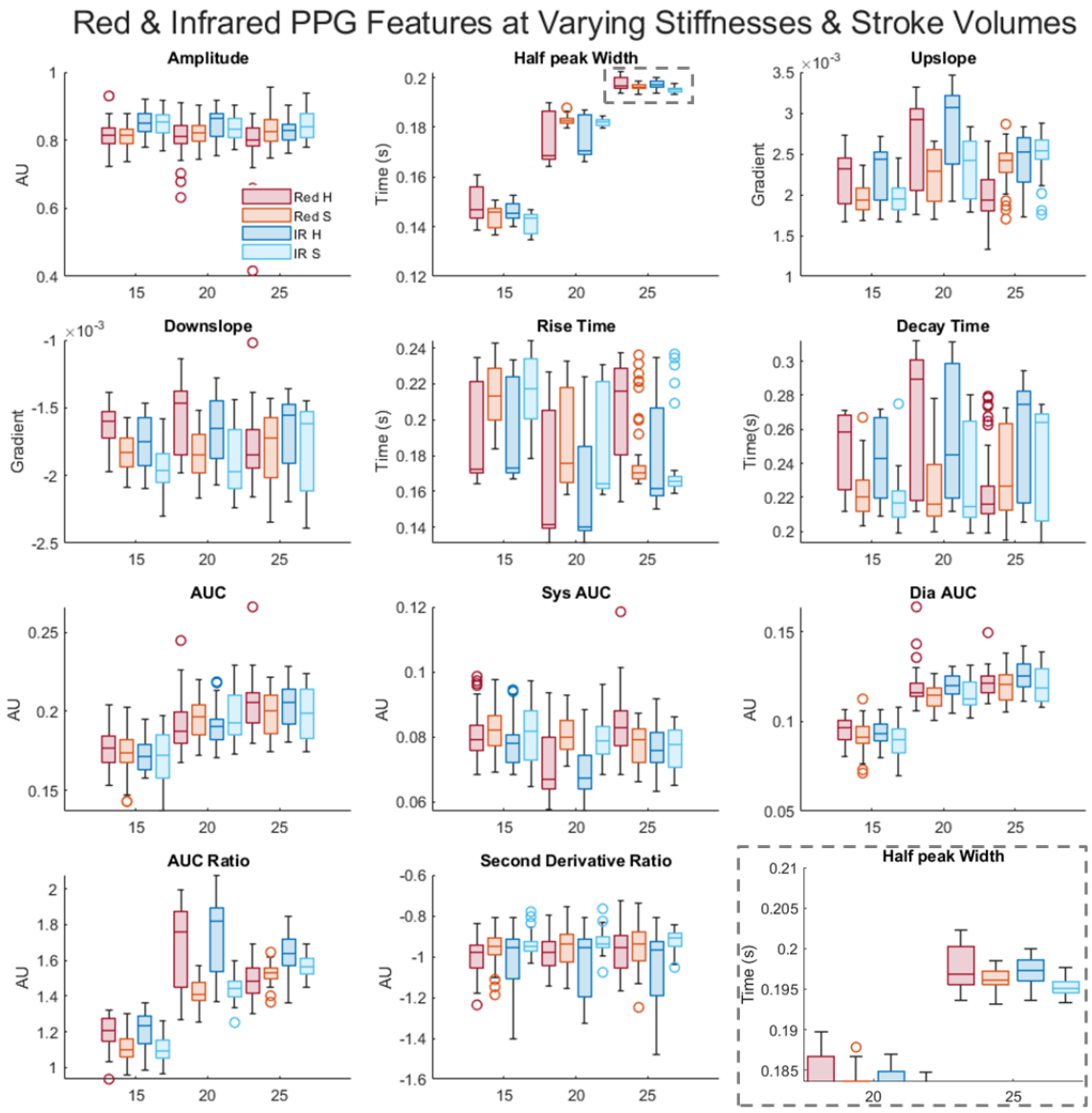

FIGURE 5-28. Boxplots of red and infrared PPG features from phantoms of varied stiffnesses, at a range of Stroke Volumes.

TABLE 5-1. P-values of Red PPG Features from Identical and Varying Phantoms. The shore 0050 and 0025 phantoms have been abbreviated to 'H' and 'S' for hard and soft. The PPG features extracted are half peak width, upslope, downslope, rise time, decay time, area under the curve (total, systolic and diastolic and ratio between them) and second derivative (acceleration) PPG ratio.

	Amp	HPW	US	DS	RT	DT	AUC	S-AYC	D-AUC	AUC Ratio	APG Ratio
HH	0.24	0.00	0.15	0.50	0.84	0.10	0.65	0.79	0.24	0.17	0.20
HS	0.52	0.00	0.19	0.35	0.65	0.41	0.71	0.57	0.47	0.07	0.82
SS	0.52	0.00	0.19	0.35	0.65	0.41	0.71	0.57	0.47	0.07	0.82

TABLE 5-2. p-values of Infrared PPG Features from Identical and Varying Phantoms.

	Amp	HPW	US	DS	RT	DT	AUC	S-AYC	D-AUC	AUC Ratio	APG Ratio
HH	0.91	0.0001	0.02	0.03	0.001	0.002	0.29	0.03	0.62	0.00	0.00
HS	0.85	0.0001	0.12	0.20	0.002	0.05	0.68	0.97	0.39	0.03	0.35
SS	0.85	0.0001	0.12	0.20	0.002	0.05	0.68	0.97	0.39	0.03	0.35

5.4 DISCUSSION

PPG signals were acquired from two phantoms in a bifurcation setup. Firstly, phantoms with identical properties were used to validate the system. Followed by phantoms with different tissue hardnesses as a proxy for vessel stiffness. Before analysing the signals obtained, the output was verified in LabVIEW and inspected in MATLAB. The raw signal, seen in FIGURE 5-18, required filtering. Filters commonly used in the literature for PPG processing where tested: Butterworth, Chebyshev I & II, and Elliptic (Liang et al., 2018). Based on the skewness quality index of nine types of filters with ten different orders, Liang et al found the Chebyshev II filter to improve signal quality the most effectively and that its optimal in the 4th order. As the main method of analysis in this study is feature extraction, it was important that the filter would remove noise while maintaining the features of the PPG signal at the same time. As such, the filters mentioned were tested to observe how they affect the signal features from this specific

experiment. The features considered were the peaks and notches of the wave. The foot of the wave was consistently noisy, so it was important that the filter would smooth this area, while keeping the peak and notch at the top of the wave. The highlighted areas in FIGURE 5-18 confirm that the Chebyshev II filter excelled in filtering and maintaining these features. The peak is distinct on many of the Chebyshev II waves, with the notch also present. The Chebyshev I filter did not filter the peak enough, resulting in noise at the top of the wave and sometimes a third notch. The Butterworth and Elliptic filters performed as well as Chebyshev II in the peak and dicrotic notch but produced fewer smooth troughs in the signal. Based on this visual observation, combined with the skewness quality index results by Liang et al, the Chebyshev II filter was applied, in the recommended 4th order, to the data before feature extraction (Liang et al., 2018).

The signal was visually inspected in MATLAB before the feature extraction process, to observe changes with varying tissue stiffness, heart rate and stroke volume. Before analysing the features, signals were displayed from the two different phantoms to see if there were any visual differences or indications of the change in tissue stiffness. As seen in FIGURE 5-19, there are no visible differences between the signal from the shore 0050 and 0025 phantoms. Feature extraction is employed to discern if this can be confirmed statistically. In terms of wavelength, the red and infrared signals appear similar, but there are subtle differences in the dicrotic notch, which is flatter in the infrared signals of both phantoms compared to the red signals. This is reflected by the differences in the statistical results and p-value tables of the features from the two wavelengths.

Representative pressure waveforms measured at the beginning and end of the rig are shown in FIGURE 5-17. Both traces retained a clear pulsatile morphology over repeated cycles, confirming that stable pulsatile conditions were maintained during PPG acquisition. A small change in waveform shape was seen between the two locations, consistent with pressure pulse propagation through the tubing and bifurcation. Although

direct flow waveforms were not recorded, these pressure traces provided a useful haemodynamic reference for the experimental system.

When comparing how the signal changed at different heart rates, it is clear from FIGURE 5-20 that as heart rate increased, the noise of the pump reduced. The setup was run at heart rates of 60, 80 and 100 beats per minute. Significant noise is seen in the signal recorded with the pump at 60 bpm. At 80 bpm, the noise is reduced but still present, and a PPG waveform can be seen. The noise is believed to be caused by the mechanical movement of the pump, which caused the rest of the setup to vibrate. This could also be improved with more elastic vessels, potentially through manual fabrication. Stroke volume did not seem to influence the noise levels. The main features of the PPG wave are visible at 100 bpm. These are the systolic and diastolic peaks, and the dicrotic notch, (Hasanzadeh et al., 2019). The presence of these points suggests that feature extraction is possible with signals obtained from tissue-vessel phantoms in this setup. In cases where all points are not present, there are other features that can still be measured (Li et al., 2022). This is then confirmed by running the feature extraction algorithm and visually verifying the detection of the features. Signals from the 100-bpm protocol were prioritised during the feature extraction and statistical analysis processes due to their reduced noise artefacts.

As well as heart rate, stroke volume was also varied. At 15 ml/stroke, the peak of the signal is below 0.09 V and the foot is at -0.055 V, resulting in a peak-to-peak voltage of around 0.145 V. This is compared to 25 ml/stroke in FIGURE 5-21, where the signal expanded by about 0.03 V at the bottom for a peak to peak of 0.175 V. The increase of 0.03 V from 0.145 to 0.175 V results in a percentage difference of 19%.

When comparing signals at the same stroke volumes from a phantom with no inner vessel, there is greater initial peak-to-peak voltage as well as a bigger change when stroke volume is increased. The PPG signal of the phantom with no vessel ranges from -1.3 V to 1.45 V, for a peak-to-peak

of 2.75 V. Therefore, the signal obtained from this phantom is 19 times larger in amplitude than the signal from a phantom with a vessel. This difference is expected as PPG is a light-based technique, relying on the reflectance and transmission of light through a vessel wall as well as the surrounding tissue. As such, the removal of the boundary of the vessel wall allowed more of the light reflected by the inner fluid to reach the sensor. This is an important change as it resulted in cleaner raw signals and higher amplitudes, which is useful for signal analysis and feature extraction. This highlights the potential for future custom vessels and phantoms for obtaining high-quality PPG signals. Furthermore, vascular structure such as thrombosis or an aneurysm can also be investigated through tissue phantoms, by using differently shaped moulds. As we have discussed in the literature review, silicone vessels can be fabricated with a wall thickness less than 1 mm, resulting in PPG signals with a higher signal-to-noise ratio (Nomoni et al., 2020b). This would be more appropriate for a tissue-vessel phantom than commercial silicone tubing which reduces the signal quality significantly, especially when combined with surrounding tissue, as we have seen. Another option for vessel stiffness experiments is to place the PPG sensor directly on the tubing, with no surrounding tissue. This would obtain a higher signal quality as the light reflected through the vessel wall will enter directly into the sensor, without propagating through any tissue. This should result in a better PPG signal which may allow for the use of commercial vessels in vessel stiffness experiments. These experiments could be done with commercial vessels of varying wall thickness. If the PPG signal quality is acceptable, which may be achieved by measuring directly on the vessel, commercial silicone tubing can be used. To summarise, there are three potential models which can produce better PPG signals for future arterial stiffness and cardiovascular disease experiments: vessel-tissue phantoms using custom micrometre walled vessels, tissue phantoms with custom inner forms, and separate silicone tubing with no tissue phantom.

After filtering and observing the changes with varying heart rate and stroke volume, the signals were run through the custom feature extraction process (Bradley and Kyriacou, 2024). The types of features chosen have been cited in literature and linked to vascular aging and cardiovascular diseases including arterial stiffness (Elgendi, 2012; Li et al., 2022; May et al., 2021). The algorithm was verified by plotting samples of the extracted features, indicating the detected points of the wave. Each run of the experiment was four minutes, producing a continuous PPG signal, which was divided into sections for the feature extraction. To avoid detection of incomplete waves, the first and last wave of each section was not used for feature detection.

Firstly, amplitude was measured by detecting the peaks, seen in FIGURE 5-22. At half the amplitude, the points of the wave on either side can be detected to measure half peak width. By detecting the onset and end points of the waves, upslope and downslope gradients could be measured from each point to the peak, shown in FIGURE 5-23. By measuring the distance on the x-axis between these points, rise time and decay time are determined. Finally, these points are considered to measure area under the curve in FIGURE 5-24. This area can also be split into systolic and diastolic phases at the dicrotic notch (Ahn, 2017). As the dicrotic notch was not consistent in the higher heart rates, the area was split at the peak of the wave. The ratio of the two areas is then calculated.

The detected PPG wave features were in the expected range, suggesting that the feature extraction algorithm results would be suitable for statistical analysis. The variables considered in this analysis were tissue stiffness, heart rate and stroke volume, against the extracted features. The differences between the red and infrared results were also observed. One-way analysis of variance was conducted using the Kruskal-Wallis test for each variable against each feature, creating a separate boxplot for each feature.

Analysis of the primary variable of interest in this experiment, tissue stiffness, is shown for the red and infrared signals in FIGURE 5-25 and FIGURE 5-26. For each feature, the boxplots are grouped into the three runs of the experiment, starting with identical 0050 shore phantoms in the bifurcation setup, followed by one 0050 shore and one 0025 shore to simulate changing arterial stiffness, and ending with two identical 0025 shore phantoms for validation.

Amplitude of the PPG wave is the first feature analysed, which is consistent across all phantoms and wavelengths, suggesting that flow through the system was consistent. This is supported by the p-values shown in the box plot and TABLE 5-1 and

TABLE 5-2. This was seen even in the varied tissue stiffness phantoms, with a p-value of 0.52, indicating that change in tissue stiffnesses could not be detected from PPG amplitude. Although the amplitude is consistent in the red and infrared signals, it should be noted that the red signal resulted in more anomalies than the infrared. However, in certain features red showed less outliers, confirming that multi-wavelength PPG sensors are beneficial, as seen in commercial devices (S. Han et al., 2019).

Half peak width shows the most variation of all the features, with p-values near 0, even in the identical phantoms. As such, half peak width is difficult to use for blood vessel assessment. Further investigation into the signals and feature extraction algorithm is required to determine the origin of this variation in results. It may be due to factors in the physical setup or the digital algorithm. Again, the red signal shows more variation and anomalous results than the infrared.

Upslopes and *downslopes* do not show variation overall between the shore 0050 and shore 0025 phantoms. In these features, the infrared results have more anomalies. The same effect is seen in rise time and decay time, with the infrared wavelength showing more variation than the red, even across identical phantoms. This effect is strongest in rise time, with

the infrared rise time variation resulting in p-values of near 0 for all phantom combinations, identical and varied. The opposite was seen in amplitude and half peek width, where the red signal had more variation. These alternations between red and infrared signals variation across features show that different wavelengths can be better depending on the feature, and a multi-wavelength system is ideal to analyse all features.

Area under the curve features are also consistent across the different phantoms, again showing that the bifurcation setup could successfully replicate identical vasculature but a greater difference in tissue stiffness is required to observe differences in the extracted features.

These features have also been analysed while changing heart rate and stroke volume. This can verify the pump system and feature extraction process by observing expected trends in the features at different heart rates and stroke volumes. For example, with increasing heart rate, the PPG waves become more frequent and closer together, in sync with the heartbeat, displayed in FIGURE 5-20. This is echoed in the half peak width analysis at different heart rates in FIGURE 5-27 which shows that with each increased heart rate, the half peak width is reduced across both phantoms and wavelengths. As this is in line with the signal changes seen, the accuracy of the peak detection is validated as well as the pump configuration. Similar effects are seen in the other features such as increasing upslope gradient with heart rate as the wave becomes steeper. Rise time and decay time both become shorter as heart rate increases, which is in accordance with the wave width changes. The same effect is seen in the features related to area under the curve. As heart rate increases, the wave is more compact resulting in less area under the wave detected. These trends in the features at different heart rates follows the expected direction when considering the wave shape changes, validating the experimental system and feature extraction code.

With changing stroke volume in FIGURE 5-28, there is less overall variance in the features compared to heart rate. Half peak width shows the most

variation, with some also seen in total area under curve and on the diastolic side. In half peak width, opposite effects are seen compared to heart rate. While half peak width reduced as heart rate increased, following the tightening of the PPG waves, the opposite occurs with stroke volume. We can see in FIGURE 5-21 that the increase in stroke volume cause the wave to become wider and taller. Therefore, the increase in half peak width with stroke volume detected by the feature extraction algorithm is expected. As such, the system and feature extraction can be verified in terms of increasing stroke volume. Therefore, half peak width could be a useful feature for estimating stroke volume. Total and diastolic area under the curve also showed an increase with stroke volume, as expected when considering the mentioned changes in shape of the wave.

5.5 CONCLUSION

This chapter begins the investigation photoplethysmography as a monitoring technology for the early screening of cardiovascular disease, specifically arterial stiffness, by developing a custom in vitro flow-rig. In vivo studies reviewed have confirmed that PPG signals detected from both sides of the body are statistically similar. When the same bilateral PPG setup was placed on patients with peripheral arterial disease, a change in the PPG signal at the occluded artery was seen.

This chapter follows by describing the design and development of a bilateral in vitro cardiovascular model to parallel the human studies, following a similar experimental protocol. This experimental setup was created with the goal of investigating changes in PPG signals in normal and diseased vascular models. Silicone tissue-vessel phantoms were created and connected to a commercial silicone tubing model of the human vasculature. To represent the heart, this system was built around a pulsatile pump which would pump a blood-mimicking fluid around the model. PPG signals were acquired from two phantoms at a time in a bifurcation, allowing for the simultaneous measurement of healthy and diseased arteries in vitro.

Following a similar protocol to the in vivo bilateral studies, the system was first validated by flowing fluid through identical phantoms and confirming the similarity of the PPG signals. This comparison was based on a custom feature extraction algorithm which detected the amplitude, half peak width, upslope and downslope, total, systolic and diastolic area under the curve and finally ratio of the areas and second derivative of each PPG wave. Amplitude, area under the curve and diastolic area under the curve were found to be stable in both red and infrared signals in the identical phantoms. The red signal was also consistent in the upslope, downslope, rise time, decay time and systolic area under the curve, whereas the infrared signal showed variance even in the identical phantoms. Further validation of the system and feature extraction was conducted by observing the variation in the detected features while changing heart rate and stroke volume. Upslope, rise time, decay time and area under the curve followed the expected trends with increasing heart rate. As did half peak width with heart rate as well as stroke volume.

With phantoms of a shore difference of 0025, a statistical difference in the PPG features could not be seen. As such, greater shore difference is suggested, as well as changes in the vessel-tissue models for the improvement of signal quality, which will enable finer detection of PPG features. Representative pressure waveforms measured at the beginning and end of the system also confirmed that the rig produced repeatable pulsatile conditions during signal acquisition.

Compared with previous in vitro studies that often investigated a single factor in isolation, this chapter establishes a bilateral platform for simultaneous comparison of paired vascular models under matched haemodynamic conditions. In this respect, the work directly addresses several of the gaps identified by introducing a controlled bilateral configuration, side-to-side validation, and a structured feature-extraction pipeline within one system. However, the present stage also confirms that

improved vessel realism and greater mechanical contrast are still required before stiffness-related differences can be resolved reliably.

5.6 Future Work

The tissue-vessel phantom signals were compared to tissue phantoms with no internal tubing. These phantoms produced higher quality raw PPGs. As such, this presents an exciting opportunity for in vitro cardiovascular disease investigations using phantoms to model varying pathologies such as arterial stiffness and atherosclerosis. Fabricated vessels also offer a high signal-to-noise ratio, making them a suitable improvement to the current tissue-vessel phantoms, potentially yielding more accurate statistical results. Finally, PPG sensors can be placed on the tubing for direct vessel flow monitoring, which could be useful for experiments involving altering vessel thicknesses with PPG feature detection. This feature detection can also be expanded to include a wider set of features, as well as the first and second PPG wave derivatives.

5.7 Summary

This chapter presents the development of an in vitro bilateral cardiovascular flow-rig designed to simulate healthy and diseased vessels for PPG research. The setup integrates a pulsatile pump, blood-mimicking fluid, silicone tubing and tissue phantoms to replicate arterial stiffness and vascular mechanics. Custom 3D-printed connecters and dual-wavelength PPG sensors were incorporated to acquire signals from parallel vessel phantoms. Experimental protocols varied heart rate and stroke volume to investigate their effects on PPG waveform features such as amplitude, peak width, slopes and area under the curve. Signal processing included noise filtering and feature extraction validated against known physiological trends.

The results demonstrated that the system could produce consistent and PPG signals between branches, with feature variations observed under differing heart rates and stroke volumes. However, changes in tissue

stiffness within the tested range did not yield statistically significant differences in extracted features, suggesting the need for greater mechanical contrast or refined phantom designs. The chapter concludes that fabricated vessel-tissue phantoms offer a promising platform for controlled vascular studies, and improvements in phantom construction may enhance PPG signal quality and sensitivity for cardiovascular disease detection. Future work will explore alternative phantom designs utilising custom-fabricated silicone vessels with varied stiffness ranges, and expanded feature extraction to advance in vitro modelling of arterial pathology.

6 DEVELOPMENT OF CUSTOM SILICONE VESSELS

6.1 INTRODUCTION

While identical phantoms comprised of commercial silicone vessels successfully produced consistent PPG signals, they were insufficient in detecting morphological changes associated with varying stiffness by adjusting the mechanical properties of the surrounding tissue. This limitation highlighted the need for more elastic, customisable vessels capable of producing higher quality PPG signals for experimental analysis.

This chapter builds on that work by exploring the fabrication of silicone vessels with adjustable stiffness. By systematically varying silicone additives, such as retarder, deadener and hardener, this study investigates the feasibility of creating vessels with tuneable mechanical properties for simulating both healthy and diseased arteries. These modified vessels, embedded within soft silicone tissue, enable the collection of PPG signals of sufficient quality to assess the relationship between vessel stiffness and PPG signal morphology.

In vitro models that replicate vascular ageing in controlled conditions offer a valuable platform for the development of non-invasive diagnostic technologies and signal processing algorithms. PPG sensors have previously been identified as promising tools for detecting changes associated with vascular ageing (Karimpour et al., 2023). Artificial vessels have been fabricated using techniques such as 3D bioprinting (Datta et al., 2017; Gao et al., 2020; Schöneberg et al., 2018). Laminar flow-based microfluidics (Du et al., 2019; Nie et al., 2018) , and coaxial scale-up printing (Liang et al., 2020). While these approaches have shown potential, they present certain limitations. For example, 3D printing methods require specialised bio-inks, and microfluidic fabrication based on laminar flow can involve complex procedures and equipment (Zhou et al., 2023).

This investigation presents the fabrication, mechanical characterisation, and PPG analysis of custom-made silicone vessels embedded within soft

tissue phantoms, designed to replicate the human healthy and unhealthy vessels in a controlled in vitro environment. The work expands on prior methods developed by the Research Centre for Biomedical Engineering at City St George's, University of London. Initial vessel fabrication using polydimethylsiloxane (PDMS) (Sylgard 184, Dow Silicones, Barry, UK) proved successful; however, the PDMS formulations offered limited control in terms of vessel elasticity.

In this chapter, the vessels were instead constructed using PlatSil Gel-10 (Polytek Development Corp., Easton, PA), a more adaptable elastomer that allows for controlled adjustment of mechanical properties through silicone additives. The focus was to assess the degree of control avhievable over vessel stiffness using formulation changes, and to characterise the full range of elasticities available using this material, building on earlier reports (Polytek Development Corp., 2021).

Mechanical testing was conducted across a series of fabricated vessels to evaluate the effects of silicone additives on elasticity, hardness, and wall thickness. This chapter also extends on previous work by offering a broader characterisation of these properties and systematically exploring the mechanical behaviour across multiple elastomer formulations (Ferizoli et al., 2024).

The fabricated vessels were surrounded by soft silicone tissue to create vessel-tissue phantoms that mimicked the compliance of biological tissues. These phantoms were then integrated into a custom-built in vitro system replicating the lower-limb cardiovascular environment, incorporating a pulsatile pump and silicone tubing. The system enabled the recording of PPG signals under consistent flow conditions.

The main aim was to determine whether the fabricated phantoms could be used to detect differences in arterial stiffness through changes in the PPG waveform. Additionally, the study evaluates how stiffness can be modulated through silicone dip-coating by varying elastomer composition.

Through this approach, this research seeks to advance the design of in vitro platforms capable of simulating vascular ageing and supporting the development of PPG-based arterial stiffness assessments.

6.2 METHODS

Custom silicone vessels were fabricated using a precise dip-coating technique involving an elastomer mixture, detailed in the following sections. Once produced, the vessels underwent tensile testing to determine their mechanical properties, and their wall dimensions were measured using a digital microscope. The vessels were then embedded into silicone tissue to form vessel-tissue phantoms. Compression tensile tests were conducted to examine tissue stiffness. Finally, the phantoms were connected to a mechanical pulsatile pump system, enabling PPG recording and analysis.

CUSTOM VESSEL MIXTURE FORMULATION

The custom vessels were fabricated using PlatSil Gel-10 elastomer, with silicone selected for its durability and heat resistance. Unlike latex, silicone maintains its shape can endure higher temperatures (Chruściel, 2022), an important property for successful curing during the dip-coating process. The elastomer mixture consists of two components, Part A and Part B, which were individually weighted using a digital precision scale (Scout, Ohaus, Parsippany, NJ) and thoroughly mixed in equal proportions. To extend the working time and prevent premature setting, a retarder was introduced intro the mixture. Adding retarder at 1% of the total elastomer weight effectively doubled the pour time (Polytek Development Corp., 2021). Depending on the desired vessel type, the softness or hardness of the final elastomer could be adjusted by incorporating either Smith's Deadener or Hardener (Polytek Development Corp., Easton, PA). After mixing, the silicone mixture was degassed in a vacuum chamber (Applied Vacuum Engineering, Bristol, UK) for three minutes, removing any trapped air bubbles before beginning the dip-coating procedure.

VESSEL DIP-COATING PROCESS

To fabricate the vessels, the prepared elastomer mixture was poured into a silicone pot which was placed in a dip-coating setup illustrated in FIGURE 6-1, following the established protocol (Nomoni et al., 2020b).

Commercial silicone tubing (Hilltop Products Limited, Warrington, UK) served as the internal form for the custom vessels and was positioned on pulleys, threading through a heating element attached to a Precision Dip Coater (Qualtech Products Industry, CO, US). One end of the tubing was fixed to a tension weight, with the other secured to the dip-coater's mechanical arm. The heating element was started, reaching and maintaining 275 °C for approximately three minutes. As the tubing was drawn through the dip pot, a coating of silicone was formed around the tubing. It was steadily drawn upwards at a controlled speed of 40 mm/min, preventing premature curing and ensuring an even coating.

The heating element was switched off once the arm reached the top, and the elastomer-coating tubing was left to fully cure. After curing, the inner form was carefully separated from the coating, leaving behind the completed custom vessel.

The wall thickness of the vessels could be adjusted by varying the amount of retarder in the formulation. Deadener and hardener could also be incorporated to produce vessels with varying elasticities.

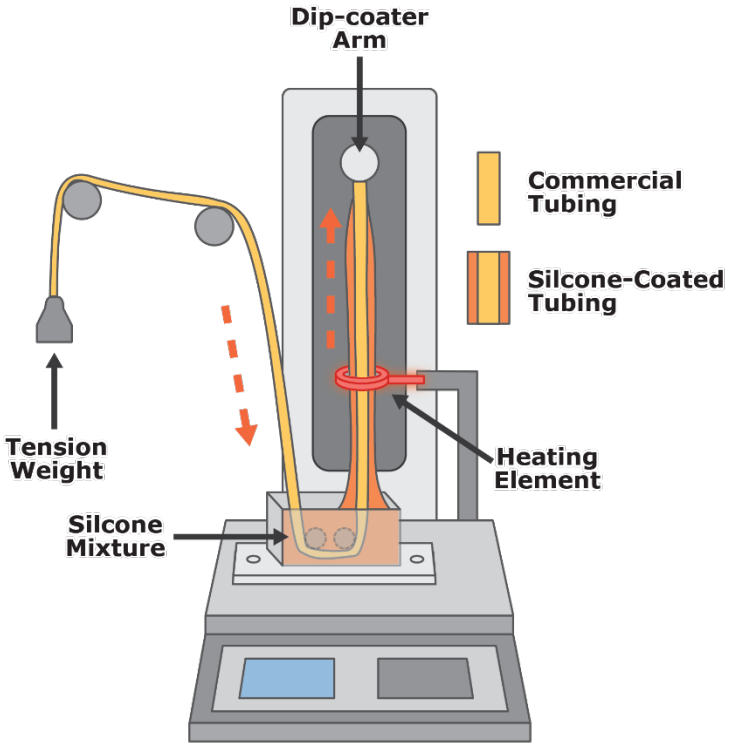

FIGURE 6-1. Dip-coating setup used to fabricate custom silicone vessels with controlled wall thickness and elasticity. The apparatus features a motorised vertical stage that pulls silicone tubing through an elastomer reservoir at a constant speed, promoting uniform coating. A pulley-weight system maintains vertical tension, while a heating element initiates curing. The coated vessel is then detached and used for integration into vessel-tissue phantoms.

VESSEL-TISSUE PHANTOM FORMATION

The surrounding tissue was prepared by mixing equal quantities of Part A and Part B of Gel-00 elastomer (Polytek Development Corp., Easton, PA). Gel-00 was chosen over Gel-10 due to its softer consistency, producing tissue with a Shore hardness of OO30, in line with the mechanical properties of natural tissues (Jafary et al., 2022). After thorough mixing, the elastomer was degassed in a vacuum chamber to remove any trapped air bubbles. The bubble-free mixture was then poured into custom-designed 3D-printed moulds to create the final vessel-tissue phantoms.

Vessel Wall Thickness Measurements

To evaluate the effect of elastomer formulation on vessel wall thickness, 1 mm long segments were cut from both ends of each fabricated vessel. These sections were stained with black paint to enhance contrast and examined under a digital microscope (Celestron, Torrance, CA), as shown in Figure 6-2. Three stained cross-sections were taken from each end, resulting in six samples per vessel. Images were captured using Celestron MicroCapture Pro software (Celestron, Torrance, CA). Wall thickness was measured on four different parts of the cross-section and averaged. The same images were also used to determine the internal diameter (ID), and the outer diameter (OD) was calculated by adding the wall thickness on both sides to the ID. Measurements from both sides were used to assess whether the fabricated dimensions remained consistent along its length after dip-coating. Vessel integrity was confirmed visually during removal from the inner form and sectioning.

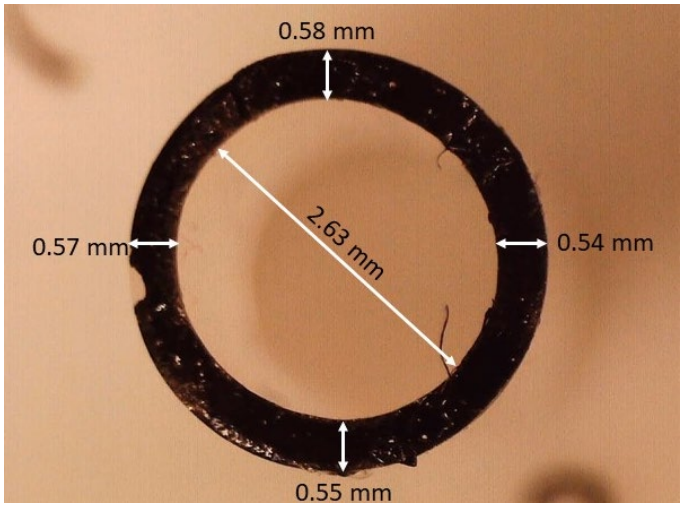

Figure 6-2. Cross-sectional microscopic view of a stained silicone vessel segment showing wall thickness and diameter measurements. The vessel was cut and coated with black paint to enhance contrast, enabling accurate thickness evaluation at multiple points around the circumference. Measurements demonstrate slight variability, with wall thickness values ranging from 0.54 mm to 0.58 mm and an internal diameter of 2.63 mm.

ELASTICITY MEASUREMENTS

Tensile testing was employed to determine the elastic modulus of each custom vessel, using the Universal Testing System (Instron 5944, Norwood, MA), as shown in FIGURE 6-3. Vessels measuring 15 cm in length were secured between two grips and vertically extended at a constant speed of 500 mm/min until failure, following the ASTM D412 standard (Instron, 2024a). Each vessel was subjected to a standardised load of 0.791 N, and Young's modulus was calculated in Bluehill Universal software (Instron, Norwood, MA), using the previously measured diameter and wall thickness values.

This process was repeated across all vessel samples to evaluate variations in elastic properties resulting from different concentrations of retarder, deadener, and hardener.

For the tissue phantoms, the system was switched to compression testing mode (FIGURE 3). Samples measuring 50 x 20 x 20 mm (L x W x H) were placed on a flat metal plate and compressed at a rate of 12 mm/min, following ASTM D575-91 guidelines, to determine Young's modulus (Instron, 2024b).

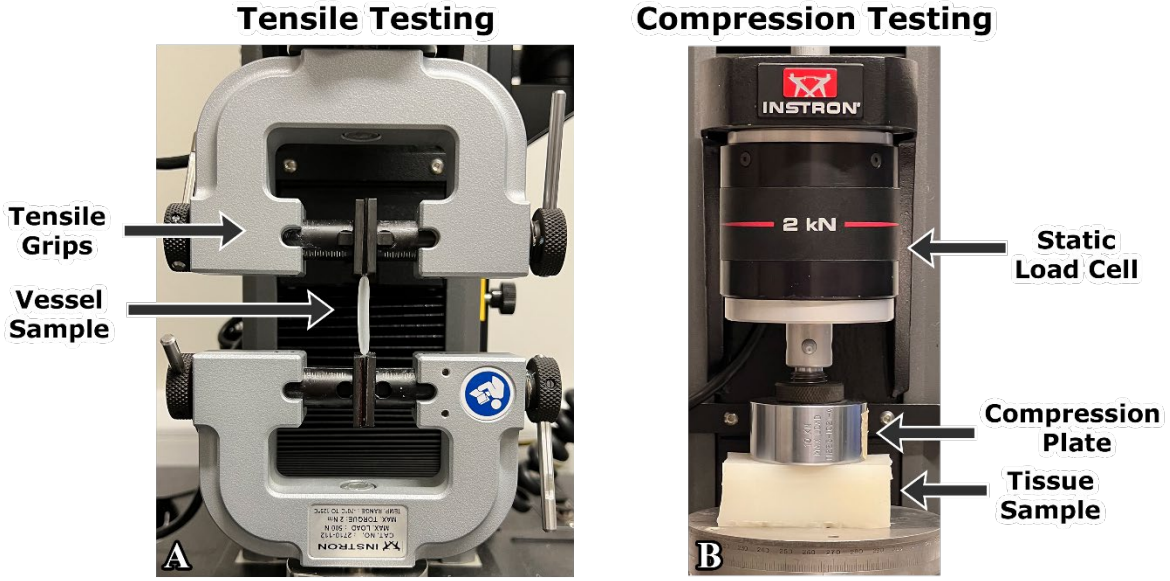

FIGURE 6-3. Universal Testing System used for elasticity and mechanical characterisation of custom vessel and tissue

samples. (A) Tensile testing configuration of silicone vessels during elasticity measurements, secured between dual grips for axial extension. **(B)** Compression testing mode for assessing tissue stiffness of silicone phantoms, between metal plates under a load cell.

HARDNESS MEASUREMENTS

To measure hardness of the cured silicone tissue mixture, the AD-100-OO Precision Shore Durometer (Checkline Europe, Netherlands) was used, as shown in FIGURE 6-4. The device was initially positioned with the footbad at a slight angle on the tissue surface, then carefully rolled into a flat position to ensure accurate readings. Measurements were taken from multiple locations on each sample and averaged. This procedure was repeated for tissue samples containing different concentrations of retarder, deadener and harderner, allowing for a comparison of how each additive influenced tissue hardness.

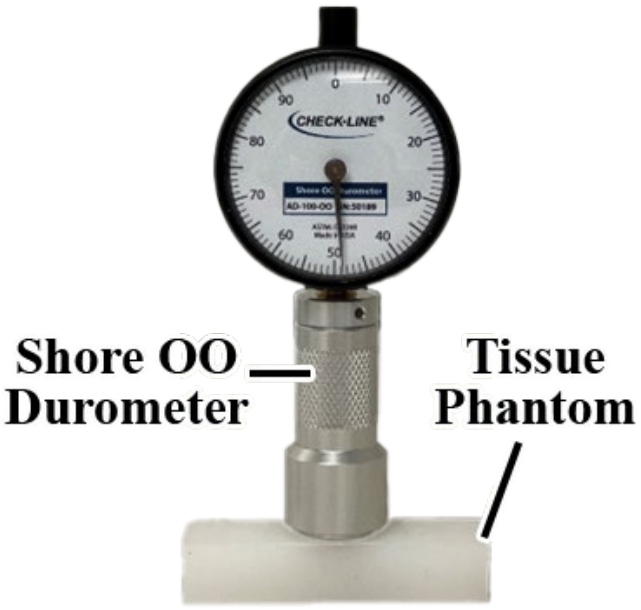

FIGURE 6-4. Shore hardness measurement of silicone tissue using a Shore OO durometer. The device is positioned vertically with its flat base in contact with the sample surface to ensure consistent readings. This method quantifies tissue stiffness, with lower values indicating softer materials suitable for mimicking compliant biological tissue.

Obtaining In Vitro PPG Signals

The custom vessel-tissue phantoms were integrated into an in vitro system comprising of a pulsatile pump, silicone tubing filled with blood-mimicking fluid (BMF), and custom PPG and pressure sensors (PendoTech, Princeton, NJ). Pulsatile flow was generated using the PD-1100 Pulsatile Pump System (BDC Laboratories, Wheat Ridge, CO), which simulated cardiac-like activity and produced a pulsatile pressure waveform. The vascular circuit was assembled using silicone tubing to form a network with two key functions: firstly, to reduce the outlet diameter to match the phantom vessels, and secondly, to recreate the distinctive pulsatile pressure waveform through bifurcations and resistances in the network.

The circulating fluid was a simple BMF, prepared by mixing methylene blue powder (Thermo Fisher Scientific, UK) with deionised water. This formulation enhanced light absorption in the red and infrared spectra, improving PPG signal quality (Whang et al., 2009). The custom vessel-tissue phantom was positioned above a PPG sensor composed of red and infrared LEDs (peak wavelengths 660 nm and 940 nm) and a photodiode (BPW34, Osram, Germany) with peak sensitivity at 900 nm. For signal acquisition and processing, the sensor was connected to a ZenPPG unit (Budidha et al., 2018), which interfaced with a data acquisition card and a LabVIEW virtual instrument (National Instruments, TX, USA).

6.3 Results

Mechanical testing was carried out on the custom vessels to evaluate the influence of additives on vessel wall thickness and elasticity. The hardness and elastic properties of the tissue samples were also assessed. In vitro PPG signals were recorded, and a preliminary amplitude analysis was conducted. These results are detailed in the following sections.

Vessel Wall Measurements

Wall thickness measurements for vessels fabricated with varying concentrations of retarder are shown in Figure 6-5. The results suggest that

retarder reduces wall thickness when included in a concentration up to 3.0%. Inner diameter (ID) values ranged from 2.55 mm to 2.78 mm, while outer diameter (OD) values varied between 3.20 mm and 3.77 mm.

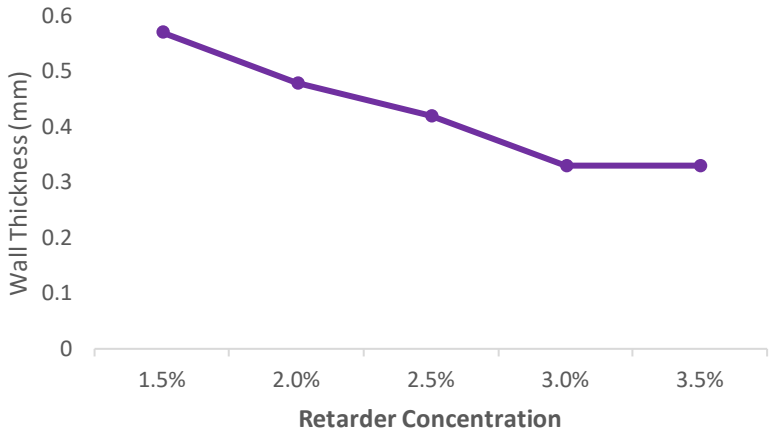

FIGURE 6-5. Effect of retarder concentration on vessel wall thickness in custom silicone formulations. Wall thickness decreased with increasing retarder content, dropping from approximately 0.57 mm at 1.5% to 0.40 mm at 3.5%.

TABLE 6-1 and TABLE 6-2 summarise the corresponding wall thickness, ID and OD measurements for vessels produced with different ratios of deadener and hardener. Wall thickness remained consistent between 0.50 mm and 0.58 mm across all samples, as expected, given that deadener and hardener are intended to modify vessel elasticity rather than wall thickness (Polytek Development Corp., 2021). Retarder concentration was held constant at 1.5%. OD values ranged from 3.96 mm to 4.04 mm in the deadener set and from 3.96 mm to 4.09 mm in the hardener set. Each formulation used equal parts of Part A and Part B, with the addition of varying amounts of Part D (deadener) or Part H (hardener). Deadener samples followed A:B:D ratios up to a maximum of 0.6 D, while hardener samples followed A:B:H ratios up to 1 H.

TABLE 6-1. Vessel wall thickness and diameter measurements for varying *deadener* concentrations. Deadener addition had

minimal effect on wall thickness, suggesting that its primary effects are elastic rather than geometric. * Ratio of Part A:Part B:deadener.

Mixture Ratio (A:B:D)*	Wall Thickness (mm)	Internal Diameter (mm)	Outer Diameter (mm)
1 : 1 : 0	0.53	3.00	3.96
1 : 1 : 0.2	0.58	2.82	4.00
1 : 1 : 0.4	0.57	2.90	4.04
1 : 1 : 0.6	0.58	2.85	4.00

TABLE 6-2. Vessel wall thickness and diameter measurements for varying *hardener* concentrations. Wall thickness and diameter values remained consistent, indicating that hardener alters vessel stiffness without affecting physical dimensions.

Mixture Ratio (A:B:H)*	Wall Thickness (mm)	Internal Diameter (mm)	Outer Diameter (mm)
1 : 1 : 0	0.53	3.00	3.96
1 : 1 : 0.2	0.54	2.98	4.06
1 : 1 : 0.4	0.50	3.02	4.02
1 : 1 : 0.6	0.51	2.95	3.96
1 : 1 : 0.8	0.53	2.96	4.01
1 : 1 : 1	0.52	3.02	4.09

ELASTICITY MEASUREMENTS

Young's modulus values obtained from tensile testing of vessels containing varying concentrations of retarder are shown in FIGURE 6-6. Measured values ranged from 0.41 MPa to 0.60 MPa, corresponding to retarder concentrations between 1.5% and 3.5%.

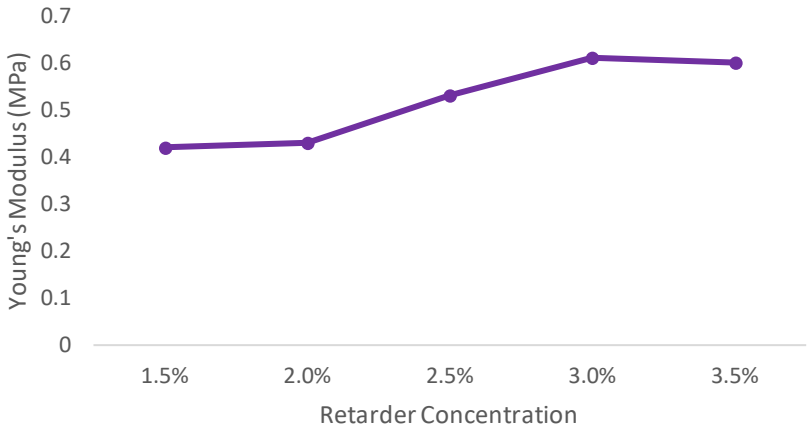

FIGURE 6-6. Elastic modulus of silicone vessels fabricated with increasing retarder concentrations. Young's modulus rose from approximately 0.41 MPa to 0.61 Mpa as retarder concentrations increased from 1.5% to 3.0%, then plateaued.

TABLE 6-3 and TABLE 6-4 present Young's modulus results for vessels formulated with different amounts of deadener and hardener. Deadener increased vessel elasticity, with a reduction in Young's modulus from 0.52 MPa to 0.20 MPa. In contrast, hardener increased stiffness, with Young's modulus rising from 0.42 MPa to 1.22 MPa. These trends are visualised in FIGURE 6-7, alongside reference values for the elastic modulus of a healthy femoral artery (adventitia and radial strain) (Brum et al., 2010).

TABLE 6-3. Young's modulus of silicone vessels fabricated with increasing concentrations of *deadener*.

Mixture Ratio (A:B:D)	Young's Modulus (MPa)
1 : 1 : 0	0.52
1 : 1 : 0.2	0.46
1 : 1 : 0.4	0.28
1 : 1 : 0.6	0.20

TABLE 6-4. Young's modulus of silicone vessels fabricated with increasing concentrations of *hardener*.

Mixture Ratio (A:B:H)	Young's Modulus (MPa)
1 : 1 : 0	0.52
1 : 1 : 0.2	0.64
1 : 1 : 0.4	0.78

1 : 1 : 0.6	0.82
1 : 1 : 0.8	0.92
1 : 1 : 1	1.22

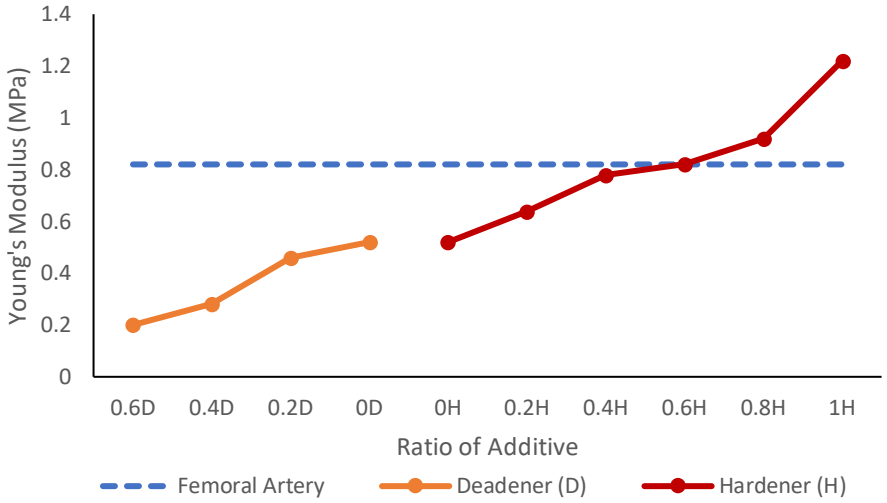

FIGURE 6-7. Tensile test results showing the effect of hardener and deadener on vessel elasticity relative to healthy femoral arteries.

An increase in deadener led to a noticeable reduction in the Young's modulus of the tissue phantoms, indicating a softening effect on the material. Conversely, higher concentrations of hardener resulted in increased Young's modulus values, reflecting greater stiffness. These results align with the normal range for tissue found in the finger, between 0.07 MPa and 0.2 MPa (Oprişan et al., 2016), shown in FIGURE 6-8.

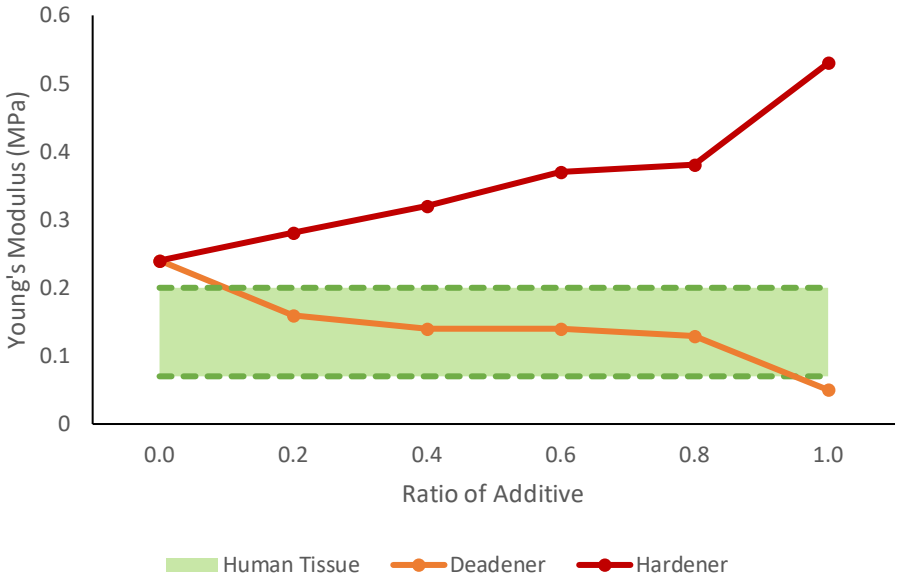

FIGURE 6-8. Compression tests indicating Young's modulus of custom tissues with varying concentrations of hardener and deadener. The normal range for finger tissue elasticity is indicated by the dotted lines (Oprişan et al., 2016).

SHORE HARDNESS OF TISSUE SAMPLES

Shore hardness measurements for tissues cured with varying levels of retarder are shown in TABLE 6-5. No significant change in hardness was observed across the tested range, with values remaining between OO47 and OO50 as retarder concentration increased from 1.5% to 3.5%.

Deadener effects on Shore hardness are presented in TABLE 6-6. A clear reduction in hardness was observed, with Shore OO25 at a 1-part deadener ratio. In contrast, TABLE 6-7 shows that tissue hardness increased with hardener concentration, as expected, reaching Shore OO67 at 1-part hardener. These trends are visualised in FIGURE 6-9, alongside the normal Shore hardness range for tissue found in the dorsal thigh (Falanga and Bucalo, 1993).

TABLE 6-5. Shore hardness of cured tissue as retarder concentration is increased.

Retarder (%)	Shore OO Hardness
1.5	48
2.0	49

2.5	49
3.0	50
3.5	47

TABLE 6-6. Shore hardness of tissue with increasing amounts of deadener.

Mixture Ratio (A:B:D)	Shore OO Hardness
1 : 1 : 0	48
1 : 1 : 0.2	44
1 : 1 : 0.4	43
1 : 1 : 0.6	39
1 : 1 : 0.8	32.5
1 : 1 : 1.0	25

TABLE 6-7. Shore hardness of tissue with increasing amounts of hardener.

Mixture Ratio (A:B:H)	Shore OO Hardness
1.0 : 1.0 : 0.0	48
1.0 : 1.0 : 0.2	52
1.0 : 1.0 : 0.4	56
1.0 : 1.0 : 0.6	61
1.0 : 1.0 : 0.8	63
1.0 : 1.0 : 1.0	67

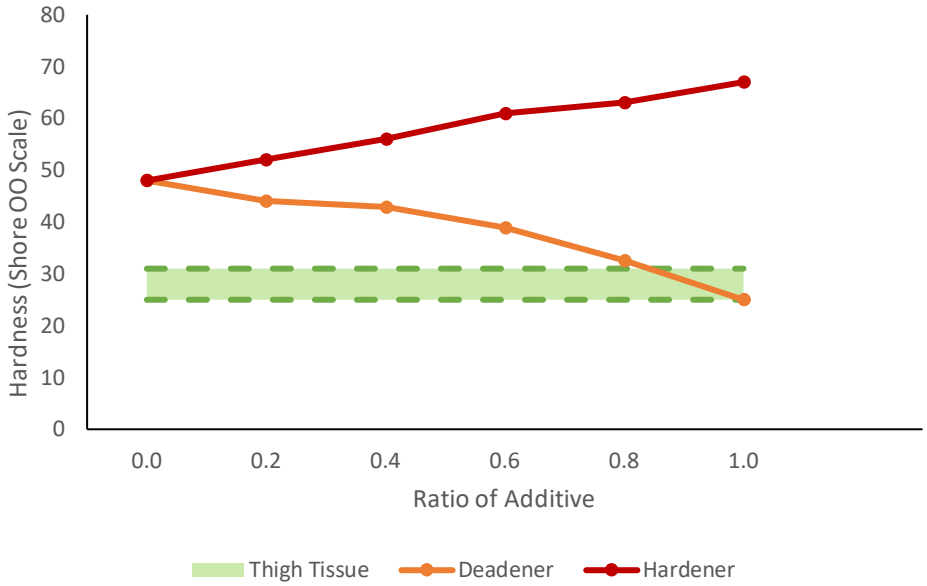

FIGURE 6-9. Variation of Shore hardness with concentrations of hardener and deadener. The normal range for dorsal thigh tissue is referenced in the shaded region (Falanga and Bucalo, 1993).

ACQUISITION OF PHOTOPLETHYSMOGRAPHY SIGNALS

PPG signals were acquired from three custom vessel-tissue phantoms, each fabricated with different additives to alter vessel elasticity. An elastic vessel was produced using deadener at a ratio of 0.2 (10% of the total mixture weight), while a stiff vessel was prepared with the same proportion of hardener. A control phantom with no additives was also included. The resulting PPG and pressure signals are presented in FIGURE 6-10. The recorded waveforms exhibited key features characteristic of human PPG signals: systolic and diastolic peaks as well as a dicrotic notch. Visual differences were observed across the phantoms; as vessel stiffness increased, the amplitude of both peaks diminished, particularly in the infrared signal.

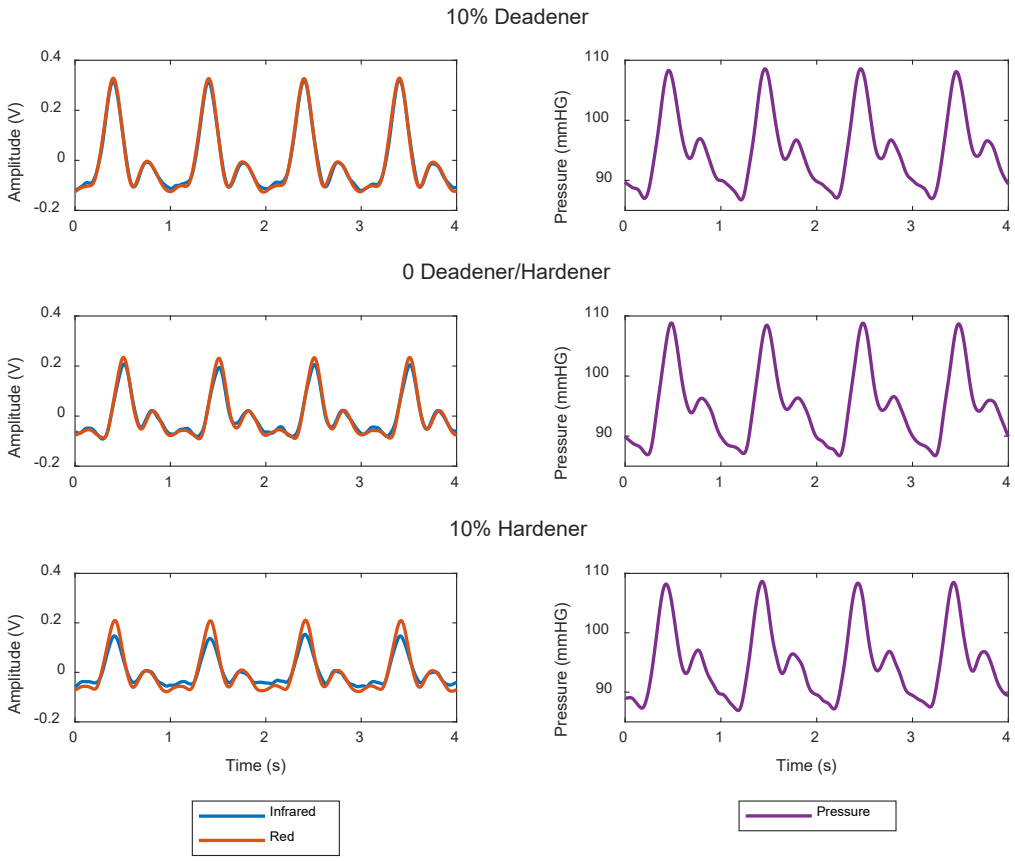

FIGURE 6-10. PPG and pressure signals from custom vessel-tissue phantoms of varying vessel stiffnesses. Vessel elasticity was adjusted by incorporating different concentrations of hardener and deadener, with additive percentages shown relative to the total elastomer mixture. The PPG signals were recorded at the mid-vessel measurement site within each phantom, while the pressure waveform was measured using the in-line pressure sensor positioned at the outlet of the phantom branch, downstream of the custom vessel.

STATISTICAL ANALYSIS OF PPG AMPLITUDE

Systolic PPG amplitude was quantified through feature extraction and is shown in the box plot in FIGURE 6-11, highlighting amplitude variations across vessel-tissue phantoms with differing stiffness. Statistical significance was assessed using a Kruskal-Wallis test, with results summarised in TABLE 6-8. The p-values obtained, 5.176×10^{-15} for red light and 1.831×10^{-14} for infrared, indicate a statistically significant difference in PPG amplitude between phantoms ($p < 0.001$). A Dunn post-hoc test was performed to evaluate pairwise differences, presented in TABLE 6-9. The

adjusted p-values confirmed that each phantom exhibited significantly different PPG amplitudes from the others ($p < 0.001$).

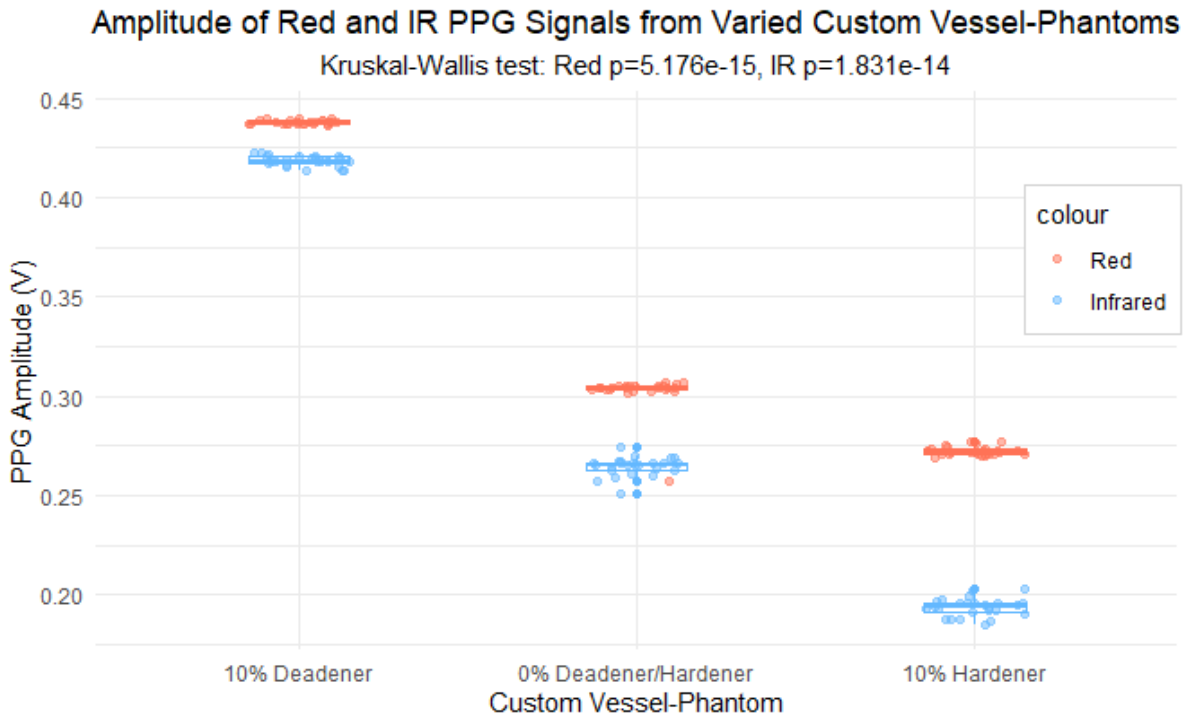

FIGURE 6-11. Box plot showing variation in red and infrared PPG amplitudes from custom vessel-tissue phantoms with different elasticities.

TABLE 6-8. Kruskal-Wallis analysis of red and infrared PPG amplitudes across phantoms.

Comparison	Chi-squared	df	p-value
Red	65.789	2	5.176e-15
Infrared	63.263	2	1.831e-14

TABLE 6-9. Dunn post-hoc test comparing PPG amplitudes between each custom phantom.

Comparison	Z	P (unadjusted)	P (adjusted)
0 D/H – 10% D	-4.055536	5.001957e-05	1.000391e-04
0 D/H – 10% H	4.055536	5.001957e-05	5.001957e-05
10% D – 10% H	4.055536	5.017550e-16	1.505265e-15

6.4 DISCUSSION

This study presents an innovative approach for investigating the impact of arterial stiffness on PPG signals using custom-designed vascular tissue phantoms. The fabrication process described can be adapted to simulate pathological conditions by altering the elastomer formulation, allowing for the modelling of both healthy and diseased vessels. The findings demonstrate that vessel wall thickness can be controlled by adjusting retarder concentrations. Furthermore, the mechanical properties of both vessels and surrounding tissue can be tuned through the addition of deadener or hardener, allowing for the customisation of softness and stiffness. Preliminary analysis of PPG signals confirmed that changes in vessel stiffness within the phantoms produced significant variations in signal amplitude, showing potential for non-invasive arterial stiffness assessment.

EFFECT OF ADDITIVES ON VESSEL THICKNESS AND ELASTICITY

Increasing retarder concentration led to a reduction in the thickness of the custom vessels. This is attributed to the extended cure time by the retarder. With a slower curing process, the silicone coating had more time to flow downward, resulting in thinner vessel walls before solidifying. Although the retarder itself does not directly alter the materials stiffness, its influence on wall thicknesses indirectly affected vessel elasticity. A thinner vessel is more elastic, with a lower Young's modulus (Bastida et al., 1998).

Deadener was incorporated to create softer, more elastic vessels that emulate the mechanical behaviour of healthy human arteries. At the highest tested concentration of 0.6 parts deadener, Young's modulus decreased from 0.52 MPa to 0.20 MPa, reflecting a substantial increase in elasticity. As anticipated, wall thickness remained relatively constant, ranging from 0.53 mm to 0.58 mm, indicating that deadener primarily influenced the material's stiffness rather than its dimensions. In contrast, hardener was introduced to reduce elasticity and recreate the stiffness of

pathological vessels. The addition of up to 1 part hardener resulted in an increase in Young's modulus from 0.52 MPa to 1.22 MPa, demonstrating reduced elasticity. Similar to the deadener group, wall thickness remained stable, between 0.50 and 0.54 mm.

Modifying Tissue Stiffness

In the silicone tissue, the addition of deadener produced a softening effect, as reflected by a reduction in Shore hardness. Conversely, incorporating hardener led to increased stiffness, shown by higher Shore hardness values. These findings demonstrate a positive relationship between tissue hardness and Young's modulus, consistent with previous research (Sun et al., 2018). The dorsal thigh typically exhibits a Shore hardness between OO25 and OO31 (Falanga and Bucalo, 1993), which can be replicated by combining equal parts of Part A, Part B, and deadener. The tissue of the human finger shows an average Young's modulus between 0.07 MPa and 0.2 MPa (Oprişan et al., 2016). This level of elasticity can be achieved by using a deader ratio between 0.2 and 0.8 relative to equal amounts of part A and Part B.

Replicatiopn of Healthy and Diseased Femoral Arteries

Peripheral arterial disease (PAD) involves narrowing or blockage of the arteries, most commonly affecting the lower limbs (Kramer, 2020). With ageing, vascular elasticity gradually declines (Segers et al., 2020). In this study, mechanical and dimensional properties of the common femoral artery were recreated in vitro. The average wall thickness of a healthy left common femoral artery is 0.55 ± 0.05 mm (Soneye et al., 2019), while vessel diameter ranges from 3.9 mm to 8.9 mm, with a mean of 6.6mm (Spector and Lawson, 2001). Reported Young's modulus values for a healthy femoral artery are approximately 0.80, 0.79 and 0.82 MPa for the intimae, adventitia and radial strain, respectively (Brum et al., 2010).

Based on results from this study, a mixture of 1A:1B:0.6H with 1.5% retarder can be used to approximate the mechanical properties of a healthy

femoral artery. When commercial silicone tubing with an outer diameter of 2.6 mm is used as the internal form, a vessel wall thickness of 0.51 mm can be achieved. This formulation corresponds to a Young's modulus of 0.82 MPa and outer diameter of 3.96 mm, within the range of the radial strain.

To replicate the characteristics of an atherosclerotic femoral artery with an elevated stiffness, the target Young's modulus is higher, at 3.6 MPa for the adventitia and 2.11 MPa for the radial strain (Brum et al., 2010). In this case, a ratio greater than 1A:1B:1H would be required to achieve this level of stiffness. However, due to material limitations, this may not be feasible with PlatSil Gel-10. However, PlatSil Gel-25 (Polytek Development Corp., Easton, PA) may be effective and should be explored to evaluate the potential for fabricating stiffer vessels.

PPG Amplitude & Vessel Elasticity

PPG signals were recorded from three phantoms incorporating vessels with different elasticities to investigate whether elasticity influenced the PPG waveform, with a focus on amplitude. The softest vessel phantom was fabricated using 0.2 parts deadener (10% of the total mixture), while the stiffest vessel phantom was created with the same ratio of hardener. The intermediate phantom was produced without any additives. Red and infrared PPG signals were analysed on a cycle-by-cycle basis, revealing that increasing vessel stiffness was associated with a reduction in PPG amplitude. This trend was statistically significant, as confirmed by Kruskal-Wallis analysis followed by Dunn post-hoc testing ($p < 0.001$).

These findings support that hypothesis that PPG signals, particularly amplitude features, can reflect changes in arterial stiffness. The observed relationship aligns with vascular physiology: stiffer vessels have reduced compliance and are therefore less capable of expanding during the arrival of the blood pulse wave. Since PPG is a volumetric technique, reduced

vessel expansion leads to smaller fluctuations in blood volume at the measurement site, resulting in a lower signal amplitude.

Pressure Signals

Accompanying pressure signals confirmed that the observed PPG waveforms were influenced by changes in pressure, with pressure traces displaying physiologically accurate morphology. While differences in PPG amplitude were evident with varying vessel stiffness, the pressure waveform remained consistent across all phantoms. This may be due to the location of the pressure sensor, which was at the outlet of the phantom, whereas the PPG sensor was located mid-vessel. Pressure signals served as a useful secondary validation, which could be expanded by incorporating additional techniques such as Doppler ultrasound for further insight intro flow-related volume changes within the vessel.

Clinical Considerations and Signal Consistency

To apply the findings of this study to clinical measurements, it is important to account for external factors that may influence the PPG waveform such as sensor contact and peripheral vasoconstriction (Karimpour et al., 2023; May et al., 2021). In the in vitro setup, both the phantoms and sensors were secured within a custom-built casing to minimise movement and maintain constant contact force throughout data acquisition.

Hydrostatic effects also play a role in in vivo measurements. The position of the sensor in relation to the heart influences arterial pressure and venous return due to gravitational effects. Previous research has shown that lowering the hand below heart level reduces both AC and DC components of the PPG signal, likely due to venous pooling. Conversely, raising the limb above heart level increases these components (Hickey et al., 2016). In this study, the in vitro system was arranged horizontally, and phantom placement was standardised to minimise hydrostatic pressure changes.

LIMITATIONS AND FUTURE WORK

Some limitations were identified during the fabrication of custom vessels. Due to the fragile nature of the material, the maximum workable ratio of deadener was found to be 1A:1B:0.6D. Beyond this threshold, the vessel adhered to the commercial silicone tubing (internal form), making removal difficult. Additionally, a minimum retarder concentration of 1.5% was required when operating the dip coater at a speed of 40 mm/min to ensure that the vessel could be pulled to its full height before curing commenced.

Future investigations should examine the effects of varying dip coater speed for more precise wall thickness control and better consistency throughout the vessel. This research could also be extended by expanding the upper limit of hardener concentrations to identify the maximum range of vessel stiffness. The current setup employed a deionised water-based fluid to replicate the characteristics of blood (Mohapatra et al., 2018), which could better simulate the Casson fluid properties of real blood by incorporating non-Newtonian fluids (Srivastava and Saxena, 1994). This introductory signal analysis can be continued through further extraction of PPG features such as peak width, area under the curve, and gradients to comprehensively understand vessel dynamics and mechanical behaviour in the context of arterial stiffness and PPG.

6.5 CONCLUSION

Recent advances in PPG highlight the need for in vitro systems capable of simulating both healthy and pathological vascular conditions to support the assessment of vascular ageing and CVD. This study presents a method for fabricating custom silicone vessels using a dip-coating technique to control vessel thickness and stiffness through adjustments in elastomer composition. By tailoring the formulation to introduce specific mechanical properties, vessel pathologies can be modelled and evaluated in contrast to healthy vessels through PPG signal analysis. This vessel and

tissue development system can be utilised in in vitro investigations in conjunction with in vivo studies.

This study aimed to fabricate custom vessels with tunable stiffness for integration intro an in vitro model. Within the system, PPG signals were recorded and analysed to asses waveform changes associated with varying vessel stiffness. The results demonstrated that PPG morphology, particularly signal amplitude, was influenced by the mechanical properties of the vessel. Statistically significant reductions in amplitude were observed with increasing stiffness, supporting the potential of PPG technology as a non-invasive tool for assessing arterial stiffness.

This chapter outlines a method for fabricating custom vessels and demonstrated how elasticity-driven changes in vessel stiffness influence the PPG signal amplitude. Improvements to the dip-coating process could facilitate the production of longer custom vessels. Additionally, alternative materials like PlatSil Gel-25 may be investigated to extend the achievable stiffness range. Further analysis full set of PPG features is recommended to deepen the understanding of the relationship between arterial stiffness and PPG waveform characteristics.

6.6 SUMMARY

This chapter presents the design, fabrication and evaluation of custom silicone vessels with adjustable mechanical properties for use in a controlled in vitro model. By adjusting concentrations of retarder, deadener, and hardener within a PlatSil Gel-10 formulation, vessel wall thickness and elasticity were successfully manipulated to replicate healthy and diseased arterial conditions. Mechanical testing confirmed that increased retarder reduced wall thickness (and thus elasticity), while deadener and hardener adjusted stiffness without affecting thickness.

Elasticity and Shore hardness measurements demonstrated that Young's modulus values could be achieved across a physiologically relevant range. Custom vessel-tissue phantoms were embedded in an in vitro circulatory

system for PPG signal acquisition during pulsatile flow. Statistical analysis confirmed that increased vessel stiffness was associated with a significant reduction in PPG signal amplitude ($p < 0.001$), aligning with physiological expectations of reduced vessel expansion in stiffer arteries.

This chapter highlights the feasibility of using dip-coated vessels with customisable elasticity in in vitro cardiovascular models. It also identifies fabrication constraints, including limits on silicone concentrations and proposes further work to refine and expand the coating processes. These advances support the development of in vitro models simulating vascular ageing for the investigation of PPG-based tools for non-invasive arterial stiffness assessment.

7 Arterial Stiffness Assessment & PPG Feature Significance Testing

7.1 Introduction

Developing the in vitro cardiovascular rig further, this investigation implements the custom silicone vessel production technique described in the previous chapter. As seen in the previous experiments, commercial silicone tubing allows for the development of robust in vitro models. While silicone dip-coating is useful for producing custom vessels with a higher elasticity to match specific human vessels, such as the radial artery of the arms or the tibial artery of the legs. By combining both types of vessels, commercial and custom, we can utilise the advantages of both to produce a durable silicone cardiovascular system, representing human properties and providing quality PPG signals at the elastic measurement site.

Continuing the investigation into CVD, the leading contributor to global mortality (Lackland and Weber, 2015; Mc Namara et al., 2019; Mensah et al., 2019), this chapter delves into vascular aging and arterial stiffness through custom vessels. The term "vascular ageing" describes the alterations that take place in the blood vessels with age, such as a loss of elasticity, which can impair the vascular system's ability to operate efficiently. Arterial stiffness results from the arteries loss of elasticity, and this is an important indicator of vascular ageing (Kohn et al., 2015). Understanding the connection between vascular ageing and arterial stiffness will help better understand age-related disorders.

With single-site PPG devices, continuous measurements are achievable since only one contact point is needed to take readings (Sun and Thakor, 2016). Another option is multi-site PPG, recorded simultaneously at several locations, such as the ears, fingers and toes, for the measurement of pulse transit time (Budidha and Kyriacou, 2014; Miglis, 2017). Previous studies have shown that multi-PPG and pulse transit time can be used to evaluate

CAD, peripheral arterial disease (PAD), and ageing (Allen et al., 2020; Bentham et al., 2018; Chan et al., 2019). Pulse transit time measurements can also be measured by pairing PPG with other physiological signals, such as electrocardiography (Miglis, 2017). This experiment utilises single-site PPG for arterial stiffness assessment due to the practicality of having only one device and measurement point, for example a smartwatch recording at the wrist, which could be employed in clinical as well as consumer settings.

This study aims to explore the relationship between arterial stiffness and vascular ageing by assessing PPG signals acquired from an in vitro vascular system, providing an indication of the utility of various pulse wave features, which would be beneficial to future arterial stiffness assessment techniques (Charlton et al., 2022) as well as exploring PPG-based arterial assessment in a controlled environment (May et al., 2021; Njoum and Kyriacou, 2018; Nomoni et al., 2019), whereby arterial stiffness can be isolated as a factor and manipulated. The hypothesis being that certain morphological features will show significant indication of vessel stiffening.

7.2 METHOD

VESSEL MANUFACTURE

Manufacturing of the custom vessels involved two parts based on a method described in the previous chapter. Firstly, the elastomer (PlatSil Gel-10 ,Polytek Development Corp., Easton, PA) was formulated and mixed for the desired vessel geometry and mechanical properties; secondly the vessel was fabricated via a combined dip-coating and curing process, using commercial silicone tubing (Hilltop Products Limited, Warrington, UK) as the vessel form. , Silicone was chosen due to its durability; in contrast to latex, silicone can maintain its form and endure high temperatures (Chruściel, 2022), crucial for the heat curing process being used in this setup. Hardener (Polytek Development Corp., Easton, PA) was added in different amounts, from 5% to 25%, in steps of 5%, to the elastomer

mixture to create five vessels of varying stiffnesses. The resultant vessels were tensile tested in a Universal Testing System (Instron 5944, Norwood, MA), indicating Young's elastic modulus values of 0.52 MPa, 0.60 MPa, 0.64 MPa, 0.78 MPa and 0.80 MPa, with an inner diameter of 2.8 mm and a wall thickness of 0.5 mm. This was representative of the dimensions of the arteries found in the forearm (Beniwal et al., 2014; Getachew et al., 2018; Madssen et al., 2006) and in the similar range of vascular elastic properties (Bernal et al., 2011; Lee et al., 2022b; McKee et al., 2011; Takashima et al., 2007).

In Vitro System, Signal Acquisition & Analysis

An in vitro setup was constructed using commercial silicone tubing that imitated the vessels found in the upper vascular system. Custom-manufactured portions were used in the areas being monitored. This setup was linked to a Pulsatile Pump System (PD-1100, BDC Laboratories, Wheat Ridge, CO). The pulsatile pump replicated the pulsatile flow characteristic of the human heart at 60 beats per minute. To mimic the optical properties of the blood and give good signals in the red and infrared wavelengths being utilised, a mixture of methylene blue powder (Thermo Fisher Scientific, UK) and deionised water was used, which was then circulated throughout the system. The custom vessels were integrated into this arrangement at locations approximating those in the vascular tree that were of interest, primarily the radial and ulnar arteries following the brachial artery bifurcation, and beneath them, a reflectance PPG sensor with a red (660 nm) and infrared (940 nm) LED was attached. Pressure sensors were positioned outside the customised region, so that the vessel segment used for PPG measurement remained uninterrupted. The sensors were connected to a custom dual-channel PPG acquisition system with a sampling rate of 2000 Hz, created by our research group at the Research Centre for Biomedical Engineering (RCBE), City St George's, University of London (Chan et al., 2019; Ferizoli et al., 2023). Raw signals were acquired by situating the sensors below the vessels, within a sensor casing to house

the sensor and hold the vessel in place, shown in FIGURE 7-1. Signals were displayed and recorded in LabVIEW (Version 2023 Q1, National Instruments, Austin, TX).

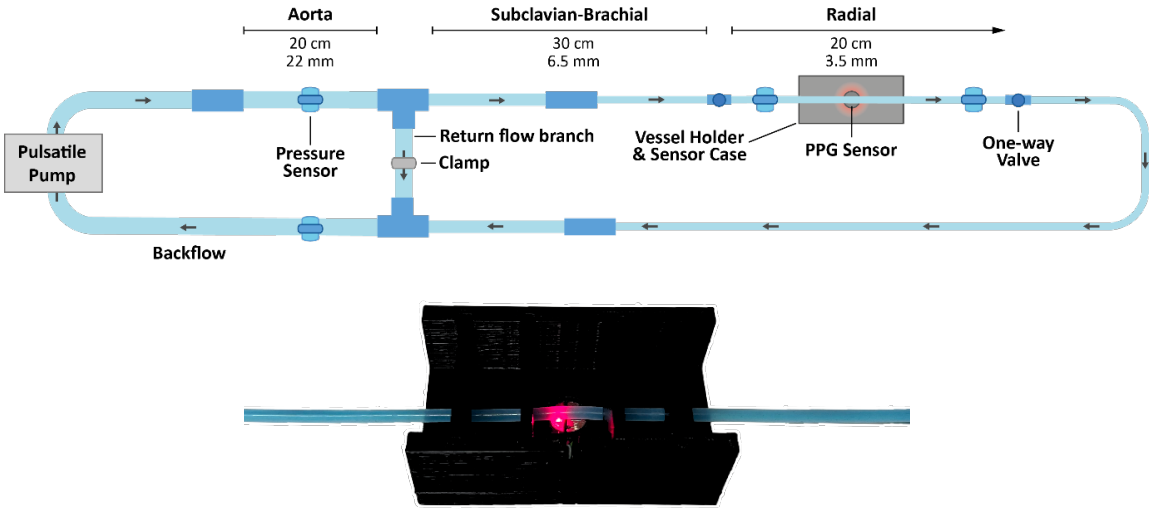

FIGURE 7-1. Schematic diagram of in-vitro setup (top) and photo of custom vessel held in PPG sensor case (bottom).

Feature extraction and analysis of the recorded signals, exemplified in FIGURE 7-2, were performed using a custom Python script, also developed at the RCBE, University of London (Bradley and Kyriacou, 2024). Recordings of 4 minutes from each vessel were split into 10 second windows, which were averaged to produce one data point per window. This produced a series of values for each feature, listed in TABLE 7-1. These results were illustrated with MATLAB (Version R2023a 9.14, MathWorks, Natick, MA) and statistically analysed and ranked by the Pearson correlation coefficient, through cross correlation computed in the R statistical programming language (Bernardo, 2023).

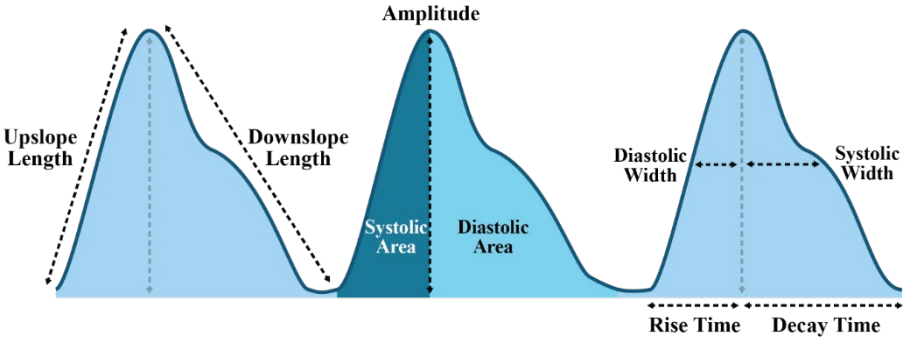

FIGURE 7-2. Example PPG features.

TABLE 7-1. Table of PPG Features.

FEATURE	DESCRIPTION
Area Under Curve (AUC)	Area of pulse
Systolic Area Under Curve (S-AUC)	Area of the systolic phase of the pulse
Diastolic Area Under Curve (D-AUC)	Area of the diastolic phase of the pulse
Area Under Curve Ratio (AUC Ratio)	Ratio between systolic and diastolic areas
Rise Time	Time taken for signal to rise from trough to peak
Decay Time	Time taken for signal to fall from peak to trough
Rise-Decay Time Ratio	Ratio of decay time to rise time
Amplitude	Median amplitude
Upslope Length	Length of tangent from trough to peak
Downslope Length	Length of tangent from peak to trough
Upslope	Gradient of pulse on rising edge
Downslope	Gradient of pulse on falling edge
Onset-End Slope	Rate of change of the pulse over the entire pulse length
Slope Ratio	Rising slope gradient (upslope) compared to falling slope gradient (downslope)
Length-Height Ratio	Ratio of the height of a pulse compared to its width
Slope Length Ratio	Ratio of the upslope length of a pulse compared to its downslope length
Upslope Length Ratio	Proportion of the total pulse length that is made up of the rising phase
Downslope Length Ratio	Proportion of the total pulse length that is made up of the falling phase
Start Datum Area	Area between PPG signal and the tangent from trough to peak (systolic phase)
End Datum Area	Area between PPG signal and the tangent from peak to trough (diastolic phase)

Datum Area Ratio	Ratio between systolic and diastolic datum areas
Max Start Datum Difference	Maximum length between PPG signal and peak-trough tangent (systolic phase)
Max End Datum Difference	Maximum length between PPG signal and trough-peak tangent (diastolic phase)
Median Start Datum Difference	Median length between PPG signal and peak-trough tangent (systolic phase)
Median End Datum Difference	Median length between PPG signal and trough-peak tangent (diastolic phase)
Pulse Width	Width of the entire pulse of one cycle (measured at 50% of height)
Systolic Width	Width of the systolic phase of the pulse (measured at 50% of height)
Diastolic Width	Width of the diastolic phase of the pulse (measured at 50% of height)
Width Ratio	Ratio between the systolic and diastolic widths (measured at 50% of height)
Variance	Deviation of signal from its mean value
Skewness	Degree of symmetry of a pulse
Kurtosis	Degree of sharpness of a pulse
Signal-to-Noise Ratio (SNR)	Level of PPG signal compared to noise
Zero-Crossing Rate (ZCR)	Number of times per second that the PPG signal crosses zero
Peak-To-Instantaneous Ratio (PIR)	Degree of change in amplitude over time

7.3 RESULTS

Red and infrared PPG signals were recorded from the custom vessels to observe differences in the signal due to varying arterial stiffness. Example red PPG signals from soft and stiff vessels are shown in FIGURE 7-3, revealing morphological differences between them. There is a clear change in amplitude in both the systolic and diastolic peaks between the two vessels. The amplitude of the soft vessel systolic peak is 0.71 V and 0.21 V for the diastolic peak, while the stiff vessel systolic and diastolic peak amplitude was 0.32 V and 0.13 V, respectively.

The signals were analysed for further morphological differences, such as slope gradient and half peak width by feature extraction. The resultant features are displayed in simple line plots, using the mean value for each feature in FIGURE 7-4, showing at a glance the trends in features across the five vessels, as stiffness increases. For example, in Area Under Curve (AUC), it can be seen that there is a strong negative correlation with vessel stiffness in the red PPG. Whereas a positive correlation is shown for both red and infrared signals in the Skewness and Kurtosis features. The features are also presented in box plot form in FIGURE 7-4, depicting the range of values for each feature.

Pearson correlation coefficients were calculated to determine the degree of correlation in the features, as well as to identify any correlations which may not be visually striking in the plots. The resultant coefficients are ranked in FIGURE 7-6 for the red and infrared PPG signal features, showing a different ranking order for the two wavelengths. Only correlation coefficients with a p-value below 0.05 are displayed, indicating statistical significance.

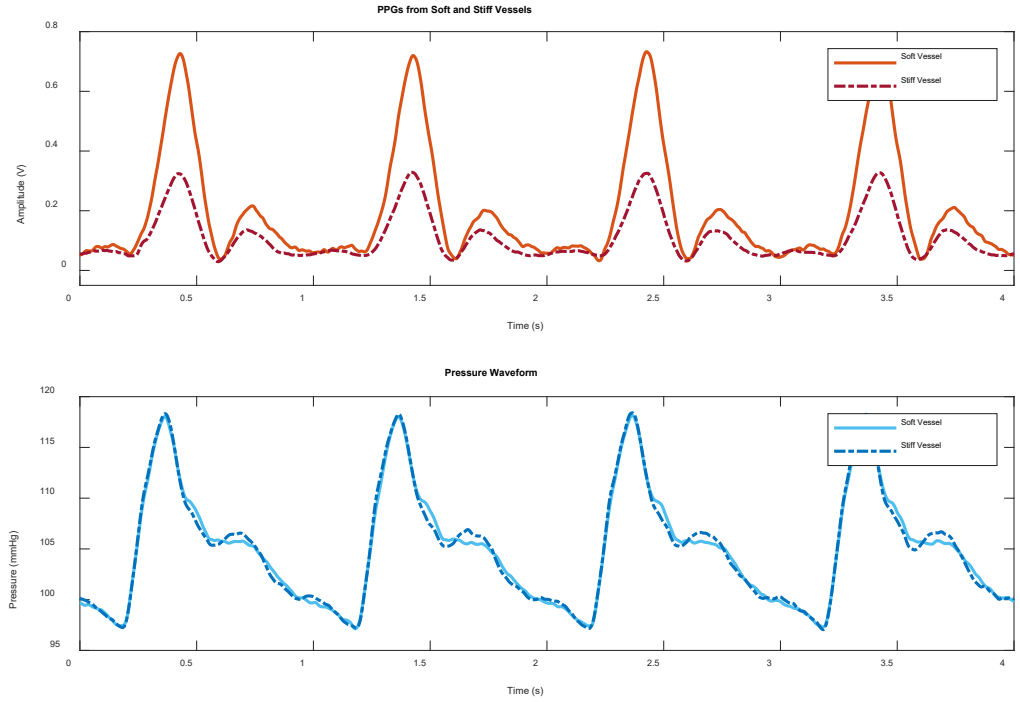

FIGURE 7-3. PPG and pressure signals from vessels with two different arterial stiffnesses. The PPG signals, which were obtained from sensors located on the vessel, depict the higher systolic and diastolic amplitudes of the soft vessel and the lower amplitudes of the stiff vessel. The pressure signals, conforming to a standard pressure pulse wave shape (Huang et al., 2019), were obtained by sensors placed after the vessel and do not show much variation between stiffnesses. The soft vessel exhibited a Young Modulus of 0.6 MPa, while the stiff vessel had a Young Modulus 0.8 MPa, representing the arterial stiffness values as highlighted in the literature (Bernal et al., 2011; Lee et al., 2022b; McKee et al., 2011; Takashima et al., 2007).

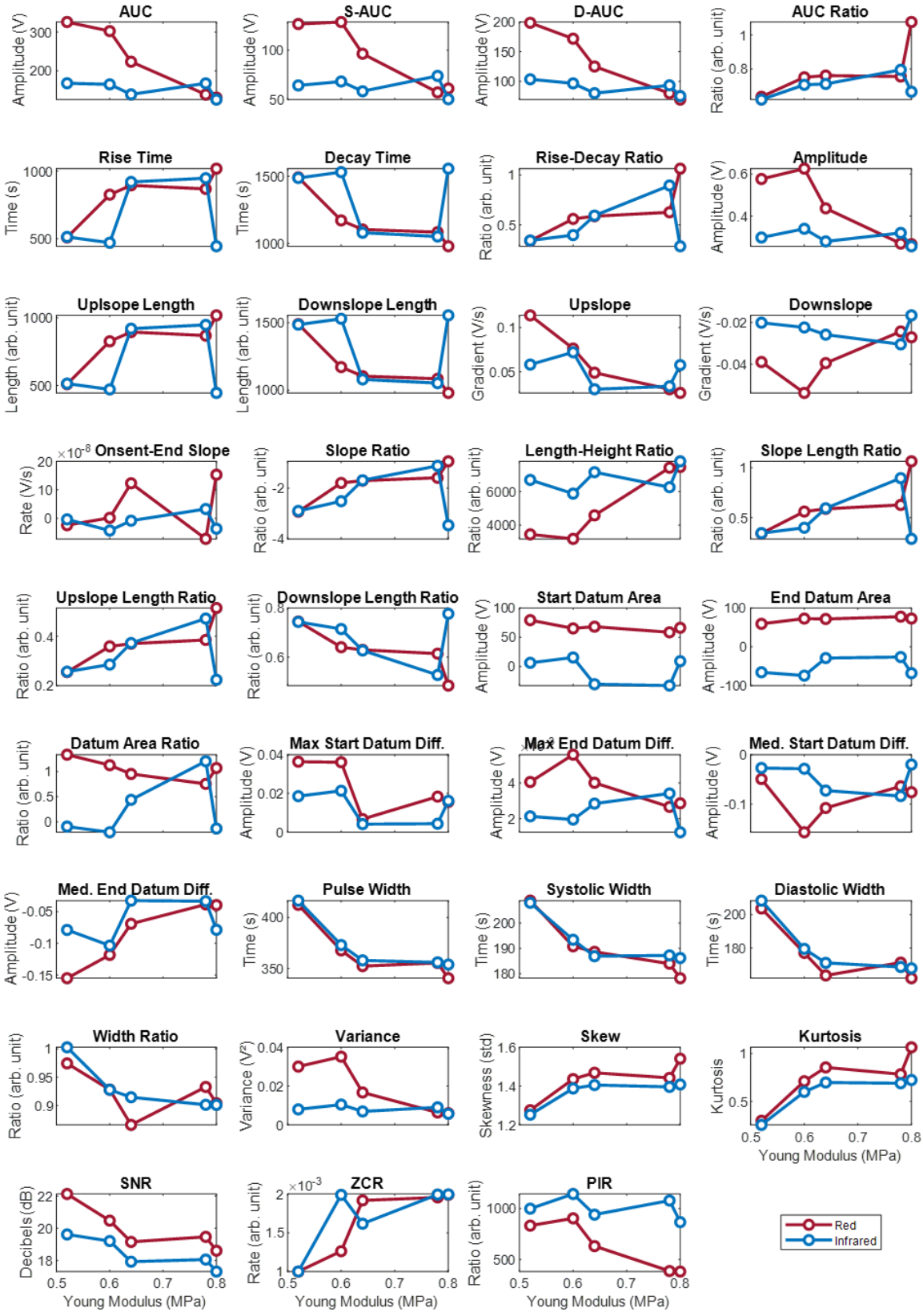

FIGURE 7-4. Line plots of the mean value of each feature, showing change in red and infrared PPG features with the custom vessels in order of increasing arterial stiffness.

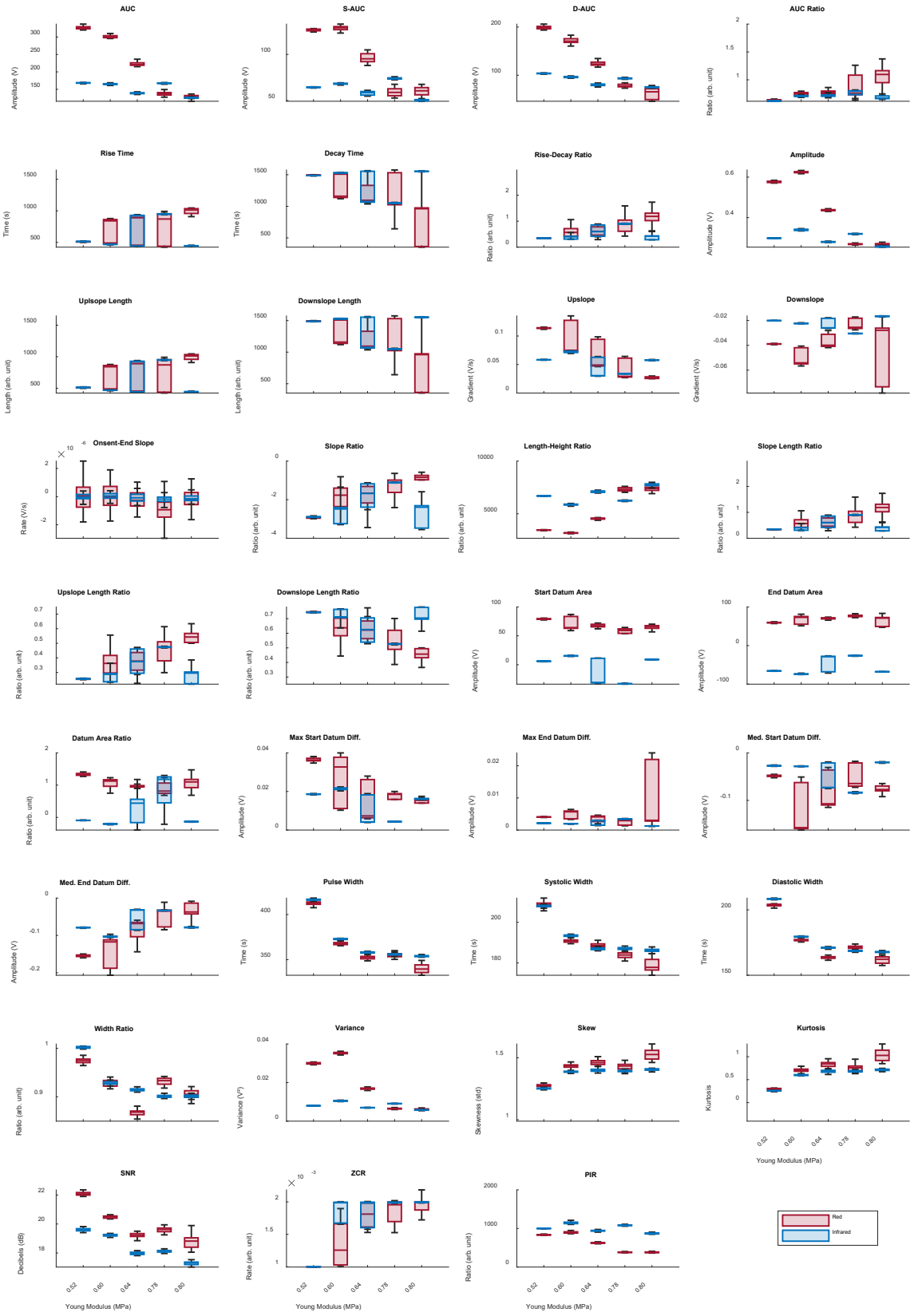

FIGURE 7-5. Box plots showing change in red and infrared PPG features with each of the custom vessels, in order of increasing arterial stiffness.

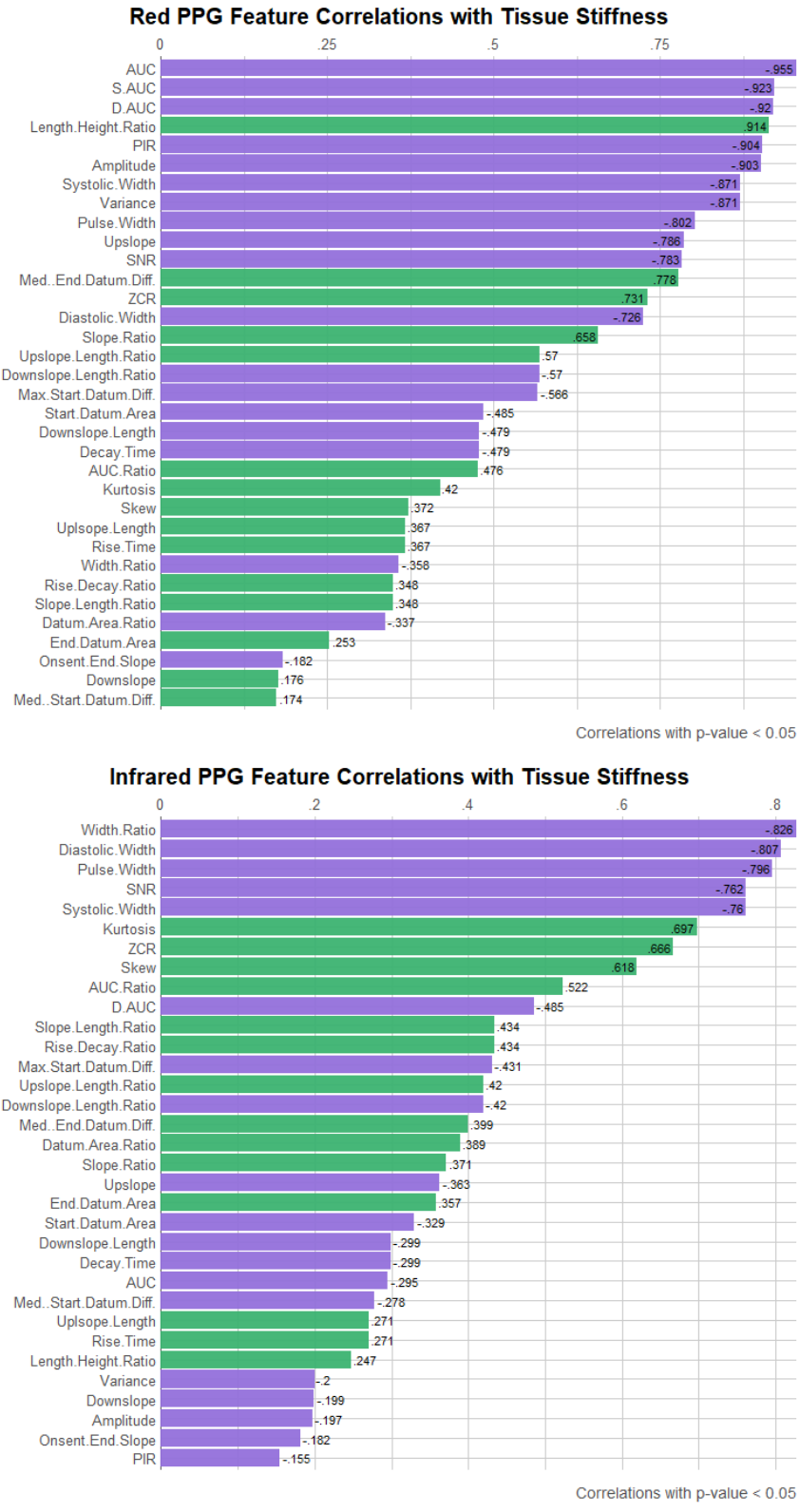

FIGURE 7-6. Red and infrared PPG features ranked by Pearson correlation coefficient with arterial stiffness. Only features which have a correlation coefficient with a corresponding p-value < 0.05 (statistically significant at 5% level) are displayed. (Green bars indicate positive correlation and purple bars indicate negative correlation.)

7.4 Discussion & Conclusions

This chapter has described the utilisation of custom vessels with varying stiffnesses to simulate vascular disease, followed by PPG signal acquisition and feature extraction on those vessels during pulsatile flow to look for significant markers in the PPG morphological features that may indicate stiffness. It has been our hypothesis that this can then be used for the detection of stiffening vessels that may indicate CVD. The vessels were created using an adjustable silicone elastomer and dip-coating process. Using this technique, vessels were created and placed in an in vitro test rig where the cardiovascular system could be emulated, consisting of a pulsatile pump and a surrounding vascular network circulating a blood-mimicking fluid, while acquiring PPG signals.

Visual observation of the PPG signals, exemplified in Figure 7-3, indicates that the vessels and in vitro system in this study were successfully able to replicate human PPG signals, including the systolic and diastolic peaks, featuring the dicrotic notch. Furthermore, the morphology of these PPGs is evidently influenced when compared to a vessel with a higher arterial stiffness (Finnegan et al., 2023). This change can be most profoundly seen in the reduction of the amplitude of the systolic peak in the stiffer vessel. A similar but lesser effect can also be noted in the diastolic peak amplitude. This initial observation can be explained by the physiology of blood flow and PPG acquisition. A stiffer artery is less able to expand; as such, a smaller change in blood volume is possible, resulting in a PPG with a lower amplitude (Cecelja and Chowienczyk, 2012). This phenomenon can be linked to other aspects of the PPG wave – with a reduction in amplitude, a reduced area under curve, pulse width and upslope/downslope would be expected (Shin, 2022). Cross-checking similar morphological features for expected trends as such provides a way of validating the feature extraction algorithm. For example, a decrease in area under curve is anticipated to result in a corresponding decrease in the pulse width.

The absence of marked pressure waveform changes is likely due to the sensor location and the different physiological quantities being measured. The pressure sensor was placed after the vessel, so it reflected the propagated system pressure pulse rather than the local vessel-wall response at the measurement site. In contrast, the PPG sensor was positioned directly on the vessel and was therefore more sensitive to local compliance changes caused by stiffening. As local vessel stiffness was varied without major changes to the overall pump conditions or extended vascular network, the pressure waveform remained broadly similar while the local volumetric response detected by PPG changed more clearly.

Further analysis of the PPG signals was conducted by feature extraction to determine the magnitude of morphological changes with each vessel and reveal potential correlations between PPG features and arterial stiffness. The values of each extracted feature were compared across the five vessels of varying vessel stiffness in FIGURE 7-4. A clear difference in PPG amplitudes with stiff and soft vessels is observed and it was expected that the amplitude feature, as well as area under curve and pulse widths (systolic and diastolic) would show a negative correlation, which is confirmed in the red line plots, helping to validate the feature extraction process. However, this correlation does not appear as strong in the amplitude and area under curve features of the infrared signal, as it does with pulse width, which is similar in both wavelengths. This suggests that the infrared signal is less susceptible to morphological changes, which may be linked to the absorption spectra of the methylene blue fluid, penetration depth of those wavelengths in this phantom or the placement of the PPG sensor on the vessel. Rise time was also expected to show a strong correlation with stiffness. Yet, although a statistically significant correlation is present, it does not rank highly in the feature ranking for red or infrared signals. Further experimentation is required to validate the statistical ranking of features. In the width ratio, a smoother negative trend is seen in the infrared signal. Overall, the red signal shows visibly larger changes

than the infrared, particularly in area under curve (including systolic and diastolic) and length-height ratio. In other features, both wavelengths have a similar trend, as seen in area under curve ratio, pulse width (including systolic and diastolic), skewness, kurtosis, and signal-to-noise ratio. The varying nature of the extracted features between the two signals highlights the importance of multi-wavelength PPG monitoring, as it allows for simultaneous signal processing and physiological measurements which offer alternatives in situations where a particular wavelength may perform better or worse than the others.

By observing the range and variability of the features, shown by the boxplots in FIGURE 7-5, the reliable features can be determined. According to the boxplots, the most stable features are those related to area, amplitude, and width, as well as indexes such as skewness, kurtosis, and signal-to-noise ratio show notable change between stiffnesses while maintaining a low variation at each vessel. This suggests that these features can be used in a wide range of applications for non-invasive measurement, as low variability and high correlation would result in reliable arterial stiffness assessment, and possible other factors such as blood pressure. This hypothesis must be followed up with patient studies to compare pulse feature reliability in vivo. These results also showcase the value of signal indexes, for example pulse skewness and kurtosis, as they can be correlated with physiological phenomena such as vascular stiffening more strongly than some geometrical features (Park and Shin, 2022; Shin, 2022). These indexes can be used alongside geometrical features to better predict cardiovascular diseases.

A ranking based on correlation coefficients can signify the most reliable PPG features for arterial stiffness measurement, which can also be employed in in vivo and in vitro studies. As shown in FIGURE 7-6, there is a significant link between arterial stiffness and the area of the PPG wave, as the three highest correlated features in red PPGs are areas under the curve. Interestingly, these features are not as highly ranked in infrared signals,

further demonstrating the versatility of multi-wavelength measurement. The top three infrared PPG features are width related, suggesting that PPG wavelengths are affected differently by physiological changes such as arterial stiffness. To further discern the morphological differences, it is worth conducting investigations utilising other commonly used PPG wavelengths such as green light.

7.5 SUMMARY

This study demonstrated the use of PPG feature extraction and significance testing to identify morphological features affected by vessel stiffness in an in vitro environment. PPG signals were recorded from a range of vessels, resembling various stages of healthy and diseased arteries, which revealed distinct morphological changes correlated to arterial stiffness. Notably, red PPG signals showed the greatest shifts in area-related features, while pulse width infrared features were more strongly associated with arterial stiffness changes. This work expands the scope of non-invasive arterial stiffness evaluation and paves the way for further research involving more rigorous in vitro experiments, such as analysis at varying heart rates and flow rates to determine differences in responsiveness to flow changes between stiffnesses; as well as parallel in vivo studies to unravel the impact of biological factors such as age and respiration on PPG pulse shape.

8 PPG & Vessel Stiffness with Varying Flow Properties Utilising Bilateral Custom Vessels

8.1 Introduction

The relationship between the PPG waveform and arterial stiffness remains complex, particularly under varying flow and heart rate conditions that occur in real physiological states. This chapter aims to address this by investigating how PPG waveforms respond to changing flow and heart rate conditions when measured from custom vessels of varying stiffness. Building upon earlier work, this chapter integrates both healthy and unhealthy vessels into a bilateral flow setup, enabling simultaneous assessment of differences in vascular response under identical haemodynamic conditions. This approach provides advantages over of sequential testing by offering controlled, uninterrupted, parallel analysis of PPG waveforms in healthy and unhealthy conditions.

The core aim of this chapter is to investigate how PPG waveforms recorded from these phantoms change in response to haemodynamic changes, and to determine which signal features are most sensitive to differences in vessel stiffness. This work represents a step forward in the development of in vitro models for vascular assessment using PPG. The findings from this study provide valuable insights that could inform future efforts to design wearable devices and algorithms for non-invasive detection of arterial stiffness and contribute to broader research into cardiovascular health monitoring.

8.2 METHOD

Combining the experimental methods developed in previous stages, this chapter embeds custom-designed silicone vessels with varied stiffness profiles into tissue moulds to produce vessel-tissue phantoms. These phantoms, previously tested individually within single-branch setups, have now been integrated into a bilateral flow configuration. This advances earlier work, where bilateral experiments were limited to commercial vessels and custom vessels were examined in isolation. By utilising custom vessels embedded within the phantom and incorporating them into the bilateral system, this setup enables the simulation of in vivo mechanical environment and allows for simultaneous comparison of vessels responses under identical flow conditions. Signals were recorded in LabVIEW, visualised with MATLAB; features extracted using Python and statistically analysed in the R programming language with custom scripts.

VESSEL FABRICATION

Two custom vessels were fabricated using the previously established dip-coating method, one representing a healthy vessel and the other mimicking pathological stiffness. Unlike earlier designs that used both silicone softener and hardener to achieve a broad range of stiffness, both vessels in this case were formulated with the only hardener, of varying levels, to achieve more physiologically relevant wall properties and maintain consistency between the vessel structures. The resulting elastic moduli were approximately 0.52 MPa for the healthy vessel and 1.22 MPa for the unhealthy vessel, representing the range of the femoral artery (Brum et al., 2010).

PHANTOM DEVELOPMENT

Following fabrication, each vessel was embedded within a tissue-mimicking phantom to produce composite vessel-tissue units. The tissue matrix was formed using a silicone blend tailored to achieve a Shore 0030 hardness, approximating the mechanical characteristics of soft biological tissue. This marks a progression from previous experiments, where custom vessels

were tested in isolation without tissue phantoms or in single branches one at a time.

Bilateral Setup

The embedded phantoms were incorporated into the bilateral flow model, replacing the commercial tubing used in earlier configurations. This integration allowed both custom vessels to be studied simultaneously under identical flow conditions, which could be controlled, enabling direct comparison of optical and mechanical properties and vascular response to varying flow, visualised in Figure 8-1.

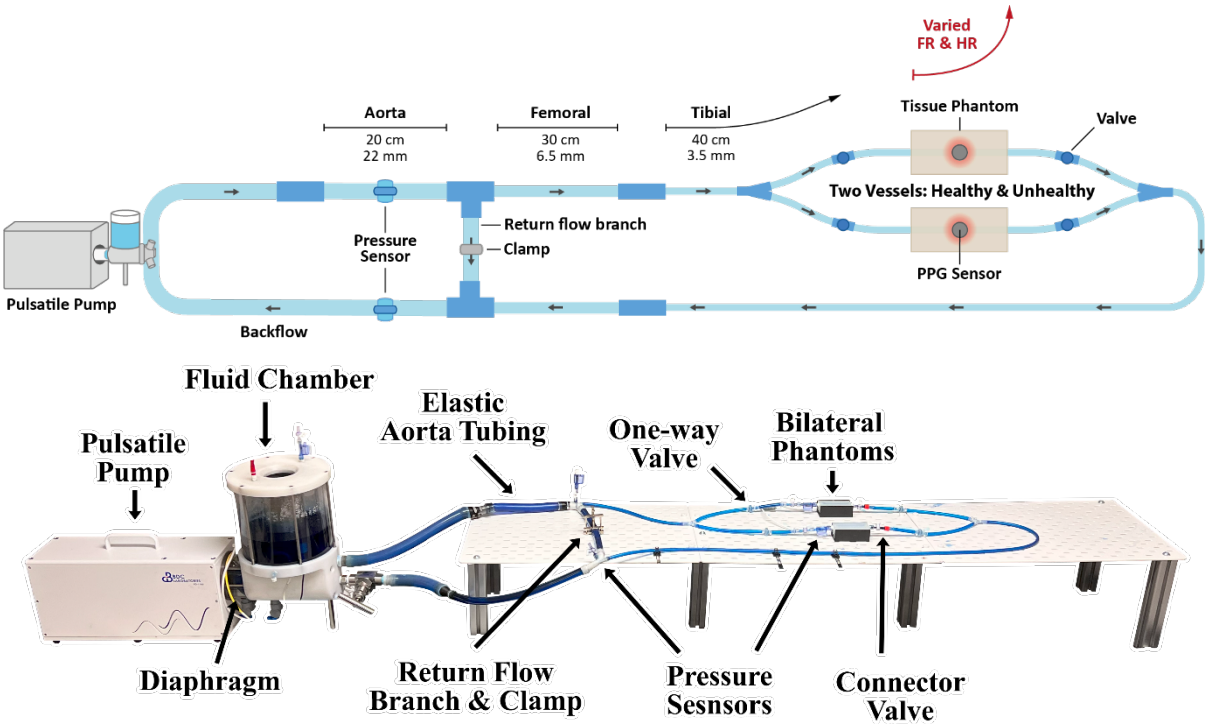

Figure 8-1. Bilateral in-vitro setup for parallel vascular assessment during varying flow dynamics.

Experimental Protocol

The bilateral setup was updated to replace the previous Harvard Apparatus pump with a BDC pulsatile pump (PD-1100, BDC Laboratories, Wheat Ridge, CO), which features adjustable flow rate controls. This modification was utilised to vary FR from 1 to 6 l/min and HR from 60 to 180 bpm. Each experimental run held one parameter constant while varying the other: for

instance, to study flow rate effects, HR was fixed (starting at 60 bpm) while FR was incremented from 1 to 6 L/min in steps. Following this, HR was increased to 90 bpm and the FR range was repeated. At each condition, segments of PPG data were collected for both phantoms and wavelengths. These raw PPG waveforms were preprocessed (filtered to remove baseline drift and high-frequency noise) and then feature extraction was performed on a pulse-by-pulse basis, averaged in 10 second windows.

Feature Extraction

A set of physiologically relevant features were defined to quantify waveform characteristics. These included time-domain features such as rise-time (time from pulse foot to peak) and decay time (time from peak to end of diastolic wave), which relate to the duration of systolic upstroke and diastolic fall. Slope-based metrics were calculated: upslope (gradient of pulse on rising edge) and downslope (gradient of pulse on falling edge). Amplitude metrics included peak amplitude of each pulse (AC height from baseline to peak) and the area under curve (AUC) of the pulse over the cardiac cycle, which was also separated into its systolic and diastolic parts to capture where in the cycle the most blood volume change occurs. Datum lines were defined as a reference to measure start and end datum area and difference, depicted in Figure 8-2.

From these, composite indices were derived; for example, the length-height ratio, defined as the ratio of pulse width to pulse height, which is high for broad, low pulses and lower for narrow, tall pulses. Another composite was the slope ratio (ratio of upslope to downslope magnitudes), indicating the symmetry of the pulse. Finally, we evaluated signal quality via signal-to-noise ratio (SNR) to compare how well-defined the pulses were in the healthy and stiff vessels under various conditions.

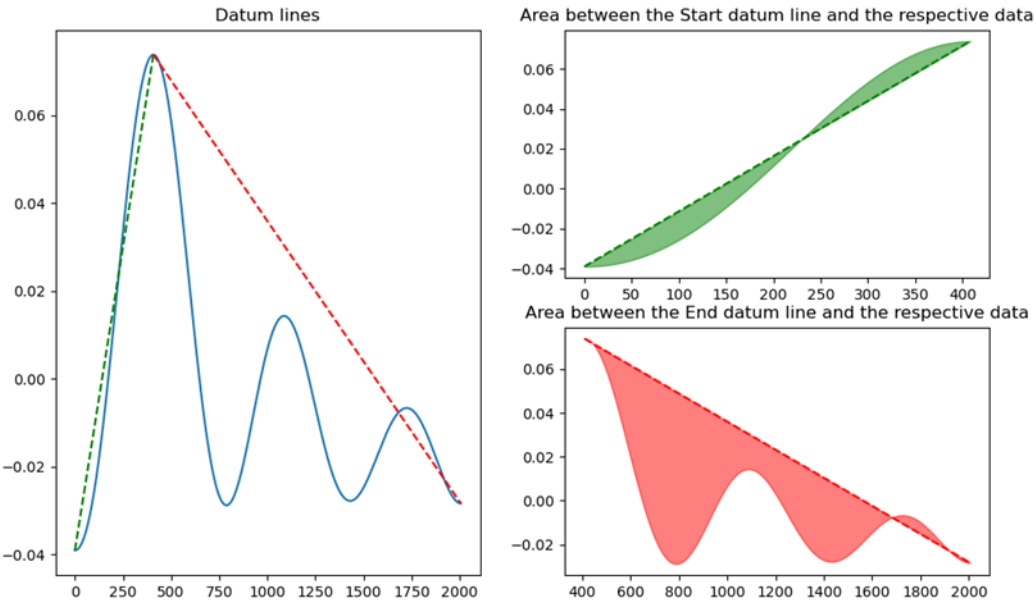

FIGURE 8-2. Visualisation of start and end datum features for PPG waveform analysis. The left panel shows a representative PPG waveform with the start datum line (green dashed line) from pulse onset to pulse peak and end datum line (red dashed line) from pulse peak to pulse end. The upper right panel illustrates the area between the start datum line and the waveform data, shaded in green, while the lower right panel shows the area between the end datum line and the waveform data, shaded in red. These areas, as well as distances, are used as features reflecting waveform morphology and potential indicators of vascular stiffness.

DATA ANALYSIS

To assess the influence of vessel stiffness on each feature across conditions, we first computed simple correlation statistics, producing a Pearson correlation coefficient between stiffness and each extracted feature, across all HR/FR settings. This was done separately for the features derived from the red and IR PPG signals. A high correlation (with a p-value < 0.05) would indicate that a feature increases or decreases when comparing the healthy and diseased vessels, suggesting it as a potential arterial stiffness indicator. Significant features were ranked in order of correlation coefficient to determine the most relevant features for vessel health detection.

To model the effects of flow and heart rate on PPG features more comprehensively, we used generalised additive models (GAMs) as part of

our regression analysis. For each feature, a GAM was fitted with FR and HR as predictor variables (using spline smoothing functions), and an interaction term to allow separate fits for healthy and diseased vessels. The GAM approach was chosen for its ability to capture potential non-linear relationships, for example, a greater difference in amplitude at higher flows. We obtained smooth curves of each feature against FR or HR for both vessels, along with 95% confidence bands.

To evaluate interaction effects, for example, whether the gap between the feature values from the healthy and diseased phantoms widens at high flow, we computed the difference between the two vessel's smooth curves and assessed its significance. This was done by pointwise statistical tests across the FR and HR intervals. If the difference curve's confidence band did not include zero (or if $p < 0.05$ at the given point), we inferred a statistically significant divergence in that feature due to stiffness, facilitated by an increase in FR or HR. This method indicated whether there was a FR–stiffness interaction, meaning the effect of stiffness on the feature depends on flow rate (and similarly for HR–stiffness interaction), with a visualisation of the trend.

8.3 Results

The results are presented in figures as follows: example PPG waveforms for healthy and unhealthy vessels and at different flow conditions to illustrate shape changes; bar charts of feature correlations with stiffness for visual ranking; and several plots of features against flow rate for both wavelengths, including the difference subplots highlighting at which flow rates healthy and diseased features differ significantly.

Waveform Morphology under Varying Flow

The raw PPG waveforms displayed revealed that flow rate has a dramatic impact on pulse amplitude and shape, and this impact differs between compliant and stiff vessels. Figure 8-3 shows infrared PPG waveforms from the healthy and unhealthy phantoms at a low flow (2 L/min, top) and a high

flow (6 L/min, bottom). At 2 L/min, both the healthy (dashed blue trace) and stiff (solid orange trace) vessels produce a similar waveform morphology and amplitude, the pulses are relatively small and smooth with only subtle differences. However, at the higher flow of 6 L/min the differences become pronounced. The healthy vessel's amplitude (0.35 V) is noticeably increased compared to the stiff vessel (0.2 V), showing a particularly sharper systolic peak compared to the diastolic.

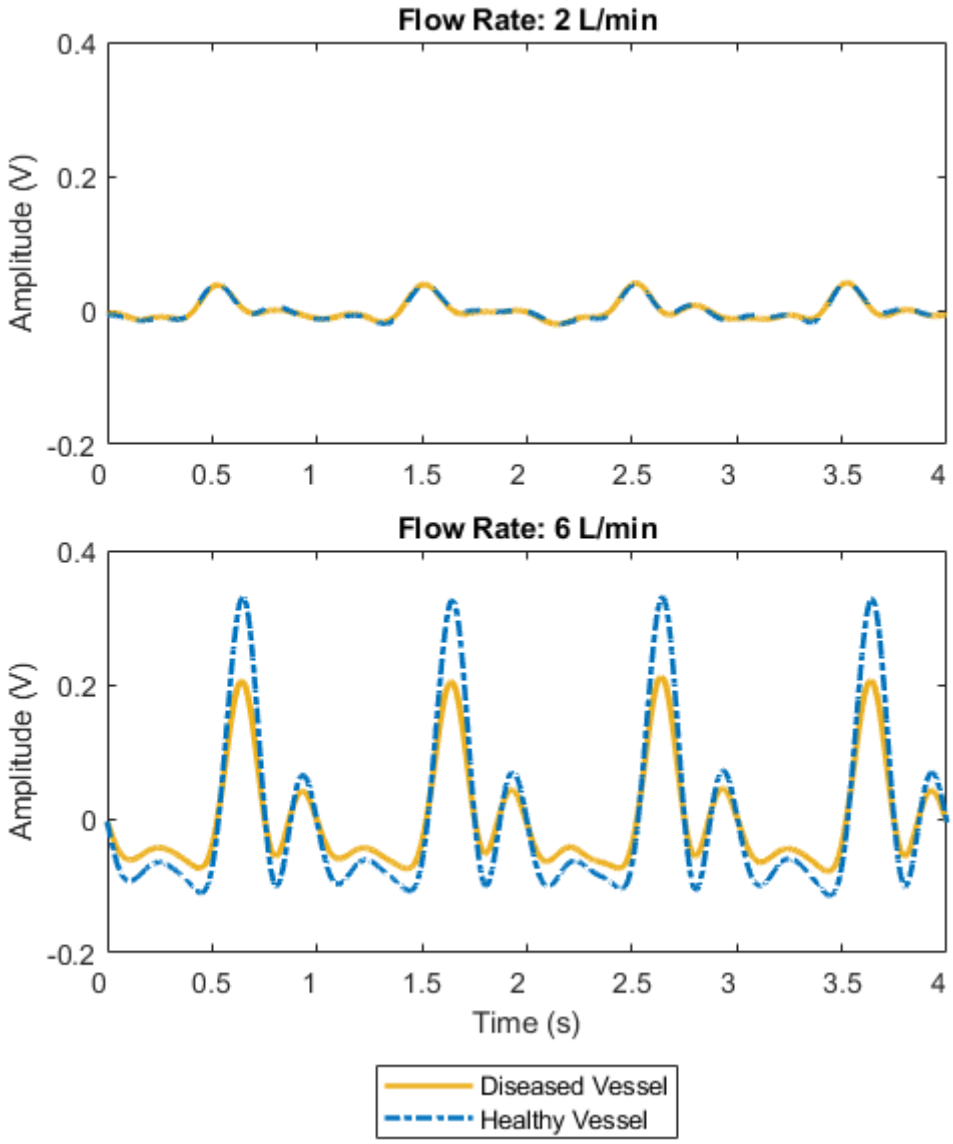

FIGURE 8-3. IR PPG waveforms from healthy and unhealthy vessels. Showing a similar morphology at a flow rate of 2 L/min (top), and an increased pulse amplitude and altered waveform morphology in the diseased vessel at a higher flow of 6 L/min (bottom).

In addition to overall amplitude changes, multi-wavelength comparison uncovered differences in how red and infrared PPG signals respond to flow and stiffness. FIGURE 8-4 compares simultaneous red and IR waveforms in each phantom at low and high flow. At 2 L/min the red and IR signals have roughly similar amplitudes, for both the healthy and diseased vessels. However, at 6 L/min, while both red and IR increase in magnitude for the soft vessel, the IR channel's is much more pronounced. The IR pulse in the becomes sharp and tall, reaching an amplitude of 0.3 V, while the red pulse peaks at 0.2 V. These waveform observations hint that the IR channel may be more sensitives to changes in haemodynamic conditions and stiffness.

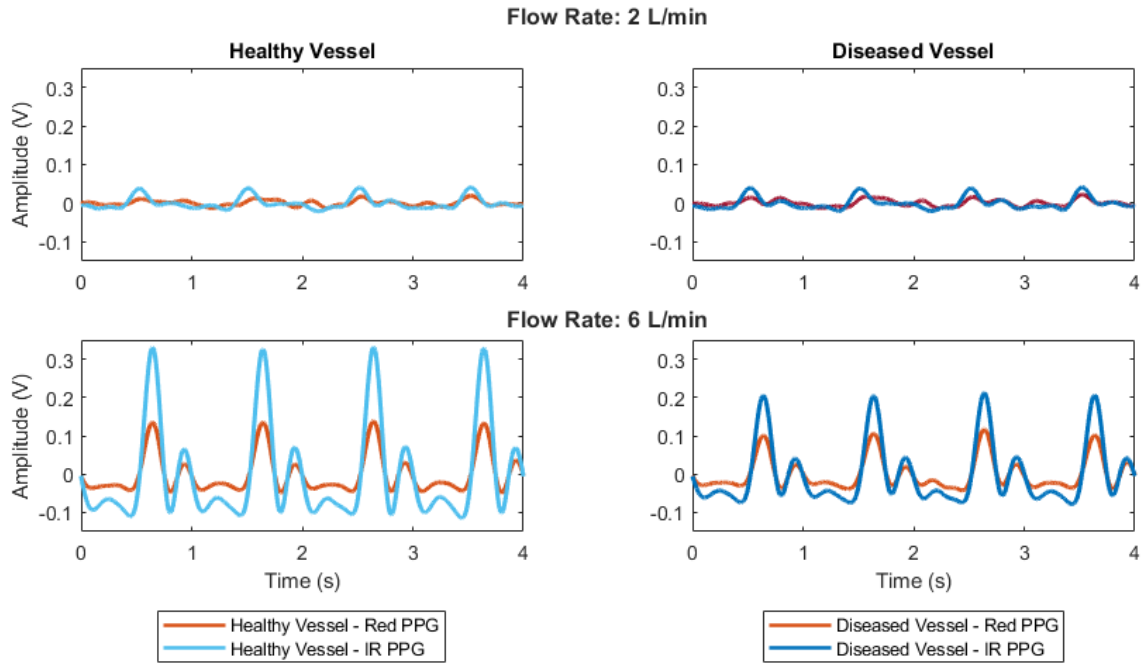

FIGURE 8-4. Red and IR PPG waveforms from healthy left panels) versus unhealthy (right panels) vessels. Showing a similar amplitude at flow rate 2 L/min (top), and an increased amplitude at 6 L/min (bottom), with the IR signals displaying a greater rate of change in amplitude.

FEATURE CORRELATIONS WITH STIFFNESS

A broad range of PPG features were extracted from these waveforms and analysed to determine which best distinguish a stiff vessel from a healthy one. FIGURE 8-5 summarises the Pearson correlation coefficients of various features with increasing vessel stiffness, for both the red and infrared channels. Features are ranked by the strength of correlation (only those with statistically significant correlation, $p < 0.05$, are shown). Blue bars denote features from the IR PPG and orange bars denote features from the red BBG. Light-coloured bars indicate a positive correlation (feature value increases as stiffness increases), whereas dark-coloured bars indicate a negative correlation (feature decreases with greater stiffness). Notably, more significant features were identified in the IR signal than in the red signal. Out of the 35 total features, 8 of the red PPG features were significantly correlated with vessel stiffness (5 positively correlated and 3 negatively correlated. In contrast, 14 IR features were significant (4 positive and 10 negative).

To systematically quantity how PPG waveform features relate to vessel stiffness and physiological conditions, the Pearson correlation coefficients between each extracted feature and the parameters of interest are listed in TABLE 8-1, showing both red and IR channels against stiffness, FR and HR, with corresponding p-values.

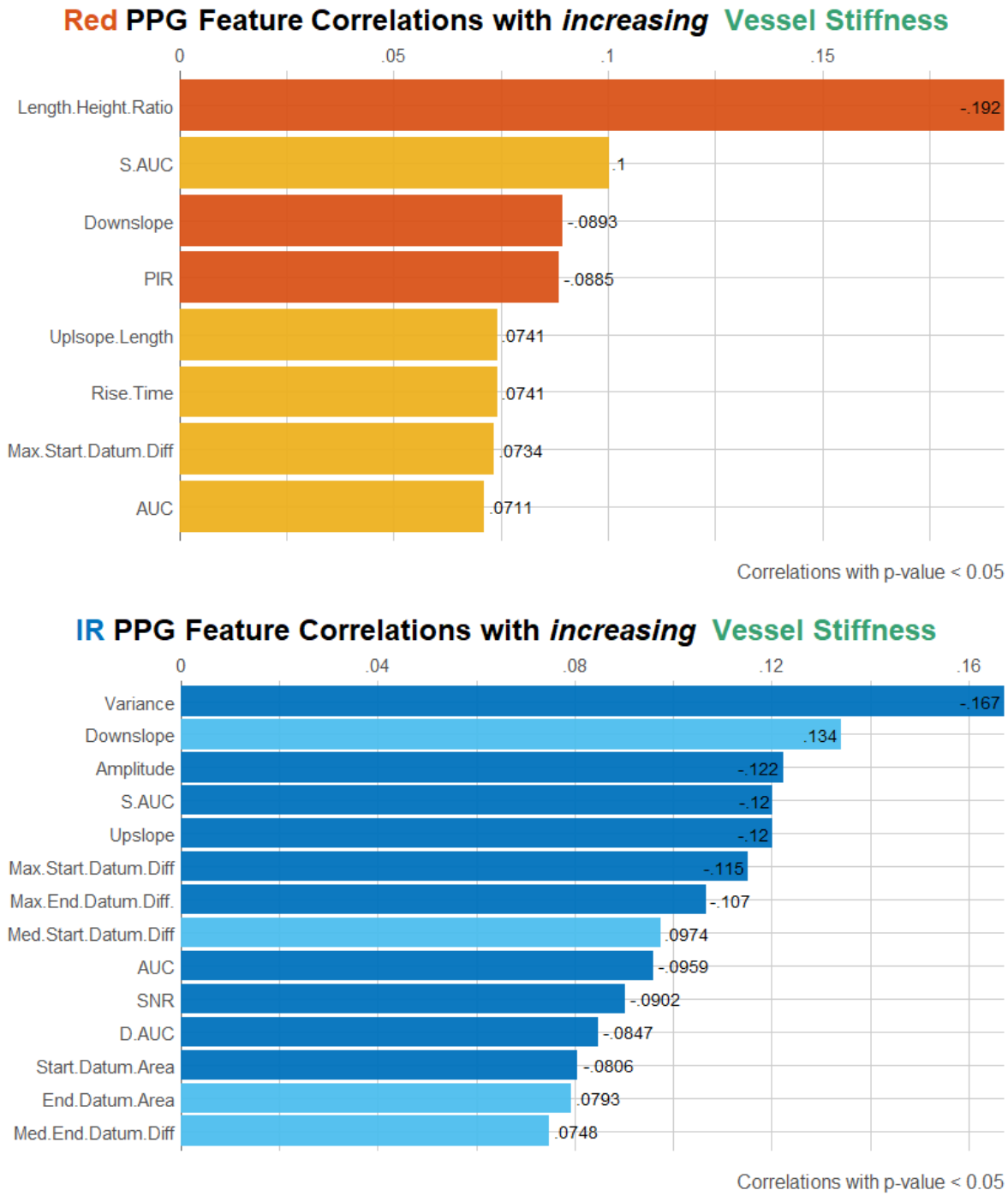

FIGURE 8-5. Red and infrared PPG feature correlations with increasing vessel stiffness, ranked by Pearson correlation coefficient. Orange bars indicate features are derived from red signals, while IR features are presented in blue. Shade indicates direction of correlation: light bars are positive correlations (features increase as vessel stiffnesses increases, while dark bars are negative correlations (features decrease as stiffness increases). Only features with a correlation coefficient with a corresponding p-value < 0.05 (statistically significant at 5% level) are included.

TABLE 8-1. Correlation coefficients (Pearson r) and p-values for red and infrared PPG waveform features against vessel stiffness, flow rate and heart rate. Positive correlations indicate features values increase with the parameter, presented in green; negative correlations indicate decreases, in red. Statistically significant correlations ($p < 0.05$) are shown, highlighting features with potential utility for stiffness detection and sensitivity to haemodynamic conditions.

	Stiffness				Flow Rate				Heart Rate			
	Red		IR		Red		IR		Red		IR	
FEATURES	corr	p value	corr	p value	corr	p value	corr	p value	corr	p value	corr	p value
AUC	0.07	$5.0 \cdot 10^{-02}$	-0.10	$8.1 \cdot 10^{-03}$	0.58	$1.7 \cdot 10^{-70}$	0.60	$8.0 \cdot 10^{-77}$	-0.52	$9.7 \cdot 10^{-54}$	-0.56	$1.3 \cdot 10^{-63}$
S.AUC	0.10	$5.6 \cdot 10^{-03}$	-0.12	$8.9 \cdot 10^{-04}$	0.69	$2.0 \cdot 10^{-107}$	0.75	$4.3 \cdot 10^{-137}$	-0.46	$2.6 \cdot 10^{-40}$	-0.47	$3.7 \cdot 10^{-42}$
D.AUC			-0.08	$1.9 \cdot 10^{-02}$	0.52	$8.3 \cdot 10^{-54}$	0.54	$6.7 \cdot 10^{-58}$	-0.56	$2.8 \cdot 10^{-64}$	-0.59	$1.6 \cdot 10^{-72}$
AUC Ratio									0.48	$1.6 \cdot 10^{-44}$	0.71	$4.9 \cdot 10^{-118}$
Rise Time	0.07	$4.1 \cdot 10^{-02}$			-0.33	$1.1 \cdot 10^{-20}$	-0.16	$1.2 \cdot 10^{-05}$	-0.09	$1.8 \cdot 10^{-02}$		
Decay Time					0.08	$3.5 \cdot 10^{-02}$			-0.72	$3.3 \cdot 10^{-122}$	-0.90	$1.2 \cdot 10^{-276}$
Rise Decay Ratio					-0.07	$4.0 \cdot 10^{-02}$			0.51	$6.9 \cdot 10^{-51}$	0.71	$2.3 \cdot 10^{-119}$
Amplitude			-0.12	$7.1 \cdot 10^{-04}$	0.73	$3.4 \cdot 10^{-126}$	0.74	$5.7 \cdot 10^{-131}$	-0.43	$6.8 \cdot 10^{-35}$	-0.44	$1.2 \cdot 10^{-36}$
Upslope Length	0.07	$4.1 \cdot 10^{-02}$			-0.33	$1.1 \cdot 10^{-20}$	-0.16	$1.2 \cdot 10^{-05}$	-0.09	$1.8 \cdot 10^{-02}$		
Downslope Length					0.08	$3.5 \cdot 10^{-02}$			-0.72	$3.3 \cdot 10^{-122}$	-0.90	$1.2 \cdot 10^{-276}$
Upslope			-0.12	$9.0 \cdot 10^{-04}$	0.73	$4.2 \cdot 10^{-128}$	0.73	$7.7 \cdot 10^{-129}$	-0.35	$8.3 \cdot 10^{-24}$	-0.38	$5.7 \cdot 10^{-27}$
Downslope	-0.09	$1.4 \cdot 10^{-02}$	0.13	$2.0 \cdot 10^{-04}$	-0.86	$1.5 \cdot 10^{-229}$	-0.90	$1.9 \cdot 10^{-280}$	-0.13	$1.9 \cdot 10^{-04}$	-0.22	$8.9 \cdot 10^{-10}$
Onset End Slope							-0.09	$1.0 \cdot 10^{-02}$				
Slope Ratio					-0.21	$5.2 \cdot 10^{-09}$			0.59	$3.4 \cdot 10^{-72}$	0.85	$5.0 \cdot 10^{-215}$
Length Height Ratio	-0.19	$8.6 \cdot 10^{-08}$			-0.87	$6.3 \cdot 10^{-230}$	-0.75	$3.7 \cdot 10^{-140}$	0.12	$1.1 \cdot 10^{-03}$	0.14	$7.7 \cdot 10^{-05}$
Slope Length Ratio					-0.07	$4.1 \cdot 10^{-02}$			0.51	$5.3 \cdot 10^{-51}$	0.71	$1.5 \cdot 10^{-119}$
Upslope Length Ratio					-0.13	$2.5 \cdot 10^{-04}$			0.57	$1.7 \cdot 10^{-67}$	0.80	$2.5 \cdot 10^{-173}$
Downslope Length Ratio					0.13	$2.5 \cdot 10^{-04}$			-0.57	$1.7 \cdot 10^{-67}$	-0.80	$2.5 \cdot 10^{-173}$
Start Datum Area			-0.08	$2.6 \cdot 10^{-02}$	0.38	$6.0 \cdot 10^{-28}$	0.39	$2.1 \cdot 10^{-28}$	-0.50	$1.5 \cdot 10^{-49}$	-0.62	$2.7 \cdot 10^{-81}$
End Datum Area			0.08	$2.9 \cdot 10^{-02}$	-0.35	$9.1 \cdot 10^{-23}$	-0.38	$8.5 \cdot 10^{-28}$	0.45	$5.0 \cdot 10^{-39}$	0.62	$7.7 \cdot 10^{-81}$
Datum Area Ratio							-0.10	$4.1 \cdot 10^{-03}$	0.10	$7.6 \cdot 10^{-03}$	0.71	$5.0 \cdot 10^{-116}$

Max Start Datum Diff	0.07	$4.3 \cdot 10^{-02}$	-0.12	$1.4 \cdot 10^{-03}$	0.65	$1.1 \cdot 10^{-93}$	0.71	$4.3 \cdot 10^{-119}$	-0.30	$3.7 \cdot 10^{-17}$	-0.39	$2.3 \cdot 10^{-28}$
Max End Datum Diff			-0.11	$3.2 \cdot 10^{-03}$	0.61	$4.5 \cdot 10^{-78}$	0.63	$1.1 \cdot 10^{-85}$	-0.33	$1.0 \cdot 10^{-20}$	-0.31	$5.6 \cdot 10^{-19}$
Med Start Datum Diff			0.10	$7.1 \cdot 10^{-03}$	-0.46	$2.3 \cdot 10^{-40}$	-0.49	$5.8 \cdot 10^{-48}$	0.52	$4.6 \cdot 10^{-54}$	0.55	$1.3 \cdot 10^{-61}$
Med End Datum Diff			0.07	$3.9 \cdot 10^{-02}$	-0.35	$4.2 \cdot 10^{-23}$	-0.32	$9.1 \cdot 10^{-20}$	0.48	$2.6 \cdot 10^{-45}$	0.58	$2.4 \cdot 10^{-68}$
Pulse Width					-0.51	$1.0 \cdot 10^{-51}$	-0.16	$1.7 \cdot 10^{-05}$	-0.18	$9.7 \cdot 10^{-07}$	-0.50	$8.1 \cdot 10^{-50}$
Systolic Width					-0.25	$1.5 \cdot 10^{-12}$			-0.25	$9.3 \cdot 10^{-13}$	-0.35	$2.8 \cdot 10^{-23}$
Diastolic Width					-0.53	$1.7 \cdot 10^{-55}$	-0.29	$2.7 \cdot 10^{-16}$	-0.36	$4.5 \cdot 10^{-24}$	-0.63	$4.1 \cdot 10^{-86}$
Width Ratio					-0.38	$1.3 \cdot 10^{-27}$	-0.42	$3.5 \cdot 10^{-34}$	-0.10	$5.3 \cdot 10^{-03}$	-0.28	$9.9 \cdot 10^{-15}$
Variance			-0.17	$3.5 \cdot 10^{-06}$	0.62	$8.6 \cdot 10^{-84}$	0.59	$9.0 \cdot 10^{-74}$	-0.39	$1.1 \cdot 10^{-28}$	-0.37	$1.6 \cdot 10^{-25}$
Skew					0.49	$1.9 \cdot 10^{-46}$	0.14	$1.3 \cdot 10^{-04}$	-0.67	$4.4 \cdot 10^{-99}$	$4.4 \cdot 10^{-99}$	$1.9 \cdot 10^{-293}$
Kurtosis					-0.13	$3.0 \cdot 10^{-04}$			-0.67	$1.5 \cdot 10^{-99}$	-0.85	$1.4 \cdot 10^{-209}$
SNR			-0.09	$1.3 \cdot 10^{-02}$	0.89	$4.6 \cdot 10^{-259}$	0.88	$3.4 \cdot 10^{-247}$	-0.33	$2.0 \cdot 10^{-20}$	-0.30	$1.3 \cdot 10^{-17}$
ZCR					0.30	$2.9 \cdot 10^{-17}$	0.09	$1.8 \cdot 10^{-02}$	0.41	$9.4 \cdot 10^{-33}$	0.52	$2.4 \cdot 10^{-54}$
PIR	-0.09	$1.4 \cdot 10^{-02}$			0.36	$3.4 \cdot 10^{-25}$	0.43	$5.2 \cdot 10^{-35}$	-0.28	$3.8 \cdot 10^{-15}$	-0.57	$1.1 \cdot 10^{-65}$

Effects of Flow Rate and Heart Rate on PPG Features

The influence of flow and heart rate on the PPG features was analysed using generalised additive model regression. Infrared features with significant trends were selected: *AUC*, *amplitude*, *upslope*, *downslope*, *start datum area*, *end datum area*, *max start datum difference*, *medium start datum difference*, *variance* and *SNR*.

The relationship of each feature with flow rate was modelled with separate curves for the healthy and unhealthy vessels utilising a generative additive model (GAM), which flexibly modelled the non-linear relationship without imposing strict linear assumptions. This is presented for the infrared features *AUC* and *amplitude* in Figure 8-6, in the upper panels, where a positive correlation with FR can be seen for both features. Confidence intervals around the fits reflect the uncertainty of the model estimates. The lower panels show the estimated pairwise differences between healthy and unhealthy signals across FR values, calculated directly from the GAMs. Shaded regions represent 95% confidence intervals for these differences, and red points denote FR levels where the difference reached statistical significance ($p < 0.05$). This analysis revealed that differences in both *AUC* and *amplitude* between healthy and unhealthy vessels became increasingly significant at higher flower rates, particularly above an FR of 4, which was a general trend seen throughout the other assessed features.

The same analytical approach was extended to the additional IR PPG-derived features presented in subsequent figures. Figure 8-7 illustrates the analysis of *upslope* and *downslope* features. Upslope showed a clear increasing trend with flow rate, while the downslope demonstrated a downward trend. The datum features are presented in the following figures: *start* and *end datum area* in Figure 8-8; *maximum* and *median start datum difference* in Figure 8-9. In *datum area*, a difference in trends was seen between the start and end, whereas in *datum difference*, a difference was seen between the maximum and median. Figure 8-10 shows the *variance*

and *signal-to-noise ratio (SNR)*. Variance displayed an increase and widening gap with FR, as in previous features, while SNR showed an overall increase but constant gap between healthy and unhealthy vessels.

In addition to the primary waveform and feature correlation analyses, further comparisons were made to asses how features from the red signal differed to the infrared, and how infrared features behaved with changing heart rate compared to flow rate, offering a broader perspective on feature behaviour beyond the main analysis. FIGURE 8-11 illustrates side-by-side comparisons of red and IR channels for *systolic area under curve (S-AUC)* and *length-height ratio*. FIGURE 8-13 extends the investigation to heart date effects in IR features, highlighting how key features such as *S-AUC*, *amplitude*, *downslope length* and *signal-to-nose ratio* evolve with increasing heart rates. FIGURE 8-12 shows how IR pulse width behaves differently for increasing heart rate compared to flow rate, facilitating direct comparison of physiological responses.

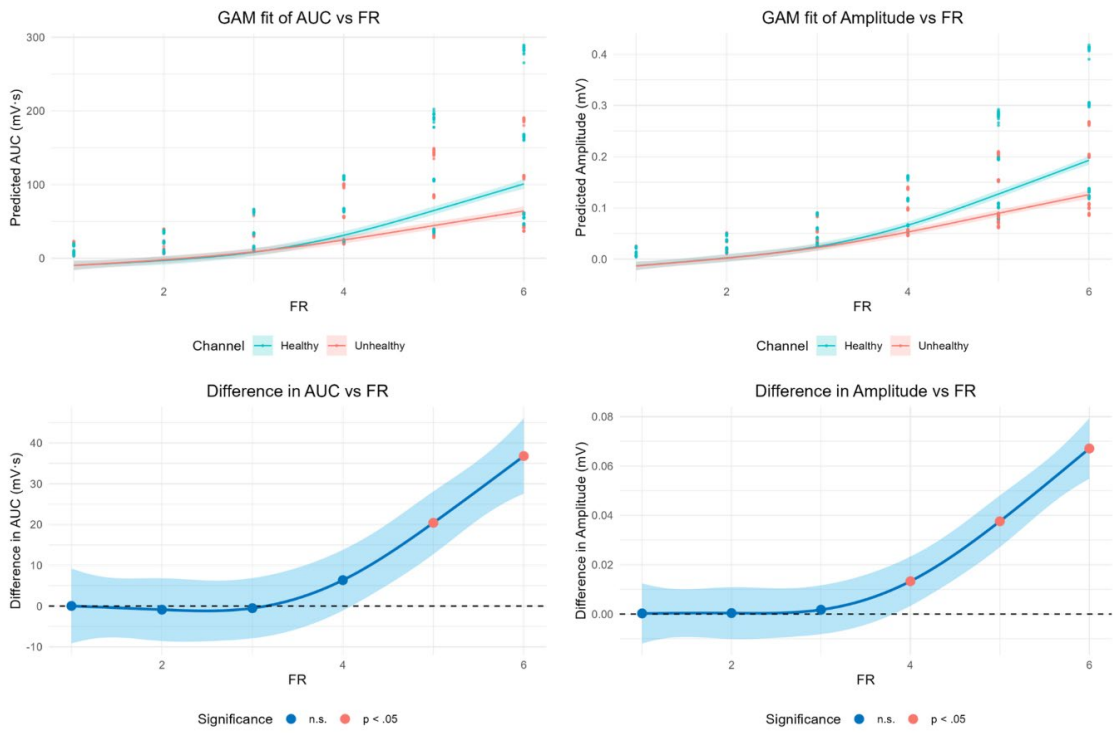

FIGURE 8-6. GAM fits of healthy and unhealthy vessels, and pairwise differences for IR area under curve (AUC) and amplitude as a function of flow rate.

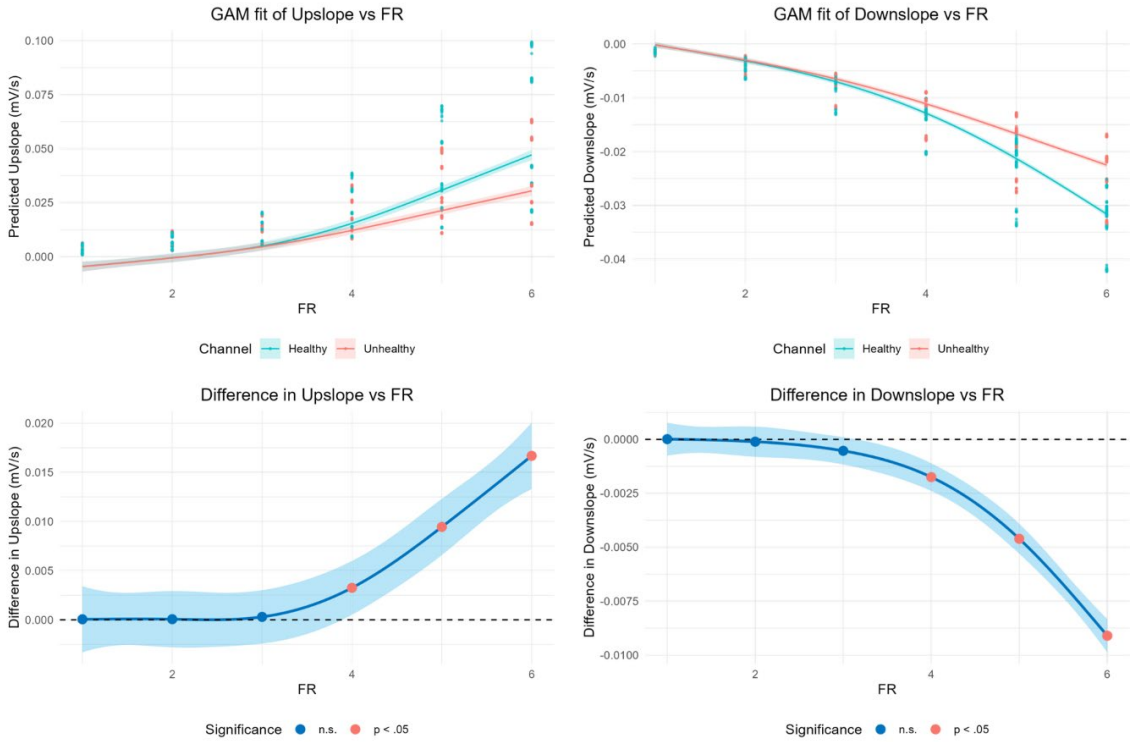

FIGURE 8-7. GAM fits of healthy and unhealthy vessels, and pairwise differences for IR *upslope* and *downslope* as a function of flow rate.

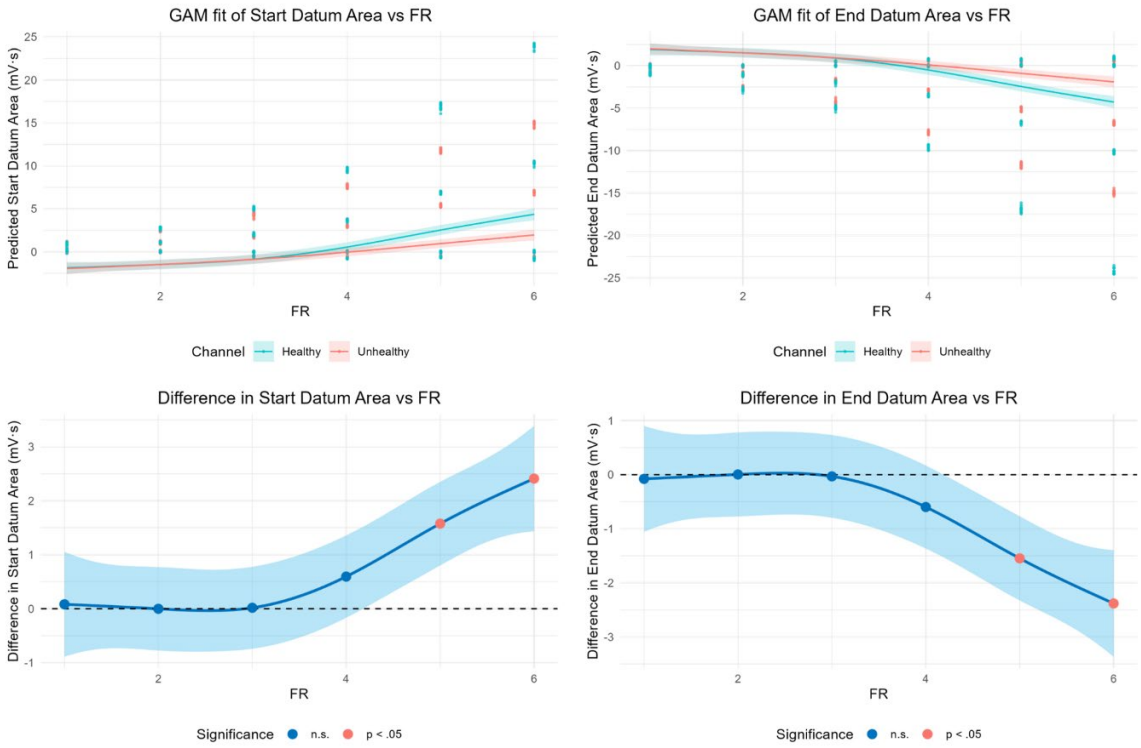

FIGURE 8-8. GAM fits of healthy and unhealthy vessels, and pairwise differences for IR *start* and *end datum* areas as a function of flow rate.

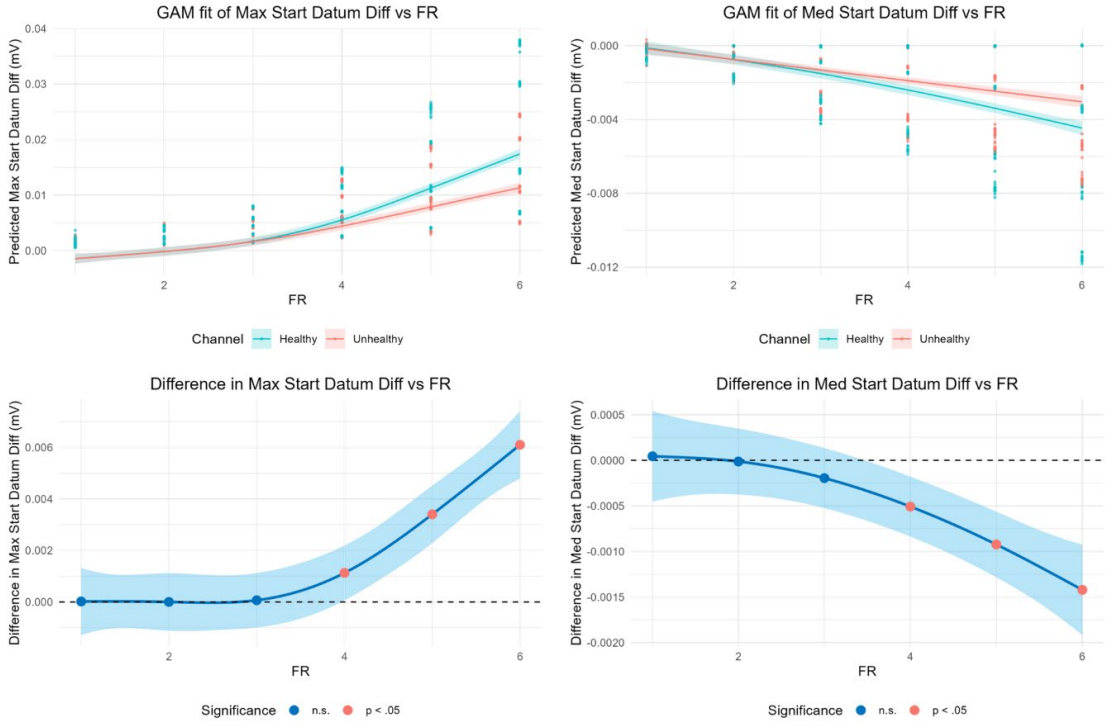

FIGURE 8-9. GAM fits of healthy and unhealthy vessels, and pairwise differences for IR *maximum* and *median* and start *datum differences* as a function of flow rate.

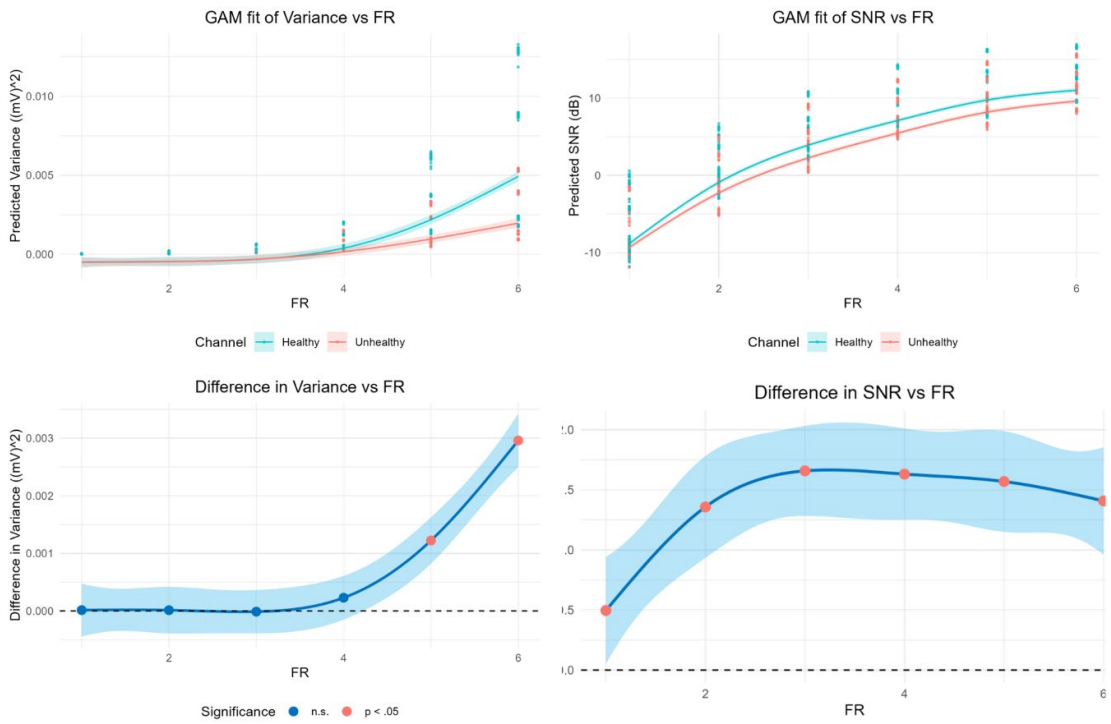

FIGURE 8-10. GAM fits of healthy and unhealthy vessels, and pairwise differences for IR *variance* and *SNR* as a function of flow rate.

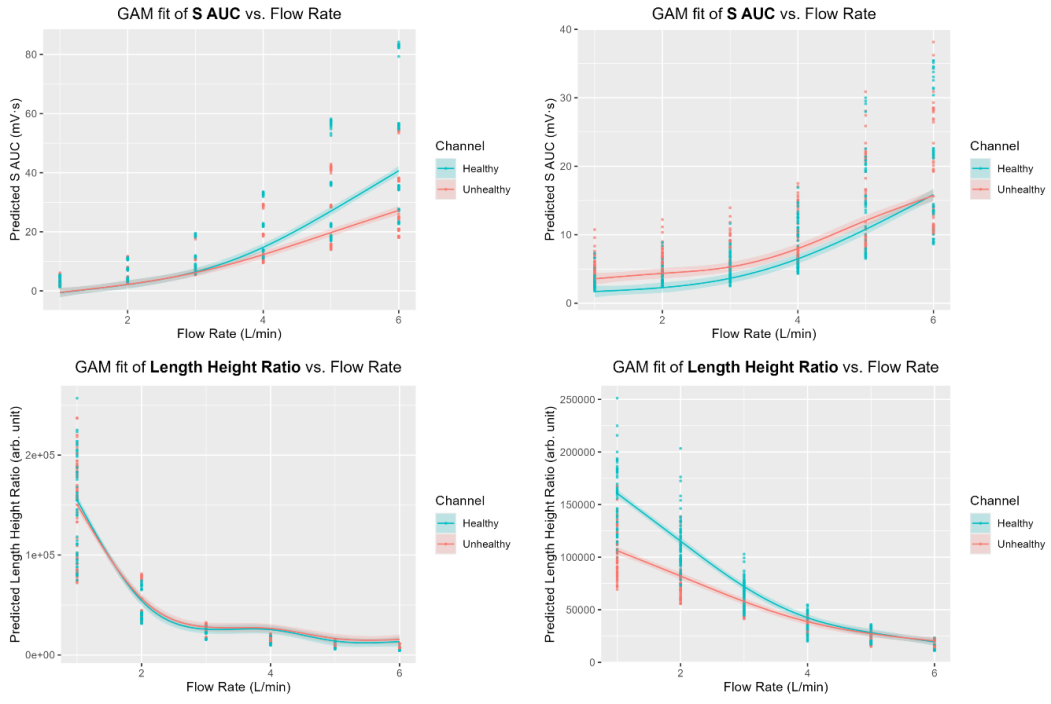

FIGURE 8-11. GAM fits comparing infrared (left panels) to red (right panels) measurements for the features: systolic area under curve (S AUC) and length height ratio.

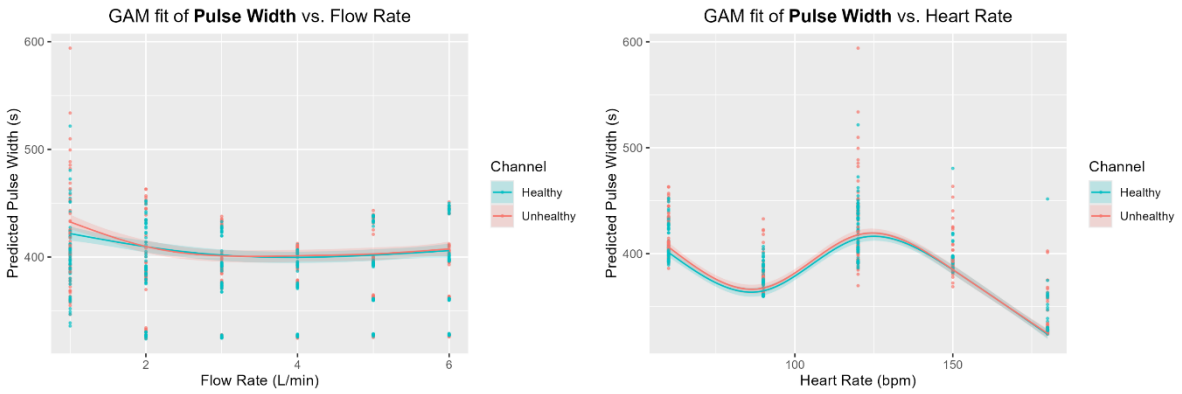

FIGURE 8-12. GAM fit comparing IR pulse width response to increasing flow rate (left) and heart rate (right).

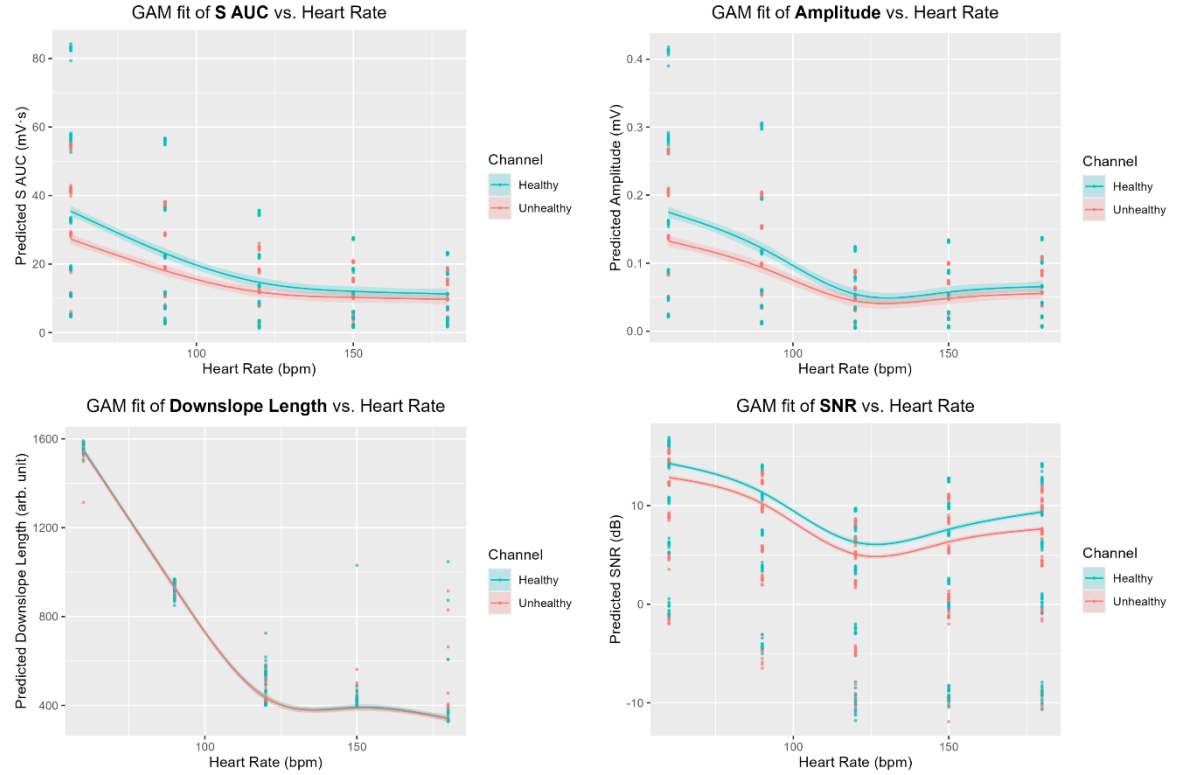

FIGURE 8-13. GAM fits of IR features against *heart rate* for healthy and unhealthy vessels.

8.4 Discussion & Conclusions

This study expands on the previous research by investigating healthy and diseased vessels in a bilateral in vitro experiment that demonstrates different vascular responses between them when under varying haemodynamic conditions. The bilateral configuration enabled simultaneous comparative assessment, eliminating experimental variability and providing a controlled environment to isolate the effects of vessel stiffness on PPG signal characteristics during varied flow properties, representing an advancement over the previous single-vessel investigation (Ferizoli et al., 2024). The integration of custom-manufactured vessels into tissue phantoms allowed for optimal human mechanical properties (0.52 MPa longitudinal elasticity for healthy, 1.22 MPa for diseased), incorporated into an in vitro bilateral system previously utilising only fixed commercial vessels (Ferizoli et al., 2023).

Morphological Analysis

The morphological changes observed with increasing flow rate demonstrated physiologically consistent patterns that validate the experimental model. For both the infrared and red wavelengths, increasing flow rate produced changes in waveform characteristics: pulse height and area visibly increased for both the systolic and diastolic portions. Visual inspection of the PPG waveforms showed a relationship between vessel stiffness and signal morphology under varying flow conditions. This was seen for both healthy and diseased vessels, with a greater increase in the healthy vessel, indicating higher elasticity (Njoum and Kyriacou, 2018). This phenomenon reflects cardiovascular physiology where elevated flow rates generate increased arterial distention, causing enhanced pulsatile blood volume changes that can be captured by PPG sensors (Elgendi, 2012).

Wavelength Sensitivity

The IR wavelength demonstrated superior sensitivity to vessel stiffness changes, compared to red light, across all flow conditions. Quantitative analysis revealed that healthy vessels under infrared illumination showed amplitude increase from approximately 0.05 V to 0.32 V as flow rate increased from 2 to 6 L/min, while stiff vessels exhibited a modest response range of 0.105 V to 0.25 V, depicted in Figure 8-3. In contrast, red wavelength signals showed amplitude changes from 0.02 V to 0.12 V for healthy and up to 0.09 V for unhealth over the same flow range, compared in Figure 8-4.

This wavelength-dependent sensitivity relates to fundamental optical properties defining light-tissue interactions. IR light achieves a greater tissue penetration depth, potentially enabling more effective interrogation of deeper vascular structures where mechanical stiffening effects are most prominent (Castaneda et al., 2018). The deeper penetration of IR light allows access to subcutaneous blood volume variations, whilst red wavelengths primarily probe superficial dermal arterioles (Moço et al., 2018). This penetration depth advantage translates directly into enhanced sensitivity for detecting mechanical changes in vessel walls that occur with arterial stiffening.

Feature Correlation Patterns

The higher sensitivity of infrared was also seen in the correlation analysis, which revealed 14 statistically significant features out of the 35 tested, 4 of which were positive and 10 negative. The tendency of negative features could be attributed to the overall shorter and smaller PPG waveforms as a result of reduced blood volume variations in a stiffer artery. In contrast, only 8 red PPG features were statistically significant, with a balance of positive and negative correlations, highlighting the varying characteristics of the two wavelengths. The types of features which were significant seemed to be balanced, with a mixture of time, amplitude and area-based features for both wavelengths.

Flow Rate & Heart Rate Interactions

Flow rate and heart rate emerged as influential factors effecting PPG features across red and infrared signals, demonstrating opposing effects on signal morphology. Flow rate increases caused positive correlations with amplitude and area-based features, shown in Figure 8-6, reflecting the larger blood volume changes associated with enhanced cardiac output (Park et al., 2022). This relationship aligns with fundamental cardiovascular physiology where increased flow rates result in greater arterial distention and consequently larger PPG amplitudes.

Heart rate increases produced predominantly negative correlations with temporal features such as decay time and pulse width, shown in Table 8-1, consistent with the PPG waveform decline and reduced temporal separation between pulses seen at higher hear rates (Aminuddin et al., 2018). The correlation coefficients of -0.90 for decay time and -0.50 for pulse width with heart rate increases indicate a strong physiological link between cardiac frequency and pulse morphology, replicable in vitro. This interaction could be applied in predicting flow rate using PPG-based algorithms adjusted for heart rate, providing a pathway for compensating temporal effects in cardiovascular monitoring systems (Md Lazin Md Lazim et al., 2020).

Regression Analysis

Generalised additive model (GAM) analysis provided insights into non-linear relationships, supported by the cross-correlation findings. PPG features responded to changing flow rate, with a clear difference between healthy and unhealthy vessels, intensified at higher flow rates. This shows potential for leveraging physical activity to elevate flow rate and enhance the detection of arterial stiffness.

Flow rate effects demonstrated wavelength-specific patterns, with red signals showing particularly strong correlation for the *length-height ratio* feature. This geometric ratio relationship suggest potential applications for

PPG shape-based vessel assessment, possibly relating to second derivative morphological indicators such as b/a and c/a ratios used in traditional pulse wave analysis (Elgendi, 2012). The absence of this geometric relationship in infrared signals remains unclear but may reflect wavelength-specific optical characteristics. As suggested by the correlation analysis, regression curves revealed clearer separation between vessels in the IR than in the red features, shown in FIGURE 8-11.

IR PPG gradients show synchronised patterns supporting the arterial phenomenon: as vessels stiffen, reduced elasticity causes smaller blood volume changes, in turn flattening out the pulse waveform (Lin et al., 2024). These shallower rising and falling gradients presented as a negative *upslope* correlation and positive for *downslope* with stiffness, seen in the GAM analysis in FIGURE 8-7.

Datum feature analysis revealed morphological indicators beyond traditional amplitude and timing measures. Datum area demonstrated contrasting behaviour: *start datum area* showed a negative correlation while *end datum area* showed a positive correlation with stiffness in FIGURE 8-8. This suggests that the effects of vessel stiffness are different in the systolic and diastolic PPG segments. Specifically, the rising and falling phases of the pulse wave visualised in FIGURE 8-2, potentially due to altered pressure wave propagation characteristics and reflection patterns.

Datum difference showed significant and contrasting correlations with stiffness. Positive correlations were seen in *maximum* values while *median* values were negative, for both the rising and falling edge as in FIGURE 8-9. This suggests that in addition to systolic and diastolic characteristics, stiffness effects are multifaceted even along the same edge, highlighting the need for multiple markers for stiffness detection. These features provide novel insights into waveform shape changes that occur with vascular pathology, expanding the analytical framework for PPG-based arterial assessment.

Signal Quality and Implications in Wearables

Signal-to-noise ratio analysis confirmed higher values in healthier vessels across both wavelengths, as expected from their greater compliance and amplitude (Wu et al., 2022). This difference remained constant across flow rate levels, seen in the uniform gap between the regression curves of the healthy and unhealthy vessels in Figure 8-10. There is a steady increase in *SNR* with flow rate, as expected, but vessel stiffness did not affect the rate of change unlike the previous features.

The stability of *SNR* measurements could potentially be utilised in wearable device development for long-term assessment of vascular health status (Burrello et al., 2021). For example, by setting a user's baseline level, and then monitoring for changes over time which could arise from ageing and lifestyle factors. The observed robustness supports the development of adaptive algorithms that maintain accuracy under varying physiological states.

Heart Rate Effects and Peak Detection Challenges

Gam analysis of heart rate effects revealed complex, non-linear relationships characterised by multiple splines rather than the consistent linear or quadratic patterns seen in flow rate effects, exemplified in Figure 8-12. This complexity potentially reflects the interaction between heart rate and vascular mechanics, where multiple physiological mechanisms operate simultaneously. *Area under curve* features demonstrated more consistent single-curve relationships, followed by *amplitude* and *downslope length*, compared in Figure 8-13.

The observation of irregular regression curves with varied heart rate may result from peak detection difficulties at certain heart rate ranges, where diastolic and systolic peaks are at similar heights, becoming indistinguishable and interfering with the feature extraction algorithm (Han et al., 2022). These findings highlight the importance of robust signal processing techniques for reliable cardiovascular parameter extraction

across varying physiological conditions and the potential for in vitro investigations to support such development.

Clinical Implications

These findings extend previous work by demonstrating simultaneous comparative analysis of custom silicone vessels under identical conditions, addressing fundamental methodological limitations in PPG research. The bilateral setup eliminated confounding variables that typically affect sequential measurements, providing more reliable insights into the relationship between vascular mechanics and PPG signal characteristics. This advancement represents a step toward translating in vitro findings to clinical applications, where controlled comparisons are more difficult.

The integration of analytical approaches including GAM modelling and comprehensive feature extraction provides a foundation for evaluating automated arterial stiffness classification systems. The identification of flow-sensitive features and the demonstration of enhanced discrimination at higher flow rates suggest strategies for clinical PPG-based assessment, potentially incorporating physiological activity to maximise diagnostic sensitivity.

8.5 Summary

This chapter examined the impact of varying flow conditions on PPG signals using custom-designed silicone vessels embedded within tissue phantoms to simulate arterial stiffness. Building upon earlier single-vessel studies, this research adopted a bilateral flow configuration, simultaneously assessing healthy ad stiff vessels under identical haemodynamic conditions. This novel setup allowed direct, controlled comparisons, addressing previous methodological limitations and enhancing the reliability of stiffness assessments using PPG.

An experimental protocol was established using a pulsatile pump system that systematically varied flow rate and heart rate independently. Waveform analysis and statistical evaluation involved extracting multiple

PPG features, including amplitude, area and gradient-based metrics, and employing generalised additive model (GAM) regression to identify significant correlations between these features and vessel stiffness.

Overall, PPG waveform morphology showed sensitivity to changes in flow rates, which were significantly different between healthy and unhealthy vessels, especially at higher flow. The infrared wavelength demonstrated greater sensitivity compared to red, suggesting deeper tissue penetration advantages in capturing vascular changes.

Interaction analysis revealed contrasting effects of flow rate and heart rate on waveform features, highlighting the complexity of interpreting PPG signals under varying physiological states. Clinically, these insights could guide the development improved wearable sensors and diagnostic algorithms for continuous vascular health monitoring, benefiting cardiovascular disease prevention and management.

Future research could expand on these findings by exploring a broader range of vessel stiffness levels, investigating additional optical wavelengths and evaluating the robustness of features under artificial noise or artefacts. Applying automated feature selection techniques could streamline identification of the most informative PPG features for classification tasks. Finally, validating these results across alternative in vitro setups would strengthen confidence in the generalisability of the model.

9 DISCUSSION

Cardiovascular disease (CVD) remains the leading cause of global mortality, responsible for 17.9 million deaths each year (Khan, 2021). Arterial stiffness, an established marker of vascular ageing and a key predictor of CVD risk, traditionally requires specialised equipment and clinical expertise for assessment. The growing integration of photoplethysmography (PPG) in wearable devices presents a promising alternative for non-invasive vascular health monitoring. This opens the door to earlier detection and continuous cardiovascular risk assessment beyond traditional clinical environments (Busati et al., 2025; Weng et al., 2024).

Current methods for assessing arterial stiffness, while clinical validated, face significant limitations in terms of accessibility and practicality. Gold-standard techniques, such as pulse wave velocity measurement, require specialised training and equipment, restricting their use to clinical settings (Karimpour et al., 2023). This gap in preventive healthcare, where early detection of vascular decline could enable timely intervention to prevent the onset of CVD. Novel applications of PPG technology offer a potential solution, providing a more accessible approach to vascular health monitoring in both clinical and non-clinical environments (Weng et al., 2024).

The research landscape surrounding PPG-based cardiovascular assessment has evolved rapidly in recent years. Recent studies have demonstrated the potential for PPG signals to predict CVD risk with comparable accuracy to traditional clinical assessments, when combining extracted PPG features with basic demographic factors such as age, sex and smoking status. Machine learning methods have also shown potential for cardiovascular disease prediction (Ejiyi et al., 2024). The in vivo data used in current research inherently limits the ability to isolate specific vascular parameters in a systematic manner.

This thesis addressed key limitations in existing PPG research by establishing in vitro methodologies to replicate controlled vascular conditions mimicking healthy and unhealthy arteries. The main hypothesis proposed that an in vitro testing platform incorporating custom-built vessels, tissue phantoms, and a bilateral flow configuration, could effectively isolate arterial stiffness as an independent variable, allowing for systematic analysis of PPG signal behaviour across various simulated CVD states under controlled flow conditions.

9.1 Key Findings and Interpretations

This research demonstrated the feasibility of using in vitro PPG investigations to assess arterial stiffness through a series of progressive developments. Initial experiments using commercial vessel phantoms in Chapter 5 highlighted their limitations in PPG signal quality and arterial stiffness detection, prompting the design of custom silicone vessels with adjustable mechanical properties.

The vessel fabrication approach introduced in Chapter 6 provided a structured method for producing vessels with elastic moduli encompassing the range of healthy to stiffened human arteries. A notable improvement over initial phantom models, which were generally limited in vascular elasticity and PPG signal quality.

Chapter 7 confirmed the effectiveness of custom vessels in recreating CVD mechanics which could be detected by PPG signals, with significant correlations observed between arterial stiffness and several features. A range of vessel elasticities were tested under fixed flow conditions, allowing for more detailed characterisation of feature behaviour across the vascular health spectrum. Consistent trends emerged, with features such as amplitude, pulse width and area under the curve showing clear relationships with vessel stiffness, ranked by significance.

The bilateral investigation presented in Chapter 8 highlighted the dynamic response of healthy and unhealthy vessels in a bilateral

arrangement under varying haemodynamic conditions, detectable through PPG analysis. Healthy and diseased vessels responded differently to changes in flow rate, with the most divergences at higher flow rates. This was demonstrated across various PPG features, including geometrical and time-based, through cross-correlation as well as regression analysis.

DEVELOPMANT OF AN IN VITRO PPG TESTING PLATFORM

The development of a custom in vitro PPG testing platform in CHAPTER 5 provided a foundation for controlled investigation of cardiovascular dynamics. The platform produced consistent PPG signals across repeated trials. Tissue phantoms using identical commercial vessels yielded statistically similar PPG features, confirming the mechanical and optical stability of the system. These findings were further supported by expected trends in feature behaviour in response to controlled changes in heart rate and stroke volume.

The feature extraction pipeline established in this study reliably identified and quantified key morphological characteristics of the PPG waveform, including amplitude, area under curve, rise time and decay time. These algorithms were validated against controlled changes in stroke volume and heart rate, confirming their ability to detect physiologically meaningful variations. The statistical analysis framework, consisting of Kruskal-Wallis testing, formed a foundation for PPG feature comparison.

Initial attempts to distinguish arterial stiffness using commercial vessel-tissue phantoms were unsuccessful, emphasising the need for custom vessel techniques tailored to optical sensing applications. While commercial vessels are suitable for general flow experiments, they lacked the elasticity and optical properties required for reliable PPG measurements. This finding underscores the custom vessel fabrication strategy established in this thesis.

The platform's applications extend beyond arterial stiffness assessment, offering a controlled environment for benchmarking algorithms across a

range of cardiovascular conditions. It enables systematic testing of PPG algorithms under scenarios that are challenging to reproduce in clinical settings, such as prolonged high heart rates, simulated arrythmias or controlled noise levels. This flexibility establishes the platform as a versatile resource for advancing the development and validation of PPG technologies across diverse cardiovascular applications.

DEVELOPMENT OF CUSTOMISABLE SILICONE VESSELS

The custom vessel fabrication method described and investigated in CHAPTER 0 presents an advancement in phantom design for optical sensing applications. Through controlled variation of retarder, deadener, and hardener concentrations within silicone mixtures, a wide range of vessel stiffness values were achieved. This systematic approach allowed for accurate replication of arterial properties across the physiological spectrum, from compliant, healthy vessels to rigid, disease-mimicking conditions.

Mechanical validation confirmed that the fabricated vessels exhibited Young's modulus values ranging from 0.20 MPa, representative of healthy elastic arteries, to 1.22 MPa, corresponding to moderately stiffened vessels–closely aligning with the reported elasticity range of the femoral artery (Brum et al., 2010). This stiffness variation was achieved through careful adjustment of deadener and hardener concentrations in the silicone formulation. Vessel wall thickness remained consistent across batches, confirming that deadener and hardener induced changes in the elastic properties of vessels, rather than geometry such as wall thickness.

Dimensional changes were achievable through changing the internal form, to produce a specific diameter, and by adjusting retarder levels, to control wall thickness. Microscopic measurements showed that wall thicknesses from 0.40 mm to 0.57 mm were possible utilising up to 1.5% deadener, representative of human vessels. This level of mechanical and geometric control expands on conventional phantom techniques with new avenues for exploring vessel behaviour under defined conditions.

Signal quality improvements achieved with custom vessels were substantial when compared to commercial alternatives. While commercial vessels were unable to produce discernible differences in PPG signals across varying stiffness levels, the custom vessels produced statistically significant amplitude distinctions ($p < 0.001$) between healthy and diseased configurations. This enhancement is attributed to the increased elasticity of the custom silicone vessels, which produced more distinct PPG waveforms, and potentially linked to optical differences.

This approach builds on existing literature by expanding capabilities of dip-coated silicone vessel fabrication. Earlier studies have established similar methods, which this research advances by presenting systematic mechanical property control techniques. The ability to tune arterial elasticity while preserving optical compatibility presents an exciting advancement in phantom development for cardiovascular research. This methodology is readily adaptable to further applications, with potential relevance for imaging modalities beyond PPG, such as ultrasound and MRI.

Stiffness Detection Across Range of Vessel Elasticities

The systematic evaluation of stiffness detection across a set of vessels, designed with ranging elasticities in Chapter 7 provided key insights into the sensitivity of PPG signals to varying degrees of arterial disease. Among the extracted features, area under the curve and pulse widths emerged as the most consistent indicators of vessel stiffness. This ranking offers a useful basis for guiding the development of automated stiffness detection algorithms optimised for clinical applications.

The statistical analysis framework applied in this study utilised non-parametric methods suited to the non-Gaussian distribution commonly observed in PPG data. Kruskal-Wallis testing, followed by Dunn post-hoc comparisons, enabled robust validation of stiffness-sensitive features. This methodology strengthens confidence that the observed feature differences reflect true physiological relationships.

This study found distinct sensitivity profiles of red and infrared signals to different markers of arterial stiffness. Red light exhibited greater sensitivity to volumetric features, such as amplitude and area under the curve, whereas infrared light was more responsive to temporal effects like pulse width and rise time. This pattern could be linked to the different penetration depths and light-tissue interaction properties of the two wavelengths, offering an insight into sensor design in clinical applications.

Long-term cardiovascular monitoring is a potential application of these findings. The ability to detect changes in arterial stiffness using PPG signals could be integrated into wearable devices for continuous, non-invasive health tracking. By establishing self-calibrated baselines tailored to individual users, it may become possible to identify gradual vascular changes over extended periods, potentially months or years, allowing for the detection of cardiovascular disease progression. This approach could shift the focus of preventative care towards earlier, data-driven intervention before clinical symptoms appear.

Recent progress in machine learning for cardiovascular risk prediction reinforces the clinical relevance of these findings. Studies achieving high predictive accuracy in vascular age estimation from PPG signals highlight the feasibility of translating controlled in vitro insights into real-world applications. The feature ranking outcomes from this research offer a valuable foundation for guiding feature selection in such models, with the potential to enhance both predictive accuracy and reliability.

Bilateral Assessment Under Varying Flow Dynamics

The bilateral experimental setup introduced in Chapter 8 builds on previous investigations by enabling direct comparison of healthy and diseased vessel conditions under identical haemodynamic conditions. By enabling simultaneous assessment of compliant and stiffened vessels within the same flow circuit, this configuration removed temporal and environmental

variability inherent in sequential testing, allowing for more reliable comparisons of PPG signal behaviours across pathological states.

Key findings highlighted strong dependencies between PPG feature behaviours and both flow rate and heart rate, with healthy and diseased vessels responding differently to haemodynamic changes. At lower flow rates, PPG signals from healthy and stiffened vessels appeared similar in amplitude and waveform shape. In contrast, at higher flow rates, a clear divergence observed: healthy vessels showed larger increases in amplitude and more distinct morphological changes, while stiffened vessels exhibited comparatively muted responses.

These findings are significant in the context of asymmetric vascular conditions such as peripheral arterial disease (PAD). The bilateral in vitro approach developed in this study, complements in vivo investigations through the ability to isolate and test specific vascular parameters under controlled conditions. By systematically adjusting vessel stiffness, the platform enables direct investigation of how stiffness alone affects PPG waveform features. This insight strengthens the interpretation of observed in vivo trends and supports more targeted feature selection for clinical monitoring. This dual approach offers a robust framework for advancing both the understanding and application of PPG in vascular assessment.

Generalised additive model (GAM) analysis revealed non-linear relationships between flow conditions and PPG features, with certain features exhibiting greater ability to differentiate between vessel conditions at higher flow rate ranges. These results suggest that applying controlled haemodynamic challenges, for example standardised exercise protocols, could be a way to perform PPG-based vascular assessments. This approach also holds promise outside clinical settings, where real-world physical activity may naturally elicit diagnostically useful signals.

9.2 NOVEL CONTRIBUTIONS

This research offers several distinctive contributions to the field of PPG-based cardiovascular assessment. The integrated in vitro testing platform, combining custom-fabricated vessels, tissue phantoms and bilateral flow control, establishes a comprehensive system designed to systematically examine PPG responses to controlled variations in arterial stiffness. This platform complements in vivo studies by enabling reproducible experimentation under precisely defined conditions, providing a level of control and repeatability that is otherwise unattainable.

Methodologically, the systematic approach to silicone vessel formulation offers a replicable framework for producing phantoms with defined mechanical properties. By mapping elastomer additive concentrations to corresponding Young's modulus values, this work establishes a reference resource that can inform future phantom design. This could also be adapted for other cardiovascular applications where targeted mechanical behaviour is required, such as aneurysm modelling or valve replacement testing.

The signal processing contributions of this work include the integration and validation of a comprehensive PPG feature extraction pipeline designed for broad applicability in cardiovascular assessment. The accompanying feature ranking methodology offers evidence-based support for algorithm development, identifying the most responsive and reliable indicators across a range of vascular conditions, including but not limited to arterial stiffness.

The bilateral assessment methodology introduced in this research offers a novel approach to comparative vascular evaluation with clear relevance for PPG applications. Conventional assessments often depend sequential measurements which can introduce variability. In contrast, the bilateral approach allows for direct, simultaneous comparison under controlled flow conditions, expanding experimental possibilities. These insights can inform and support parallel in vivo measurements, contributing to more robust clinical evaluation strategies.

9.3 Implications and Real-World Applications

The findings from this research carry implications across cardiovascular research and PPG technology development. The in vitro setup offers a controlled, repeatable environment for benchmarking and validating PPG algorithms, addressing a key limitation in the current landscape of wearables. As machine learning and algorithm development accelerates in this space, standardised validation protocols, such as those presented in this paper, are critical.

Clinical applications include the potential for early vascular ageing screening using dynamic testing protocols integrated into wearable devices. The observation that flow-induced changes amplify distinctions between healthy and stiffened vessels supports the development of clinical assessments incorporating controlled haemodynamic challenges to enhance diagnostic sensitivity. Such approaches may support the detection of preclinical vascular disease, allowing for earlier intervention and reducing the risk of future cardiovascular events.

Another important application lies in the practical pathway toward personalised device calibration. By establishing individual baselines, monitoring algorithms can be tailored to account for each person's unique physiological profile. This addition to population-based references values, utilising individualised change detection, could improve sensitivity while reducing false positives, marking a step forward in the accuracy and reliability of CVD assessment through long-term wearable monitoring.

The economic implications include potential cost reductions in cardiovascular screening through the use of widely available smartphones and wearable technology. Recent studies demonstrate comparable cardiovascular risk prediction accuracy using PPG compared to traditional clinical assessments requiring blood pressure measurements. The systematic feature optimisation presented in this research could further

improve these approaches, working towards CVD screening in resource-limited settings where traditional diagnostic equipment is unavailable.

9.4 Limitations of the Experimental Model

Several key limitations should be considered in relation to the phantom-based approach used in this research. The simplified vessel geometry, although essential for maintaining experimental control, does not replicate the full complexity or branching architecture of real arterial networks. Biological arteries exhibit dynamic compliance driven by smooth muscle activity and layered structural composition. Therefore, their stiffness adapts to physiological conditions, a behaviour not replicated in static phantom models (Wesley et al., 2024).

Geometric constraints in the vessel fabrication process limited the range of achievable vessel lengths and wall thicknesses. The workable deadener limit restricted how soft the vessels could be made, while the material properties of PlatSil Gel-10 limited the upper range of achievable vessel stiffness, representative of advanced atherosclerosis. Ongoing work is addressing these limitations through the investigation of alternative silicone elastomers and fabrication methods.

Differences in optical properties between silicone phantoms and human tissue represent another important limitation. The scattering and absorption behaviour of silicone differs from skin and subcutaneous tissue, potentially affecting light penetration and reflection. Current research addresses this by incorporating light-scattering additives and exploring layered phantom designs to more closely mimic the optical behaviour of real tissue (Goldfain et al., 2022).

The controlled experimental environment, while essential for systematic investigation, inevitably excluded many factors that influence real-world PPG measurements. Variables such as skin pigmentation, motion artefacts and ambient light interference were not accounted for in this phantom-based setup. Furthermore, the fluid used in experiments was a simplified

substitute and did not replicate the complex rheological behaviours of real blood, including its non-Newtonian properties and cellular composition. The bilateral platform, while enabled controlled comparisons, relied on simplified flow patterns that may not fully reflect the complexity of real cardiovascular haemodynamics. Phenomena such as wave reflection, interactions between arterial segments and branching flow dynamics were not replicated in the experimental setup.

9.5 Future Directions and Clinical Translation

Translating these in vitro findings into clinical practice will require systematic validation in human studies. Future work should explore whether the feature sensitivities seen in the phantom model are consistent in real-world clinical settings. Bilateral data from in vitro and in vivo may be analysed together, which could support the development of more reliable algorithms for clinical use.

The development of standardised protocols for cardiovascular assessment represents another valuable future direction. The observation that flow-induced changes improve the distinction between healthy and disease vessels points to potential clinical applications involving controlled exercise or stress testing. Further research could also explore how assessment algorithms could be integrated with wearable monitoring technologies for practical implementation.

Machine learning applications based on the feature ranking methods from this research offer a promising route toward clinical translation. By systematically validating the sensitivity of specific features to arterial stiffness, this work provides a foundation for developing data-driven classification algorithms. Future studies should evaluate the performance of these algorithms across varied patient populations and a range of cardiovascular conditions to assess their generalisability and clinical utility.

Long-term longitudinal studies, using either bilateral or single-site PPG measurements, represent another promising line of future work.

Demonstrating the ability to detect gradual vascular deterioration over months or years will require extended human studies. Such work could provide valuable insight into the natural course of vascular ageing and help assess the impact of early intervention strategies on long-term cardiovascular health.

Further developing the phantom system to more closely replicate physiological complexity would be a natural step forward. Possible improvements include incorporating multi-layered vessels and embedding branching geometries that align more closely with human anatomy. Adding layered tissue structures with varying optical properties would allow the phantom to more accurately reflect the effects of skin pigmentation and subcutaneous composition on PPG signal formation. These improvements would more closely mimic the physiological interactions between, pressure flow and vessel mechanics observed in vivo.

Expanding phantom technology to other cardiovascular applications presents opportunities for broader impact. The systematic formulation approach developed in this study could be adapted to investigate a range of vascular conditions, including aneurysm formation and peripheral arterial disease. Integrating additional sensing or imaging modalities, such as ultrasound or MRI, into phantom systems could create comprehensive validation platforms to support medical device testing and clinical research.

9.6 SUMMARY

This research has shown that in vitro methods can be a provide a practical way to study how PPG signals respond to changes in blood vessel properties. Using custom silicone vessels with adjustable stiffness in a bilateral flow setup, it was possible to explore how different disease conditions affect PPG features. These findings offer a foundation for future algorithm development, validation and integration with clinical and wearable applications.

The key contributions of this work include the development of a comprehensive in vitro system for PPG-based cardiovascular research, the design of customisable silicone vessels with tuneable mechanical properties, the systematic validation of feature sensitivity to arterial stiffness, and the demonstration of bilaterial comparison methods for distinguishing between healthy and diseased vessel conditions. Together, these advances lay the groundwork for future clinical applications and technology development in the growing field of wearable health technologies.

While there are limitations related to the phantom environment and controlled experimental setup, the systematic approach developed in this work offers insights that complement and extend current clinical research. Combined with recent advances in machine learning and wearable technology, these findings point to CVD prevention and early detection through accessible, non-invasive monitoring.

10 CONCLUSION

This thesis set out to develop a bilateral in vitro vessel and tissue phantom system for investigating cardiovascular disease mechanisms using photoplethysmography (PPG), particularly detecting and assessing arterial stiffness. The work aimed to overcome key limitations in current PPG-based assessment by creating a controlled experimental environment that allows specific vascular parameters to be isolated and studied systematically.

The primary objectives of developing custom vessel fabrication techniques, establishing reproducible PPG signal acquisition protocols, and demonstrating arterial stiffness detection were successfully achieved. Custom silicone vessels with clinically relevant elasticities ranging from healthy to diseased were systematically produced using controlled elastomer formulations. When embedded within tissue-mimicking phantoms, these vessels generated high-quality PPG signals, enabling detection of stiffness-related changes between vessels.

Statistical analysis identified several PPG features that correlated significantly with vessel stiffness, supporting the system's ability to detect differences in vascular condition. The bilateral experimental setup demonstrated consistent differences between healthy and diseased vessels across a range of flow conditions, with clearer separation observed at higher flow rates.

The development of a comprehensive feature extraction pipeline, validated, through systematic testing across a range of vessel stiffness levels, offers support for future algorithm development in clinical contexts. The findings confirm that PPG technology can reliably detect stiffness variations in controlled settings, reinforcing its potential for non-invasive cardiovascular assessment in both clinical and wearable device applications.

Beyond establishing a controllable testing environment, this research provides a platform for generating high-quality, labelled data under controlled vascular conditions to support the development of robust PPG analysis algorithms. By systematically isolating arterial stiffness and comparing bilateral signal behaviours, the in vitro system can help train and validate algorithms for detecting asymmetrical vascular changes, such as those seen in peripheral arterial disease. These algorithms can then be applied to real-world bilateral or single-site PPG measurements in human subjects, enhancing the reliability and clinical utility of wearable health monitoring technologies.

Strengths, Limitations and Future Directions

The controlled in vitro environment in this research enabled systematic exploration of arterial stiffness effects on PPG signals, free from the variability present in human studies. The bilateral comparison setup reduced external influences and allowed consistent, side-by-side analysis of healthy and unhealthy vessels. The ability to tune vessel properties and validate feature sensitivity using statical methods offers a strong foundation for algorithm development and clinical translation.

However, the phantom system has inherent limitations. It lacks the anatomical and physiological complexity of living tissues, including variations in skin tone, motion artefacts and ambient light interference. While the simplified geometry and fluid dynamics allowed precise control, they do not fully replicate real-world cardiovascular characteristics, such as layered structures and branching vessel geometries.

Future work should focus on bridging this gap by further developing the system to be more physiologically representative, as well as the integration of in vitro and in vivo data for training and testing classification algorithms. Developing personalised and population-level models based on validated features could support deployment in wearables. Expanding the phantom may also broaden its relevance in applications such as ultrasound and MRI.

Longitudinal studies using long-term PPG analysis algorithms could help track vascular deterioration over time, enabling earlier and more personalised intervention strategies.

Final Reflection

This research contributes to a growing shift in cardiovascular care, from hospital-based diagnosis to continuous, personalised monitoring through wearable devices. By establishing a controlled framework for understanding how PPG signals respond to arterial changes, this work opens new possibilities for preventive healthcare outside a clinical environment.

As wearable technologies become more integrated into daily life, the ability to extract meaningful health information from everyday signals will be critical. The tools and methodologies developed here, though technical in nature, ultimately serve this broader goal. They provide a foundation for building reliable,

interpretable and equitable cardiovascular monitoring devices.

Looking ahead, this work supports a vision where individuals can monitor heart health proactively, and healthcare systems can intervene earlier using low-cost, non-invasive technologies. In this sense, it is not just a technical contribution but part of a wider effort to make cardiovascular care more preventative, data-driven, and inclusive.

REFERENCES

Abay, T.Y., Kyriacou, P.A., 2018. Photoplethysmography for blood volumes and oxygenation changes during intermittent vascular occlusions. J Clin Monit Comput 32, 447–455. https://doi.org/10.1007/s10877-017-0030-2

ACR, 2020. Magnetic Resonance Imaging (MRI) - Body [WWW Document]. Radiologyinfo.org. URL https://www.radiologyinfo.org/en/info/bodymr (accessed 9.21.22).

AHA, 2017. Why High Blood Pressure is a "Silent Killer" [WWW Document]. www.heart.org. URL https://www.heart.org/en/health-topics/high-blood-pressure/why-high-blood-pressure-is-a-silent-killer (accessed 10.26.22).

Ahn, J., 2017. New Aging Index Using Signal Features of Both Photoplethysmograms and Acceleration Plethysmograms. Healthcare Informatics Research 23, 53–59. https://doi.org/10.4258/hir.2017.23.1.53

Al Fahoum, A.S., Abu Al-Haija, A.O., Alshraideh, H.A., 2023. Identification of Coronary Artery Diseases Using Photoplethysmography Signals and Practical Feature Selection Process. Bioengineering (Basel) 10, 249. https://doi.org/10.3390/bioengineering10020249

Aldrich, J.E., 2007. Basic physics of ultrasound imaging. Critical Care Medicine 35, S131. https://doi.org/10.1097/01.CCM.0000260624.99430.22

Alivon, M., Vo-Duc Phuong, T., Vignon, V., Bozec, E., Khettab, H., Hanon, O., Briet, M., Halimi, J.-M., Hallab, M., Plichart, M., Mohammedi, K., Marre, M., Boutouyrie, P., Laurent, S., 2015. A novel device for measuring arterial stiffness using finger-toe pulse wave velocity: Validation study of the pOpmètre®. Archives of Cardiovascular Diseases 108, 227–234. https://doi.org/10.1016/j.acvd.2014.12.003

Allen, J., 2007. Photoplethysmography and its application in clinical physiological measurement. Physiol. Meas. 28, R1–R39. https://doi.org/10.1088/0967-3334/28/3/R01

Allen, J., Murray, A., 2003. Age-related changes in the characteristics of the photoplethysmographic pulse shape at various body sites. Physiol. Meas. 24, 297–307. https://doi.org/10.1088/0967-3334/24/2/306

Allen, J., Murray, A., 2002. Age-related changes in peripheral pulse timing characteristics at the ears, fingers and toes. J Hum Hypertens 16, 711–717. https://doi.org/10.1038/sj.jhh.1001478

Allen, J., Murray, A., 2000. Similarity in bilateral photoplethysmographic peripheral pulse wave characteristics at the ears, thumbs and toes. Physiol. Meas. 21, 369–377. https://doi.org/10.1088/0967-3334/21/3/303

Allen, J., O'Sullivan, J., Stansby, G., Murray, A., 2020. Age-related changes in pulse risetime measured by multi-site photoplethysmography.

Physiol. Meas. 41, 074001. https://doi.org/10.1088/1361-6579/ab9b67

Almarshad, M.A., Islam, M.S., Al-Ahmadi, S., BaHammam, A.S., 2022. Diagnostic Features and Potential Applications of PPG Signal in Healthcare: A Systematic Review. Healthcare (Basel) 10, 547. https://doi.org/10.3390/healthcare10030547

American Heart Association, 2017. What is Cardiovascular Disease? [WWW Document]. www.heart.org. URL https://www.heart.org/en/health-topics/consumer-healthcare/what-is-cardiovascular-disease (accessed 9.20.22).

Aminuddin, A., Tan, I., Butlin, M., Avolio, A.P., Kiat, H., Barin, E., Megat Mohd Nordin, N.A., Chellappan, K., 2018. Effect of increasing heart rate on finger photoplethysmography fitness index (PPGF) in subjects with implanted cardiac pacemakers. PLoS One 13, e0207301. https://doi.org/10.1371/journal.pone.0207301

Anderson, R.H., Baker, E.J., Redington, A., Rigby, M.L., Penny, D., Wernovsky, G., 2009. Paediatric Cardiology. Elsevier Health Sciences.

Aoyagi, T., 2003. Pulse oximetry: its invention, theory, and future. J Anesth 17, 259–266. https://doi.org/10.1007/s00540-003-0192-6

Apple, 2020. Apple Reveals bringing the Apple Watch PPG Sensor to Beats Earphones to monitor the heart & perform ECG [WWW Document]. Patently Apple. URL https://www.patentlyapple.com/2020/10/apple-reveals-bringing-the-apple-watch-ppg-sensor-to-beats-earphones-to-monitor-the-heart-perform-ecg.html (accessed 9.11.22).

Armañac-Julián, P., Kontaxis, S., Lázaro, J., Rapalis, A., Brazaitis, M., Marozas, V., Laguna, P., Bailón, R., Gil, E., 2025. Vascular reactivity characterized by PPG-derived pulse wave velocity. Biomedical Signal Processing and Control 105, 107641. https://doi.org/10.1016/j.bspc.2025.107641

Asakura, T., Karino, T., 1990. Flow patterns and spatial distribution of atherosclerotic lesions in human coronary arteries. Circ Res 66, 1045–1066. https://doi.org/10.1161/01.res.66.4.1045

Axelife, 2022. pOpmètre [WWW Document]. Axelife. URL https://www.axelife.fr/en/le-popmetre-en/ (accessed 8.14.22).

Axelife, 2019. pOpmètre appareil diagnostic de l'artériosclérose (vieillissement artériel). Axelife. URL https://www.axelife.fr/en/le-popmetre-en/ (accessed 9.14.22).

Baratchi, S., Singleman, C., Beis, D., Leung, L., Yalcin, H., Benslimane, F., Alser, M., Zakaria, Z., Sharma, A., Abdelrahman, H., 2019. Adaptation of a Mice Doppler Echocardiography Plato Measure Cardiac Flow Velocities for Embryonic Chicken and Adult Zebrafish. Frontiers in Bioengineering and Biotechnology 7, 96. https://doi.org/10.3389/fbioe.2019.00096

Bartels, K., Thiele, R.H., 2015. Advances in photoplethysmography: beyond arterial oxygen saturation. Can J Anesth/J Can Anesth 62, 1313–1328. https://doi.org/10.1007/s12630-015-0458-0

Bastida, S., I. Eguiazábal, J., Gaztelumendi, M., Nazábal, J., 1998. On the thickness dependence of the modulus of elasticity of polymers. Polymer Testing 17, 139–145. https://doi.org/10.1016/S0142-9418(97)00042-1

Bellinazzi, V.R., Sposito, A.C., Schreiber, R., Mill, J.G., Krieger, J.E., Pereira, A.C., Nadruz, W., 2014. Response to Cold Pressor Test Predicts Long-Term Changes in Pulse Wave Velocity in Men. American Journal of Hypertension 27, 157–161. https://doi.org/10.1093/ajh/hpt213

Beniwal, S., Bhargava, K., Kausik, S.K., 2014. Size of distal radial and distal ulnar arteries in adults of southern Rajasthan and their implications for percutaneous coronary interventions. Indian Heart J 66, 506–509. https://doi.org/10.1016/j.ihj.2014.08.010

Bentham, M., Stansby, G., Allen, J., 2018. Innovative Multi-Site Photoplethysmography Analysis for Quantifying Pulse Amplitude and Timing Variability Characteristics in Peripheral Arterial Disease. Diseases 6, 81. https://doi.org/10.3390/diseases6030081

Berger, A., 2002. Magnetic resonance imaging. BMJ 324, 35.

Bernal, M., Nenadic, I., Urban, M.W., Greenleaf, J.F., 2011. Material property estimation for tubes and arteries using ultrasound radiation force and analysis of propagating modes. J Acoust Soc Am 129, 1344–1354. https://doi.org/10.1121/1.3533735

Bernardo, L., 2023. Lares.

Bhattacharya, K., 2020. Takuo Aoyagi—a Tribute to the Brain Behind Pulse Oximetry. Indian J Surg 82, 1332–1333. https://doi.org/10.1007/s12262-020-02365-x

BHF, 2017a. ECG [WWW Document]. URL https://www.bhf.org.uk/informationsupport/tests/ecg (accessed 9.21.22).

BHF, 2017b. Echocardiogram [WWW Document]. URL https://www.bhf.org.uk/informationsupport/tests/echocardiogram (accessed 9.21.22).

BHF, 2017c. Why might I not be able to have an MRI scan? [WWW Document]. URL https://www.bhf.org.uk/informationsupport/heart-matters-magazine/medical/ask-the-experts/pacemaker-and-mri-scan (accessed 9.24.22).

BHF, 2017d. Chest x-ray [WWW Document]. URL https://www.bhf.org.uk/informationsupport/tests/chest-x-ray (accessed 9.24.22).

BIOPAC, 2021. Laser Doppler Flow | Research | BIOPAC. BIOPAC Systems, Inc. URL https://www.biopac.com/application/laser-doppler-flow/ (accessed 2.25.21).

BM, 2017. English: An illustration depicting an echocardiogram procedure.

Bogusz-Górna, K., Polańska, A., Danczak-Pazdrowska, A., Żaba, R., Sumińska, M., Fichna, P., Kędzia, A., 2023. Non-invasive detection of early microvascular changes in juveniles with type 1 diabetes.

Cardiovascular Diabetology 22. https://doi.org/10.1186/s12933-023-02031-y

Boice, E.N., Berard, D., Gonzalez, J.M., Torres, S.I.H., Knowlton, Z.J., Avital, G., Snider, E.J., 2022. Development of a Modular Tissue Phantom for Evaluating Vascular Access Devices. Bioengineering 9, 319. https://doi.org/10.3390/bioengineering9070319

Bradley, G.R.E., Kyriacou, P.A., 2024. Exploring the dynamic relationship: Changes in photoplethysmography features corresponding to intracranial pressure variations. Biomedical Signal Processing and Control 98, 106759. https://doi.org/10.1016/j.bspc.2024.106759

Brown, S., Liyanage, S., Mikrou, P., Singh, A., Ewer, A.K., 2020. Newborn pulse oximetry screening in the UK: a 2020 survey. The Lancet 396, 881. https://doi.org/10.1016/S0140-6736(20)31959-0

Brum, J., Balay, G., Bia, D., Benech, N., Ramos, A., Armentano, R., Negreira, C., 2010. Improvement of Young modulus estimation by ultrasound using static pressure steps. Physics Procedia, International Congress on Ultrasonics, Santiago de Chile, January 2009 3, 1087–1094. https://doi.org/10.1016/j.phpro.2010.01.141

Bruss, Z.S., Raja, A., 2022. Physiology, Stroke Volume, in: StatPearls. StatPearls Publishing, Treasure Island (FL).

BSX Technologies, 2016. Red Light versus Green Light. bsxtechnologies. URL https://medium.com/bsxtechnologies/red-light-versus-green-light-74fdd5fe7027 (accessed 9.8.22).

Budidha, K., Kyriacou, P.A., 2014. Investigation of Pulse Transit Times utilizing multisite reflectance photoplethysmography under conditions of artificially induced peripheral vasoconstriction. Annu Int Conf IEEE Eng Med Biol Soc 2014, 1965–1968. https://doi.org/10.1109/EMBC.2014.6943998

Budidha, K., Rybynok, V., Kyriacou, P.A., 2018. Design and Development of a Modular, Multichannel Photoplethysmography System. IEEE Transactions on Instrumentation and Measurement 67, 1954–1965. https://doi.org/10.1109/TIM.2018.2810643

Burrello, A., Pagliari, D.J., Risso, M., Benatti, S., Macii, E., Benini, L., Poncino, M., 2021. Q-PPG: Energy-Efficient PPG-Based Heart Rate Monitoring on Wearable Devices. IEEE Transactions on Biomedical Circuits and Systems 15, 1196–1209. https://doi.org/10.1109/TBCAS.2021.3122017

Busati, A., Altabaa, O., Hamad, O., 2025. Photoplethysmography-Based Technologies for Cardiovascular Disease Detection: Challenges and Opportunities. International Journal of Research and Scientific Innovation XII, 794–802. https://doi.org/10.51244/IJRSI.2025.12030060

Cao, R., Azimi, I., Sarhaddi, F., Niela-Vilen, H., Axelin, A., Liljeberg, P., Rahmani, A.M., 2022. Accuracy Assessment of Oura Ring Nocturnal Heart Rate and Heart Rate Variability in Comparison With Electrocardiography in Time and Frequency Domains: Comprehensive

Analysis. J Med Internet Res 24, e27487. https://doi.org/10.2196/27487

Cao, Y., Chen, H., Li, F., Wang, Y., 2021. Crisp-BP: continuous wrist PPG-based blood pressure measurement, in: Proceedings of the 27th Annual International Conference on Mobile Computing and Networking, MobiCom '21. Association for Computing Machinery, New York, NY, USA, pp. 378–391. https://doi.org/10.1145/3447993.3483241

Casson, A.J., Vazquez Galvez, A., Jarchi, D., 2016. Gyroscope vs. accelerometer measurements of motion from wrist PPG during physical exercise. ICT Express, Special Issue on Emerging Technologies for Medical Diagnostics 2, 175–179. https://doi.org/10.1016/j.icte.2016.11.003

Castaneda, D., Esparza, A., Ghamari, M., Soltanpur, C., Nazeran, H., 2018. A review on wearable photoplethysmography sensors and their potential future applications in health care. Int J Biosens Bioelectron 4, 195–202. https://doi.org/10.15406/ijbsbe.2018.04.00125

CC, 2022a. Cardiovascular Disease: Types, Causes & Symptoms [WWW Document]. Cleveland Clinic. URL https://my.clevelandclinic.org/health/diseases/21493-cardiovascular-disease (accessed 10.25.22).

CC, 2022b. Atherosclerosis: Causes, Symptoms, Risks & Tests [WWW Document]. Cleveland Clinic. URL https://my.clevelandclinic.org/health/diseases/16753-atherosclerosis-arterial-disease (accessed 10.26.22).

CC, 2021. High Blood Pressure (Hypertension): Causes and Symptoms [WWW Document]. Cleveland Clinic. URL https://my.clevelandclinic.org/health/diseases/4314-hypertension-high-blood-pressure (accessed 10.26.22).

Cecelja, M., Chowienczyk, P., 2012. Role of arterial stiffness in cardiovascular disease. JRSM Cardiovasc Dis 1, cvd.2012.012016. https://doi.org/10.1258/cvd.2012.012016

Cefalu, C.A., 2011. Theories and mechanisms of aging. Clin Geriatr Med 27, 491–506. https://doi.org/10.1016/j.cger.2011.07.001

Chakravorty, A., 2018. Researchers unveil new strategy to correct for motion during MRI scans [WWW Document]. Waisman Center. URL https://www.waisman.wisc.edu/2018/08/23/researchers-unveil-new-strategy-to-correct-for-motion-during-mri-scans/ (accessed 9.24.22).

Chan, Cooper, Hosanee, Welykholowa, Kyriacou, Zheng, Allen, Abbott, Lovell, Fletcher, Elgendi, 2019. Multi-Site Photoplethysmography Technology for Blood Pressure Assessment: Challenges and Recommendations. JCM 8, 1827. https://doi.org/10.3390/jcm8111827

Chang, C.-C., Chen, C.-A., Ho, C.-I., Tsai, P.-Y., Wang, T.-D., 2024. Update on Estimation of Blood Pressure and Pulse Wave Velocity Using Signals Obtained from Wearable Devices.

Charlton, P.H., Allen, J., Bailón, R., Baker, S., Behar, J.A., Chen, F., Clifford, G.D., Clifton, D.A., Davies, H.J., Ding, C., Ding, X., Dunn, J., Elgendi, M., Ferdoushi, M., Franklin, D., Gil, E., Hassan, M.F., Hernesniemi, J., Hu, X., Ji, N., Khan, Y., Kontaxis, S., Korhonen, I., Kyriacou, P.A., Laguna, P., Lázaro, J., Lee, C., Levy, J., Li, Y., Liu, C., Liu, J., Lu, L., Mandic, D.P., Marozas, V., Mejía-Mejía, E., Mukkamala, R., Nitzan, M., Pereira, T., Poon, C.C.Y., Ramella-Roman, J.C., Saarinen, H., Shandhi, M.M.H., Shin, H., Stansby, G., Tamura, T., Vehkaoja, A., Wang, W.K., Zhang, Y.-T., Zhao, N., Zheng, D., Zhu, T., 2023. The 2023 wearable photoplethysmography roadmap. Physiol Meas 44, 111001. https://doi.org/10.1088/1361-6579/acead2

Charlton, P.H., Mariscal Harana, J., Vennin, S., Li, Y., Chowienczyk, P., Alastruey, J., 2019. Modeling arterial pulse waves in healthy aging: a database for in silico evaluation of hemodynamics and pulse wave indexes. Am J Physiol Heart Circ Physiol 317, H1062–H1085. https://doi.org/10.1152/ajpheart.00218.2019

Charlton, P.H., Marozas, V., 2022. 12 - Wearable photoplethysmography devices, in: Allen, J., Kyriacou, P. (Eds.), Photoplethysmography. Academic Press, pp. 401–439. https://doi.org/10.1016/B978-0-12-823374-0.00011-6

Charlton, P.H., Paliakaitė, B., Pilt, K., Bachler, M., Zanelli, S., Kulin, D., Allen, J., Hallab, M., Bianchini, E., Mayer, C.C., Terentes-Printzios, D., Dittrich, V., Hametner, B., Veerasingam, D., Žikić, D., Marozas, V., 2022. Assessing hemodynamics from the photoplethysmogram to gain insights into vascular age: a review from VascAgeNet. American Journal of Physiology-Heart and Circulatory Physiology 322, H493–H522. https://doi.org/10.1152/ajpheart.00392.2021

Chatterjee, S., Budidha, K., Kyriacou, P.A., 2020. Investigating the origin of photoplethysmography using a multiwavelength Monte Carlo model. Physiol. Meas. 41, 084001. https://doi.org/10.1088/1361-6579/aba008

Cheng, K., Monaghan J, M., Kenny, A., Rana, B., Steeds, R., Mackay, C., Van der Westhuizen, D., 2018. 3D echocardiography: benefits and steps to wider implementation - The British Journal of Cardiology [WWW Document]. URL https://bjcardio.co.uk/2018/05/3d-echocardiography-benefits-and-steps-to-wider-implementation/ (accessed 9.21.22).

Cheung, Y., 2010. CHAPTER 6 - Systemic Circulation, in: Anderson, R.H., Baker, E.J., Penny, D.J., Redington, A.N., Rigby, M.L., Wernovsky, G., Price, G. (Eds.), Paediatric Cardiology (Third Edition). Churchill Livingstone, Philadelphia, pp. 91–116. https://doi.org/10.1016/B978-0-7020-3064-2.00006-0

Chruściel, J.J., 2022. Modifications of Textile Materials with Functional Silanes, Liquid Silicone Softeners, and Silicone Rubbers—A Review. Polymers (Basel) 14, 4382. https://doi.org/10.3390/polym14204382

Clement, M., Daniel, G., Trelles, M., 2005. Optimising the design of a broad-band light source for the treatment of skin. J Cosmet Laser Ther 7, 177–189. https://doi.org/10.1080/14764170500344575

Cleveland Clinic, 2021. Heart Rate Variability (HRV): What It Is and How You Can Track It [WWW Document]. Cleveland Clinic. URL https://my.clevelandclinic.org/health/symptoms/21773-heart-rate-variability-hrv (accessed 9.14.22).

Cluett, J., 2022. How Contrast Dye Is Used to See Inside the Body [WWW Document]. Verywell Health. URL https://www.verywellhealth.com/contrast-dye-2548866 (accessed 9.26.22).

Colquhoun, D., Dunn, L.K., McMurry, T., Thiele, R.H., 2013. The relationship between the area of peripherally-derived pressure volume loops and systemic vascular resistance. J Clin Monit Comput 27, 689–696. https://doi.org/10.1007/s10877-013-9493-y

Colvonen, P.J., 2021. Response To: Investigating sources of inaccuracy in wearable optical heart rate sensors. npj Digit. Med. 4, 1–2. https://doi.org/10.1038/s41746-021-00408-5

Coutinho, T., 2014. Arterial Stiffness and Its Clinical Implications in Women. Canadian Journal of Cardiology 30. https://doi.org/10.1016/j.cjca.2014.03.020

Cybulski, G., 2011. Ambulatory Impedance Cardiography, in: Cybulski, G. (Ed.), Ambulatory Impedance Cardiography: The Systems and Their Applications. Springer, Berlin, Heidelberg, pp. 39–56. https://doi.org/10.1007/978-3-642-11987-3_3

Daly, S.M., Leahy, M.J., 2013. 'Go with the flow ': A review of methods and advancements in blood flow imaging. Journal of Biophotonics 6, 217–255. https://doi.org/10.1002/jbio.201200071

Datta, P., Ayan, B., Ozbolat, I.T., 2017. Bioprinting for vascular and vascularized tissue biofabrication. Acta Biomater 51, 1–20. https://doi.org/10.1016/j.actbio.2017.01.035

Davenport, J.J., Hickey, M., Phillips, J.P., Kyriacou, P.A., 2017. Dual pO2/pCO2 fibre optic sensing film. Analyst 142, 1711–1719. https://doi.org/10.1039/C7AN00173H

de Pinho Ferreira, N., Gehin, C., Massot, B., 2020a. A Review of Methods for Non-Invasive Heart Rate Measurement on Wrist. IRBM 42. https://doi.org/10.1016/j.irbm.2020.04.001

de Pinho Ferreira, N., Gehin, C., Massot, B., 2020b. Ambient Light Contribution as a Reference for Motion Artefacts Reduction in Photoplethysmography, in: 13th International Conference on Biomedical Electronics and Devices. SCITEPRESS - Science and Technology Publications, Valletta, Malta, pp. 23–32. https://doi.org/10.5220/0008878800230032

Dehkordi, P., Garde, A., Molavi, B., Ansermino, J.M., Dumont, G.A., 2018. Extracting Instantaneous Respiratory Rate From Multiple Photoplethysmogram Respiratory-Induced Variations. Front Physiol 9, 948. https://doi.org/10.3389/fphys.2018.00948

D'Orazio, J., Jarrett, S., Amaro-Ortiz, A., Scott, T., 2013. UV Radiation and the Skin. Int J Mol Sci 14, 12222–12248. https://doi.org/10.3390/ijms140612222

Du, X.-Y., Li, Q., Wu, G., Chen, S., 2019. Multifunctional Micro/Nanoscale Fibers Based on Microfluidic Spinning Technology. Adv Mater 31, e1903733. https://doi.org/10.1002/adma.201903733

E, R., C, R., F, B., I, M., S, P., F, S., 2010. The different photoplethysmographic patterns can help to distinguish patients with primary and sclerodermic Raynaud phenomenon. The American journal of the medical sciences 340. https://doi.org/10.1097/MAJ.0b013e3181eecfad

Eduok, U., Etim, U., Umoren, S., 2012. Coconut coir dust as a low cost adsorbent for the removal of cationic dye from aqueous solution. Journal of Saudi Chemical Society 77. https://doi.org/10.1016/j.jscs.2012.09.014

Ejiyi, C.J., Qin, Z., Nneji, G.U., Monday, H.N., Agbesi, V.K., Ejiyi, M.B., Ejiyi, T.U., Bamisile, O.O., 2024. Enhanced Cardiovascular Disease Prediction Modelling using Machine Learning Techniques: A Focus on CardioVitalnet. Network: Computation in Neural Systems 0, 1–33. https://doi.org/10.1080/0954898X.2024.2343341

Electricalvoice, 2017. Blood Flowmeters | Electricalvoice [WWW Document]. URL https://electricalvoice.com/types-of-blood-flowmeters/#Types_of_Blood_Flowmeters (accessed 3.1.21).

Electrophysiology, T.F. of the E.S. of C. the N.A.S. of P., 1996. Heart Rate Variability. Circulation 93, 1043–1065. https://doi.org/10.1161/01.CIR.93.5.1043

Elentra, 2022. Normal ECG [WWW Document]. URL https://elentra.healthsci.queensu.ca/assets/modules/ECG/normal_ecg.html (accessed 9.21.22).

Elgendi, M., 2020. PPG Signal Analysis: An Introduction Using MATLAB®. CRC Press.

Elgendi, M., 2012. On the Analysis of Fingertip Photoplethysmogram Signals. Curr Cardiol Rev 8, 14–25. https://doi.org/10.2174/157340312801215782

Elgendi, M., Fletcher, R., Liang, Y., Howard, N., Lovell, N.H., Abbott, D., Lim, K., Ward, R., 2019. The use of photoplethysmography for assessing hypertension. npj Digit. Med. 2, 1–11. https://doi.org/10.1038/s41746-019-0136-7

ESP, 2018. Doppler Effect and Measuring Velocity of Blood in the Circulation. Education for the Sonographic Professional | ESP Inc. URL https://www.esp-inc.com/doppler-effect-velocity-of-blood-2/ (accessed 9.26.22).

Estornell Erill, J., 2004. Non-Invasive Coronary Angiography With Multislice CT: at Last an Alternative to Conventional Coronary Angiography? Rev Esp Cardiol 57, 198–200. https://doi.org/10.1016/S1885-5857(06)60136-9

Falanga, V., Bucalo, B., 1993. Use of a durometer to assess skin hardness. Journal of the American Academy of Dermatology 29, 47–51. https://doi.org/10.1016/0190-9622(93)70150-R

Fallow, B.A., Tarumi, T., Tanaka, H., 2013. Influence of skin type and wavelength on light wave reflectance. J Clin Monit Comput 27, 313–317. https://doi.org/10.1007/s10877-013-9436-7

Faria, A.N., Zanella, M.T., Kohlman, O., Ribeiro, A.B., 2002. Treating diabetes and hypertension in the obese patient. Arquivos Brasileiros de Endocrinologia & Metabologia 46, 137–142.

Farnsworth, B., 2021. What Is ECG and How Does It Work? [WWW Document]. Imotions. URL https://imotions.com/blog/what-is-ecg/ (accessed 9.21.22).

FDA, 2018. What are the Radiation Risks from CT? FDA.

FDA, 2017. Benefits and Risks. FDA.

Feigenbaum, H., 1983. Echocardiography: An overview. Journal of the American College of Cardiology 1, 216–224. https://doi.org/10.1016/S0735-1097(83)80023-0

Feiner, J.R., Severinghaus, J.W., Bickler, P.E., 2007. Dark Skin Decreases the Accuracy of Pulse Oximeters at Low Oxygen Saturation: The Effects of Oximeter Probe Type and Gender. Anesthesia & Analgesia 105, S18. https://doi.org/10.1213/01.ane.0000285988.35174.d9

Felman, A., 2019. Cardiovascular disease: Types, symptoms, prevention, and causes [WWW Document]. URL https://www.medicalnewstoday.com/articles/257484 (accessed 9.20.22).

Ferizoli, R., Karimpour, P., May, J.M., Kyriacou, P.A., 2024. Arterial stiffness assessment using PPG feature extraction and significance testing in an in vitro cardiovascular system. Sci Rep 14, 2024. https://doi.org/10.1038/s41598-024-51395-y

Ferizoli, R., Karimpour, P., May, J.M., Kyriacou, P.A., 2023. A Bilateral In Vitro Model for Cardiovascular Disease Investigations Using Photoplethysmography Sensors, in: 2023 IEEE BioSensors Conference (BioSensors). Presented at the 2023 IEEE BioSensors Conference (BioSensors), pp. 1–4. https://doi.org/10.1109/BioSensors58001.2023.10281067

Finapres, 2008. Finapres - Continuous non-invasive hemodynamics. URL https://www.finapres.com/ (accessed 9.15.22).

Fine, J., Branan, K.L., Rodriguez, A.J., Boonya-ananta, T., Ajmal, Ramella-Roman, J.C., McShane, M.J., Coté, G.L., 2021. Sources of Inaccuracy in Photoplethysmography for Continuous Cardiovascular Monitoring. Biosensors (Basel) 11, 126. https://doi.org/10.3390/bios11040126

Finnegan, E., Davidson, S., Harford, M., Watkinson, P., Tarassenko, L., Villarroel, M., 2023. Features from the photoplethysmogram and the electrocardiogram for estimating changes in blood pressure. Sci Rep 13, 986. https://doi.org/10.1038/s41598-022-27170-2

Folts, J.D., 1974. The Electromagnetic Flowmeter and Its Use in the Operating Room 10.

Gao, Q., Xie, C., Wang, P., Xie, M., Li, H., Sun, A., Fu, J., He, Y., 2020. 3D printed multi-scale scaffolds with ultrafine fibers for providing excellent biocompatibility. Mater Sci Eng C Mater Biol Appl 107, 110269. https://doi.org/10.1016/j.msec.2019.110269

GBS, 2015. The desired interaction of these ablative lasers is to precisely remove a thin layer. GBS. URL https://gbslaser.com/ablative-lasers-skin-refurfacing/ (accessed 9.2.22).

GE, 2019. | GE Healthcare (United Kingdom) [WWW Document]. URL https://www.gehealthcare.co.uk/insights/article/breaking-the-mri-sound-barrier (accessed 9.24.22).

Georgiou, K., Larentzakis, A.V., Khamis, N.N., Alsuhaibani, G.I., Alaska, Y.A., Giallafos, E.J., 2018. Can Wearable Devices Accurately Measure Heart Rate Variability? A Systematic Review. Folia Med (Plovdiv) 60, 7–20. https://doi.org/10.2478/folmed-2018-0012

Getachew, D., Astatkie, A., Lemma, K., 2018. Diameter, Vessel Thickness and Angle of Bifurcation of the Radial Artery in Ethiopian Cadavers. Journal of Morphological Sciences 35, 129–135. https://doi.org/10.1055/s-0038-1669905

Goldfain, A., Lemaillet, P., Allen, D.W., Briggman, K., Hwang, J.C., 2022. Polydimethylsiloxane tissue-mimicking phantoms with tunable optical properties. NIST 27.

GSFC, 2020. Imagine the Universe! [WWW Document]. Goddard Space Flight Center | National Aeronautics and Space Administration (NASA). URL https://imagine.gsfc.nasa.gov/features/yba/M31_velocity/spectrum/doppler_more.html (accessed 9.26.22).

Han, D., Bashar, S.K., Lazaro, J., Ding, E., Whitcomb, C., McManus, D.D., Chon, K.H., 2019. Smartwatch PPG Peak Detection Method for Sinus Rhythm and Cardiac Arrhythmia, in: 2019 41st Annual International Conference of the IEEE Engineering in Medicine and Biology Society (EMBC). Presented at the 2019 41st Annual International Conference of the IEEE Engineering in Medicine and Biology Society (EMBC), pp. 4310–4313. https://doi.org/10.1109/EMBC.2019.8857325

Han, D., Bashar, S.K., Lázaro, J., Mohagheghian, F., Peitzsch, A., Nishita, N., Ding, E., Dickson, E.L., DiMezza, D., Scott, J., Whitcomb, C., Fitzgibbons, T.P., McManus, D.D., Chon, K.H., 2022. A Real-Time PPG Peak Detection Method for Accurate Determination of Heart Rate during Sinus Rhythm and Cardiac Arrhythmia. Biosensors 12, 82. https://doi.org/10.3390/bios12020082

Han, S., Roh, D., Park, J., Shin, H., 2019. Design of Multi-Wavelength Optical Sensor Module for Depth-Dependent Photoplethysmography. Sensors 19, 5441. https://doi.org/10.3390/s19245441

Haq, A., Zafar, K., Fatima, M., Shafique, M., 2018. Effects of Different Nail Polish Colors on Arterial Blood Oxygen Saturation Values (SpO2) in Pakistani Population, in: Proceedings of the 2018 3rd International Conference on Biomedical Imaging, Signal Processing, ICBSP 2018.

Association for Computing Machinery, New York, NY, USA, pp. 6–9. https://doi.org/10.1145/3288200.3288202
Hartmann, V., Liu, H., Chen, F., Hong, W., Hughes, S., Zheng, D., 2019. Toward Accurate Extraction of Respiratory Frequency From the Photoplethysmogram: Effect of Measurement Site. Frontiers in Physiology 10. https://doi.org/10.3389/fphys.2019.00732
Hasanzadeh, N., Ahmadi, M.M., Mohammadzade, H., 2019. Blood Pressure Estimation Using Photoplethysmogram Signal and Its Morphological Features. IEEE Sensors Journal PP, 1–1. https://doi.org/10.1109/JSEN.2019.2961411
Hayes, M.J., Smith, P.R., 1998. Artifact reduction in photoplethysmography. Appl. Opt., AO 37, 7437–7446. https://doi.org/10.1364/AO.37.007437
HCA, 2021. Private MRI Scans in London | Costs & Procedure [WWW Document]. URL https://www.hcahealthcare.co.uk/our-services/tests/mri (accessed 9.21.22).
Henriksen, A., Haugen Mikalsen, M., Woldaregay, A.Z., Muzny, M., Hartvigsen, G., Hopstock, L.A., Grimsgaard, S., 2018. Using Fitness Trackers and Smartwatches to Measure Physical Activity in Research: Analysis of Consumer Wrist-Worn Wearables. J Med Internet Res 20, e110. https://doi.org/10.2196/jmir.9157
Hersant, J., Ramondou, P., Thouveny, F., Daligault, M., Feuilloy, M., Saulnier, P., Abraham, P., Henni, S., 2021. Arterial Digital Pulse Photoplethysmography in Patients with Suspected Thoracic Outlet Syndrome: A Study of the "Ca+Pra" Maneuver. Diagnostics 11, 1128. https://doi.org/10.3390/diagnostics11061128
Hickey, M., Phillips, J.P., Kyriacou, P.A., 2016. Investigation of peripheral photoplethysmographic morphology changes induced during a hand-elevation study. J Clin Monit Comput 30, 727–736. https://doi.org/10.1007/s10877-015-9761-0
Hong, J., Jin, W., Nandi, M., Alastruey, J., 2026. Real-time classification of blood pressure changes using photoplethysmography and deep learning. Biomedical Signal Processing and Control 112, 108380. https://doi.org/10.1016/j.bspc.2025.108380
Hoog Antink, C., Mai, Y., Peltokangas, M., Leonhardt, S., Oksala, N., Vehkaoja, A., 2021. Accuracy of heart rate variability estimated with reflective wrist-PPG in elderly vascular patients. Sci Rep 11, 8123. https://doi.org/10.1038/s41598-021-87489-0
Hornak, J.P., 1996. The Basics of MRI. Rochester Institute of Technology.
Hosanee, M., Chan, G., Welykholowa, K., Cooper, R., Kyriacou, P.A., Zheng, D., Allen, J., Abbott, D., Menon, C., Lovell, N.H., Howard, N., Chan, W.-S., Lim, K., Fletcher, R., Ward, R., Elgendi, M., 2020. Cuffless Single-Site Photoplethysmography for Blood Pressure Monitoring. Journal of Clinical Medicine 9, 723. https://doi.org/10.3390/jcm9030723
HPMC, 2015. Having an Echocardiogram: What You Need to Know [WWW Document]. UPMC HealthBeat. URL

https://share.upmc.com/2015/08/what-is-an-echocardiogram/ (accessed 9.21.22).
Hsieh, H.-Y., Luo, C.-H., Ye, J.-W., Tai, C.-C., 2019. Two-electrode-pair electrocardiogram with no common ground between two pairs. Rev Sci Instrum 90, 114703. https://doi.org/10.1063/1.5016939
Huang, C., Chambers, D., Matthews, G. (Eds.), 2019. Arterial Pressure Waveforms, in: Basic Physiology for Anaesthetists. Cambridge University Press, Cambridge, pp. 155–157. https://doi.org/10.1017/9781108565011.038
Instron, 2024a. The Definitive Guide to ASTM D412 Tensile Testing of Elastomers Available online [WWW Document]. URL https://www.instron.com/en/testing-solutions/astm-standards/astm-d412/ (accessed 8.3.25).
Instron, 2024b. ASTM D575-91: Standard Test Methods for Rubber Properties in Compression. URL https://www.instron.com/en/testing-solutions/astm-standards/astm-d575/ (accessed 8.3.25).
ITN, 2020. Current Evidence for Cardiac CT Calls for Change in Recommendations and Reimbursements [WWW Document]. Imaging Technology News. URL http://www.itnonline.com/article/current-evidence-cardiac-ct-calls-change-recommendations-and-reimbursements (accessed 9.25.22).
Jafary, R., Armstrong, S., Byrne, T., Stephens, A., Pellegrino, V., Gregory, S.D., 2022. Fabrication and Characterization of Tissue-Mimicking Phantoms for Ultrasound-Guided Cannulation Training. ASAIO Journal 68, 940. https://doi.org/10.1097/MAT.0000000000001593
Jani, B., Rajkumar, C., 2006. Ageing and vascular ageing. Postgrad Med J 82, 357–362. https://doi.org/10.1136/pgmj.2005.036053
Jha, P., 2021. Coronary artery bypass graft | Radiology Reference Article | Radiopaedia.org [WWW Document]. Radiopaedia. https://doi.org/10.53347/rID-16152
JHM, 2022. Atherosclerosis [WWW Document]. URL https://www.hopkinsmedicine.org/health/conditions-and-diseases/atherosclerosis (accessed 10.25.22).
Joyce, S., O'Connor, O.J., Maher, M.M., McEntee, M.F., 2020. Strategies for dose reduction with specific clinical indications during computed tomography. Radiography 26, S62–S68. https://doi.org/10.1016/j.radi.2020.06.012
Jubran, A., 2015. Pulse oximetry. Crit Care 19, 272. https://doi.org/10.1186/s13054-015-0984-8
Kang, H.G., Lee, S., Ryu, H.U., Shin, Y., 2018. Identification of Cerebral Artery Stenosis Using Bilateral Photoplethysmography. Journal of Healthcare Engineering 2018, 3253519. https://doi.org/10.1155/2018/3253519
Karimpour, P., May, J.M., Kyriacou, P.A., 2023. Photoplethysmography for the Assessment of Arterial Stiffness. Sensors (Basel) 23, 9882. https://doi.org/10.3390/s23249882

Khan, T., 2021. Cardiovascular diseases [WWW Document]. URL https://www.who.int/health-topics/cardiovascular-diseases (accessed 10.26.22).

Khoo, M.C.K., Chalacheva, P., 2019. Respiratory modulation of peripheral vasoconstriction: a modeling perspective. J Appl Physiol (1985) 127, 1177–1186. https://doi.org/10.1152/japplphysiol.00111.2019

Kim, K.B., Baek, H.J., 2023. Photoplethysmography in Wearable Devices: A Comprehensive Review of Technological Advances, Current Challenges, and Future Directions. Electronics 12, 2923. https://doi.org/10.3390/electronics12132923

Kocak, M., 2021. Magnetic Resonance Imaging (MRI) - Special Subjects [WWW Document]. MSD Manual Consumer Version. URL https://www.msdmanuals.com/en-gb/home/special-subjects/common-imaging-tests/magnetic-resonance-imaging-mri (accessed 9.24.22).

Kohn, J.C., Lampi, M.C., Reinhart-King, C.A., 2015. Age-related vascular stiffening: causes and consequences. Front Genet 6, 112. https://doi.org/10.3389/fgene.2015.00112

Kohsaka, S., Makaryus, A.N., 2008. Coronary Angiography Using Noninvasive Imaging Techniques of Cardiac CT and MRI. Curr Cardiol Rev 4, 323–330. https://doi.org/10.2174/157340308786349444

Kolin, A., 1959. Electromagnetic Blood Flow Meters. Science 130, 1088–1097.

Kramer, C.M. (Ed.), 2020. Imaging in Peripheral Arterial Disease: Clinical and Research Applications. Springer International Publishing, Cham. https://doi.org/10.1007/978-3-030-24596-2

Kraudel, R., 2021. Are PPG sensors less accurate for people with darker skin? [WWW Document]. Valencell. URL https://valencell.com/blog/are-ppg-sensors-less-accurate-for-people-with-darker-skin/ (accessed 9.13.22).

Krishnaswamy, A., Baranoski, G.V.G., 2004. A Study on Skin Optics.

Kwak, B.R., Bäck, M., Bochaton-Piallat, M.-L., Caligiuri, G., Daemen, M.J.A.P., Davies, P.F., Hoefer, I.E., Holvoet, P., Jo, H., Krams, R., Lehoux, S., Monaco, C., Steffens, S., Virmani, R., Weber, C., Wentzel, J.J., Evans, P.C., 2014. Biomechanical factors in atherosclerosis: mechanisms and clinical implications. Eur Heart J 35, 3013–3020, 3020a–3020d. https://doi.org/10.1093/eurheartj/ehu353

Kwon, A., Kim, G.-H., Kim, M.-S., 2022. Clinical implications of central blood pressure measured by radial tonometry and automated office blood pressure measured using automatic devices in cardiovascular diseases. Front Cardiovasc Med 9, 906021. https://doi.org/10.3389/fcvm.2022.906021

Kyriacou, P., Allen, J., 2022. Photoplethysmography. Elsevier. https://doi.org/10.1016/C2020-0-00098-8

Kyriacou, P.A., 2006. Pulse oximetry in the oesophagus. Physiol Meas 27, R1-35. https://doi.org/10.1088/0967-3334/27/1/R01

Kyriacou, P.A., Moye, A.R., Choi, D.M., Langford, R.M., Jones, D.P., 2001. Investigation of the human oesophagus as a new monitoring site for blood oxygen saturation. Physiol Meas 22, 223–232. https://doi.org/10.1088/0967-3334/22/1/325

Lackland, D.T., Weber, M.A., 2015. Global burden of cardiovascular disease and stroke: hypertension at the core. Can J Cardiol 31, 569–571. https://doi.org/10.1016/j.cjca.2015.01.009

Lao, C., Che, U., Chen, W., Pun, S., Mak, P., Wan, F., Vai, M., 2012. Portable Heart Rate Detector Based on Photoplethysmography with Android Programmable Devices for Ubiquitous Health Monitoring System. International Journal of Advances in Telecommunications, Electrotechnics, Signals and Systems 2. https://doi.org/10.11601/ijates.v2i1.22

Lazazzera, R., Belhaj, Y., Carrault, G., 2019. A New Wearable Device for Blood Pressure Estimation Using Photoplethysmogram. Sensors (Basel) 19, 2557. https://doi.org/10.3390/s19112557

Lee, B., Jeong, J.-H., Hong, J., Park, Y.-H., 2022a. Correlation analysis of human upper arm parameters to oscillometric signal in automatic blood pressure measurement. Sci Rep 12, 19763. https://doi.org/10.1038/s41598-022-24264-9

Lee, B., Jeong, J.-H., Hong, J., Park, Y.-H., 2022b. Correlation analysis of human upper arm parameters to oscillometric signal in automatic blood pressure measurement. Sci Rep 12, 19763. https://doi.org/10.1038/s41598-022-24264-9

Lee, C., Shin, H.S., Lee, M., 2011. Relations between ac-dc components and optical path length in photoplethysmography. JBO 16, 077012. https://doi.org/10.1117/1.3600769

Lee, J., Matsumura, K., Yamakoshi, K., Rolfe, P., Tanaka, S., Yamakoshi, T., 2013. Comparison between red, green and blue light reflection photoplethysmography for heart rate monitoring during motion. Annu Int Conf IEEE Eng Med Biol Soc 2013, 1724–1727. https://doi.org/10.1109/EMBC.2013.6609852

Lee, S.-H., Jun, S.-H., Yeom, J., Park, S.-G., Lee, C.-K., Kang, N.-G., 2018. Optical clearing agent reduces scattering of light by the stratum corneum and modulates the physical properties of coenocytes via hydration. Skin Res Technol 24, 371–378. https://doi.org/10.1111/srt.12439

Li, Y., Xu, Y., Ma, Z., Ye, Y., Gao, L., Sun, Y., 2022. An XGBoost-based model for assessment of aortic stiffness from wrist photoplethysmogram. Computer Methods and Programs in Biomedicine 226, 107128. https://doi.org/10.1016/j.cmpb.2022.107128

Liang, Q., Gao, F., Zeng, Z., Yang, J., Wu, M., Gao, C., Cheng, D., Pan, H., Liu, W., Ruan, C., 2020. Coaxial Scale-Up Printing of Diameter-Tunable Biohybrid Hydrogel Microtubes with High Strength, Perfusability, and Endothelialization. Advanced Functional Materials 30, 2001485. https://doi.org/10.1002/adfm.202001485

Liang, Y., Elgendi, M., Chen, Z., Ward, R., 2018. An optimal filter for short photoplethysmogram signals. Sci Data 5, 180076. https://doi.org/10.1038/sdata.2018.76

Lin, W.-H., Zheng, D., Li, G., Chen, F., 2024. Age-Related Changes in Blood Volume Pulse Wave at Fingers and Ears. IEEE Journal of Biomedical and Health Informatics 28, 5070–5080. https://doi.org/10.1109/JBHI.2023.3282796

Liu, B., Zhang, Z., Di, X., Wang, X., Xie, L., Xie, W., Zhang, J., 2021. The Assessment of Autonomic Nervous System Activity Based on Photoplethysmography in Healthy Young Men. Front. Physiol. 12. https://doi.org/10.3389/fphys.2021.733264

Liu, S.-H., Cheng, D.-C., Su, C.-H., 2017. A Cuffless Blood Pressure Measurement Based on the Impedance Plethysmography Technique. Sensors 17. https://doi.org/10.3390/s17051176

Madssen, E., Haere, P., Wiseth, R., 2006. Radial Artery Diameter and Vasodilatory Properties After Transradial Coronary Angiography. The Annals of Thoracic Surgery 82, 1698–1702. https://doi.org/10.1016/j.athoracsur.2006.06.017

Mansouri, S., Alhadidi, T., Chabchoub, S., Salah, R.B., 2018. Impedance cardiography: recent applications and developments. Biomedical Research 29. https://doi.org/10.4066/biomedicalresearch.29-17-3479

Matthews, B., Vongsavan, N., 1993. Advantages and limitations of laser Doppler flow meters. Int Endod J 26, 9–10. https://doi.org/10.1111/j.1365-2591.1993.tb00531.x

May, J.M., Mejía-Mejía, E., Nomoni, M., Budidha, K., Choi, C., Kyriacou, P.A., 2021. Effects of Contact Pressure in Reflectance Photoplethysmography in an In Vitro Tissue-Vessel Phantom. Sensors 21, 8421. https://doi.org/10.3390/s21248421

Mayfair, 2020. How does an ultrasound work? Mayfair Diagnostics. URL https://www.radiology.ca/article/how-does-ultrasound-work/ (accessed 9.21.22).

MC, 2022. CT coronary angiogram [WWW Document]. Mayo Clinic. URL https://www.mayoclinic.org/tests-procedures/ct-coronary-angiogram/about/pac-20385117 (accessed 9.26.22).

Mc Namara, K., Alzubaidi, H., Jackson, J.K., 2019. Cardiovascular disease as a leading cause of death: how are pharmacists getting involved? Integr Pharm Res Pract 8, 1–11. https://doi.org/10.2147/IPRP.S133088

McKee, C.T., Last, J.A., Russell, P., Murphy, C.J., 2011. Indentation versus tensile measurements of Young's modulus for soft biological tissues. Tissue Eng Part B Rev 17, 155–164. https://doi.org/10.1089/ten.TEB.2010.0520

McNaught, A.D., Wilkinson, A., 1997. Compendium of Chemical Terminology: IUPAC Recommendations. Blackwell Science.

Md Lazin Md Lazim, M.R., Aminuddin, A., Chellappan, K., Ugusman, A., Hamid, A.A., Wan Ahmad, W.A.N., Mohamad, M.S.F., 2020. Is Heart

Rate a Confounding Factor for Photoplethysmography Markers? A Systematic Review. International Journal of Environmental Research and Public Health 17, 2591. https://doi.org/10.3390/ijerph17072591

Medina-Lezama, J., Narvaez-Guerra, O., Herrera-Enriquez, K., Morey-Vargas, O.L., Bolaños-Salazar, J.F., Abugattas, J.P., Zea-Diaz, H., Chirinos-Revilla, J.L., Fernandez-Sivincha, J.G., Delgado-Lazo, V., Chirinos, D.A., Townsend, R.R., Chirinos, J.A., 2018. Hemodynamic Patterns Identified by Impedance Cardiography Predict Mortality in the General Population: The PREVENCION Study. Journal of the American Heart Association 7, e009259. https://doi.org/10.1161/JAHA.118.009259

Mehta, S., Kwatra, N., Jain, M., McDuff, D., 2024. Examining the challenges of blood pressure estimation via photoplethysmogram. Sci Rep 14, 18318. https://doi.org/10.1038/s41598-024-68862-1

Mejía-Mejía, E., Kyriacou, P.A., 2022. Photoplethysmography-Based Pulse Rate Variability and Haemodynamic Changes in the Absence of Heart Rate Variability: An In-Vitro Study. Applied Sciences 12, 7238. https://doi.org/10.3390/app12147238

Mensah, G.A., Roth, G.A., Fuster, V., 2019. The Global Burden of Cardiovascular Diseases and Risk Factors. Journal of the American College of Cardiology 74, 2529–2532. https://doi.org/10.1016/j.jacc.2019.10.009

MHRA, 2021. The use and regulation of pulse oximeters (information for healthcare professionals) [WWW Document]. GOV.UK. URL https://www.gov.uk/guidance/the-use-and-regulation-of-pulse-oximeters-information-for-healthcare-professionals (accessed 9.18.22).

Micheels, J., Alsbjorn, B., Sorensen, B., 1984. Laser doppler flowmetry. A new non-invasive measurement of microcirculation in intensive care? Resuscitation 12, 31–39. https://doi.org/10.1016/0300-9572(84)90056-x

Miglis, M.G., 2017. Pulse-Transit Time [WWW Document]. URL https://www.sciencedirect.com/topics/psychology/pulse-transit-time (accessed 12.3.23).

Mizeva, I.A., Podolyan, N.P., Mamontov, O.V., Sakovskaia, A.V., Kamshilin, A.A., 2025. Local nature of 0.1 Hz oscillations in microcirculation is confirmed by imaging photoplethysmography. Biomedical Signal Processing and Control 100, 107188. https://doi.org/10.1016/j.bspc.2024.107188

Moço, A.V., Stuijk, S., de Haan, G., 2018. New insights into the origin of remote PPG signals in visible light and infrared. Sci Rep 8, 8501. https://doi.org/10.1038/s41598-018-26068-2

Mohapatra, P., Sreeletha Premkumar, P., Sivaprakasam, M., 2018. A Yellow–Orange Wavelength-Based Short-Term Heart Rate Variability Measurement Scheme for Wrist-Based Wearables. IEEE Transactions on Instrumentation and Measurement 67, 1091–1101. https://doi.org/10.1109/TIM.2017.2786677

Mower, W.R., Sachs, C., Nicklin, E.L., Baraff, L.J., 1997. Pulse oximetry as a fifth pediatric vital sign. Pediatrics 99, 681–686. https://doi.org/10.1542/peds.99.5.681

Mozos, I., Malainer, C., Horbańczuk, J., Gug, C., Stoian, D., Luca, C.T., Atanasov, A.G., 2017. Inflammatory Markers for Arterial Stiffness in Cardiovascular Diseases. Front Immunol 8, 1058. https://doi.org/10.3389/fimmu.2017.01058

Mukkamala, R., Hahn, J.-O., Chandrasekhar, A., 2022. 11 - Photoplethysmography in noninvasive blood pressure monitoring, in: Allen, J., Kyriacou, P. (Eds.), Photoplethysmography. Academic Press, pp. 359–400. https://doi.org/10.1016/B978-0-12-823374-0.00010-4

Muntner, P., Shimbo, D., Carey, R.M., Charleston, J.B., Gaillard, T., Misra, S., Myers, M.G., Ogedegbe, G., Schwartz, J.E., Townsend, R.R., Urbina, E.M., Viera, A.J., White, W.B., Wright, J.T., 2019. Measurement of Blood Pressure in Humans: A Scientific Statement From the American Heart Association. Hypertension 73, e35–e66. https://doi.org/10.1161/HYP.0000000000000087

MW, 2022. Exploring Slices from a 3-Dimensional MRI Data Set - MATLAB & Simulink Example [WWW Document]. URL https://www.mathworks.com/help/images/exploring-slices-from-a-3-dimensional-mri-data-set.html (accessed 9.23.22).

Najjar, S.S., Lakatta, E.G., Gerstenblith, G., 2011. CHAPTER 25 - Cardiovascular Aging: The Next Frontier in Cardiovascular Prevention, in: Blumenthal, R.S., Foody, J.M., Wong, N.D. (Eds.), Preventive Cardiology: Companion to Braunwald's Heart Disease. W.B. Saunders, Philadelphia, pp. 415–432. https://doi.org/10.1016/B978-1-4377-1366-4.00025-1

Naka, K.K., Papathanassiou, K., Bechlioulis, A., Kazakos, N., Pappas, K., Tigas, S., Makriyiannis, D., Tsatsoulis, A., Michalis, L.K., 2012. Determinants of vascular function in patients with type 2 diabetes. Cardiovasc Diabetol 11, 127. https://doi.org/10.1186/1475-2840-11-127

Nall, R., 2022. Electrocardiogram: Procedure, Risks & Results [WWW Document]. Healthline. URL https://www.healthline.com/health/electrocardiogram (accessed 9.21.22).

Nara, S., Kaur, M., Lal Verma, K., 2014. Novel Notch Detection Algorithm for Detection of Dicrotic Notch in PPG Signals. IJCA 86, 36–39. https://doi.org/10.5120/15081-3520

National Health Service, 2022. NHS England » COVID Oximetry @home [WWW Document]. URL https://www.england.nhs.uk/nhs-at-home/covid-oximetry-at-home/ (accessed 9.21.22).

National Health Service, 2021. Electrocardiogram (ECG) [WWW Document]. nhs.uk. URL https://www.nhs.uk/conditions/electrocardiogram/ (accessed 9.21.22).

National Health Service, 2020. Angiography [WWW Document]. nhs.uk. URL https://www.nhs.uk/conditions/angiography/ (accessed 9.26.22).

National Health Service, 2019a. Atherosclerosis (arteriosclerosis) [WWW Document]. nhs.uk. URL https://www.nhs.uk/conditions/atherosclerosis/ (accessed 10.25.22).

National Health Service, 2019b. High blood pressure (hypertension) [WWW Document]. nhs.uk. URL https://www.nhs.uk/conditions/high-blood-pressure-hypertension/ (accessed 10.26.22).

National Health Service, 2019c. What is blood pressure? [WWW Document]. nhs.uk. URL https://www.nhs.uk/common-health-questions/lifestyle/what-is-blood-pressure/ (accessed 9.14.22).

National Health Service, 2018. MRI scan - How it's performed [WWW Document]. nhs.uk. URL https://www.nhs.uk/conditions/mri-scan/what-happens/ (accessed 9.24.22).

National Health Service, 2017a. Cardiovascular disease [WWW Document]. nhs.uk. URL https://www.nhs.uk/conditions/cardiovascular-disease/ (accessed 9.20.22).

National Health Service, 2017b. Echocardiogram [WWW Document]. nhs.uk. URL https://www.nhs.uk/conditions/echocardiogram/ (accessed 9.21.22).

National Health Service, 2017c. MRI scan [WWW Document]. nhs.uk. URL https://www.nhs.uk/conditions/mri-scan/ (accessed 9.21.22).

National Health Service, 2017d. MRI scan - Who can have one [WWW Document]. nhs.uk. URL https://www.nhs.uk/conditions/mri-scan/who-can-have-it/ (accessed 9.24.22).

National Health Service, 2014. Vascular Ultrasound [WWW Document]. Ashford & St. Peter's Hospitals NHS Foundation Trust. URL https://www.ashfordstpeters.nhs.uk/ultrasound-scans/804-vascular-ultrasound (accessed 9.26.22).

Neskovic, A.N., Hagendorff, A., Lancellotti, P., Guarracino, F., Varga, A., Cosyns, B., Flachskampf, F.A., Popescu, B.A., Gargani, L., Zamorano, J.L., Badano, L.P., Imaging, on behalf of the E.A. of C., 2012. Emergency echocardiography: the European Association of Cardiovascular Imaging recommendations. European Heart Journal - Cardiovascular Imaging 14, 1.

Nguyen, L.S., Squara, P., 2017. Non-Invasive Monitoring of Cardiac Output in Critical Care Medicine. Front Med (Lausanne) 4, 200. https://doi.org/10.3389/fmed.2017.00200

NHLBI, 2013. English: Figure A shows how the ultrasound probe (transducer) is placed over the carotid artery. Figure B is a color ultrasound image showing blood flow (the red color in the image) in the carotid artery. Figure C is a waveform image showing the sound of flowing blood in the carotid artery.

NIBIB, 2022a. Magnetic Resonance Imaging (MRI) [WWW Document]. URL https://www.nibib.nih.gov/science-education/science-topics/magnetic-resonance-imaging-mri (accessed 9.21.22).

NIBIB, 2022b. X-rays [WWW Document]. URL https://www.nibib.nih.gov/science-education/science-topics/x-rays (accessed 9.24.22).

NIBIB, 2016. Ultrasound [WWW Document]. URL https://www.nibib.nih.gov/science-education/science-topics/ultrasound (accessed 9.21.22).

NICE, 2023. Hypertension in adults: diagnosis and management, National Institute for Health and Care Excellence: Guidelines. National Institute for Health and Care Excellence (NICE), London.

Nicolò, A., Massaroni, C., Schena, E., Sacchetti, M., 2020. The Importance of Respiratory Rate Monitoring: From Healthcare to Sport and Exercise. Sensors (Basel) 20, 6396. https://doi.org/10.3390/s20216396

Nie, J., Gao, Q., Wang, Y., Zeng, J., Zhao, H., Sun, Y., Shen, J., Ramezani, H., Fu, Z., Liu, Z., Xiang, M., Fu, J., Zhao, P., Chen, W., He, Y., 2018. Vessel-on-a-chip with Hydrogel-based Microfluidics. Small 14, e1802368. https://doi.org/10.1002/smll.201802368

Nielsen, K., Zhao, L., Stamnes, J., Stamnes, K., Moan, J., 2008. The optics of human skin: Aspects important for human health. Solar Radiation and Human Health 1.

Nitzan, M., Adar, Y., Hoffman, E., Shalom, E., Engelberg, S., Ben-Dov, I.Z., Bursztyn, M., 2013. Comparison of Systolic Blood Pressure Values Obtained by Photoplethysmography and by Korotkoff Sounds. Sensors 13, 14797–14812. https://doi.org/10.3390/s131114797

Nitzan, M., Romem, A., Koppel, R., 2014. Pulse oximetry: fundamentals and technology update. Med Devices (Auckl) 7, 231–239. https://doi.org/10.2147/MDER.S47319

Njoum, H., 2017. Investigations of photoplethysmography in the assessment of haemodynamics, vascular mechanics and haemorheology (doctoral). City, University of London.

Njoum, H., Kyriacou, P.A., 2018. In vitro validation of measurement of volume elastic modulus using photoplethysmography. Medical Engineering & Physics 52, 10–21. https://doi.org/10.1016/j.medengphy.2017.11.011

Njoum, H., Kyriacou, P.A., 2017. Photoplethysmography for the Assessment of Haemorheology. Sci Rep 7, 1406. https://doi.org/10.1038/s41598-017-01636-0

Nomoni, M., Kyriacou, P.A., May, J.M., 2019. A Pulsatile Optical Tissue Phantom for the Investigation of Light-Tissue Interaction in Reflectance Photoplethysmography, in: 2019 41st Annual International Conference of the IEEE Engineering in Medicine & Biology Society (EMBC). Presented at the 41st Annual International Conference of the IEEE Engineering in Medicine and Biology Society,

IEEE, Berlin, Germany, pp. 3204–3207. https://doi.org/10.1109/EMBC.2019.8857036

Nomoni, M., May, J.M., Kyriacou, P.A., 2020a. Novel Polydimethylsiloxane (PDMS) Pulsatile Vascular Tissue Phantoms for the In-Vitro Investigation of Light Tissue Interaction in Photoplethysmography. Sensors (Basel) 20. https://doi.org/10.3390/s20154246

Nomoni, M., May, J.M., Kyriacou, P.A., 2020b. Fabricating Novel PDMS Vessels for Phantoms in Photoplethysmography Investigations. Annu Int Conf IEEE Eng Med Biol Soc 2020, 4458–4461. https://doi.org/10.1109/EMBC44109.2020.9176476

Omeh, D.J., Shlofmitz, E., 2022. Angiography, in: StatPearls. StatPearls Publishing, Treasure Island (FL).

Oprişan, C., Cârlescu, V., Barnea, A., Prisacaru, G., Olaru, D.N., Plesu, G., 2016. Experimental determination of the Young's modulus for the fingers with application in prehension systems for small cylindrical objects. IOP Conf. Ser.: Mater. Sci. Eng. 147, 012058. https://doi.org/10.1088/1757-899X/147/1/012058

O'Rourke, M.F., Pauca, A., Jiang, X.-J., 2001. Pulse wave analysis. British Journal of Clinical Pharmacology 51, 507–522. https://doi.org/10.1046/j.0306-5251.2001.01400.x

Ouyang, V., Ma, B., Pignatelli, N., Sengupta, S., Sengupta, P., Mungulmare, K., Fletcher, R.R., 2021. The use of multi-site photoplethysmography (PPG) as a screening tool for coronary arterial disease and atherosclerosis. Physiol. Meas. 42, 064006. https://doi.org/10.1088/1361-6579/abad48

Pai, R.K., 2021. Cardiac Output [WWW Document]. URL https://myhealth.alberta.ca:443/Health/Pages/conditions.aspx?hwid=tx4080abc (accessed 9.17.22).

Park, J., Seok, H.S., Kim, S.-S., Shin, H., 2022. Photoplethysmogram Analysis and Applications: An Integrative Review. Front Physiol 12, 808451. https://doi.org/10.3389/fphys.2021.808451

Park, J., Shin, H., 2022. Vascular Aging Estimation Based on Artificial Neural Network Using Photoplethysmogram Waveform Decomposition: Retrospective Cohort Study. JMIR Med Inform 10, e33439. https://doi.org/10.2196/33439

Patterson, J. a. C., Guang-Zhong Yang, null, 2011. Ratiometric artifact reduction in low power reflective photoplethysmography. IEEE Trans Biomed Circuits Syst 5, 330–338. https://doi.org/10.1109/TBCAS.2011.2161304

Pereira, M.M., Torrado, J., Bock, J., Sosa, C., Diaz, A., Bia, D., Zócalo, Y., 2022. Wave separation analysis-derived indexes obtained from radial and carotid tonometry in healthy pregnancy and pregnancy-associated hypertension: Comparison with pulse wave analysis-derived indexes. Front. Cardiovasc. Med. 9. https://doi.org/10.3389/fcvm.2022.997452

Pharmattila, 2019. Magyar: Metilén kék abszorbciós spektruma (modification of Methylene_blue_absorption_spectrum).

Phillips, J.P., Cibert-Goton, V., Langford, R.M., Shortland, P.J., 2013. Perfusion assessment in rat spinal cord tissue using photoplethysmography and laser Doppler flux measurements. J Biomed Opt 18, 037005. https://doi.org/10.1117/1.JBO.18.3.037005

Phillips, J.P., Langford, R.M., Chang, S.H., Kyriacou, P.A., Jones, D.P., 2011. Photoplethysmographic measurements from the esophagus using a new fiber-optic reflectance sensor. J Biomed Opt 16, 077005. https://doi.org/10.1117/1.3598858

Picone, D.S., Schultz, M.G., Otahal, P., Aakhus, S., Al, -Jumaily Ahmed M., Black, J.A., Bos, W.J., Chambers, J.B., Chen, C.-H., Cheng, H.-M., Cremer, A., Davies, J.E., Dwyer, N., Gould, B.A., Hughes, A.D., Lacy, P.S., Laugesen, E., Liang, F., Melamed, R., Muecke, S., Ohte, N., Okada, S., Omboni, S., Ott, C., Peng, X., Pereira, T., Pucci, G., Rajani, R., Roberts, -Thomson Philip, Rossen, N.B., Sueta, D., Sinha, M.D., Schmieder, R.E., Smulyan, H., Srikanth, V.K., Stewart, R., Stouffer, G.A., Takazawa, K., Wang, J., Westerhof, B.E., Weber, F., Weber, T., Williams, B., Yamada, H., Yamamoto, E., Sharman, J.E., 2017. Accuracy of Cuff-Measured Blood Pressure. Journal of the American College of Cardiology 70, 572–586. https://doi.org/10.1016/j.jacc.2017.05.064

Pilt, K., May, J.M., Kyriacou, P.A., 2021. In-Vitro Investigation of Flow Profiles in Arteries Using the Photoplethysmograph, in: 2021 43rd Annual International Conference of the IEEE Engineering in Medicine & Biology Society (EMBC). Presented at the 2021 43rd Annual International Conference of the IEEE Engineering in Medicine & Biology Society (EMBC), IEEE, Mexico, pp. 7211–7214. https://doi.org/10.1109/EMBC46164.2021.9629713

Pinheiro, N., Couceiro, R., Henriques, J., Muehlsteff, J., Quintal, I., Goncalves, L., Carvalho, P., 2016. Can PPG be used for HRV analysis? Annu Int Conf IEEE Eng Med Biol Soc 2016, 2945–2949. https://doi.org/10.1109/EMBC.2016.7591347

Polytek Development Corp., 2021. PlatSil Silicone Gels Technical Bulletin.

Pouratian, N., Toga, A.W., 2002. 5 - Optical Imaging Based on Intrinsic Signals, in: Toga, A.W., Mazziotta, J.C. (Eds.), Brain Mapping: The Methods (Second Edition). Academic Press, San Diego, pp. 97–140. https://doi.org/10.1016/B978-012693019-1/50007-1

Přibil, J., Přibilová, A., Frollo, I., 2020. Comparative Measurement of the PPG Signal on Different Human Body Positions by Sensors Working in Reflexive and Transmission Modes. Engineering Proceedings 2, 69. https://doi.org/10.3390/ecsa-7-08204

Puiu, T., 2021. What's an MRI and how does it work? ZME Science. URL https://www.zmescience.com/science/what-is-mri-052354/ (accessed 9.24.22).

Red light, green light: Why Fitbit's sensor shake-up is a huge deal [WWW Document], 2017. . Wareable. URL

https://www.wareable.com/fitbit/fitbit-red-light-optical-sensor-technology-2034 (accessed 9.8.22).

Reguig, F.B., 2016. Photoplethysmogram signal analysis for detecting vital physiological parameters: An evaluating study, in: 2016 International Symposium on Signal, Image, Video and Communications (ISIVC). Presented at the 2016 International Symposium on Signal, Image, Video and Communications (ISIVC), pp. 167–173. https://doi.org/10.1109/ISIVC.2016.7893981

Remmen, J.J., Aengevaeren, W.R.M., Verheugt, F.W.A., Van der Werf, T., Luijten, H.E., Bos, A., Jansen, R.W.M.M., 2002. Finapres arterial pulse wave analysis with Modelflow® is not a reliable non-invasive method for assessment of cardiac output. Clinical Science 103, 143–149. https://doi.org/10.1042/cs1030143

Riva, C.E., Harino, S., Petrig, B.L., Shonat, R.D., 1992. Laser Doppler flowmetry in the optic nerve. Exp Eye Res 55, 499–506. https://doi.org/10.1016/0014-4835(92)90123-a

Roldan, M., Chatterjee, S., 2021. Brain Light-Tissue Interaction Modelling: Towards a non-invasive sensor for Traumatic Brain Injury. pp. 1292–1296. https://doi.org/10.1109/EMBC46164.2021.9630909

Rouger, M., 2022. CT or MRI – which is better for imaging stable cardiac chest pain? [WWW Document]. URL https://healthcare-in-europe.com/en/news/ct-or-mri-which-is-better-for-imaging-stable-cardiac-chest-pain.html (accessed 9.25.22).

Sadiku, M.N.O., 2001. Elements of Electromagnetics. Oxford University Press.

Sahroni, A., Hassya, I.A., Rifaldi, R., Jannah, N.U., Irawan, A.F., Rahayu, A.W., 2019. HRV Assessment Using Finger-tip Photoplethysmography (PulseRate) as Compared to ECG on Healthy Subjects During Different Postures and Fixed Breathing Pattern. Procedia Computer Science, The Fifth Information Systems International Conference, 23-24 July 2019, Surabaya, Indonesia 161, 535–543. https://doi.org/10.1016/j.procs.2019.11.153

Sandell, J.L., Zhu, T.C., 2011. A review of in-vivo optical properties of human tissues and its impact on PDT. J Biophotonics 4, 773–787. https://doi.org/10.1002/jbio.201100062

Saritas, T., Greber, R., Venema, B., Puelles, V.G., Ernst, S., Blazek, V., Floege, J., Leonhardt, S., Schlieper, G., 2019. Non-invasive evaluation of coronary heart disease in patients with chronic kidney disease using photoplethysmography. Clinical Kidney Journal 12, 538–545. https://doi.org/10.1093/ckj/sfy135

Sayyed, S., 2013. What's the difference between cardiac MRI and cardiac CT [WWW Document]. URL https://www.nebraskamed.com/heart/imaging/whats-the-difference-between-cardiac-mri-and-cardiac-ct (accessed 9.25.22).

Scardulla, F., Cosoli, G., Spinsante, S., Poli, A., Iadarola, G., Pernice, R., Busacca, A., Pasta, S., Scalise, L., D'Acquisto, L., 2023. Photoplethysmograhic sensors, potential and limitations: Is it time

for regulation? A comprehensive review. Measurement 218, 113150. https://doi.org/10.1016/j.measurement.2023.113150

Schaefer-Prokop, C., Neitzel, U., Venema, H.W., Uffmann, M., Prokop, M., 2008. Digital chest radiography: an update on modern technology, dose containment and control of image quality. Eur Radiol 18, 1818–1830. https://doi.org/10.1007/s00330-008-0948-3

Scheeren, T.W.L., Schober, P., Schwarte, L.A., 2012. Monitoring tissue oxygenation by near infrared spectroscopy (NIRS): background and current applications. Journal of Clinical Monitoring and Computing 26, 279. https://doi.org/10.1007/s10877-012-9348-y

Schöneberg, J., De Lorenzi, F., Theek, B., Blaeser, A., Rommel, D., Kuehne, A.J.C., Kießling, F., Fischer, H., 2018. Engineering biofunctional in vitro vessel models using a multilayer bioprinting technique. Sci Rep 8, 10430. https://doi.org/10.1038/s41598-018-28715-0

Schultz-Ehrenburg, U., Blazek, V., 2001. Value of Quantitative Photoplethysmography for Functional Vascular Diagnostics: Current Status and Prospects. Skin Pharmacology and Applied Skin Physiology 14, 316–323. https://doi.org/10.1159/000056362

Schwartz, D.T., 2008. Counter-Point: Are We Really Ordering Too Many CT Scans? West J Emerg Med 9, 120–122.

Scott, E.A., Sandler, G.A., 1978. Electromagnetic blood flowmeters and flow probes: theoretic and practical considerations. Am J Vet Res 39, 1567–1571.

Segers, P., Rietzschel, E.R., Chirinos, J.A., 2020. How to Measure Arterial Stiffness in Humans. Arterioscler Thromb Vasc Biol 40, 1034–1043. https://doi.org/10.1161/ATVBAHA.119.313132

Seok, D., Lee, S., Kim, M., Cho, J., Kim, C., 2021. Motion Artifact Removal Techniques for Wearable EEG and PPG Sensor Systems. Frontiers in Electronics 2.

Sharman, J.E., Tan, I., Stergiou, G.S., Lombardi, C., Saladini, F., Butlin, M., Padwal, R., Asayama, K., Avolio, A., Brady, T.M., Murray, A., Parati, G., 2023. Automated 'oscillometric' blood pressure measuring devices: how they work and what they measure. J Hum Hypertens 37, 93–100. https://doi.org/10.1038/s41371-022-00693-x

SHC, 2017. Types of Angiograms [WWW Document]. Stanford Health Care. URL https://stanfordhealthcare.org/medical-tests/a/angiogram-arteriogram/types.html (accessed 9.26.22).

Shcherbina, A., Mattsson, C.M., Waggott, D., Salisbury, H., Christle, J.W., Hastie, T., Wheeler, M.T., Ashley, E.A., 2017. Accuracy in Wrist-Worn, Sensor-Based Measurements of Heart Rate and Energy Expenditure in a Diverse Cohort. Journal of Personalized Medicine 7, 3. https://doi.org/10.3390/jpm7020003

Sheffield, S., 2017. The Electrocardiogram (EKG or ECG) [WWW Document]. GetBodySmart. URL https://www.getbodysmart.com/circulatory-system/ekg/ (accessed 9.21.22).

Shin, H., 2022. XGBoost Regression of the Most Significant Photoplethysmogram Features for Assessing Vascular Aging. IEEE Journal of Biomedical and Health Informatics 26, 3354–3361. https://doi.org/10.1109/JBHI.2022.3151091

Shirwany, N.A., Zou, M., 2010. Arterial stiffness: a brief review. Acta Pharmacol Sin 31, 1267–1276. https://doi.org/10.1038/aps.2010.123

Shmerling, R.H., 2017. How's your heart rate and why it matters? [WWW Document]. Harvard Health. URL https://www.health.harvard.edu/heart-health/hows-your-heart-rate-and-why-it-matters (accessed 9.14.22).

Slapničar, G., Mlakar, N., Luštrek, M., 2019. Blood Pressure Estimation from Photoplethysmogram Using a Spectro-Temporal Deep Neural Network. Sensors (Basel) 19, 3420. https://doi.org/10.3390/s19153420

SMIL, 2022. Benefits and Risks of Vascular Ultrasound in Arizona– Southwest Medical Imaging [WWW Document]. Southwest Medical Imaging. URL https://www.esmil.com/heart-vascular-scans/vascular-ultrasound/benefits-risks.php (accessed 9.26.22).

Smith, M., Sachdev, P., 2022. Cardiac Output: Normal Rate, Low Output Causes, & How To Increase It [WWW Document]. URL https://www.webmd.com/heart/heart-cardiac-output (accessed 9.17.22).

SMT Medical, 2013. Vascular Diagnostics - VICORDER - Products - SMT Medical GmbH [WWW Document]. URL https://www.smt-medical.com/en/products/vicorder.html (accessed 9.15.22).

Soneye, M.A., Adekanmi, A.J., Obajimi, M.O., Aje, A., 2019. Intima-media thickness of femoral arteries and carotids among an adult hypertensive Nigerian population: A case-control study to assess their use as surrogate markers of atherosclerosis. Ann Afr Med 18, 158–166. https://doi.org/10.4103/aam.aam_57_18

Spaccarotella, C.A.M., Migliarino, S., Mongiardo, A., Sabatino, J., Santarpia, G., De Rosa, S., Curcio, A., Indolfi, C., 2021. Measurement of the QT interval using the Apple Watch. Sci Rep 11, 10817. https://doi.org/10.1038/s41598-021-89199-z

Spector, K.S., Lawson, W.E., 2001. Optimizing safe femoral access during cardiac catheterization. Catheter Cardiovasc Interv 53, 209–212. https://doi.org/10.1002/ccd.1150

Srivastava, V.P., Saxena, M., 1994. Two-layered model of Casson fluid flow through stenotic blood vessels: applications to the cardiovascular system. J Biomech 27, 921–928. https://doi.org/10.1016/0021-9290(94)90264-x

Stergiou, G.S., Palatini, P., Parati, G., O'Brien, E., Januszewicz, A., Lurbe, E., Persu, A., Mancia, G., Kreutz, R., European Society of Hypertension Council and the European Society of Hypertension Working Group on Blood Pressure Monitoring and Cardiovascular Variability, 2021. 2021 European Society of Hypertension practice

guidelines for office and out-of-office blood pressure measurement. J Hypertens 39, 1293–1302. https://doi.org/10.1097/HJH.0000000000002843

Stoyneva, Z., 2012. Clinical application of laser Doppler flowmetry in neurology. Perspectives in Medicine, New Trends in Neurosonology and Cerebral Hemodynamics – an Update 1, 89–93. https://doi.org/10.1016/j.permed.2012.03.009

Stroke Association, 2014. Ischaemic stroke [WWW Document]. Stroke Association. URL https://www.stroke.org.uk/what-is-stroke/types-of-stroke/ischaemic-stroke (accessed 9.20.22).

Sun, W.-J., Kothari, S., Sun, C.C., 2018. The relationship among tensile strength, Young's modulus, and indentation hardness of pharmaceutical compacts. Powder Technology 331, 1–6. https://doi.org/10.1016/j.powtec.2018.02.051

Sun, Y., Thakor, N., 2016. Photoplethysmography Revisited: From Contact to Noncontact, From Point to Imaging. IEEE Transactions on Biomedical Engineering 63, 463–477. https://doi.org/10.1109/TBME.2015.2476337

SVH, 2017. St Vincent's Heart Health [WWW Document]. URL https://www.svhhearthealth.com.au/procedures/imaging/chest-x-ray (accessed 9.24.22).

Sviridova, N., Zhao, T., Aihara, K., Nakamura, K., Nakano, A., 2018. Photoplethysmogram at green light: Where does chaos arise from? Chaos, Solitons & Fractals 116, 157–165. https://doi.org/10.1016/j.chaos.2018.09.016

Takashima, K., Kitou, T., Mori, K., Ikeuchi, K., 2007. Simulation and experimental observation of contact conditions between stents and artery models. Medical engineering & physics 29, 326–35. https://doi.org/10.1016/j.medengphy.2006.04.003

Tamura, T., Maeda, Y., Sekine, M., Yoshida, M., 2014. Wearable Photoplethysmographic Sensors—Past and Present. Electronics 3, 282–302. https://doi.org/10.3390/electronics3020282

Tanaka, A., 2022. Analysis of a microcirculatory windkessel model using photoplethysmography with green light: A pilot study. IEICE Electron. Express 19, 20220371–20220371. https://doi.org/10.1587/elex.19.20220371

Teferra, M., 2017. Electromagnetic Blood Flow meter: Review. International Journal of Latest Research in Engineering & Technology 3, 21–26.

Thaulow, E., Erikssen, J.E., 1991. How important is heart rate? J Hypertens Suppl 9, S27-30. https://doi.org/10.1097/00004872-199112007-00007

Thomas-Jean, F., Obeid, H., Boutouyrie, P., Hallab, M., Coucke, P., Danchin, N., Pannier, B., 2016. [PP.11.22] ARTERIAL STIFFNESS RECORDINGS WITH POPMETRE® IN A GENERAL PRIMARY CARE POPULATION: THE IPC COHORT. Journal of Hypertension 34, e183. https://doi.org/10.1097/01.hjh.0000491850.03804.86

Thomson, S.D., Jung, S., 2025. Fingertip Impedance Plethysmography: A New Window Into Peripheral Blood Flow, in: 2025 IEEE 21st International Conference on Body Sensor Networks (BSN). Presented at the 2025 IEEE 21st International Conference on Body Sensor Networks (BSN), pp. 1–4. https://doi.org/10.1109/BSN66969.2025.11337753

Tsakok, M.T., Gleeson, F.V., 2018. The chest radiograph in heart disease. Medicine 46, 453–457. https://doi.org/10.1016/j.mpmed.2018.05.007

UVAH, 2017. Having an Exam That Uses Contrast Dye? Here's What You Need to Know. University of Virgina Health | UVA Radiology and Medical Imaging Blog for Patients. URL https://blog.radiology.virginia.edu/medical-contrast/ (accessed 9.26.22).

Van Bortel, L.M., Laurent, S., Boutouyrie, P., Chowienczyk, P., Cruickshank, J.K., De Backer, T., Filipovsky, J., Huybrechts, S., Mattace-Raso, F.U.S., Protogerou, A.D., Schillaci, G., Segers, P., Vermeersch, S., Weber, T., Artery Society, European Society of Hypertension Working Group on Vascular Structure and Function, European Network for Noninvasive Investigation of Large Arteries, 2012. Expert consensus document on the measurement of aortic stiffness in daily practice using carotid-femoral pulse wave velocity. J Hypertens 30, 445–448. https://doi.org/10.1097/HJH.0b013e32834fa8b0

van der Meer, R.W., Diamant, M., Westenberg, J.J.M., Doornbos, J., Bax, J.J., de Roos, A., Lamb, H.J., 2007. Magnetic resonance assessment of aortic pulse wave velocity, aortic distensibility, and cardiac function in uncomplicated type 2 diabetes mellitus. J Cardiovasc Magn Reson 9, 645–651. https://doi.org/10.1080/10976640601093703

Van Son, C.R., Eti, D.U., 2021. Screening for COVID-19 in Older Adults: Pulse Oximeter vs. Temperature. Frontiers in Medicine 8.

VH, 2022. Private MRI Scan without Referral in UK | Vista Health [WWW Document]. URL https://www.vista-health.co.uk/services/mri-services/cardiac-mri-scan (accessed 9.21.22).

Wang, C., Li, Z., Wei, X., 2013. Monitoring heart and respiratory rates at radial artery based on PPG. Optik 124, 3954–3956. https://doi.org/10.1016/j.ijleo.2012.11.044

Wang, T.-W., Chen, W.-X., Chu, H.-W., Lin, S.-F., 2020. Single-Channel Bioimpedance Measurement for Wearable Continuous Blood Pressure Monitoring. IEEE Transactions on Instrumentation and Measurement PP. https://doi.org/10.1109/TIM.2020.3035578

Ward, K.R., Ivatury, R.R., Barbee, R.W., Terner, J., Pittman, R., Filho, I.P.T., Spiess, B., 2006. Near infrared spectroscopy for evaluation of the trauma patient: a technology review. Resuscitation 68, 27–44. https://doi.org/10.1016/j.resuscitation.2005.06.022

Webster, J.G., 1997. Design of Pulse Oximeters. CRC Press.

Weng, W.-H., Baur, S., Daswani, M., Chen, C., Harrell, L., Kakarmath, S., Jabara, M., Behsaz, B., McLean, C.Y., Matias, Y., Corrado, G.S.,

Shetty, S., Prabhakara, S., Liu, Y., Danaei, G., Ardila, D., 2024. Predicting cardiovascular disease risk using photoplethysmography and deep learning. PLOS Glob Public Health 4, e0003204. https://doi.org/10.1371/journal.pgph.0003204

Wesley, C.D., Neutel, C.H.G., De Meyer, G.R.Y., Martinet, W., Guns, P.-J., 2024. Unravelling the impact of active and passive contributors to arterial stiffness in male mice and their role in vascular aging. Sci Rep 14, 18337. https://doi.org/10.1038/s41598-024-68725-9

Whang, T.-J., Huang, H.-Y., Hsieh, M.-T., Chen, J.-J., 2009. Laser-Induced Silver Nanoparticles on Titanium Oxide for Photocatalytic Degradation of Methylene Blue. Int J Mol Sci 10, 4707–4718. https://doi.org/10.3390/ijms10114707

World Health Organisation, 2021. Cardiovascular diseases (CVDs) [WWW Document]. URL https://www.who.int/news-room/fact-sheets/detail/cardiovascular-diseases-(cvds) (accessed 9.20.22).

World Health Organisation, 2013. A global brief on hypertension: silent killer, global public health crisis: World Health Day 2013. World Health Organization.

Wu, M.-T., Liu, I.-F., Tzeng, Y.-H., Wang, L., 2022. Modified photoplethysmography signal processing and analysis procedure for obtaining reliable stiffness index reflecting arteriosclerosis severity. Physiol. Meas. 43, 085001. https://doi.org/10.1088/1361-6579/ac7d91

Xing, X., Huang, R., Hao, L., Jiang, C., Dong, W.-F., 2023. Temporal complexity in photoplethysmography and its influence on blood pressure. Front. Physiol. 14. https://doi.org/10.3389/fphys.2023.1187561

Xing, X., Ma, Z., Xu, S., Zhang, M., Zhao, W., Song, M., Dong, W.-F., 2021. Blood pressure assessment with in-ear photoplethysmography. Physiol. Meas. 42, 105009. https://doi.org/10.1088/1361-6579/ac2a71

Yang, D., Zhu, J., Zhu, P., 2015. SpO2 and heart rate measurement with wearable watch based on PPG, in: 2015 IET International Conference on Biomedical Image and Signal Processing (ICBISP 2015). Presented at the 2015 IET International Conference on Biomedical Image and Signal Processing (ICBISP 2015), pp. 1–5. https://doi.org/10.1049/cp.2015.0784

Yousef, H., Alhajj, M., Sharma, S., 2022. Anatomy, Skin (Integument), Epidermis, in: StatPearls. StatPearls Publishing, Treasure Island (FL).

Yuda, E., Shibata, M., Ogata, Y., Ueda, N., Yambe, T., Yoshizawa, M., Hayano, J., 2020. Pulse rate variability: a new biomarker, not a surrogate for heart rate variability. Journal of Physiological Anthropology 39, 21. https://doi.org/10.1186/s40101-020-00233-x

Zahner, G.J., Gruendl, M.A., Spaulding, K.A., Schaller, M.S., Hills, N.K., Gasper, W.J., Grenon, S.M., 2017. THE ASSOCIATION BETWEEN ARTERIAL STIFFNESS AND PERIPHERAL ARTERY DISEASE AS

MEASURED BY RADIAL ARTERY TONOMETRY. J Vasc Surg 66, 1518–1526. https://doi.org/10.1016/j.jvs.2017.06.068

Zhou, L., Li, Y., Tu, Q., Wang, J., 2023. A 3D printing mold method for rapid fabrication of artificial blood vessels. Colloids and Surfaces A: Physicochemical and Engineering Aspects 662, 130952. https://doi.org/10.1016/j.colsurfa.2023.130952

Zieman, S.J., Melenovsky, V., Kass, D.A., 2005. Mechanisms, Pathophysiology, and Therapy of Arterial Stiffness. Arteriosclerosis, Thrombosis, and Vascular Biology 25, 932–943. https://doi.org/10.1161/01.ATV.0000160548.78317.29

Zouridakis, G., 2003. Biomedical Technology and Devices Handbook. CRC Press, Boca Raton. https://doi.org/10.1201/9780203491492